Universidad de Valladolid

ESCUELA DE INGENIERÍAS INDUSTRIALES

PROGRAMA DE DOCTORADO EN INGENIERIA

TERMODINAMICA DE FLUIDOS

TESIS DOCTORAL:

CONVERSION OF CO_2 CAPTURED BY AMMONIA INTO VALUE-ADDED CHEMICALS

Presentada por Juan Ignacio del Río Blandón para optar al grado de doctor con mención internacional por la Universidad de Valladolid

Directores:

Profesora María Dolores Bermejo Roda

Profesor Ángel Martín Martínez

Supervisor Internacional:

Profesor Pavel Gurikov

DEDICATORIA

A mis padres y hermana, a todos aquellos familiares que han sido una inspiración, a aquellos que han cumplido su ciclo, y a todas aquellas personas que a lo largo de la vida han influenciado para bien este trasegar.

AGRADECIMIENTOS

A mis tutores Lola y Ángel, y a la profesora Maria José Cocero, por la confianza depositada y por posibilitar el cumplimiento de este sueño. Por enseñarme además lo que es ser buenas personas.

Al profesor Eduardo Perez, por su incondicional amistad y su valioso apoyo en las primeras etapas del proyecto.

A la Universidad de Valladolid, por el contrato predoctoral, por la financiación y tantas oportunidades brindadas.

To professors Irina Smirnova, Pavel Gurikov and Baldur Schroeter from Institute of Thermal Separation Processes at the Technische Universität. Hamburg (TUHH), for the dedication and interest during and after my doctoral stay.

A Nuria la secretaria del departamento, y los técnicos de laboratorio en Valladolid: Mónica, Enrique, Araceli y Beatriz, por acompañar y facilitar día a día nuestro trabajo.

A los compañeros y amigos de grupo de investigación, por las risas, cafés, tertulias, disgustos, consejos, ayudas y quedadas, terminan siendo como hermanos. A los estudiantes de grado David León y Miguel Almarza, por su dedicación y valiosas contribuciones al proyecto.

A Isa y Dani, porque, más que técnicos de laboratorio, son amigos incondicionales. Por los tantos momentos en que pudimos hacer lo que nos apasiona, ciencia y música. Y con ellos, a Leyre y Alberto, también compinches de banda.

A Jon y Omar, mis queridos amigos y camaradas de banda, cómplices también de ese otro sueño irrenunciable, la música.

A Jacobo, David, Carmen y Penélope, por su amistad inspiradora, por las tantas quedadas en Valladolid que por momentos olvidaba quién era.

A la compañía Befesa y a los proyectos:

i) optimización de la reducción hidrotermal de CO2 para desarrollar un proceso de captura y utilización de CO2 integrado (OPTICO2) RTI2018-097456-B-I00 Ministerio de Ciencia, Innovación y Universidades.
ii) Revalorización de CO2 mediante un proceso integrado de captura y conversión de CO2 con aminas (AMICO2) (VA248P18). Junta de Castilla y León.
iii) Reciclado químico de CO2 mediante conversión hidrotermal en un reactor en continuo (AQUACO2NV) ENE2014-53459-R. Ministerio de Economía Y Competitividad (MINECO).

TABLE OF CONTENTS

OBJECTIVES

The present PhD thesis focuses on utilizing captured CO_2 for the sustainable production of formic acid and green hydrogen. These value-added chemicals are of great interest today for reducing the reliance on fossil sources, facilitating the transition toward a circular economy. In this context, formic acid can play a dual role, as energy source (either through hydrogen storage or direct application in fuel cells) or as platform chemical. Likewise, green hydrogen is experiencing an increasing demand as its technologies of production and application are rapidly securing a commercial stage of development. Therefore, the main goal of the thesis was integrating the capture of CO_2 with hydrogen generation for producing **formic acid** and **green hydrogen**, under the lens of both CO_2 and hydrogen economies. To do it so, the following research objectives were stablished, divided in **Part 1, Part 2** and **Part 3** of the thesis.

Part 1: State of the art technologies - looking for CO_2 and H_2 economies consolidation

- Reviewing of the reports of the past decade, along with the most recent reports about the current global situation in terms of economic and environmental challenges, developing the motivation and background that gathers the milestones related to the carbon capture utilization and storage (CCU) to achieve the world-claimed CO_2-Goals for 2030-2050 (Chapter 1).

Part 2: On the catalytic study of the reduction of ammonia-CO_2 absorption derivatives as starting materials for production of value-added chemicals

- Evaluation of starting materials for the hydrothermal production of formic acid under mild reaction conditions (Chapter 2)
- Parametric study of effects of the main process variables on formic acid production. (Chapter 2)

- Screening and comparison of different supported metal catalysts and reducing metals in search for the most actives metal/catalyst system for CO_2 reduction and H_2 generation (Chapter 3).
- Use of CO2RS/CO2LS streams as reaction media on the hydrogen generation in a simultaneous process with reduction of capture CO_2. (Chapter 3)
- Development of alternative carbonaceous support from renewable sources with improved production costs, and carbon footprint through facile and ecofriendly production process (Chapter 4). (International collaboration with Technical University of Hamburg TUHH).
- Thorough characterization of commercial and synthesized catalysts and exhausted metals with state-of-the-art technologies (Chapters 2, 3 and 4)

Part 3: On the design and construction of a semicontinuous facility for integrating CO_2 and hydrogen economies and its concept proof by experimental study

- Design and construction of a novel semicontinuous facility for the green hydrogen generation using metals and industrial wastes under superheated water condition. (Chapter 5)
- Proof of concept evaluation of using CO2-Rich stream (CO2RS) and a CO2 Capture-Solvent Lean stream (CO2LS) as activators of the hydrogen generation from the metal water-splitting reaction in a semi-continuous fashion (Chapter 5)

ABSTRACT

In chapter 1 the analysis of indicators of the state of progress and relevance of CO_2 utilization technologies revealed that the sector of fuels and chemical products (formic acid and hydrogen among them), has the greatest relevance compared to other non-traditional emerging technologies (mineral carbonation, chemical and material processing, power sector and others). In chapter 2, the batch study of the catalytic reduction process of CO_2 in hydrothermal media showed that, as starting material, ammonium carbamate had the best yield towards formic acid at a mild reaction temperature of 120 ºC, while sodium bicarbonate presented the highest yield, but at a higher temperature of 250 ºC. The formic acid yield, from ammonium carbamate, is limited by the thermal decomposition of the reducible species HCO_3^- and of the formate ion, for which the yield started to decrease at temperatures higher than 120 ºC. The formic acid yield was directly proportional to the catalyst (palladium over activated carbon) concentration in the reaction solution, obtaining a yield of almost 40% for the highest concentration of 60%, suggesting that the process is highly sensitive to the nature and quantity of the catalyst. Through the characterization of the spent solid after successive reuse reactions, it was identified that the aluminum is not completely consumed, even up to the fifth reuse. In addition, it was possible to elucidate the evolution of the catalyst in the different reuse cycles, with the H_2-TPR analysis. This allowed to identify the formation of palladium hydride species, which can play a reductive role of the captured CO_2 into formic acid. In chapter 3, the batch study of the hydrothermal reduction of captured CO_2 in ammonia was extended to the evaluation of different reducing metals and catalysts, as well as their incidence in the simultaneous production of green hydrogen. Among a pool of selected catalysts, differentiated by the type of support and active metal, palladium 5% wt over activated carbon was the only one that showed activity towards the production of formic acid, for all the reducing metals used. Among these metals, zinc showed the highest autogenous pressure, corresponding to a higher yield of green hydrogen up to 26%. This chapter also analyzed the effect of the particle size of the reducing metal and its purity, using 500 µm aluminum and aluminum residue from the company BEFESA, in the form of spall (or chips). Compared to the powder size (<5 µm), the 500 µm size, both for pure aluminum and for the residue,

decreased the formic yield, but this allowed demonstrating that the residue shows activity towards the *in situ* generation of green hydrogen. In this chapter, for the study of green hydrogen generation, two media/streams were considered, one rich in captured CO_2 (CO2RS), and another free of CO_2 or fresh solvent (CO2LS), in experiments with no catalyst and for 10 hours. In general, zinc presented faster H_2 generation rates under both types of streams at all times, with a yield of up to 63.7% with aqueous carbamate. Aluminum activation was generally slower, it only started to be significant at 6 h with SB, for an H_2 yield of 11%. The XRD analysis of the solids showed, in addition to the expected oxides of the metals used, the appearance of metal carbonates, suggesting that part of the carbamate conversion is due to this product. In chapter 4, the synthesis of metal-crosslinked aerogels (MCAs) and metal-decorated carbogels (MDCs) was performed within the framework of the doctoral stay. In the first synthesis step, hydrogel preparation, the concentration of the metal precursor solution in the gelation bath was varied, but the final metal content stabilized at a concentration of 170 mmol/L. Pd^{+2} showed the highest incorporation in aerogel, with a final metal content of up to 13%, which is higher than those found in the reviewed literature, and after pyrolysis the Pd-carbogel was notably the one that lost less mass, with only 58%, up to 600 ºC. At different pyrolysis temperatures (150 – 600 ºC) there was a decreasing trend in textural features, with a large change after approximately 285ºC, associated with an expected shrinkage. SEM-BSE of carbogels showed an evolution of nanoparticle clusters through the different pyrolysis temperatures, developing well-defined forms for Ni- and Cu-carbogels at 600 ºC, with average size of 14 nm +/- 7 nm and 85 nm +/- 29nm, respectively. XRD and TPR results of Ni-, Cu-, Pt- and Pd-carbogels indicated that the particles are composed of elemental metals and metal oxides in varying proportions, while Pd-aerogel was the only aerogel to show the exclusive presence of the zero-valence state by XPS and TPO analyses. When Pd-aerogel was tested as a catalyst in the hydrothermal reduction reaction of captured CO_2, the yield of formic acid was 34.3%, in contrast to the blank reaction (without catalyst) that did not show H_2 consumption and/or formic acid signal in the HPLC chromatogram. On the other hand, the reaction with Pd powder as catalyst (control reaction) showed a negligible formic acid yield of 2.97%. For the first time, chapter 5 proposes a novel facility operated in semi-continuous, of self-construction, for the use of the basic solvent streams that mediate in typical CO_2 capture plants (CO2RS and CO2LS streams) for the

generation of green hydrogen, using metals. One of the novelties is that the process is conducted with superheated water (also called subcritical water), which is defined as liquid water pressurized at temperatures ranging from the boiling point (100 ºC) and the supercritical temperature (374 ºC). The experimental study showed that the H_2 production increased in the order Mn<Al<Fe<Zn, using aqueous ammonium carbamate as CO2RS stream. The yield was proportional to temperature and concentration, and indirectly to particle size. Once again, the aluminum residue in the form of spall (or chips) from the company BEFESA showed a high performance, reaching a yield of 12% for the size of 250 µm, using aqueous ammonium carbamate as CO2RS. The yield of H_2 was proportional to the variables temperature and carbamate concentration, while the variable stream flow did not show a significant effect. It is noteworthy that aqueous sodium bicarbonate (a CO2RS stream) showed a higher yield compared to carbamate, reaching a relative yield of 71% of H_2, using Al, in only 0.5 h of steady state operation time, at 200 ºC and a concentration of 1.0 mol/L. Likewise, 0.5 mol/L aqueous NaOH (CO2LS) showed the highest relative yield of H_2 (up to 85.5%), using Al, in only 50 min. Likewise, as in chapter 3, the interaction of CO2RS with metals was detected by the formation of metal carbonates, and by ATR-FTIR the formation of aluminum hydrides was detected. The results of this chapter allowed concluding that aqueous sodium bicarbonate and sodium are strong bases that should be better used in activating less active metals like Al and Mn. For its part, highly active metals like Zn and Fe should be better used with less basic aqueous streams like ammonium carbamate, ammonia and MEA.

Part 1. State of the art technologies - looking for CO_2 and H_2 economies consolidation

CHAPTER 1

BACKGROUND

The global CO_2-Goals for 2030-2050

Actions towards ambitious 2030 climate targets are being accelerated by the opportunity that supposes economic response to COVID-19 recovery scenario through stimulus packages [1][2]. Oil and gas companies are experiencing market values instability, while valuation of battery electric vehicle (EV) companies is exponentially raising [3][4]. About 50% of the energy production by 2050 will come from fossil fuels [5], so the transition to net zero greenhouse gas emissions by this era demands progress in the development of new and improved clean energy technologies, where carbon capture utilization and storage (CCUS) has an important role, although still requiring the integration of its technical advances with economic and regulatory frameworks in order to deploy as practical and feasible options [6][7]. For its part, hydrogen economy is rapidly growing as a pathway for decarbonizing the energy used worldwide [3], but its acceptance and fitting in a net-zero economy is conditioned to the overcoming of its numerous hazards [8], and to the announcement of COP 26 about cutting in 30% the methane leakage associated to the production and supply chains of natural gas-based hydrogen [3]. However, to the date, COVID-19 and Ukraine-Russian crises are bringing about the reorientation of policies that are favoring the speeding up of renewables deployment for mitigating the reliance on fossil fuels from vulnerable importers [9][10]. As an example, the European commission has recently launched the “Hydrogen Accelerator” program to encourage the development of infrastructure of different sources, storage facilities and ports for hydrogen [11].

Carbon capture and storage (CCS): the solvents-based CO_2 capture perspective

To meet the global targets, the IEA emphasizes the importance of CCUS technologies, capable of providing up to 20% of the emissions cuts needed by 2050 [12], calling for immediate and large-scale deployment of clean and efficient energy technologies [2]. Today, Carbon capture is sought to be more efficient by its implementation in streams with high content of CO_2, for example 10-15% for fossil

power plants, and up to 23 % from ironmaking industry [13], compared to the direct air capture (DAC) with only 0.04% CO_2 content of the atmosphere [14]. This technology permits concentrating the capture CO_2 for further storage at geological storage, considered a competent method for long-term storage because of its accessibility and economics [15]. In this sense, the solvent based post-combustion CO_2 capture processes, with subsequent geo-sequestration, occupy an important share in the efforts for CO_2 emissions abatement need for the future, but its implementation has been delayed today mainly by the preferred use of CO_2 for enhanced oil recovery (CO2-EOR) process [16], given its higher profitability. The carbon capture and storage (CCS) technologies based on the absorption of CO_2 use aqueous solutions of basic solvents known as CO_2 Capture-Solvent Lean stream (CO2LS) in absorber/stripper columns, yielding a CO_2-Rich stream (CO2RS). The main solvents used, aqueous MEA (monoethanolamine), NaOH (sodium hydroxide) and ammonia (NH_3), are reviewed and compared in Table 1, based on references [17-26].

Table 1. Comparison of main solvent-based CO_2 capture technologies

Solvent	**Maximum capture Capacity g CO_2/g solvent)**	**Advantages**	**Disadvantages**
Aqueous MEA (7 wt%)	0.4	Less volatile, good stability of absorbent, has less corrosion and degradation issues, also capture NO_x, SO_2	Poorer absorption efficiency, high regeneration energy, facile degradation
Aqueous Ammonia (7 wt%)	1.2	heat of absorption is much lower than in the case of amines, regeneration is cheaper economically and energetically	Easy to volatilize and leak, high vapor pressure and low molecular weight, thermal instability of products, corrosion to equipment, not suitable at high temperature. larger absorber column than traditional MEA based process

Aqueous NaOH (5 wt%)	2.1*	Low solvent cost, High accessibility, Low toxicity and non-volatility	Precipitation in reboiler and pipeline of the process, strong corrosion, resulting in higher operating costs, absorbent is non-renewable, not readily generable with a mild thermal or pressure swing

* Units in mg of total CO_2 absorbed/g of NaOH solution

In general, ammonia-based capture process is more efficient than amines because of its higher capture capabilities, lower heat requirement and costs, and higher regeneration. At commercial scale there are several R&D and pilot plants (ALSTOM, Powerspan, CSIRO, KIER and RIST) [13]. Although the technology of CO_2 absorption by amines (e.g., aqueous MEA) is a well-known technology, its application in thermal power plants and other CO_2 emission points has prohibitive costs, which limit its widespread implementation in the industry. Reducing the economic penalty associated with CO_2 capture would allow its application to be extended. Hydroxides-based capture technologies (e.g., aqueous NaOH) use more familiar solvents, with high availability in the market, but presents strong corrosion problems, and for higher capture capacities must operate at high concentrations. However, the selection of the method to be implemented will depend on inlet CO_2 concentration, operative conditions and total gas flow rate, among other parameters.

Carbon capture utilization and storage (CCUS): Toward a CO_2-Economy consolidation

Pushing the CO_2 “under the carpet” seems to be not sufficient in the growing demand for products and services nowadays, thus giving birth to new techniques of CCUS that incorporates transformation processes to the value chain into useful products, such as polymers, fuels or chemicals [27]. CO_2-derived polymers, CO_2 carbonation and methanol production constitute the most technologically advanced methods of utilization [28]. Polyols production with 20 wt% of capture CO_2 allows a greenhouse gases (GHG) reductions of 11–19% [29], and the mixes of concrete/CO_2 can produce a net CO_2 reduction of 18 kg/m^3 concrete [30]. Some of the current leading economies are not only investing in CCS technologies, but treating CO_2 as a resource that can be utilized as C1 building block in organic synthesis because of its abundance and low cost [31][32]. For instance, the

comparative techno-economic analysis of Mikhelkis *et al*. [33], for a case of study of a Stockholm's district bio-and waste-based incineration plant, allowed concluding that a hybridized approach that combines CCS and CCUS (in suitable proportions) is the most worth investing option in the future. In this approach, CO_2 is reacted with slag from the stainless-steel industry to produce building blocks, a commercially value product in construction sector. This makes the sequestration of larger quantities of CO_2 a more economical way than only CCS by showing a saving of 17% over the total costs per year.

Table 2. State of progress and relevance indicators of CO_2 utilization technologies (adapted and modified from Valluri *et al.* [34]).

Sector	Usage	Qualitative Impact	Impact value assigned	Average TRL	Score
Fuels and chemicals	Fuels (methanol, ethanol, syngas, methane); Chemicals (formic acid, oxalic acid); Urea production	High	7.5	5.5	41.25
Food	Dry ice; Drinks carbonation; Baking soda (bicarbonate); Food preservative	Medium	5	10	50
Chemical and materials processing industry	Iron and steel making; Acid mine drainage rare earth extraction; Steel slag carbonation	Medium	5	7	35
Oil and gas	Enhanced oil recovery	Very high	10	10	100
Mineral carbonation	Concrete building materials;	Medium	5	7.5	37.5

	Red-mud (Bauxite residue) neutralization.				
Power sector	Working fluid in power cycle	Medium	5	3.5	17.5
Other	Solvent (Supercritical CO_2); Refrigerant; Dry cleaning	Low	2.5	6	15

Based on the recent estimations of Valluri *et al.* on the opportunities and challenges in CO_2 utilization, one can score-up the different technologies of CO_2 utilization (see Table 2), by assigning an equivalent numerical value to the qualitative impact estimated by the author, where “low” accounts for 2.5, and high for 10, thus generating a new variable called **Impact value assigned**. Then, one can multiply it by its average TRL (Technology readiness level), thus generating the variable “**Score”**. The results can be observed plotted in Fig. 1 by the present work, reflecting, in the first place the current status concerning the already CO_2 utilization in oil and gas sector (score 100), largely implemented since 70’s decade [35], along with food sector (score 50), having the oldest direct utilizations of CO_2 in carbonating beverages and preserving foods, since the beginning of 20th century [36]. Interestingly, this sector is closely followed by fuels and chemicals (score 41.25) (the focus of the present thesis), and mineral carbonation (score 37.5) sectors. When computing a percentage share per sector from the assigned scores, is observed that the production of fuels and chemicals (like methanol and formic acid (FA)), have the highest relevancy within the other emerging technologies.

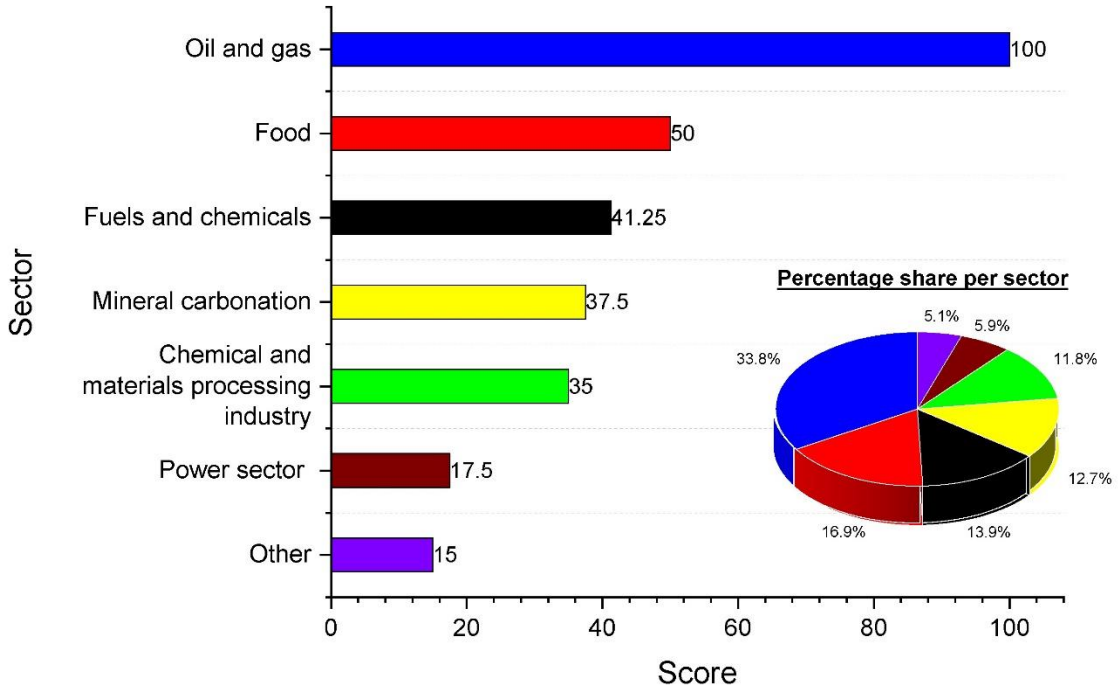

Fig. 1. Relevancy indicators of CO_2 utilization technologies

The catalytic hydrothermal process: a strategic way for integrating CO_2 capturing with production of value-added fuels and chemicals

Like H_2O, a covalently bonded compound, gaseous CO_2 is one of the most stable molecules owing to the linear doble covalent bonds that carbon atom forms with two oxygen atoms [37]. The two C=O double bonds have a high dissociation energy of c.a. 750 kJ/mol [38], therefore its conversion into value added chemicals and fuels without any catalyst or sufficient energy input to overcome its thermodynamical stability is almost impossible [39]. Hydrothermal media of reaction becomes a novel and promising strategy for reducing capture CO_2 because permits, i) overcoming the high energy requirements of reducing gaseous CO_2, by its capture in water as an easier HCO_3^- reducible species, ii) the usage of heterogeneous catalysts with high activity and easy separation and reutilization, iii) the usage of biomass-derived and metal reductants from wastes, iv) the usage of traditional equipment and materials with techno-economical potential.

CHAPTER 1

The field of heterogeneous catalyst for CO_2 reduction is continuously exploring new and more efficient, cheaper and sustainable ways of supporting metals like Ni, Cu, Pd, Pt, Co, as the most active transition metals for hydrogenation of carbon-carbon double bonds under moderate conditions [40]. In this sense, carbon aerogels (carbogels) appeared in 1980s [41], as a promising alternative for natural carbonaceous materials, owing to the possibility of controlling its purity, mechanical strength and porosity from the synthesis steps. Other features like the large specific area, low density, low thermal and high electrical conductivity and hydrophobicity makes them ideal as supports for catalysts [42]. The tailorable textural and structural features of carbogels make possible to overcome some of the constraints encountered in heterogeneous catalysts, like metal-species aggregates formation, pore blocking and leaching of active sites. For this, polysaccharides have gained much interest as an inexpensive and abundant carbon source, especially those derived from species with large capability of fixing carbon dioxide, such as the brown algae [43]. This represents an opportunity in the context of sustainable development, by encouraging the algae CO_2 capture with added value. Up to 60% of the total sugars in brown algae are alginate, an anionic biopolymer that can be easily crosslinked with cations for the preparation of hydrogels [44], and also for capturing pollutant cations as a bioremediation of environments contaminated with toxic heavy metals [45][46].

On the other hand, water is a green solvent that rapidly changes its physicochemical properties when heated, conferring improved solvation features of gaseous and organic compounds [47]. The in-situ generation of hydrogen in the hydrothermal media occurs when put water in contact with zero valent metals, such as Al, Zn, Mn, Fe, (among others) through the metal-water splitting mechanism ($M^0+H_2O \rightarrow MO_x + H_2$) [48-51]. This hydrogen avoids the hazard issues of storage and transportation. In hydrothermal media, the generated hydrogen can easily reduce CO_2 by donation and/or hydrogenation mechanism in presence of catalysts, following the overall reaction pathway: $M^0+H_2O \rightarrow M_xO_y+H_2+CO_2 \rightarrow HCOOH$ [52]. However, the main drawback of using metals as raw material is that they should be reduced again for a new cycle of hydrogen generation, but is a feasible redox process through solar energy input [53]. Efforts have also been focused on utilizing other inexpensive feedstocks, like alcohols, ketones, saccharides and phenols which are biomass-derived

reductants that have shown potential for integrating both CO_2 reduction and biomass conversion by hydrothermal processes [54][55]. In this direction, other possible CO_2 reductions processes have been intensively investigated, such as photocatalysis and electrocatalysis [56].

Formic acid, as the main product of CO_2 reduction, has been traditionally used in many industrial applications [57][58]:

- as reducing and decalcifying agent in dyeing and finishing of textiles
- as an agent for plumping and dehairing hides in leather tanning
- as a solution for electroplating
- as a rubber coagulating agent in the creation of latex rubber and in regenerating old rubber
- as a component in the manufacture of commercial paint strippers and metal salts, including nickel, cadmium, and potassium
- and other uses in medicine, pesticides, dyes, agriculture and environmental protection are recognized [52]

Even so, there is an increasing interest today in pointing formic acid to the fuels market, specifically as a promising hydrogen energy carrier with potential in transportation sector, thanks to its non-toxic and environmentally benign feature, with low flammability under ambient conditions, making possible to easily adapt the existing gasoline infrastructure FA distribution [59]. The selectively release of hydrogen electricity generation by feeding FA directly into a fuel cell looks promising as well, under penalty of his still immature technological stage [60]. If more endeavors join the worldwide research on hydrogen production from renewables (solar and wind), this hydrogen storage and distribution concept based on FA will find its way within the future hydrogen economy.

CHAPTER 1

Green and blue hydrogen: top chemicals toward sustainability

Today, the industry is preparing itself to make step forward in the transition of grey hydrogen, from fossil methane reformation, to more sustainable presentations of hydrogen, mainly blue and green. Blue hydrogen has been defined as the one obtained by methane steam reforming with CO_2 capturing, so no emissions are involved, at least theoretically. Green hydrogen is the most ambitious, since no emissions are involved at all, and it comes basically from the electrolysis of water, powered by renewable sources of energy like solar and wind [61][62]. They constitute the future of hydrogen economy, based on a cleaner fuel with high energy yield (122 kJ/g), 2.75 times bigger than hydrocarbons [63][10], that could substitute in the future the natural gas (NG) used to cover the energy demand, by converting existing NG pipelines into a dedicated hydrogen infrastructure [64]. While green hydrogen is a key-goal for EU, based on its IPCEI rules (important projects of common European interests) [65], blue hydrogen may have an important place as an intermediate solution in the coming decades, especially if the CO_2 capture rate can be kept to 99% [66], but its reduced impact on the greenhouse effect has not been fully proven [67]. Despite this, blue hydrogen has the potential in the middle term as a cheaper option (especially by 2030 [68]), with greater potential for industrial scaling [69][70].

The literature review of Acar *et al*. [71] is illustrative and conclusive in comparing the performance of hydrogen production sources and systems, storage and end-use technologies, based on the 3S approach (route to sustainability) previously introduced by Dincer [72]:

- Sources of hydrogen: biomass, geothermal, hydro, nuclear, solar and wind
- Systems of a) production: biological, electrical, photonic and thermal, and b) storage: chemical hydrides, compressed gas, cryogenic liquid, metal hydrides and nanomaterials.
- Services: power, heating, cooling, fresh water and fuels.

In this work, the rank (0-10 range) of each system was calculated based on environmental, economic, social, technical and reliability criteria. From its assessment, upon considering all performances criteria, it is interesting noting that solar had the highest average ranking (7.4/10) as the source of hydrogen; electrical is the most advantageous production system (7.6/10), followed closely by thermal (6.6/10), which is the focus of the present thesis; and nanomaterials are the most advantageous storage option (8.4/10). In the future, it is expected that aluminum will gain an important place in the value chain of hydrogen generation ($Al+3H_2O \rightarrow Al(OH)_3+1.5H_2+426.5kJ$) because is one of the most affordable methods of generation using cheap and abundant material, with the possibility of recovery of heat, from the exothermal reaction, and yields environmentally benign by-products of commercial value [73].

Research opportunities

To the date, much literature has emphasized in chemistry and thermodynamics aspects of the reduction of CO_2 into value added chemicals using thermochemical and electrochemical methods. However, the intensification of the process remains as an opportunity for economizing the unit operations between the CO_2 captured and its conversion into value added chemicals. Safer and more efficient way of hydrothermally reducing captured CO_2 is required in ongoing studies for improving its techno-economic competitiveness versus other traditional methods based on electrical and photonics. To achieve it, alternatives to the traditional materials used as catalysts must be explored, in order to improve the production costs and carbon footprint from the elaboration process. While CO_2 economy and Hydrogen economy are treated separately in most cases, the opportunity lies as well in identifying its integration, for as they can perfectly match from an engineering point of view, becoming strategic in achieving sustainability goals, once found solutions to its major technical challenges. To achieve it, we propose for the first time the use of CO2RS/CO2LS streams as activators of the green hydrogen generation. This is a novel concept that will potentially integrate two of the current strategic goals for the sustainable development.

REFERENCES

[1] E. Commission, “Stepping up Europe’s 2030 climate ambition Investing in a climate-neutral future for the benefit of our people,” *J. Chem. Inf. Model.*, vol. 53, pp. 1689–1699, 2020.

[2] A. Pham, B. C. Emard, and J. Hausen, “COVID-19 Economic Impacts and GAC’s Role in the Green Recovery,” *Aftershocks*.

[3] M. van der Spek *et al.*, “Perspective on the hydrogen economy as a pathway to reach net-zero CO 2 emissions in Europe,” *Energy Environ. Sci.*, vol. 15, no. 3, pp. 1034–1077, 2022.

[4] J. D. Hunt, A. Nascimento, N. Nascimento, L. W. Vieira, and O. J. Romero, “Possible pathways for oil and gas companies in a sustainable future: From the perspective of a hydrogen economy,” *Renew. Sustain. Energy Rev.*, vol. 160, p. 112291, 2022.

[5] B. P. Center, “Annual energy outlook 2020,” *Energy Inf. Adm. Washington, DC*, vol. 12, pp. 1672–1679, 2020.

[6] J. Deutch, “Is net zero carbon 2050 possible?,” *Joule*, vol. 4, no. 11, pp. 2237–2240, 2020.

[7] E. Martin-Roberts, V. Scott, S. Flude, G. Johnson, R. S. Haszeldine, and S. Gilfillan, “Carbon capture and storage at the end of a lost decade,” *One Earth*, vol. 4, no. 11, pp. 1569–1584, 2021, doi: https://doi.org/10.1016/j.oneear.2021.10.002.

[8] M. C. Clarke, “Can the hydrogen economy concept be the solution to the future energy crisis?,” *Aust. J. Multi-Disciplinary Eng.*, pp. 1–15, 2022.

[9] L. Rodríguez-Fernández, A. B. F. Carvajal, and V. F. de Tejada, “Improving the concept of energy security in an energy transition environment: Application to the gas sector in the European Union,” *Extr. Ind. Soc.*, p. 101045, 2022.

[10] S. E. Hosseini, “Transition away from fossil fuels toward renewables: lessons from Russia-Ukraine crisis,” *Futur. Energy*, vol. 1, no. 1, 2022.

[11] European Commission, “REPowerEU: Joint European action for more affordable, secure and sustainable energy,” 2022. https://ec.europa.eu/commission/presscorner/detail/en/ip_22_1511 (accessed Apr. 19, 2022).

[12] R. IEA, “Energy technology perspectives 2020,” *Spec. Rep. Carbon Capture, Util. Storage.*,

2020.

[13] C. H. Rhee, J. Y. Kim, K. Han, C. K. Ahn, and H. D. Chun, “Process analysis for ammonia-based CO2 capture in ironmaking industry,” *Energy Procedia*, vol. 4, pp. 1486–1493, 2011.

[14] L. Schernikau and W. H. Smith, “Climate impacts of fossil fuels in todays electricity systems,” *J. South. African Inst. Min. Metall.*, vol. 122, no. 3, pp. 133–145, 2022.

[15] M. N. Anwar *et al.*, “CO2 capture and storage: a way forward for sustainable environment,” *J. Environ. Manage.*, vol. 226, pp. 131–144, 2018.

[16] K. A. Mumford, Y. Wu, K. H. Smith, and G. W. Stevens, “Review of solvent based carbon-dioxide capture technologies,” *Front. Chem. Sci. Eng.*, vol. 9, no. 2, pp. 125–141, 2015.

[17] F. Shakerian, K.-H. Kim, J. E. Szulejko, and J.-W. Park, “A comparative review between amines and ammonia as sorptive media for post-combustion CO2 capture,” *Appl. Energy*, vol. 148, pp. 10–22, 2015.

[18] G. Puxty, R. Rowland, and M. Attalla, “Comparison of the rate of CO2 absorption into aqueous ammonia and monoethanolamine,” *Chem. Eng. Sci.*, vol. 65, no. 2, pp. 915–922, 2010.

[19] T. N. Borhani and M. Wang, “Role of solvents in CO2 capture processes: The review of selection and design methods,” *Renew. Sustain. Energy Rev.*, vol. 114, p. 109299, 2019.

[20] S.-J. Han, M. Yoo, D.-W. Kim, and J.-H. Wee, “Carbon dioxide capture using calcium hydroxide aqueous solution as the absorbent,” *Energy & Fuels*, vol. 25, no. 8, pp. 3825–3834, 2011.

[21] Y. Peng, B. Zhao, and L. Li, “Advance in post-combustion CO2 capture with alkaline solution: a brief review,” *Energy Procedia*, vol. 14, pp. 1515–1522, 2012.

[22] M. Yoo, S.-J. Han, and J.-H. Wee, “Carbon dioxide capture capacity of sodium hydroxide aqueous solution,” *J. Environ. Manage.*, vol. 114, pp. 512–519, 2013.

[23] A. Jongpitisub, K. Siemanond, and A. Henni, “Simulation of carbon-dioxide-capture process using aqueous ammonia,” in *Computer Aided Chemical Engineering*, vol. 37, Elsevier, 2015, pp. 1301–1306.

[24] N. Dave, T. Do, G. Puxty, R. Rowland, P. H. M. Feron, and M. I. Attalla, “CO2 capture by aqueous amines and aqueous ammonia–a comparison,” *Energy Procedia*, vol. 1, no. 1, pp.

949–954, 2009.

[25] V. Darde, W. J. M. van Well, E. H. Stenby, and K. Thomsen, “CO2 capture using aqueous ammonia: kinetic study and process simulation,” *Energy Procedia*, vol. 4, pp. 1443–1450, 2011.

[26] H. Jilvero, F. Normann, K. Andersson, and F. Johnsson, “Thermal integration and modelling of the chilled ammonia process,” *Energy Procedia*, vol. 4, pp. 1713–1720, 2011.

[27] A. Saravanan *et al.*, “A comprehensive review on different approaches for CO2 utilization and conversion pathways,” *Chem. Eng. Sci.*, vol. 236, p. 116515, 2021.

[28] Q. Zhu, “Developments on CO2-utilization technologies,” *Clean Energy*, vol. 3, no. 2, pp. 85–100, 2019.

[29] N. von der Assen and A. Bardow, “Life cycle assessment of polyols for polyurethane production using CO 2 as feedstock: insights from an industrial case study,” *Green Chem.*, vol. 16, no. 6, pp. 3272–3280, 2014.

[30] S. Monkman and M. MacDonald, “On carbon dioxide utilization as a means to improve the sustainability of ready-mixed concrete,” *J. Clean. Prod.*, vol. 167, pp. 365–375, 2017.

[31] Q. Liu, L. Wu, R. Jackstell, and M. Beller, “Using carbon dioxide as a building block in organic synthesis,” *Nat. Commun.*, vol. 6, no. 1, pp. 1–15, 2015.

[32] T. Sakakura, J.-C. Choi, and H. Yasuda, “Transformation of carbon dioxide,” *Chem. Rev.*, vol. 107, no. 6, pp. 2365–2387, 2007.

[33] L. Mikhelkis and V. Govindarajan, “Techno-economic and partial environmental analysis of carbon capture and storage (CCS) and carbon capture, utilization, and storage (CCU/S): case study from proposed waste-fed district-heating incinerator in Sweden,” *Sustainability*, vol. 12, no. 15, p. 5922, 2020.

[34] S. Valluri, V. Claremboux, and S. Kawatra, “Opportunities and challenges in CO2 utilization,” *J. Environ. Sci.*, vol. 113, pp. 322–344, 2022.

[35] D. Merchant, “Enhanced oil recovery–the history of CO2 conventional wag injection techniques developed from lab in the 1950’s to 2017,” 2017.

[36] N. Kaliyan, R. V Morey, W. F. Wilcke, K. Alagusundaram, and P. Gayathri, “Applications of

carbon dioxide in food and processing industries: current status and future thrusts," in *2007 ASAE Annual Meeting*, 2007, p. 1.

[37] F. Winter, R. A. Agarwal, J. Hrdlicka, and S. Varjani, *CO2 Separation, purification and Conversion to Chemicals and Fuels*. Springer, 2019.

[38] D. Jiang, Q. Song, Y. Xu, and D. Li, "Photocatalytic CO 2 Reduction," *Photo-and Electro-Catalytic Process. Water Split. N2 Fixing, CO2 Reduct.*, pp. 541–567, 2022.

[39] G. Zhao, X. Huang, X. Wang, and X. Wang, "Progress in catalyst exploration for heterogeneous CO 2 reduction and utilization: a critical review," *J. Mater. Chem. A*, vol. 5, no. 41, pp. 21625–21649, 2017.

[40] G. Agrimi *et al.*, *Biorefineries: an introduction*. Walter de Gruyter GmbH & Co KG, 2015.

[41] R. W. Pekala, "Organic aerogels from the polycondensation of resorcinol with formaldehyde," *J. Mater. Sci.*, vol. 24, no. 9, pp. 3221–3227, 1989.

[42] J.-H. Lee and S.-J. Park, "Recent advances in preparations and applications of carbon aerogels: A review," *Carbon N. Y.*, vol. 163, pp. 1–18, 2020.

[43] O. K. Lee and E. Y. Lee, "Sustainable production of bioethanol from renewable brown algae biomass," *Biomass and Bioenergy*, vol. 92, pp. 70–75, 2016.

[44] E. M. Ahmed, "Hydrogel: Preparation, characterization, and applications: A review," *J. Adv. Res.*, vol. 6, no. 2, pp. 105–121, 2015.

[45] S. A. Qamar, M. Qamar, A. Basharat, M. Bilal, H. Cheng, and H. M. N. Iqbal, "Alginate-based nano-adsorbent materials–Bioinspired solution to mitigate hazardous environmental pollutants," *Chemosphere*, p. 132618, 2021.

[46] H. Maleki, "Recent advances in aerogels for environmental remediation applications: A review," *Chem. Eng. J.*, vol. 300, pp. 98–118, 2016.

[47] M. Castro-Puyana, M. L. Marina, and M. Plaza, "Water as green extraction solvent: Principles and reasons for its use," *Curr. Opin. Green Sustain. Chem.*, vol. 5, pp. 31–36, 2017.

[48] X. Zeng, H. Zhong, G. Yao, and F. Jin, "Hydrothermal Water Splitting for Hydrogen Production with Iron," in *Hydrothermal Reduction of Carbon Dioxide to Low-Carbon Fuels*, CRC Press, 2017, pp. 47–60.

[49] H. Zhong, L. Wang, Y. Yang, R. He, Z. Jing, and F. Jin, “Ni and Zn/ZnO Synergistically Catalyzed Reduction of Bicarbonate into Formate with Water Splitting,” *ACS Appl. Mater. Interfaces*, vol. 11, no. 45, pp. 42149–42155, 2019.

[50] C. He, G. Tian, Z. Liu, and S. Feng, “A Mild Hydrothermal Route to Fix Carbon Dioxide to Simple Carboxylic Acids,” *Org. Lett.*, vol. 12, no. 4, pp. 649–651, 2010, doi: 10.1021/ol9025414.

[51] F. Jin *et al.*, “High-yield reduction of carbon dioxide into formic acid by zero-valent metal/metal oxide redox cycles,” *Energy Environ. Sci.*, vol. 4, no. 3, pp. 881–884, 2011, doi: 10.1039/C0EE00661K.

[52] X. Liu, H. Zhong, C. Wang, D. He, and F. Jin, “CO2 reduction into formic acid under hydrothermal conditions: A mini review,” *Energy Sci. Eng.*

[53] S. Abanades, “Metal oxides applied to thermochemical water-splitting for hydrogen production using concentrated solar energy,” *ChemEngineering*, vol. 3, no. 3, p. 63, 2019.

[54] M. I. Chinchilla, F. A. Mato, Á. Martín, and M. D. Bermejo, “Hydrothermal CO2 Reduction by Glucose as Reducing Agent and Metals and Metal Oxides as Catalysts,” *Molecules*, vol. 27, no. 5, p. 1652, 2022.

[55] M. Andérez-Fernández, E. Pérez, A. Martín, and M. D. Bermejo, “Hydrothermal CO2 reduction using biomass derivatives as reductants,” *J. Supercrit. Fluids*, 2017.

[56] J. Ma, *Photo-and Electro-Catalytic Processes: Water Splitting, N2 Fixing, CO2 Reduction*. John Wiley & Sons, 2022.

[57] S. Uhm, S. T. Chung, and J. Lee, “Characterization of direct formic acid fuel cells by Impedance Studies: In comparison of direct methanol fuel cells,” *J. Power Sources*, vol. 178, no. 1, pp. 34–43, 2008.

[58] C. A. S. Numbers, “Formic acid.”

[59] J. Eppinger and K.-W. Huang, “Formic acid as a hydrogen energy carrier,” *ACS Energy Lett.*, vol. 2, no. 1, pp. 188–195, 2017.

[60] K. Müller, K. Brooks, and T. Autrey, “Hydrogen storage in formic acid: a comparison of process options,” *Energy & Fuels*, vol. 31, no. 11, pp. 12603–12611, 2017.

[61] N. Van Hulst, “The clean hydrogen future has already begun,” *IEA Comment. Int. Energy Agency. https//www. iea. org/comme ntari es/the-clean-hydro gen-futur e-has-alrea dy-begun. Accessed April*, vol. 1, p. 2021, 2019.

[62] M. Yu, K. Wang, and H. Vredenburg, “Insights into low-carbon hydrogen production methods: Green, blue and aqua hydrogen,” *Int. J. Hydrogen Energy*, vol. 46, no. 41, pp. 21261–21273, 2021.

[63] S. Eker and F. Kargi, “Hydrogen gas production from electrohydrolysis of industrial wastewater organics by using photovoltaic cells (PVC),” *Int. J. Hydrogen Energy*, vol. 35, no. 23, pp. 12761–12766, 2010.

[64] A. Wang, K. van der Leun, D. Peters, and M. Buseman, “European hydrogen backbone: How a dedicated hydrogen infrastructure can be created,” 2020.

[65] L. L. Meldahl, “A clean hydrogen market in the making. Comparing Norway’s and the Netherland’s roles in the European hydrogen transition.” NTNU, 2021.

[66] C. Philibert, “Perspectives on a Hydrogen Strategy for the European Union,” *Etudes l’Ifri, Ifri*, 2020.

[67] R. W. Howarth and M. Z. Jacobson, “How green is blue hydrogen?,” *Energy Sci. Eng.*, vol. 9, no. 10, pp. 1676–1687, 2021.

[68] J. Neff, C. Bataille, and B. Shaffer, “The role of hydrogen in decarbonizing Alberta’s electricity system,” *Sch. Public Policy Publ.*, 2021.

[69] D. Hjeij, Y. Biçer, and M. Koç, “Hydrogen strategy as an energy transition and economic transformation avenue for natural gas exporting countries: Qatar as a case study,” *Int. J. Hydrogen Energy*, 2021.

[70] J. Lof, “SURVEY OF HEAVY-DUTY HYDROGEN FUEL CELL ELECTRIC VEHICLES.”

[71] C. Acar and I. Dincer, “Review and evaluation of hydrogen production options for better environment,” *J. Clean. Prod.*, vol. 218, pp. 835–849, 2019.

[72] I. Dincer and C. Acar, “A review on clean energy solutions for better sustainability,” *Int. J. Energy Res.*, vol. 39, no. 5, pp. 585–606, 2015.

[73] G.-L. Ma, H.-B. Dai, D.-W. Zhuang, H.-J. Xia, and P. Wang, “Controlled hydrogen generation

by reaction of aluminum/sodium hydroxide/sodium stannate solid mixture with water," *Int. J. Hydrogen Energy*, vol. 37, no. 7, pp. 5811–5816, 2012.

Part 2. On the catalytic study of the reduction of ammonia-CO_2 absorption derivatives as starting materials for production of value-added chemicals

CHAPTER 2

Catalytic hydrothermal conversion of CO_2 captured by ammonia into formate using aluminum-sourced hydrogen at mild reaction conditions*

Abstract

The catalytic conversion of CO_2 captured in aqueous media into formate was studied using aluminum-sourced hydrogen in a batch reaction system. To do so, the main ammonia-based CO_2 absorption derivatives: ammonium carbamate, carbonate and bicarbonate and sodium bicarbonate were selected as CO_2 source. The performance of the different species was determined under mild hydrothermal reaction conditions (120 °C), using Pd/C 5 wt% catalyst. In these conditions, the formate yield and selectivity increase in the order ammonium bicarbonate < sodium bicarbonate < ammonium carbonate < ammonium carbamate. Ammonium bicarbonate and sodium bicarbonate reagents needed higher temperature (250 °C) for an increased yield. Results with ammonium carbamate as starting material indicate a significant effect of time and catalyst content on formate yield, which ranged between 4 and 38%. Experiments with gaseous H_2 showed that a comparable yield with Al can be obtained at a similar level of pressure. The reutilization and characterization of the reaction solid, comprising exhausted aluminum and Pd/C catalyst, showed that the aluminum was not completely oxidized up to the 5th re-use, and Pd can play a reducing role through the formation of palladium hydride species. The process can be improved by operating at higher pressure and lower temperature, to avoid loss of yield by dehydration of formate.

Keywords: *CO_2 utilization, Hydrothermal reduction, Formic Acid, Ammonium carbamate, Aluminum-water splitting*

* *This chapter has been published as: del Río, J.I., Pérez, E., León, D., Martín, Á., Bermejo, M.D. Catalytic hydrothermal conversion of CO_2 captured by ammonia into formate using aluminum-sourced hydrogen at mild reaction conditions Journal of Industrial and Engineering Chemistry, Volume 97, 25 May 2021*

CHAPTER 2

Introduction

The concentration of greenhouse gases, mainly CO_2 from burning fossil fuels, has increased the global concern for climate change [1]. The Paris Agreement has the objective of limiting global warming to less than 2 °C above the temperature in pre-industrial times by reducing CO_2 emissions, and pursuing efforts to limit the temperature increase to 1.5 °C [2]. To achieve it, the European Union and the rest of the international community encourage the use of renewable energies, but it can be foreseen that for many years it will still be necessary to use fossil fuels for the production of electricity and as fuel in the automotive industry [3–5]. Therefore, other solutions are considered, such as CO_2 capture and storage technologies (CCS) [6], and the Carbon Capture Utilization (CCU), which would significantly reduce the CO_2 emissions of thermal power stations and chemical industries such as ammonia, hydrogen, steel and cement production [7]. The amine-based CCS technology is one of the most attractive solutions nowadays, but the high cost of the desorption step entails to consider further possibilities. Recently, the French company Alston developed a technology known as “Chilled Ammonia”, based on a similar principle [8]. Instead of using an amine aqueous solution, combustion gases are absorbed into an ammonia aqueous solution (28 wt%) at low temperature (2–10 °C). CO_2 is then immobilized by forming ammonium bicarbonate (1), carbonate (2), and carbamates (3) [9].

$$CO_2 + NH_3 + H_2O \rightarrow CO_3H^-NH_4^+ \quad (1)$$

$$CO_3H^-NH_4^+ + NH_3 \rightarrow CO_3^{2-}(NH_4^+)_2 \quad (2)$$

$$CO_2 + 2NH_3 \rightarrow NH_2COO^-NH_4^+ \quad (3)$$

Typically, 0.33–0.67 mol CO_2/mol NH_3 can be absorbed [10]. As in the case of amines, regeneration is produced by desorption at temperatures between 100–150 °C, and pressures between 0.3–13.6 MPa. This process has the advantage that the heat of absorption is much lower than in the case of amines, and therefore the regeneration is cheaper economically and energetically, but it presents the

disadvantage of using considerable cooling. The European Union has launched the SET Plan (Strategic Energy Technology Plan) to encourage the use of CO_2 as a source of carbon for the production of fuels, chemicals and energy storage, in search for a CO_2 zero emission cycle [11]. Considering this approach, the CO_2 should not be seen as a residue but as a renewable resource and a sustainable C1 building block in organic synthesis because of its abundance, low cost, non-toxicity, and non-flammability [12]. Nowadays, one the most developed processes of CO_2 conversion is the production of polycarbonates by copolymerization of CO_2 with epoxides [13]. Conversion of carbon dioxide, C (IV) into other chemical or fuels requires reduction of carbon in one or several steps. The reduction steps for C1 species are: CO_2 (IV) → Formic acid (II) → Formaldehyde (0) → Methanol (-II) → Methane (-IV) (Roman Numerals refer to oxidation states). Different methods of reduction have been investigated, including photochemical reduction, electrochemical reduction and hydrogenation of CO_2 [14]. The final reduced species produced depends on the reaction conditions and the catalyst used. The production of formic acid (FA) by catalytic CO_2 hydrogenation was first proposed nearly a century ago [15]. Since the 70's the reduction of CO_2 has been studied with homogeneous catalysts, due to their high performances [16]. It was only in the 80's that Pd/ C catalyst was introduced for synthesizing formate from H_2 and bicarbonate [17–19]. The uses of formic acid include food additive, preservative, insecticide, industrial material for synthetic processes and hydrogen storage. In the recent years, formic acid has been presented as a promising media for hydrogen storage, to be used in direct liquid fuel cells, owing to its relatively high hydrogen content (4.4 wt%) and higher energy density [20], where the fuel cell runs successfully over formic acid concentrations between 5 and 20 mol L-1 [21]. Other advantages are: (1) it is nontoxic and biodegradable, (2) it is liquid at ambient conditions, and (3) it is easy to store and transport [16].The hydrothermal reduction can be a feasible alternative to overcome the thermochemical stability of gaseous CO_2, as the reduction of HxCOy species derived from its capture in water requires less energy. The abiotic formation of organic compounds in Earth is taken as reference, where the CO_2 and/or CO is reduced by H_2 on a catalytic surface in hydrothermal media [22,23]. Although the use of gaseous hydrogen is currently based on a non-sustainable economy, it can be potentially obtained by environmentally friendly and economically hydrogen production technologies like the Aluminum-

water splitting, see reaction (4). In this reaction, hydrogen can be produced in situ in a safe way, getting advantage of the water present in the reaction media [24]. The hydrogen formed as free radicals in water at high temperature is more active than the so- called dry hydrogen (molecular H_2), which is much more chemically stable [25,26]. In spite of the need of further economic assessments to ensure feasibility of aluminum as feedstock, the process is promising in terms of sustainability, owing to the recyclability of aluminum from scrap using renewable energy [27], as aluminum can be regenerated through a solar thermochemical cycle [28–30]. Besides, the hydrogen mass yield of the Aluminum-water splitting of 11.1% is competitive with other renewable sources of hydrogen like steam gasification of biomass (hydrogen yield potential of 7.6–12.6%), and can be obtained under milder reaction temperature, where gasification requires above 700 °C [31].

$$2Al + 6H_2O \rightarrow 2Al(OH)_3 + 3H_2 \quad (4)$$

Table 1 summarizes the yields reported in the literature as function of reaction conditions for the hydrothermal conversion of CO_2 into formate. In most cases, sodium bicarbonate has been preferred as the starting material for the hydrothermal reduction of CO_2, using Ni [32,33], Fe [34] or Pd supported on carbon [35] as catalysts, and/or reductants like Al, Mg, Mn and Zn. Metals like Zn and Al produce the highest yields [33,35–37]. In our previous research, the use of zinc allowed to obtain a yield of 75% of formic acid from the reduction of sodium bicarbonate in batch system at 300 °C and 2 h [38]. Also, the use of biomass derivatives (glucose) allowed reducing sodium bicarbonate in hydrothermal media with efficiencies of up to 60%, in batch system at 300 °C and 3 h [39]. Na and K bicarbonates showed higher FA yield (86–92%) than its carbonates (71–76%) [40]. The ammonium bicarbonate had a negligible performance (6.5%) compared to the previous ones. Takahashi et al. [32] studied the effect of Fe-powder and Ni-powder as reducing agents of gaseous CO_2 in hydrothermal media. The main product obtained was methane, except when K_2CO_3 was used as a carbon source, which generates basic conditions and mainly produces formic acid, increasing its performance with high temperatures. The mild reaction conditions on the hydrothermal reduction of CO_2, catalyzed by Pd/C (5 wt%), were studied by Stalder et al. [18]. They used sodium bicarbonate

(concentration of 1.0 M) as carbon source, a pressure of 1.0–1.7 atm of hydrogen and room temperature, obtaining sodium formate with final concentration up to 0.5 M, but the reaction time was too long (24–46 h). He et al. [34] who reduced CO_2 in hydrothermal media in presence of iron nanoparticles at temperatures between 80 and 200 °C and times between 5 and 200 h concluded that by increasing time and temperature the yield of both formic acid and acetic acid was improved. Nevertheless, the final concentration of formic acid was low, of 8.5 mmol/L. Zhu et al. [41] reduced sodium bicarbonate with 2-pyrrolidone as a reducing agent to obtain formic acid using Pd/C (5 wt%) and other metals as catalyst, but only Pd/C and Cr showed good performance.

Many works attempted the reduction of CO_2 in the form of sodium or potassium bicarbonate, which corresponds to the product from capturing CO_2 into NaOH and KOH aqueous solutions, respectively. Not much research has been done in reducing CO_2 captured in ammonia and amines, even though these derivatives (carbamates and carbonates) can be more easily hydrogenated at mild temperatures than bicarbonates (in ethanol-rich solutions), and are more reactive than carbonates and bicarbonates of inorganic cations [42,43]. As example, Su et al. [42] reduced ammonium carbamate to formic acid in hydrothermal media, aided by ethanol co-solvent, using Pd/C catalyst at room temperature with gaseous hydrogen. They showed that the higher reactivity of bicarbonates is conditional andsolvent-dependent. Pulidindi etal. [44] hydrothermally reduced ammonium carbonate using $NaBH_4$ as reducing agent, in batch reaction using a domestic microwave oven as heating system (2.45 GHz, 1100 W at 100% power), under atmospheric pressure in the presence of air, obtaining a yield of 75 wt% of formate with an irradiation time of 5 min at 90 °C.

Table 1. Overview of the catalytic hydrothermal conversion of CO_2 into formate using different sources of hydrogen in batch reactors.

CO_2 source	Hydrogen source/reducing Agent	Temperature (ºC)	Time (h)	Catalyst	Formate Yield (%)	Ref.
Sodium bicarbonate	Zn/ZnO	225	0.5-4	Ni powder	81	[33]
Sodium bicarbonate	Al	250-325	2	-	64	[35]
Sodium bicarbonate	Al	260-320	0.5-3	Pd/C (5%wt)	70	[39]
Sodium bicarbonate	Zn	250-325	0-10	-	80	[36]
Sodium bicarbonate	Zn	250-400	0-3	-	75	[37]
Sodium bicarbonate	gaseous-H_2	Room	24-46	Pd/C (5 wt%)	54	[18]
Sodium bicarbonate	2-pyrrolidone	250-350	0.5-2.5	Pd/C (5 wt%)	30	[41]
Sodium bicarbonate	glucose	300	3	-	60*	[38]
Sodium bicarbonate	isopropanol	260–320	0.5-2.5	-	70	[48]
Carbonates and bicarbonates of Na, K, Ca and NH_4	gaseous-H_2	200	2	NiNPore	0-92	[40]
Carbonates and bicarbonates of Na, K, and NH_4	gaseous-H_2	20-80	1-15	Palladium Nanocatalysts	95.6	[47]
Potassium carbonate	Ni, Fe	200-350	1-6	Ni	25	[32]
Ammonium carbamate/carbonate	gaseous-H_2	20-60	1-8	Pd/C (5 wt%)	92	[42]
Ammonium carbonate	$NaBH_4$	90	0.1	-	75	[44]
CO_2 gas	Fe nanoparticles	80-200	5-200	Fe nanoparticles	8.5**	[34]

* With respect to the initial molar concentration of glucose

** Units are in mmol*L^{-1}

However, in none of these reports, the comparison of ammonia- based CO_2 absorption derivatives (ammonium carbamate, carbon- ate and bicarbonate) has been studied as starting materials for the hydrothermal production of formic acid under mild reaction conditions using aluminum water-splitting reaction as hydrogen source. Not much research has been done in reducing CO_2 captured in ammonia and amines, even though its derivatives can be more easily hydrogenated at mild temperatures. This route is important because it allows obtaining value-added chemicals like formic acid, without separation, purification or compression steps between the CO_2 capture and its conversion, thus involving a safer and efficient way of producing hydrogen from aluminum. In this work, the implementation of a commercial catalyst allowed lowering the temperature of the reduction process in search for mild reaction conditions. This approach allowed selecting the best starting material for a parametric study to determine the effect of the main process variables on the yield, selectivity and conversion in the formic acid production. The evaluation of the chemical-state evolution and reusability of the resulting reaction solid allowed determining the reducing species available in the synergy Al powder-Pd/C catalyst, based on thorough characterization.

CHAPTER 2

Materials and methods

Chemicals

Ammonium carbamate (AC) (99%), ammonium carbonate (ACA) (≥30.0% NH_3 basis), ammonium bicarbonate (AB) (≥99.0%) and sodium bicarbonate (SB) (100%) were used as carbon source, and diluted in deionized water. Fine powder of commercial Pd/C catalysts of 5 wt% of metal loading was used as received. Aluminum fine powder (Al) (<5μm, 99.5%) was employed for the *in situ* generation of hydrogen. All reagents, except aluminum and sodium hydroxide pellets (Panreac) and sodium bicarbonate (COFARCAS-Spain), were purchased from Sigma-Aldrich. Hydrogen (99.99%) was provided by Linde. All chemicals were used without further purification.

Catalytic experiments

Hydrothermal reactions for the reduction of the ammonia-based CO_2 captured species, using Al powder as hydrogen source and Pd/C as catalyst, were conducted in a stainless steel stirred reactor from Parr Instruments (Series 4791 Micro Stirred Reactors of 25 mL, maximum pressure of 200 bar, and maximum temperature of 350 °C), at 500 RPM, with autogenous pressure and heating at a ramp of 14 ºC/min using a band heater. The pressure meter device had an error of ±2 bar. Before each run, all the solids were weighed (Al, catalyst and the respective carbon source) and diluted/suspended in water. Once the reactor was sealed, a gentle flow of nitrogen was passed through the head-space to purge the remaining air out of the system. After the reaction, the vessel was rapidly immersed in a cold water bath. Then, the liquid sample was collected and filtered through a 0.22 mm filter, while the solid was stored under N_2 atmosphere for characterization.

It was established a reference central point of reaction conditions, comprising the values: 120 ˚C, 2 h (constant temperature), Al:Carbon Source molar ratio of 6:1, 15 wt% catalyst with respect to the initial weight of carbon source, and 70% of reactor filling in volume at room temperature. Then, the effect

of the process variables on the production of formic acid (FA) from ammonium carbamate was assayed by varying the reaction conditions as follows: temperature (80-300 ˚C), reaction time (0.5-5 h), Al:AC molar ratio (1.5:1 - 9:1), catalysts content (7.5-60 wt%), calculated as grams of catalyst/grams of carbamate), liquid filling (50-85% of the total volume of the vessel), using an initial concentration of carbamate of 0.5 M (initial pH=9.2, at room temperature).

All the carbon sources were evaluated in order to determine their reactivity as starting material for the production of formic acid at the central point of reaction conditions and at 250 ºC. Sodium bicarbonate was used as reference feedstock, given its wide use as carbon source.

The effect of alkalinity of the initial reaction solution of carbamate was evaluated at the central point conditions by adding NaOH before the reaction, until reaching, at room temperature, a pH of 10.1 and 12.5, separately. During reaction, a variation of the pH values is expected. Experiments with AC at the central point were also carried out with gaseous hydrogen as the reducing agent, for contrasting the performance of aluminum. To do it so, the reactor was charged with the corresponding amount of AC, water and catalyst, followed by a gentle flow of hydrogen passed through the head-space to purge the remaining air out of the system, and finally pressurized with hydrogen.

The evaluation of the reutilization of the resulting solid after reaction (a mixture of exhausted aluminum and Pd/C catalyst) was done through 5 reuses at the central point, using carbamate. Before every reuse, the solid was filtered and dried in-situ in the reactor, by attaching a vacuum pump to the reactor, while passing nitrogen at 50 °C for 30 min.

Product analyses

The liquid samples were analyzed by HPLC (Waters, Alliance separation module e2695) using an Aminex 87H (Bio-Rad) column with RI detector (Waters, 2414 module). The mobile phase was 5 mM H_2SO_4 with a flow rate of 0.6 mL/min. The temperatures of the column and the detector were 60 °C

and 30 °C, respectively. The yield and selectivity to formic acid, as well as conversion of the carbon source were calculated as shown in equations 5 to 7.

$$Y_{FA} = \frac{C_{FA,f}}{C_{cs,i}} x100 \quad (5)$$

$$X_{CS} = \frac{C_{cs,f} - C_{cs,i}}{Ccs,i} x100 \quad (6)$$

$$S_{FA} = \frac{Y_{FA}}{X_{CS}} x100 \quad (7)$$

Where $C_{FA,f}$ is the final molar concentration of formic acid, $C_{CS,i}$ is the initial molar concentration of carbon source and $C_{CS,f}$ is the final molar concentration of carbon source. S_{FA} is the selectivity.

In order to measure the concentration of H_2 in the gas phase at the end of reaction, the reactor was cooled down and the gas collected using a Tedlar® bag. The sample was injected to a Bruker 430 GC-TCD (Palo Alto, USA) equipment, with water trap and a CP-Molsieve 5A (15 m × 0.53 mm × 15 μm) and a CP-Pora BOND Q (25 m × 0.53 mm × 15 μm) columns. The injector, detector and oven temperatures were maintained at 150 °C, 175 °C and 40 °C, respectively. Helium was used as the carrier gas at 13.7 cm^3/min.

Solid Characterization

The solid samples were dried in an oven under vacuum overnight at 45 °C, to remove the remaining moisture. They were analyzed by X-ray diffraction (XRD), using a BRUKER D8 DISCOVER A25 equipment, with 3 kW Generator, 2.2 kW type FFF Cu-ceramic tube, LynxEye Detector, operating at 40 kV and 30 mA. The database used for identifying the phases was the PDF-2 Released 2013 (ICDD). For evaluating the oxidative stability of the catalyst after reaction at the central point, first and last reutilization, Temperature Programmed Reduction (H_2-TPR) was conducted using the commercial Micromeritics TPD/TPR 2900 unit. Firstly, the sample was loaded into a U-shaped quartz cell (100 mm × 3.76 mm i.d.) and heated at 10 ºC/min to 150ºC and maintained for 1 h under a flow

of 50 cm^3/min of pure nitrogen (99,999%, Air Liquide), in order to remove air and moisture. Afterwards, the temperature was returned to ambient and then ramped up to 900 °C under a flow of H_2/N_2 (5% v/v; 50 $cm^3\,min^{-1}$, Air Liquide) at a rate of 10 °C·min^{-1}. Hydrogen consumption was monitored by a thermal conductivity detector (TCD) with data acquisition/manipulation using the ChemiSoft TPX V1.03™ software. Before the detector, an ice trap was used to retain any water formed in the analyses. Transmission electron microscopy (TEM) was performed to determine possible changes in the particle size distribution and shape of the Pd/C catalyst after the hydrotreatment. For that, the samples were ultrasonically dispersed in water-MilliQ and suspended on a copper grid before the analysis, and analyzed in a JEOL JEM-1011 HR equipment (JEOL, Tokyo, Japan) at 100kV.

RESULTS AND DISCUSSION

Comparative results using different sources of carbon.

Fig. 1 shows the results of the reactivity of the different carbon sources at 120 ºC and at 250 ºC. Highest yield (20%) and selectivity (55%) towards formate were obtained with carbamate at 120 ºC, while carbonate displays a similar selectivity but at a higher temperature (250 °C), with slightly increased yield of 24%. It is worth noting that AB showed the worst performance at any temperature, with a maximum yield of 11% and selectivity of 25%, while SB only reached its highest performance at 250 ºC, with a yield and selectivity of 57% and 72%, respectively. The results indicate that under mild hydrothermal reaction conditions, using *in-situ* produced hydrogen, the FA yield and selectivity increase in the order AB<SB<ACA<AC, where AB and SB reagents need higher temperature (250 °C) for a better yield. Equilibrium constants were computed and used for estimating the concentration of each species of the ammonium speciation in water, for a given temperature, according to the work of Ahn et al. [45]. This shows that the fact that AC and ACA are more reactive as starting materials at mild temperature is probably because in water as solvent at 120 ºC, AC and ACA generate 27% more concentration of HCO_3^- anion (0.42 mol/L) in the equilibrium than that obtained from AB (0.33

mol/L) [45]. Moreover, ammonium bicarbonate decomposes into ammonia and CO_2 presenting more loss of the anion to yield a higher concentration of gaseous CO_2 (0.17 mol/L) than for AC and ACA (0.08 mol/L). The similar activity of carbamate and carbonate is because they both easily decompose into HCO_3^- (see Fig. 2), which is the reducible species, and that happens because the ammonium cation (NH_4^+) can donate its proton (H^+) to other species due to its weak acid nature [46]. HCO_3^- is the reducible species as suggested in the mechanism of hydrogenation of $NaHCO_3$ by water splitting with Al by Yao et al. [35]. High temperatures are not favorable to carbamate and carbonate because the reduction competes with a thermal decomposition step.

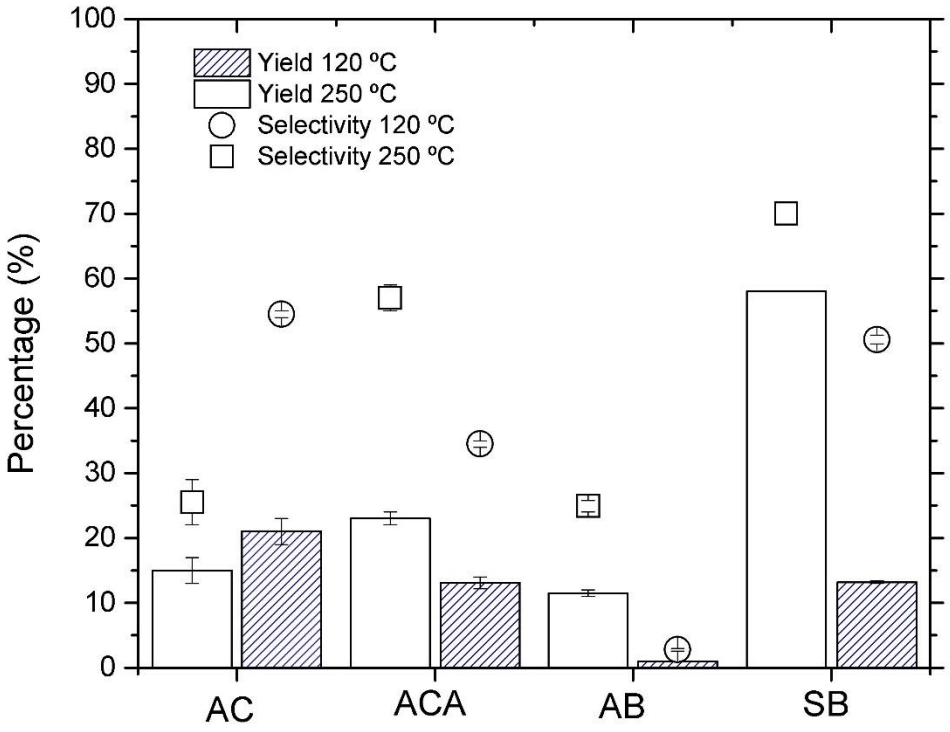

Fig. 1. Performance comparison of different carbon source conversion at 120 and 250 ºC toward FA yield and selectivity. Reaction conditions: 2 h, Al:carbon source molar ratio of 6, 15% catalyst, 70% of filling and 0.5 M of initial concentration. (FA: formic acid, AC: ammonium carbamate, ACA: ammonium carbonate, AB: ammonium bicarbonate and SB: sodium bicarbonate).

It is worth noting that a significant yield of 57% was obtained from reducing SB at an increased temperature of 250 ºC, while at this temperature AB only yields 11% of FA, in accordance with Wang et al. [40], who obtained higher FA yield out of SB (86.6%) than AB (7.2%). This is because the concentration of HCO_3^- (the reducible species) is higher when we use Na^+ than NH_4^+ at elevated temperatures (200 ºC), as shown in the calculated equilibrium between HCO_3^- and CO_3^{2-} with sodium cation, using the aforementioned model of Ahn et al. [45]. HCO_3^- concentration from sodium bicarbonate is not affected by the temperature increase, in the range of 0 to 350 ºC, whereas ammonium bicarbonate is more affected by thermal decomposition. i.e. Reaction b in Fig. 2 is less favored. On the contrary, high temperature may favor the reduction step. Na^+ and K^+ cations does not promote the hydrogenation of carbonates and bicarbonates at low temperature [47], but the reduction of $NaHCO_3$ can be handled up to 300 ºC before affecting the formate concentration, as shown by Shen et al. [48].

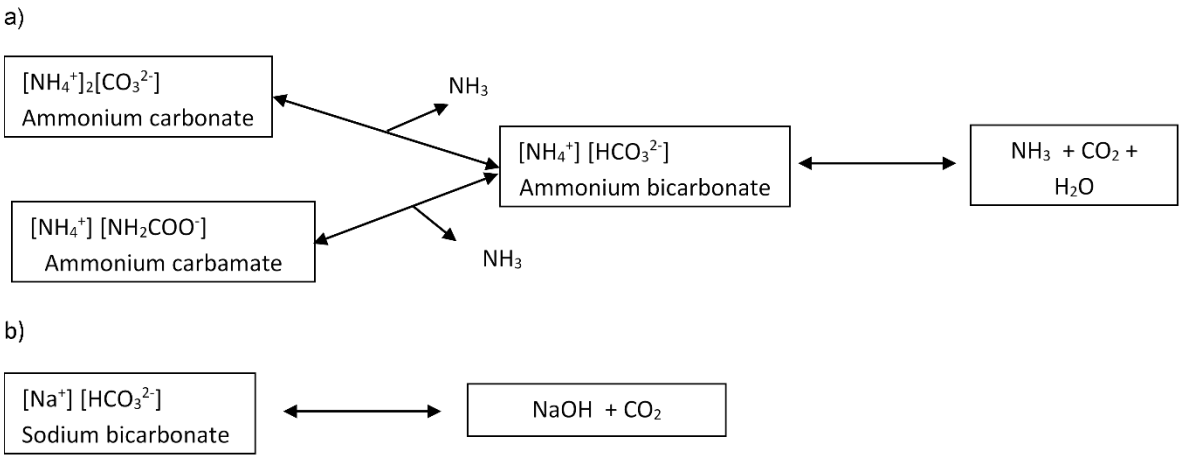

Fig. 2. Decomposition equilibria of a) ammonia-based CO_2 absorption derivatives and b) sodium hydroxide-based CO_2 absorption derivatives.

In general, the lower yield of formate obtained from ammonium salts may be owed to the high yield of hydrogen coming from dehydration reaction of ammonium formate at the tested reaction temperature of 120 ºC, in accordance to Su *et al.* [47]. However, this can be made up by the fact that, as hydrogen storage method, it is desired to produce formate with NH_4^+ countercation rather

than with Na^+, because the volumetric hydrogen density is expected to be higher, as it depends on the solubility of the salt. Thereby, the solubility of ammonium formate (~22 mol/L) is nearly double of sodium formate (~12 mol/L) at room temperature. What is more, higher yields (>90%) of hydrogen as fuel, from the decomposition of ammonium formate, are obtained, owing that NH_4^+ easily donates H^+ protons to complete the reaction (8), while for the sodium formate is more difficult as the proton must be taken from the H_2O, reaction (9), making it more stable to temperature [47, 49]. Another advantage is that the ammonium formate can be utilized in solid state, so its decomposition for producing hydrogen will leave no residue.

$$NH_4^+HCOO^- \rightarrow NH_3 + CO_2 + H_2 \quad (8)$$

$$Na^+HCOO^- + H_2O \rightarrow NaOH + CO_2 + H_2 \quad (9)$$

Experimental results for ammonium carbamate

Influence of temperature

Fig. 3 depicts the results of yield, conversion and selectivity as a function of the reaction temperature. It can be appreciated that a minimum yield (4%) is obtained at the lowest temperature of 80 ºC, with the highest selectivity (70%), but low conversion (10%). In the region 120-200 °C the yield stabilizes around 20%, but higher temperature makes the yield and selectivity to decrease, owing to the thermal decomposition of AC to CO_2 and ammonia, and the ammonium formate to CO_2, ammonia and H_2 [42, 50]. The increase of conversion can be attributed to decomposition of HCO_3^- that becomes gaseous CO_2 (detected by GC-TCD) which is a by-product along with traces of formaldehyde and methanol (detected by HPLC).

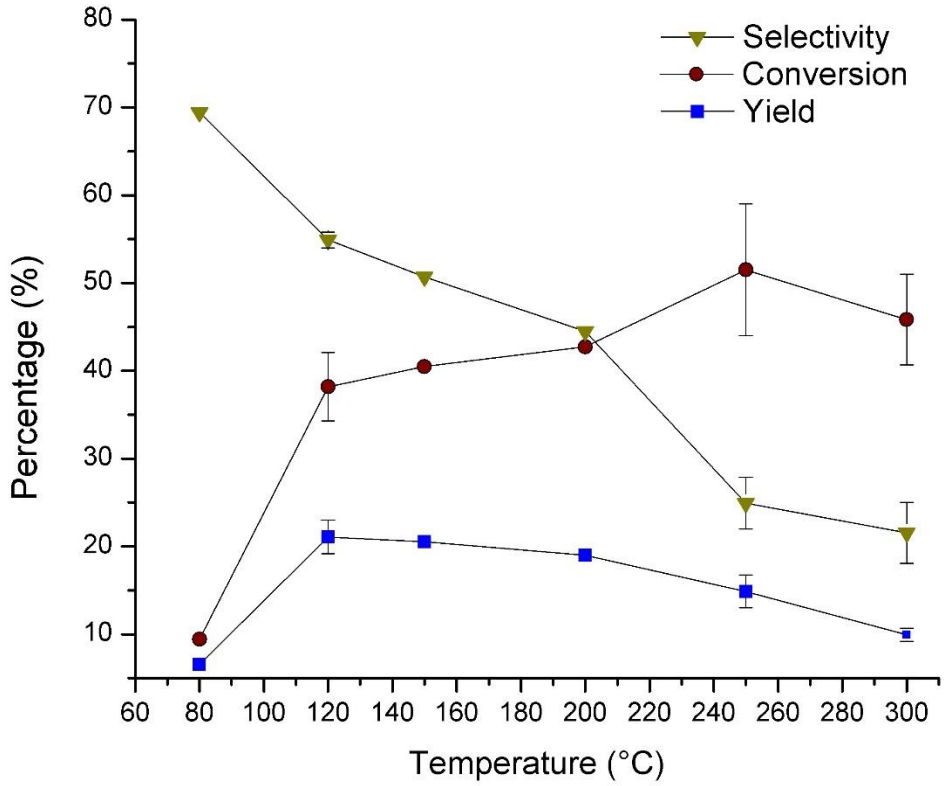

Fig. 3. Effect of temperature over yield and selectivity of FA, and conversion of AC. Reaction conditions are: 2 h, Al:AC molar ratio of 6, 15% catalyst, 70% filling and 0.5 M of AC initial concentration.

At 300 ºC the dry-based gas composition was 66.7% H_2, 30.2% N_2, 1.1% CO_2, 1.97% O_2 and traces of CH_4 (<0.005%). At 120 °C was 73.2% H_2, 25.4% N_2, 0.67% CO_2 and 0.67% O_2 (other components are not identified by the chromatographic system). Given that NH_3 decomposition into N_2 and H_2 is a high temperature process (usually above 400 °C for complete conversion [51, 52]), the nitrogen reported in the gas phase corresponds to the purge done before reaction. The lower concentration of hydrogen in the gas phase at 300 ºC, compared to 120 ºC (central point), can be explained by the fact that the aluminum-water splitting reaction has an optimum temperature of 70-90 ºC, in which the highest rate of hydrogen production is reached [53]. Likewise, at higher temperature the availability of dissolved hydrogen in the liquid phase for the reduction of HCO_3^- ions is lower, and the ammonium-

formate dehydration rate is accelerated, thus contributing to the observed drop of FA yield at 300 ºC. Both the hydrogen production using aluminum and the selectivity towards formic acid ($HCOO^-$ stability) are improved by alkaline conditions [32, 37, 54, 55], so high temperatures should be avoided because the alkalinity is reduced by NH_4^+ dissociation into NH_3 and H^+. Likewise, He et al. [34] concluded that slightly acidic media does not favor the reduction of CO_2, probably due to low solubility in water.

Influence of reaction time

The influence of time in the reaction at 120 ºC is presented in Fig. 4. A high selectivity (72%) is achieved at 0.5 h, indicating that the FA is formed faster than other possible products. In general, previous authors [35, 36], who studied the reduction of sodium bicarbonate during up to 3 hours using aluminum as reductant, found that the conversion was promoted by an increase of reaction time. Similarly, in our study the conversion is still increasing after 4 hours, but toward undesired products. However, it is clear that the selectivity decreases proportionally to time, so it is not convenient to increase time because the parameters to be optimized are yield and selectivity.

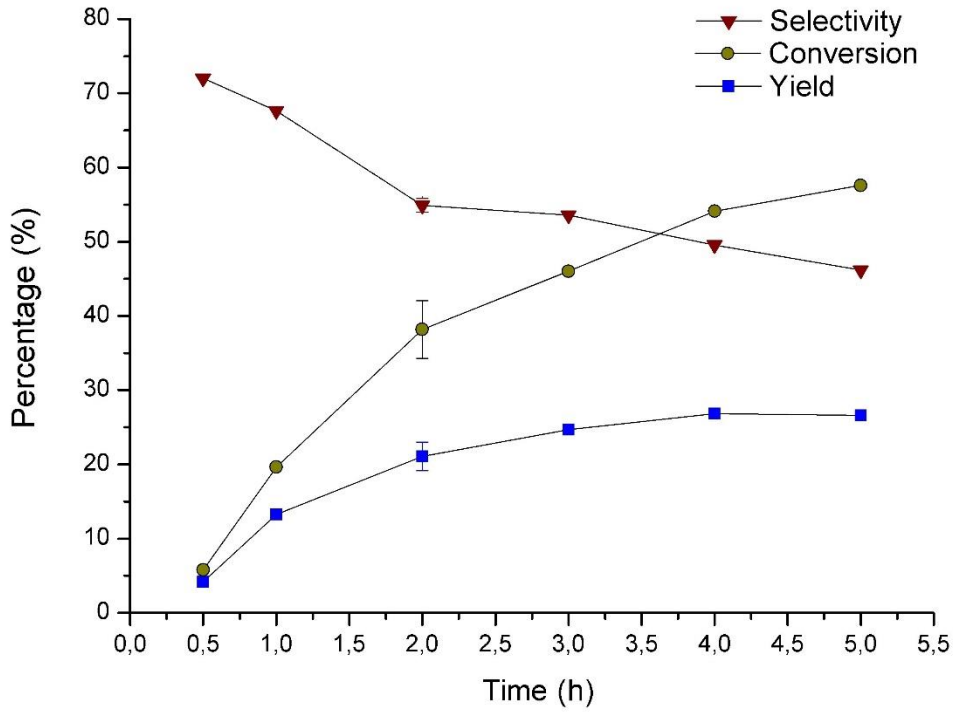

Fig. 4. Effect of time over FA yield and selectivity, and AC conversion. Reaction conditions are: 120 ºC, Al:AC molar ratio of 6, 15% catalyst, 70% filling and 0.5 M of AC initial concentration.

Influence of catalyst content

A reaction blank, using activated carbon powder instead of catalyst (0% of Pd load), showed a negligible yield of 2%. A reaction using Pd powder (without activated carbon) at the central point of reaction conditions, keeping the proportion of metal with respect to the initial weight of carbon source as in the test of 15% wt Pd/C content, yielded less than 1% of FA. This supports the following facts: a) the hydrogenation/reduction of ammonia-based CO_2 captured species in hydrothermal media requires the presence of a selective catalyst such as Pd/C, b) The active site of the catalyst is the Palladium and c) the dispersion of Pd into a matrix increases greatly the contact area and mass transfer. It seems that Pd/C and aluminum powder conform a good catalytic system for the reduction of SB at 250 ºC (FA yield of 57% as aforementioned), given that when using Pd/C with a liquid

reductant (pyrrolidone), even at higher temperature of 300 ºC and 2 h, the yield is only 17.8%, and 30% at 350 ºC [41]. Likewise, when reducing SB without catalyst, and only with 6 mmol of Al at 250 ºC for 2 h the yield is 19% [36]. In a recent work by Zhong et al. [33], the addition of Ni powder as catalyst in the reduction of SB with Zn/ZnO yielded 81% of formate at 225 ºC. This support the need of a selective catalyst for an increased yield under a moderate temperature.

These results confirm that the reaction mechanism occurs in two steps: the reduction of water to obtain H_2 by oxidizing Al, followed by a reduction of bicarbonate heterogeneously catalyzed by Pd^0. A reaction pathway is proposed in Fig. 5. The first reaction (a) describe the production of molecular hydrogen from the water splitting using aluminum. In the second one (b), is described the reduction of bicarbonate ion in aqueous media, starting with the H_2 adsorption into a surface-palladium site of the catalyst composite, followed by the weakening of the H-H bond that allows the hydrogenation and the loss of one mole of water to yield the formate.

a) $2Al+6H_2O \rightarrow 2Al(OH)_3+3H_2$

b)

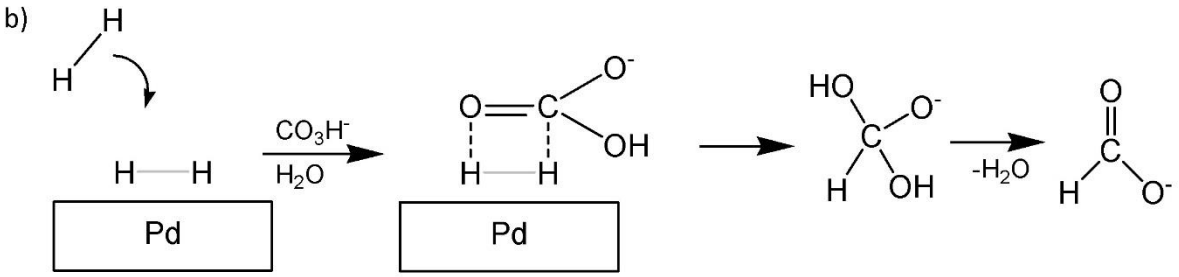

Fig. 5. a) Hydrogen production from aluminum-water splitting, and b) Reaction pathway for the reduction of ammonium carbamate over Pd/C catalyst surface.

Fig. 6 shows the influence of the amount of catalyst in the reduction of AC at 120 ºC. When no catalyst is used, the yield and selectivity is almost zero, indicating that the mild reaction conditions of carbamate reduction are feasible only through an active and selective catalyst like Pd/C. However, the conversion is 20% because the carbamate is thermally decomposed into NH_3 and CO_2. The

response variables are linearly proportional to the catalyst content, and start to level off above 30% with respect to carbamate (0.02 g catalyst/mL of reaction solution). This is in accordance with Wiener et al. [19], who reduced sodium and potassium bicarbonate in batch system with dry hydrogen (7 atm), employing Pd/C (5%wt) catalyst, and observed that the rate of reaction rose linearly up to a certain amount of catalyst (in this work, 0.03 g catalyst/mL of reaction solution). The results at 60% of catalyst show that Pd/C is highly selective toward FA (85%), while the yield is of ca. 40%, and the conversion tends to stabilize in 45%.

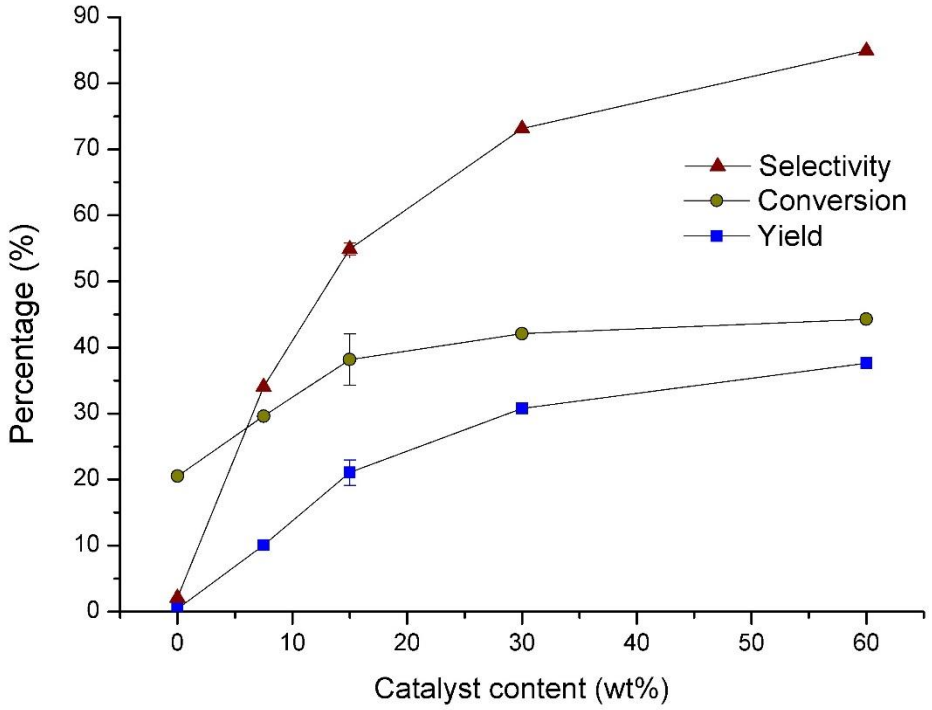

Fig. 6. Effect over FA yield and selectivity, and AC conversion of catalyst Pd/C 5wt % content with respect to ammonium carbamate. Reaction conditions are: 120 ºC, 2 h, Al:AC ratio of 6, 70% filling and 0.5 M of AC initial concentration.

Influence of pressure (filling level)

As the reactor works with autogenic pressure, the final pressure can be increased by increasing the percentage of volume filled in the reactor with the liquid phase. In such a way, the space left for the gas phase is lower and thus the gas pressure is increased. The concentration of carbamate is kept constant at 0.5 M by recalculating the amount needed for the varying liquid phase volume. In Fig. 7 can be appreciated that the liquid filling has a modest effect over FA yield at a filling percentage of 85%, related to the higher pressure produced of 1.1 MPa that accounts for dissolved hydrogen of $8.4x10^{-6}$ mol H_2/g H_2O, compared to the central point of reaction conditions of 70% with a pressure of 0.6 MPa that accounts for $4.6x10^{-6}$ mol H_2/g H_2O, according to the solubility data generated by Wiebe *et al.* [56]. Nevertheless, the effect is more clear when using zinc as reductant, as modelled in our previous research at 300 ºC and 75% of filling [38], owing to the higher pressure produced of 21 MPa, which accounts for dissolved hydrogen of $1.6x10^{-4}$ mol H_2/g H_2O.

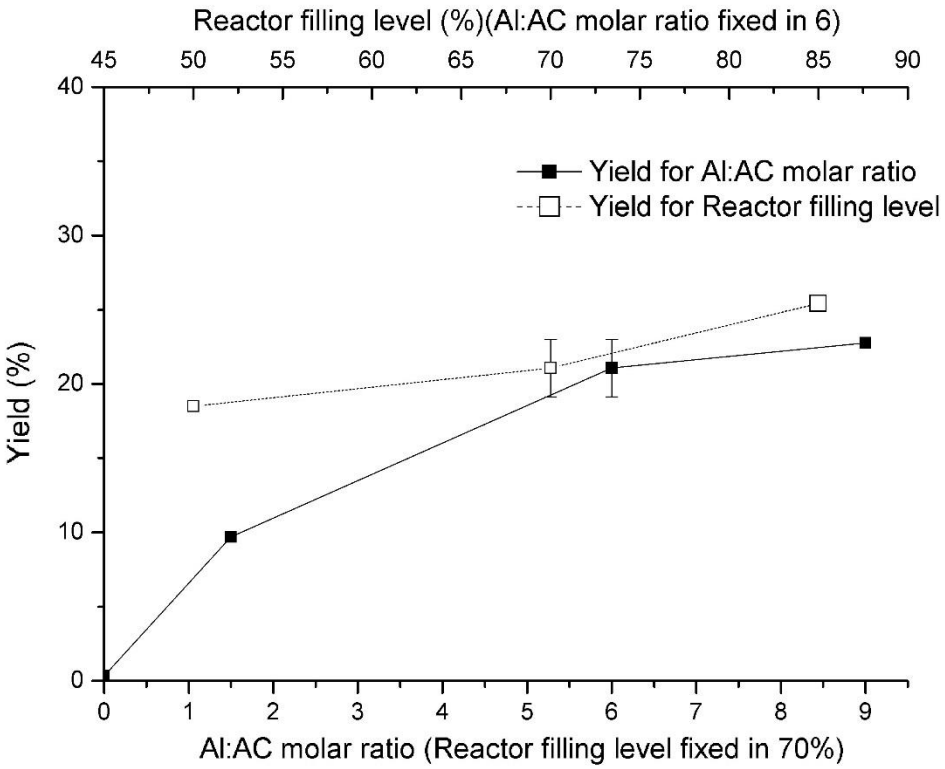

Fig. 7. Effect of filling and Al:AC molar ratio over FA yield. Reaction conditions are: 120 ºC, 2 h, and 0.5 M of AC initial concentration.

Influence of Al:AC molar ratio

The Al:AC molar ratio had a remarkable effect over FA yield in the range 1.5-6 (see Fig. 7), which represents an excess of 2.25 and 9 times the stoichiometric ratio of Al:H_2 of 0.67 (based on Fig. 5), respectively. The yield is not significantly improved when the Al:AC molar ratio is increased up to 9, which represents an excess of 13.5 times the stoichiometric ratio, most probably because of the large amount of solids inside the reactor which are out of the working range of the agitator. A previous work with sodium bicarbonate by Zhong et al. [35], also reported that the excess of aluminum promoted the formation of formic acid using catalyst Pd/C (5 wt%).

Reduction with gaseous-H_2

The behavior of aluminum, as hydrogen source, against gaseous-H_2 in the reduction of AC was analyzed at different stoichiometric excesses of the reaction 10, where the stoichiometry is 1:1. For reduction with hydrogen generated by aluminum, the excesses were calculated as the molar ratio Al:AC (1.5 and 6) divided by 0.67 (moles of aluminum per mole of hydrogen, see reaction 4), thus yielding hydrogen excesses of 2.25 and 9 over the stoichiometric amount. For reduction with gaseous-H_2 low stoichiometric excesses of 0.35, 1 and 2.25, representing initial pressures at room temperature of 0.4, 1.15 and 2.6 MPa, respectively, were selected for two reasons. The first one, to be under the maximum pressure of the reactor and, secondly, to compare not only to the stoichiometric amount but also to lower pressures as happens to the Al experiments where the pressure reached is much lower.

$HCO_3^- + H_2 \rightarrow HCOO^- + H_2O$ (10)

Table 2 shows the yield results for both reductants. It is observed that yields using Al (9.7%) are lower than using H_2 (56.7%), at equal hydrogen excess of 2.25. If instead comparing data with the same excess over the stoichiometric amount, data with a similar level of pressure are compared: data with 0.35 excess over the stoichiometric (yield =15.6%) for gaseous-H_2 and excess of 9 for Al (yield=21.1) the yield is slightly higher for Al experiments, but the yields are comparable.

Table 2. Comparison results of FA yield for experiments with gaseous H_2 and aluminum as reducing agents. Reaction conditions are (Central point): 120 ºC, 2 h, Al:AC ratio of 6, 15% of catalyst (Pd/C 5wt %), 70% filling and 0.5 M of AC initial

Hydrogen source	Hydrogen Stoichiometric excess	Final Absolute Pressure (MPa)**	FA Yield (%)
gaseous H_2	0.35	0.5	15.6 ± 1.0
	1	1.1	30.2 ± 1.0
	2.25	2.4	56.3 ± 1.0
aluminum	2.25	0.3	9.7 ± 1.9
	9	0.6	21.1 ± 1.9
	9*	1.1	25.4 ±1.9

Fig. 8 indicates that using both sets of data the yield is linearly proportional to pressure (R=0,986), which is produced by gaseous H_2. This can be indicative that, in both cases H_2 is the reductant, and the only role of Al would be releasing H_2. In this way it is different from other hydrothermal reduction processes using Zn as reductant in which the reduction yields more than twice the reduction using gaseous H_2 [37]. Secondly, the slow release of H_2 from Al makes that the pressure is lower than using gaseous H_2, and thus, decrease the solubility of H_2 in the liquid phase penalizing in this way the reaction rate. From the results of yield in Table 2, it is clear that a high excess of aluminum is not sufficient to release enough H_2 to reach the performance showed by gaseous H_2 in batch. To improve this process, efforts must be directed to increase the operational pressure. One solution is to speed up the release or H_2, for example, increasing the pH to release the H_2 faster. According to the results shown in table 3, in which the pH is increased by adding NaOH, the increase of pH from 9.2 to 10.1, increases Yield from 19.2 to 25.2 with an increment of pressure of 0.2 MPa. Nevertheless, at pH 12.5 the yield decreased dramatically although the pressure is almost three times that of pH=10.1 (see Table 3). This could be explained by the fact that at pH=12.5 the chemical equilibrium favors the formation of carbonate instead of HCO_3^- (the reducible specie), according to the model of Ahn et al.

[45]. This results are in good agreement with Onoki *et al.* [57], who found that pH should be kept below 11, so an excessive addition of NaOH inhibits reduction from HCO_3^- to useful carbonic compounds like CH_4 and $HCOO^-$ under the hydrothermal conditions.

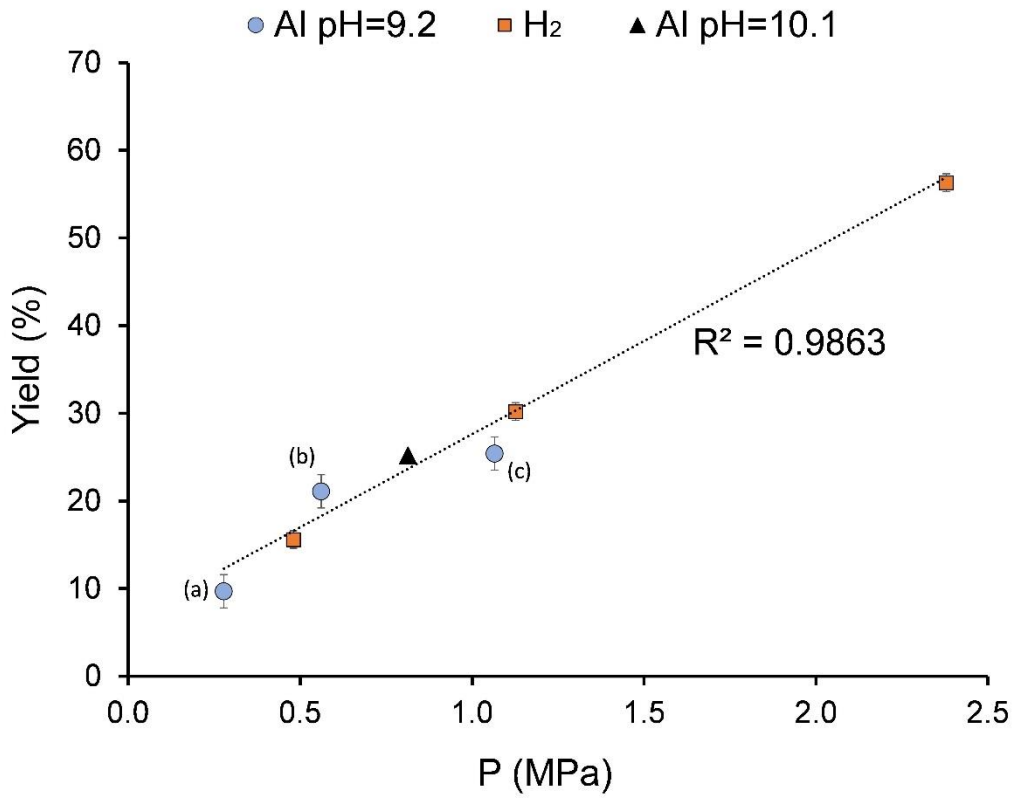

Fig. 8. Proportionality of FA yield to pressure using Aluminum and hydrogen as reducing agents. (Data of Al pH= 9.2 are at stoichiometric excesses of 2.25 (a), 9 (b) and 9* (c)).

Table 3. FA yield results at different initial pH of carbamate solution using aluminum as reductant. Reaction conditions are (Central point): 120 ºC, 2 h, Al:AC ratio of 6, 15% of catalyst (Pd/C 5wt %), 70% filling and 0.5 M of AC initial concentration.

pH	Final Absolute Pressure (MPa)	FA Yield (%)
9.2	0.6	19.2 ± 1.9
10.13	0.8	25.2 ± 1.0
12.5	2.0	3.43 ± 1.0

Another solution to improve the process using Al, could be the use of a more suitable reaction system. Using a continuous reaction system has the advantage that pressure can be controlled independently of the filling of the reactor or Al content, thus a higher working pressures for increasing the solubility of H_2 would be achievable, and may allow optimizing two temperature zones for the aluminum-water splitting and formate formation. In addition, the continuous flow would allow the instantaneous removal of the hydrolysis product (aluminum hydroxide) that covers on the aluminum surface and inhibits the H_2 release [55].

Solid characterization

In our previous experience with Zn as reductant of sodium bicarbonate in hydrothermal media, this metal is completely oxidized in the early stages of the reaction [38]. In order to verify if the Al behaves similarly, a set of reutilization cycles were performed. Owing to the configuration of the reactor it is not possible to isolate the exhausted aluminum from the catalyst. The resulting solid from the reaction, comprising partially oxidized aluminum and Pd/C catalyst, was recovered and reutilized without washing. Based on Table 4, a certain amount of aluminum was consumed in the first use, as the yield dropped from 22.7 to 9.5% obtained in the first re-use (second use). However, Al it is not totally oxidized since, even up to the 5^{th} re-use, the reductant is able to yield 4.8% of formate, suggesting

that hydrogen is still produced but in a deficient amount with low pressure, limiting its solubility in water, as discussed before. This is in agreement with the low pressure found in the experiments with aluminum compared to an equivalent amount of H_2, as explained in section 3.2. It is also consistent with the observations of Setiani *et al.* [60] who found that the aluminum was only partially reacted for reactions at ≤ 270 ºC after 24 h reaction, generating 30 mmol of hydrogen over the theoretical maximum of 60 mmol.

Table 4. Reutilization results (%wt) of reaction solid (Al+Pd/C)

Re-use	FA Yield (%)	AC Conversion (%)	FA Selectivity (%)
0*	22.7	42.1	53.9
1	9.5	26.9	35.5
2	7.4	28.5	26.0
3	6.6	24.0	27.6
4	6.0	25.3	23.7
5	4.8	23.4	20.6

Fig. 9 shows the XRD patterns of the remaining solid after reaction, at different temperatures and after the 5th re-use. At 40° there is an appreciable peak, corresponding to Pd (PDF 00-046-1043). At every reaction temperature tested, the cubic structure of aluminum powder, with diffraction peaks at 2θ = 38, 45, 65 and 78°, is present [59, 60] confirming that is not completely exhausted. However, there is also evidence of aluminum oxidation, reflected by peaks at 2θ = 14.5, 28, 49, 55 and 72°, which corresponds mostly to bohemite AlO(OH) (PDF 00-021-1307) [61].

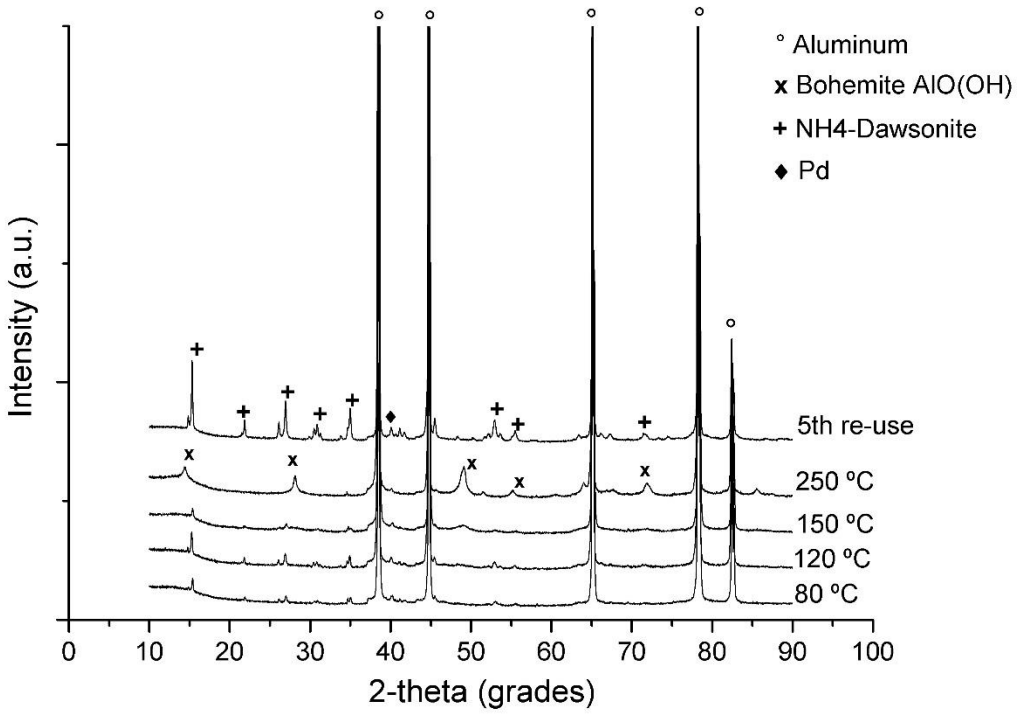

Fig. 9. Comparative XRD patterns of reaction solid at different temperatures and after five reuses.

The presence of the by-product ammonium aluminum carbonate hydroxide ($NH_4Al(OH)_2CO_3$) (or NH_4-dawsonite) (PDF 76-1923) (known as a potential precursor in the field of alumina synthesis [62]) is detected after the 5th re-use. It seems that after oxidation, Al (III) precipitates with CO_3^{2-} and NH_4^+ anions present in the medium to form this new compound.

The temperature programmed reduction (TPR) technique allows determining the reduction temperature of metallic oxides of a catalyst, and the amount of hydrogen consumed, revealing its reducibility [63]. In this work the TPR analysis is presented for the resulting solid after the central point of reaction conditions (Re-use 0), for the 1st re-use and the 5th. In Fig. 10 a first small negative peak appears at the low temperature in the range of 69-75 °C, characteristic of decomposition of superficial palladium hydride specie (β-PdH_x, where x>0.6) [64-67], tentatively formed during the hydrothermal process and/or at ambient temperature under H_2/N_2 flow of the TPR experiment. This phenomena of H_2 adsorption into palladium as hydride specie has been thoroughly studied [68]. The positive peak

present in the three samples in the range 194-235 ºC corresponds to hydrogen consumption of the PdO species strongly interacting with the support [69], where a complete reduction of Pd^{2+} to Pd^{0} takes place [70]. This represent a catalyst depletion and is more evident in the reactions where the solid is re-used, as the PdO reduction peak is larger. Since Al, as the main reductant, is depleted, Pd can play that role instead. This can explain the residual yield observed in the reutilization studies. Because Pd facilitates the H atom migration to the carbon support [71], the negative peak present in the tree samples in the range 630-675 ºC can be explained by the desorption of adsorbed hydrogen on the carbon support (following the reaction $Pd\text{-}H_x \rightarrow Pd + x/2H_2$). This high temperature hydrogen evolution is promoted by the PdO strongly bonded to the support that in turn follows the reaction $(2+x)/2\ H_2 + PdO \rightarrow Pd\text{-}H_x + H_2O$ that occurs at ambient temperature. The asymmetry of this hydrogen desorption peaks correspond with distinct desorption stages, depending on the proximity of palladium hydride specie to the surface [72]. The formation of aluminum hydride during the hydrothermal process and/or TPR analyses should be discarded, given that its decomposition temperature (negative peak) is usually between 150-170 ºC [73].

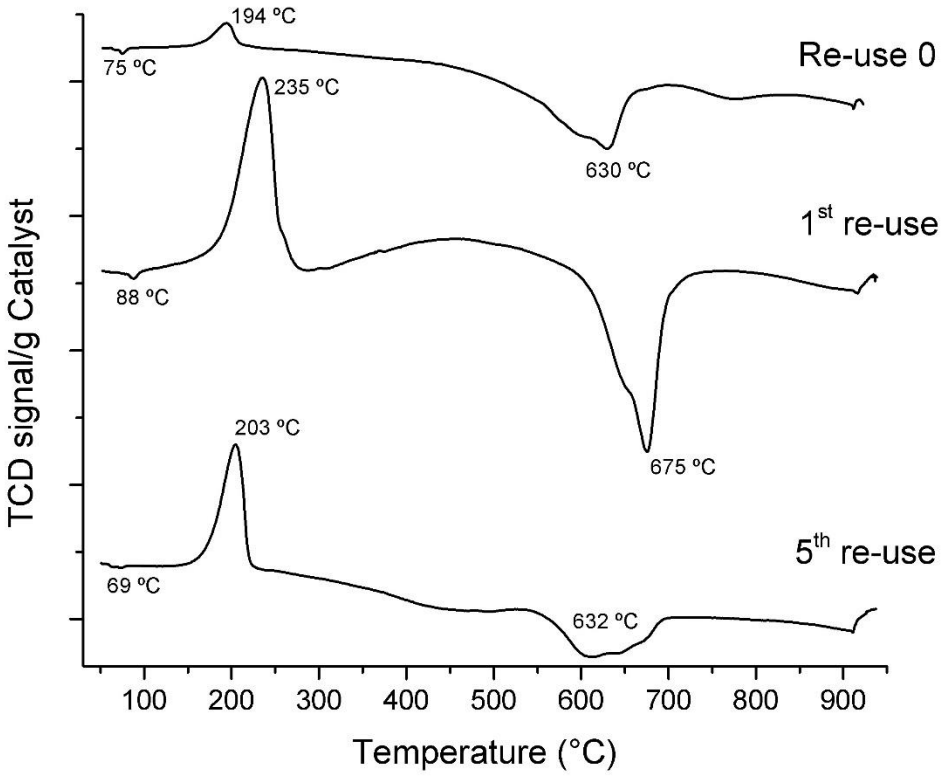

Fig. 10. TPR profile of resulting solid (Al+Pd/C 5 wt%) after central point of reaction conditions (Re-use 0), 1st and 5th re-use.

The morphology of the reaction solid was analyzed by Transmission Electron Microscopy (TEM). From Fig. 11a it can be observed at 20 nm the nano-particles of Pd (5 wt%) active sites, well distributed, with an average particle size of 4.3 ±1.0 nm, calculated with the software ImageJ 1.52a. From Fig. 11b it can be observed at 20 nm that the metalic dispersion of the catalyst after the 5th re-use has not been seriously compromised, but grain growing of Pd particles is warned, making the average particle size to increase to 7.6 ±3.1nm, which may have consecuences over the catalytic performance.

This analyses allowed concluding that the drop of yield and selectivity observed in table 4 is mostly ascribed to the following facts: a) partial inactivation of aluminum by formation of bohemite, causing

a diminishing of hydrogen production, and b) partial inactivation of catalyst by oxidation of Pd active sites (PdO formation). A potential leaching of palladium and aluminum from solids to the reaction solution during each re-use cycle should be considered as a factor affecting the overall catalytic performance.

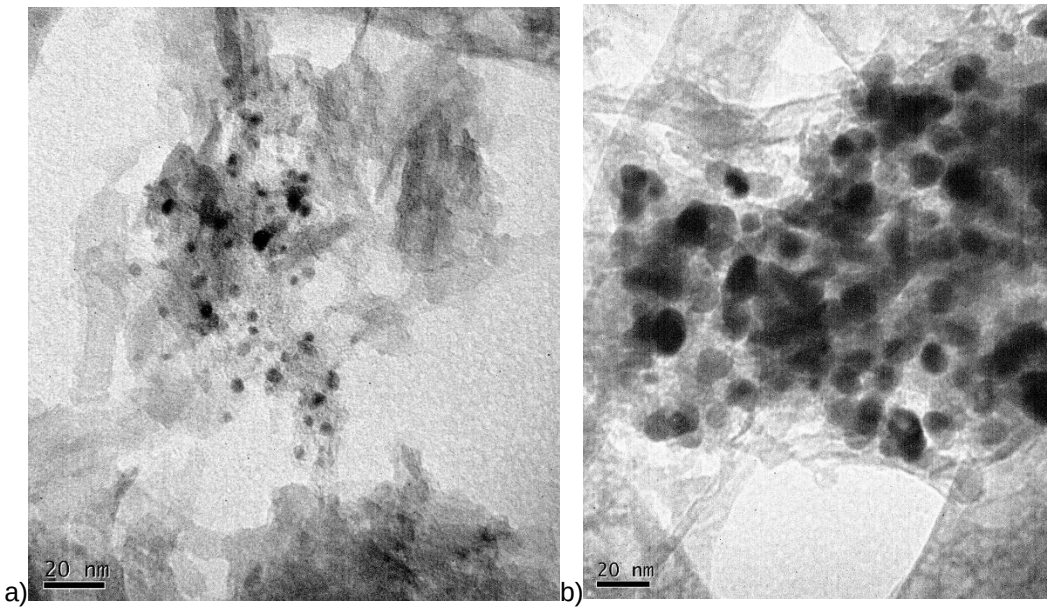

Fig. 11. TEM image of resulting solid, a) after reaction in the central point (20 nm), b) after 5th re-use (20 nm)

Conclusions

In the process to obtain formic acid from the catalytic conversion of CO_2 captured in aqueous media, ammonium carbamate showed the best performance under mild reaction temperature (120 ºC) as starting material, while ammonium carbonate, ammonium bicarbonate and sodium bicarbonate reagents need higher temperature (250 °C) for an increased yield. Time variable had a significant effect and after 4 h of reaction the yield stabilized in 27%. The response variables are proportional to the catalyst content, and start to level off above 30% of Pd/C with respect to carbamate, obtaining a yield of ca. 40%. The increase of autogenic pressure of 1.1 MPa, by increasing the liquid filling up to 85% of the volume of the reactor, had a modest effect over FA yield. Although an excess of aluminum

is required, the formate yield is not significantly improved at the highest Al:AC ratio of 9. The process can be improved by operating at higher pressure and lower temperature, to avoid loss of yield by dehydration of formate. Experiments using gaseous H_2 as reductant, showed higher yield of formate, but also higher pressure inside the reactor. When comparing data with a similar level of pressure the yield is slightly higher for Al experiments, but the yields are comparable. The slow release of H_2 from the Aluminum hinders the process. The reutilization and characterization of the reaction solid, comprising exhausted aluminum and Pd/C catalyst, showed that most of the aluminum was consumed in the first use, but XRD analyses confirmed it was not completely oxidized up to the 5^{th} re-use. Pd can play a reducing role through the formation of palladium hydride species, as it was observed through the TPR analyses.

REFERENCES

[1] M. Pérez-Fortes, E. Tzimas, JRC Science Hub: ZG Petten, the Netherlands (2016)

[2] J. Rogelj, M. Den Elzen, N. Höhne, T. Fransen, H. Fekete, H. Winkler, R. Schaeffer, F. Sha, K. Riahi, M. Meinshausen, Nature, 534 (2016) 631. https://doi.org/10.1038/nature18308

[3] E.J. Maginn, J. Phys. Chem. Lett. (2010) 3478-3479. https://doi.org/10.1021/jz101582c

[4] P. Styring, E.A. Quadrelli, K. Armstrong, Carbon dioxide utilisation: closing the carbon cycle, first ed, Elsevier, Amsterdam, (2014).

[5] T. Covert, M. Greenstone, C.R. Knittel, J. Econ. Perspect. 30 (2016) 117-138. https://doi.org/10.1257/jep.30.1.117

[6] H. Yang, Z. Xu, M. Fan, R. Gupta, R.B. Slimane, A.E. Bland, I. Wright, J. Environ. Sci. 20 (2008) 14-27. https://doi.org/10.1016/s1001-0742(08)60002-9

[7] B. Llamas, B. Navarrete, F. Vega, E. Rodriguez, L.F. Mazadiego, Á. Cámara, P. Otero, Greenhouse Gas Emissions–Carbon Capture, Storage and Utilisation, in: B. Llamas, J. Pous (eds), Greenhouse Gases, InTech, Croatia, 2016, pp. 81-114.

[8] E. Gal, Ultra Cleaning Combustion Gas Including the Removal of CO 2, Patent No, WO2006022885, (2006).

[9] C.K. Ahn, H.W. Lee, M.W. Lee, Y.S. Chang, K. Han, C.H. Rhee, J.Y. Kim, H.D. Chun, J.M. Park, Enrgy. Proced. 4 (2011) 541-547. https://doi.org/10.1016/j.egypro.2011.01.086

[10] A. Bandyopadhyay, Carbon capture and storage: CO2 management technologies, first ed, Apple Academic Press, (2014).

[11] H.B. Gray, Powering the planet with solar fuel, Nat. Chem. 1 (2009) 112. https://doi.org/10.1038/nchem.141

[12] Q.-W. Song, Z.-H. Zhou, L.-N. He, Green Chem. 19 (2017) 3707-3728. https://doi.org/10.1039/C7GC00199A

[13] K. Nakano, K. Kobayashi, T. Ohkawara, H. Imoto, K. Nozaki, J. Am, Chem, Soc, 135 (2013) 8456-8459. https://doi.org/10.1021/ja4028633

[14] J. Wu, Y. Huang, W. Ye, Y. Li, Adv Sci. 4 (2017) 1700194. https://doi.org/10.1002/advs.201700194

[15] G. Bredig, S.R. Carter, Ber. Dtsch. Chem. Ges. 47 (1914) 541-545. https://doi.org/10.1002/cber.19140470188

[16] W.-H. Wang, X. Feng, M. Bao, Transformation of carbon dioxide to formic acid and methanol, first ed, Springer, Singapore, (2018).

[17] A.M. Klibanov, B.N. Alberti, S.E. Zale, Biotechnol. bioeng. 24 (1982) 25-36. https://10.1002/bit.260240104.

[18] C.J. Stalder, S. Chao, D.P. Summers, M.S. Wrighton, J. Am. Chem. Soc. 105 (1983) 6318-6320. https://doi.org/10.1021/ja00358a026

[19] H. Wiener, J. Blum, H. Feilchenfeld, Y. Sasson, N. Zalmanov, J. Catal. 110 (1988) 184-190. https://doi.org/10.1016/0021-9517(88)90308-9

[20] S. Uhm, S.T. Chung, J. Lee, J. Power. Sources. 178 (2008) 34-43. https://doi.org/10.1016/j.jpowsour.2007.12.016

[21] C. Rice, S. Ha, R. Masel, P. Waszczuk, A. Wieckowski, T. Barnard, J. Power. Sources. 111 (2002) 83-89. https://doi.org/10.1016/S0378-7753(02)00271-9

[22] C. Masters, The Fischer-Tropsch Reaction, in: F.G.A Stone, R. West (eds), Advances in Organometallic Chemistry, New York, 1979, pp. 61-103.

[23] Á. Martín, A. Navarrete, M.D. Bermejo, J. Supercrit. Fluid. 134 (2018) 141-149. https://doi.org/10.1016/j.supflu.2017.11.021

[24] H.Z. Wang, D.Y.C. Leung, M.K.H. Leung, M. Ni, Renew. Sust. Energ. Rev. 13 (2009) 845-853. https://doi.org/10.1016/j.rser.2008.02.009

[25] F. Jin, X. Zeng, Z. Jing, H. Enomoto, Ind. Eng. Chem. Res. 51 (2012) 9921-9937. https://doi.org/10.1021/ie202721q

[26] F. Jin, Y. Gao, Y. Jin, Y. Zhang, J. Cao, Z. Wei, R.L. Smith Jr, Energ. Environ. Sci. 4 (2011) 881-884. https://doi.org/10.1039/C0EE00661K

[27] M. Kutz, Environmentally conscious materials and chemicals processing, first ed, Wiley Online Library, (2007).

[28] A. Steinfeld, P. Kuhn, A. Reller, R. Palumbo, J. Murray, Y. Tamaura, Int. J. Hydrogen. Energ. 23 (1998) 767-774. https://doi.org/10.1016/S0360-3199(97)00135-3

[29] L. D'Souza, Mater. Renewable Sustainable Energy. 2 (2013) 7. https://doi.org/10.1007/s40243-013-0007-0

[30] Y.S. Cho, J.H. Kim, Int. J. Hydrogen Energy, 36 (2011) 8192-8202. https://doi.org/10.1016/j.ijhydene.2011.04.133

[31] S. Turn, C. Kinoshita, Z. Zhang, D. Ishimura, J. Zhou, Int. J. Hydrogen Eneqv. 23 (1998) 64-648. https://doi.org/10.1016/S0360-3199(97)00118-3

[32] H. Takahashi, L.H. Liu, Y. Yashiro, K. Ioku, G. Bignall, N. Yamasaki, T. Kori, J. Mater. Sci. 41 (2006) 1585-1589. https://doi.org/10.1007/s10853-006-4649-5

[33] H. Zhong, L. Wang, Y. Yang, R. He, Z. Jing, F. Jin, ACS Appl. Mater. Interfaces. 11 (2019) 42149-42155. https://doi.org/10.1021/acsami.9b14039

[34] C. He, G. Tian, Z. Liu, S. Feng, Org. Lett. 12 (2010) 649-651. https://doi.org/10.1021/ol9025414

[35] H. Zhong, H. Yao, J. Duo, G. Yao, F. Jin, Catal. Today 274 (2016) 28, doi: http://dx. doi.org/10.1016/j.cattod.2016.05.010.

[36] G. Yao, X. Zeng, Y. Jin, H. Zhong, J. Duo, F. Jin, Int. J. Hydrogen Energy. 40 (2015) 14284-14289. https://doi.org/10.1016/j.ijhydene.2015.04.073

[37] F. Jin, X. Zeng, J. Liu, Y. Jin, L. Wang, H. Zhong, G. Yao, Z. Huo, Sci. Rep. 4 (2014) 4503. https://doi.org/10.1038/srep04503

[38] D. Roman-Gonzalez, A. Moro, F. Burgoa, E. Pérez, A. Nieto-Márquez, Á. Martín, M.D. Bermejo, J. Supercrit. Fluids. 140 (2018) 320-328. https://doi.org/10.1016/j.supflu.2018.07.003

[39] M. Andérez-Fernández, E. Pérez, A. Martín, M. Bermejo, J. Supercrit. Fluids. (2017). https://doi.org/10.1016/j.supflu.2017.10.010

[40] T. Wang, D. Ren, Z. Huo, Z. Song, F. Jin, M. Chen, L. Chen, Green Chem. 19 (2017) 716-721. https://doi.org/10.1039/C6GC02866G

[41] Y. Zhu, Y. Yang, X. Wang, H. Zhong, F. Jin, Energy Sci. Eng. (2019). https://doi.org/10.1002/ese3.317

[42] J. Su, M. Lu, H. Lin, Green Chem. 17 (2015) 2769-2773. https://doi.org/10.1039/C5GC00397K

[43] Y.E. Kim, J.A. Lim, S.K. Jeong, Y.I. Yoon, S.T. Bae, S.C. Nam, Bull. Korean Chem. Soc. 34 (2013) 783-787. https://doi.org/10.1021/ef500561a

[44] I.N. Pulidindi, B.B. Kimchi, A. Gedanken, J. CO2 Util. 7 (2014) 19-22. https://doi.org/10.1016/j.jcou.2014.06.002

[45] C.K. Ahn, H.W. Lee, Y.S. Chang, K. Han, J.Y. Kim, C.H. Rhee, H.D. Chun, M.W. Lee, J.M. Park, Int. J. Greenhouse Gas Control. 5 (2011) 1606-1613. https://doi.org/10.1016/j.ijggc.2011.09.007

[46] G.B. Kauffman, J. Chem. Educ. 65 (1988) 28. https://doi.org/10.1021/ed065p28

[47] J. Su, L. Yang, M. Lu, H. Lin, ChemSusChem. 8 (2015) 813-816. https://doi.org/10.1002/cssc.201403251

[48] Z. Shen, Y. Zhang, F. Jin, Green Chem. 13 (2011) 820-823. https://doi.org/10.1039/C0GC00627K

[49] S. Rajagopal, M. Anwer, A. Spatola, Catalytic transfer hydrogenation and hydrogenolysis by formic acid and its salts, In: Basava C., Anantharamaiah G.M. (eds), Peptides, Birkhäuser Boston, 1994, pp. 11-26.

[50] R. Bennett, P. Ritchie, D. Roxburgh, J. Thomson, Trans. Faraday Soc. 49 (1953) 925-929. https://doi.org/10.1039/TF9534900925.

[51] R.W. McCabe, J. Catal. 79 (1983) 445-450. https://doi.org/10.1252/jcej.14we431

[52] S. Mukherjee, S.V. Devaguptapu, A. Sviripa, C.R. Lund, G. Wu, Appl. Catal., B, 226 (2018) 162-181. https://doi.org/10.1016/j.apcatb.2017.12.039

[53] D. Stockburger, J. Stannard, B. Rao, W. Kobasz, C. Tuck, On-line hydrogen generation from aluminum in an alkaline solution, In: Proc Symp Hydrogen Storage Mater Batteries Electrochem, New York, 1992, pp. 431-444.

[54] L. Soler, J. Macanas, M. Muñoz, J. Casado, Int. J. Hydrogen Energy, 32 (2007) 4702-4710. https://doi.org/10.1016/j.ijhydene.2007.06.019

[55] X. Huang, T. Gao, X. Pan, D. Wei, C. Lv, L. Qin, Y. Huang, J. Power Sources. 229 (2013) 133-140. https://doi.org/10.1016/j.jpowsour.2012.12.016

[56] R. Wiebe, V. Gaddy, C. Heinss Jr, Ind. Eng. Chem., 24 (1932) 823-825. https://doi.org/10.1021/ie50271a024

[57] T. Onoki, H. Takahashi, T. Kori, N. Yamasaki, T. Hashida, AIP Conf. Proc., American Institute of Physics, 2006, pp. 61-64. https://doi.org/10.1063/1.2207074

[58] P. Setiani, N. Watanabe, R.R. Sondari, N. Tsuchiya, Mater. Renewable Sustainable Energy, 7 (2018) 10. https://doi.org/10.1007/s40243-018-0118-8

[59] M. Ravichandran, A. Naveen Sait, V. Anandakrishnan, J. Mater. Res. 29 (2014) 1480-1487. https://doi.org/10.1557/jmr.2014.143

[60] H. Kwon, M. Leparoux, Nanotechnology, 23 (2012) 415701. https://doi.org/10.1088/0957-4484/23/41/415701

[61] Y. Liu, D. Ma, X. Han, X. Bao, W. Frandsen, D. Wang, D. Su, Mater. Lett. 62 (2008) 1297-1301. https://doi.org/10.1016/J.MATLET.2007.08.067

[62] R. Lafficher, M. Digne, F. Salvatori, M. Boualleg, D. Colson, F. Puel, Powder Technol. 320 (2017) 565-573. https://doi.org/10.1016/j.powtec.2017.07.080

[63] M. Reiche, M. Maciejewski, A. Baiker, Catal. Today, 56 (2000) 347-355. https://doi.org/10.1016/S0920-5861(99)00294-1

[64] H. Huang, X. Ye, H. Huang, L. Zhang, D.Y. Leung, Chem. Eng. J. 230 (2013) 73-79. https://doi.org/10.1016/j.cej.2013.06.035

[65] N.K. Nag, The J. Phys. Chem. B. 105 (2001) 5945-5949. https://doi.org/10.1021/jp004535q

[66] C.W.A. Chan, Y. Xie, N. Cailuo, K.M.K. Yu, J. Cookson, P. Bishop, S.C. Tsang, New environmentally friendly catalysts containing Pd–interstitial carbon made from Pd–glucose precursors for ultraselective hydrogenations in the liquid phase, Chem. Commun. 47 (2011) 7971-7973. https://doi.org/10.1039/C1CC12681D

[67] F. Manchester, A. San-Martin, J. Pitre, J. Phase Equilib. 15 (1994) 62-83. https://doi.org/10.1007/BF02667685

[68] G. Chen, W.-T. Chou, C.-t. Yeh, Appl. Catal. 8 (1983) 389-397. https://doi.org/10.1016/0166-9834(83)85009-X

[69] A. Aznarez, A. Gil, S. Korili, RSC Adv. 5 (2015) 82296-82309. https://doi.org/10.1039/C5RA15675K

[70] W. Juszczyk, Z. Karpiński, I. Ratajczykowa, Z. Stanasiuk, J. Zieliński, L.L. Sheu, W.M.H. Sachtler, J. Catal. 120 (1989) 68-77. https://doi.org/10.1016/0021-9517(89)90251-0

[71] B.D. Adams, A. Chen, Mater. Today. 14 (2011) 282-289. https://doi.org/10.1016/S1369-7021(11)70143-2

[72] R. Stumpf, Phys. Rev. Lett. 78 (1997) 4454. https://doi.org/10.1103/PhysRevLett.78.4454

[73] J. Graetz, Int. Sch. Res. Notices, 2012 (2012). https://doi.org/10.5402/2012/863025

CHAPTER 3

Assessment of selected catalysts and reducing metals for the simultaneous conversion of captured CO_2 and hydrogen generation

Abstract

The hydrothermal reduction of carbon dioxide dissolved in water in the form of carbamate has been studied using hydrogen released by metals. Different experiments have been carried out by mixing reducing metals such as aluminum, zinc, manganese and iron with different commercial catalysts: palladium, platinum and copper supported on activated carbon, and ruthenium supported on alumina, and raw activated carbon. From these experiments, the selectivity, conversion and yield have been calculated, showing aluminum and Pd/C as the best metal/catalyst system, with a yield of 15.61%, selectivity of 27.8%, and a conversion of 55.42%. The hydrogen generated is a value-added chemical of great interest given its wide market and demand nowadays. Therefore, in this chapter the hydrogen generation in different basic hydrothermal medias (aqueous solutions of ammonium carbamate, sodium bicarbonate and ammonia) was studied, and it was analyzed the hydrogen and pressure evolution during 10 h. Aluminum Spall, from BEFESA company, showed potential to be used as cheap reducing agent in the conversion of captured CO_2. The increase of size of the metal (Al) showed a detriment effect over FA yield. The type of hydrogen produced fall into the category of green, when no CO_2 was released, and blue when the captured CO_2 formed metal carbonates in the solid byproduct, determined by XRD analyses. Other techniques like N_2-absorption isotherms (area BET) and SEM-BSE analyses were performed to characterize the solid samples. Among the metals, Zn showed the best performance toward H_2 yield, up to 63.7% in 10 h under aqueous AC solution as CO2RS.

Keywords: *Catalysts screening, hydrogen evolution, formic acid production, metal-water splitting*

CHAPTER 3

Introduction

Current changes in worldwide economic scenario, as a product of the reactivation endeavors in post-covid era, are challenging the achievement of the past-decades objectives of cutting the CO_2 emissions and reducing oil and natural gas dependency. The increase of demand of fossil fuels to 2040 can increase to 30% [1], and the necessity of mitigating the subsequent CO_2 emissions is still on the table. In this context, one successful carbon capture and storage (CCS) technology is based on the absorption of CO_2 with aqueous solutions of ammonia (generally known as CO_2 Capture-Solvent Lean stream (CO2LS) for any basic dissolution) in absorber/stripper columns, yielding a CO_2-Rich stream (CO2RS) containing an equilibria of ammonia bicarbonate, carbonate and carbamate [2][3]. Other techniques have been proposed to capture CO_2, such as chemical looping combustion (CLC), which is a method to capture CO_2 produced from the combustion of fossil fuels and requires the use of two-phase membranes to achieve high CO_2 capture and separation from the gas stream [4][5]. Once captured, CO_2 is stored in depleted oil and gas fields, in deep saline aquifer formations and in deep coal seams that cannot be mined anymore and are widely distributed around the world in all sedimentary basins, usually several kilometers below the earth's surface [3]. To store CO_2, it must be transported from the production site to the place of storage or use. CO_2 is transported via gas pipelines, ships or trains, depending on how economical the means of transport are [6].

In addition to capturing and storing CO_2, there are different CO_2 utilization approaches, framed in the so-called *CO_2-Economy*. In the first place, it can be used directly without no chemical conversion in applications such as refrigerant (supercritical state), in food and beverages, as fire extinguisher, in concrete materials, in oil wells, medicine, etc [7]. In the second place, its indirect utilization implies the chemical transformation into other final complex products, such as useful chemicals and fuels [8-10]. CO_2-derived fuels with high energy density are gaining more attention as energy vectors for fulfilling the energy storage demands [11], where formic acid (FA), methane and methanol are prominent [12-14].

CHAPTER 3

Hydrothermal catalytic reduction of captured CO_2 using reducing metals is one of the methods to obtain formic acid that remains on the research focus [15][16]. In our most recent work, the endeavors laid the implementation of milder reactions conditions for ammonia-based CO_2 absorption derivatives, while contrasting its performance toward more common substrates like sodium bicarbonate, using commercial Pd 5 wt% over activated carbon catalyst (Pd5AC) [17]. Likewise, catalytic metals like ruthenium displayed high efficiency in reducing CO_2 to formate when supported on alumina or activated carbon, using sodium bicarbonate as a source of CO_2, at 80°C, 5 MPa of H_2 and a reaction time of one hour [18]. This study concluded that the optimum ruthenium content is 2% because higher ruthenium percentages reduce its Turnover Number (TON). Not many antecedents are available for Pt based catalyst in the reduction of captured CO_2 with reducing metals, though abundant reports are for electrochemical and photocatalytical conversion of CO_2 [19-22]. However, the reduction of captured CO_2 by Pt based catalyst into formate has been proved with glycerol as reducing agent [23]. Several works have attempted the reduction of captured CO_2 with Cu based catalyst and organic reductants. In the report of Wang *et al* [24], $Pd_{0.5}Cu_{0.5}$/C catalyst was synthesized for the reduction of bicarbonate with methanol into formate with 68% production efficiency, while Huo *et al.* reduced bicarbonate to methanol at temperatures as high as 350ºC using Zn as reductant and Cu as catalyst. In this work, the methanol yield increased consequently with the addition of different amounts of Cu [25]. Other advances have been recently accomplished with homogeneous catalysts containing Ru, Rh or Ir [26][27], displaying high selectivity and yield to formate, even at mild conditions, but still dealing with several drawbacks when facing industrial scale up, concerning its separation and recyclability [28].

On the other hand, metals used as reductants for CO_2 hydrogenation are of great interest not only because they are utilized as *in situ* reducing agent, but also because they generate itself molecular hydrogen by the metal water-splitting reaction, that is favored under alkaline conditions [29]. The byproducts generated from this reaction are hydroxides and metal oxides, which are of great interest in the construction, water treatment and catalysis industry. For aluminum, the production of alumina from boehmite is well known [30]; zinc hydroxide is used as a precursor for the preparation of catalysts

and other zinc-requiring compounds [31]; iron oxide is used in the preparation of catalysts, especially those that use it as a magnetic material for their preparation, for reddish color paints, in medicine to treat hemoglobin problems, among others [32]. Most hydroxides are to be used in water treatment to remove phosphates from wastewater due to their excellent adsorption capacities, good reaction kinetics and selectivity [33]. However, at the light of a circular-economy and zero-emissions practice, in the field of CO_2 hydrogenation it would make more sense to reduce these oxidated byproducts back to the zero-valent metals for reutilization, in a process driven by solar power [34]. In this process, the hydrogen produced from water can be categorized as green, if using renewable energy sources in the process without carbon emissions (green) [35].

It is clear that the reduction of captured CO_2 as bicarbonate using reducing metals like Mn, Al and Zn, have shown effectiveness, displaying yields up to 81% and 2 h [36][12]. Despite these works, not much literature is available about the comparison of different supported metal catalysts, reducing metals and CO2RS/CO2LS streams on the simultaneous reduction of captured CO_2 from the ammonia-based process and hydrogen generation from metal-water splitting reaction.

The present study aims at two main objectives: i) evaluating different types of commercial catalyst in the reduction of captured CO_2 in aqueous ammonia, where the hydrogen needed is generated by a metal-water splitting reaction *in situ*, conforming a metal/catalyst system. ii) Studying the generation of hydrogen with the different metal/catalyst systems and CO2RS/CO2LS, by means of a pressure and hydrogen evolution analysis for 10 hours. These studies are important because allow stablishing a screening of different possible catalysts for the reduction process, while understanding the influence of the reaction media on the hydrogen generation. These results will feed a potential integration of carbon capture process and the green hydrogen production in the frame CO_2 and hydrogen economies. This assessment allowed determining the most active catalyst and metals for CO_2 reduction and H_2 generation *in situ*, while the solids byproducts were analyzed based on a thorough characterization.

CHAPTER 3

Materials and methods

Chemicals

Ammonium carbamate (AC) (99%), and sodium bicarbonate (SB) (100%) were used as carbon source. Fine powder of commercial Pd/C catalyst of 5 wt% (Pd5AC), Cu/C catalyst of 3 wt% (Cu3C), Pt/C catalyst of 5 wt% (Pt5AC) and Ru/Al_2O_3 catalyst of 5 wt% (Ru5Alu) were used as received. The reducing metals used were aluminum powder (Al) (<5 µm, 99.5%), granular aluminum (<1 mm, 99.7% trace metals basis, Sigma-Aldrich), Aluminum spall residue, zinc powder (Zn) (<5 µm, 99.5%), Iron powder (Fe) (≥99%), manganese powder (Mn) (<5 µm, ≥99%). Activated charcoal RX3-Extra (Norit) was used for catalyst support blank experiments. All reagents, except aluminum powder (Panreac) and sodium bicarbonate (COFARCAS-Spain), were purchased from Sigma-Aldrich. Granular aluminum (<1 mm, 99.7% trace metals basis, Sigma-Aldrich) and aluminum spall (provided by BEFESA company) were sieved into 500 µm size, and employed as reactants without any other treatment.

Experiments for catalysts assessment

The comparison of the different metals as hydrogen generators from water, as well as the evaluation of the different catalyst for the capture CO_2 conversion were carried out in batch using a Parr Instruments stainless steel reactor (25 mL Micro Stirred Reactors Series 4791, maximum pressure 200 bar, maximum temperature 350 °C) with stirring at 700 rpm, autogenous pressure and ramp heating of 14 °C/min using a band heater. Before each run, metal and catalyst system were weighed. Ammonium carbamate was weighed and diluted in water so that its initial concentration was 0.5 mol/L. Once the reactor was sealed, a gentle flow of nitrogen was passed through the headspace to purge the remaining air out of the system, followed by heating up, at 14 ºC/min, to a constant temperature of 120 °C. Once reached, reaction proceeded for 2 h. After the reaction, the vessel was quickly immersed in a cold-water bath. For the catalytic experiments conditions were fixed at 6 moles of

reducing metal per carbamate mole, 3.8 mmol of catalyst metal (for a comparison basis of metals Pd, Ru, Pt and Cu) per mole of carbamate, and 70% of the volume of the reactor filling at room temperature.

Experiments for hydrogen generation

In order to see how affects the use of both CO2RS and CO2LS in the batch hydrogen generation experiments of hydrogen release were conducted for 10 h at 120 ºC, using 24 mmol of Al and Zn, separately, in 0.5 mol/L aqueous solution of carbamate (initial pH=9.2), sodium bicarbonate (initial pH=10.1) (as CO2RS), and NH_3 (as CO2LS) in the same Parr reactor. Gas samples were taken in intervals of 2 h, using Tedlar® bags, to quantify the hydrogen concentration by GC-TCD. In these experiments a reduced liquid filling volume percentage of 35% was employed to avoid draining out of liquid and solids at the moment of the gas sampling due to the depressurization.

Products characterization

Liquids

Once the reactor was cooled down, the liquid sample was collected and filtered through a 0.22 mm filter. For quantifying formic acid (FA), carbamate and sodium bicarbonate concentrations the liquid samples were analyzed by HPLC (Waters, Alliance separation module e2695) using an RAZEX™ ROA-Organic Acid H+ column with RI detector (Waters, 2414 module). The mobile phase was 25 mM H_2SO_4 with a flow rate of 0.5 mL/min. The temperatures of the column and the detector were 40 °C and 30 °C, respectively. The yield and selectivity to formic acid, as well as conversion of the carbamate were calculated as shown in equations 1 to 3:

$$Y_{FA} = \frac{C_{FA,f}}{C_{cs,i}} x100 \quad (1)$$

$$X_{CS} = \frac{C_{cs,f} - C_{cs,i}}{Ccs,i} x100 \quad (2)$$

$$S_{FA} = \frac{Y_{FA}}{X_{CS}} x100 \quad (3)$$

$$TON = \frac{nHCOOH}{ncatalyst_{metal} * Metal\_dispersion} x100 \quad (4)$$

Where Y_{FA} is the yield of formic acid, X_{CS} is the conversion of carbamate, S_{FA} is the selectivity of formic acid, $C_{FA,f}$ is the final molar concentration of formic acid, $C_{CS,i}$ is the initial molar concentration of carbon source and $C_{CS,f}$ is the final molar concentration of carbon source and. TON (4) is the Turnover Number, calculated as the number of moles of formate ($nHCOOH$) that can be converted by one mole of surface active metal site of the catalyst ($ncatalyst\_metal * Metal\_dispersion$) [37]. For the Pd5AC Sigma Aldrich catalyst the metal dispersion (23.3%) was reported elsewhere [38].

Solids

The solid byproducts of the reactions comprise the mixture of exhausted metal and catalyst, which cannot be separated by conventional methods. They were characterized by X-ray diffraction (XRD). Before analysis, the samples were dried in an oven under vacuum overnight at 45 °C, to remove the remaining moisture. A BRUKER D8 DISCOVER A25 equipment was used, with 3 kW Generator, 2.2 kW type FFF Cu-ceramic tube, LynxEye Detector, operating at 40 kV and 30 mA. The database used for identifying the phases was the PDF-2 Released 2013 (ICDD). Textural properties analysis of the solids after reaction were conducted in an ASAP 2420 equipment with nitrogen adsorption at 77 K, all samples were degassed prior to each analysis. The surface area was determined by the BET method, and the pore size and volume by BJH method. SEM micrographs observations were conducted over the solid byproduct after CO_2 reduction experiments, comprising a mixture of exhausted metal and catalyst, in order to determine the morphology and surface particle changes. For this, a Quanta 200FEG ESEM (Environmental Scanning Electron Microscope) equipment was used, operating at 20kV. The samples were coated with gold in a K575 sputter coater, and the images generated with a BSED detector.

Gases

Pressure was registered by a Picotech instrument-Technology ADC-20 & TERM, attached to a pressure transducer Desin TPR-20 (error ± 2 bar). With this information, the amount of mol of hydrogen produced ($n\mathrm{H2}$) were calculated using equations 5 and 6:

$$n\mathrm{H2} = \frac{P_{s,f} * V_{s,f}}{R * T_{s,f}} * xH2 \quad (5)$$

$$V_{s,f} = V_{s,t} - V_{s,l} \quad (6)$$

Where, $P_{s,f}$ is the final absolute pressure; $T_{s,f}$ is the temperature; $V_{s,f}$ is the final overhead volume; $V_{s,t}$ is the total volume of the reaction system; $V_{s,l}$ is the final volume of liquid collected; R is the ideal gas constant (83.14472 L*mbar*K^{-1}*mol^{-1}); *xH2* is the fractional molar composition of hydrogen, measured by a GC-TCD Varian 4900 equipment, using Molsieve 5A-10m and Poraplot Q -10m columns. Then, the molar yield of hydrogen ($Y\mathrm{H2}$) is calculated as shown in eq. 6.

$$Y\mathrm{H2} = \frac{n\mathrm{H2}}{n\mathrm{M}} * 100 \quad (6)$$

Where, $n\mathrm{H2}$ is the number of mol of hydrogen produced; $n\mathrm{M}$ is the number of mol of metal used. The catalytical experiments of CO_2 reduction were duplicated in order to stablish the experimental error.

CHAPTER 3

RESULTS AND DISCUSSION

Screening of catalyst for the reduction of captured CO_2

Fig. 1 plots the yield, conversion and selectivity of FA and final reactor pressure as a function of the catalyst and metal type, at 120 ºC and 2 h. Only Pd5AC catalyst showed activity toward FA formation, up to 15.4 ± 2.1% and TON=175 when using Al as reductant, followed by Mn (5±0.5%) (TON=57), Fe (4.6±1.5%) (TON=54) and Zn (2.2± 0.3%) (TON=24). Su *et al* conducted similar experiments with carbamate in ethanol, but under high pressure (2.75MPa) of molecular hydrogen during 1 h reaction in anhydrous ethanol at 20 ºC and 1 hour reaction, where Ru and Pt 5% over AC were nearly inactive, and Pd5AC was the catalyst with the best performance [38]. Comparatively, for a similar TON=162 (FA yield of 17.6%) Su *et al* used high pressure of molecular hydrogen (2.75MPa) and ethanol 30%. The benefits where the decrease in temperature (20 ºC) and time (1 h). This means that intake of ethanol and hydrogen as expensive raw materials can be compensated by a cheaper reductant like aluminum (preferably from residues for economic feasibility) and mild temperature, with the possibility of generating value added green hydrogen. In the work of Jin *et al* [12] aluminum, as reducing metal, also had the highest relative efficiency, against Zn, Mn and Fe, for hydrothermally converting bicarbonate into formate. In the case of Cu_3C, it is more likely to produce methanol from carbon dioxide in a two-step process, first producing formic acid, and then converting it to methanol under hydrothermal conditions [39]. Perhaps, more severe reaction conditions (temperature, time, wt % catalyst, pressure) to see activity of the tested Pt, Cu and Ru catalysts toward capture CO_2 reduction would be necessary. Hence the mild reaction conditions worked only for Pd5AC.

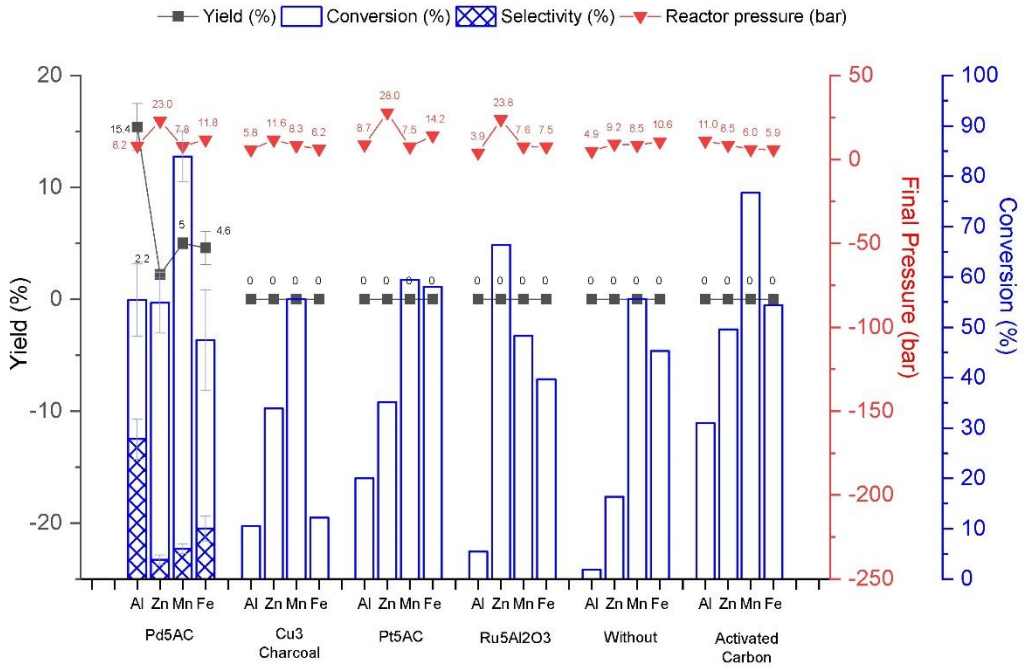

Fig. 1. Catalytical performance of different metal/catalyst systems in terms of FA yield, AC conversion and final pressure of reactor. Reaction conditions: 2 h, metal:carbamate molar ratio of 6, catalyst metal:carbamate molar ratio of 3.8 mmol, 70% of filling and 0.5 M of initial concentration.

The resulting yield of the system Al/Pd5AC is about 5% lesser compared to our previous publication (c.a. 20%) [17], under the same conditions of 120 ºC, 2 h, Al:AC molar ratio of 6 and 70% volume filling, because, in the present work, it was used lesser amount of catalyst metal (Pd) of 3.8 mmol (or 10% total catalyst with respect to carbamate), instead of 5.5 mmol (or 15% total catalyst with respect to carbamate). The metal that has the highest selectivity with respect to formic acid is Al, with a selectivity of 27.8%, followed by Fe (10%), Mn (6%) and Zn (4%). On the other hand, the highest conversion of carbamate in the presence of Pd5AC was achieved with Mn (84%), while Al and Zn had similar conversion (55.4% and 54.9%, respectively), followed by Fe (conversion of 47.4%). With most of the catalysts, except Ru5Al, Mn showed the highest conversion. Interestingly, it can be observed that the conversion with Al never surpassed 20% (Pt5AC), except for Pd5AC (c.a. 60%), because the CO_2 reduction to FA formation was the highest.

Analysis of FA and H_2 yield in presence and absence of catalysts

Based on final reactor's pressure presented in Fig. 1, it is clear that, among the metals, Zn had always the highest value, up to 28 bars (with Pt5AC), where it seems that all catalysts accelerated the gas release from the reaction solution, if compared to the pressure without catalyst (up to 10.6 bar, with Fe) and with active carbon (up to 11 bar, with Al). Fig. 2 presents the comparison of FA and hydrogen for all metals and catalysts combinations, where Zn, accordingly to pressure evolution aforementioned, had the highest H_2 yield of up to 26% with Pt5AC, and 20% with Pd5AC, while aluminum showed 7.3 and 7.4% with activated carbon and catalyst Pd5AC, respectively. This indicates that the carbonaceous supports may play a role in the H_2 generation, where the metal powder could be dispersed onto the support's surface area (highest value for Pt5AC of 1490.6 m^2/g), thus increasing the contact area between metal and water. To support this state, a different support, such as alumina support (low surface area 168.6 m^2/g), did not promoted H_2 generation (less than 0.1% with $Ru5Al_2O_3$).

It draws attention that with the combination Al/Pd5AC the FA yield was higher than with Zn/Pd5AC, given that it was demonstrated that with Zn the H_2 yield is much higher. This can be explained on the light of the textural properties results of each metal/catalyst residue after reaction, considering that the mixture of these solids may have structural consequences, specially over the textural features of the catalyst. Firstly, it must be taken into account that the surface area of Pd5AC catalyst before reaction is 948 m^2/g (a typical value for the activated carbon support), and that for Al and Zn powder before reaction is 0.11 and 0.24 m^2/g, respectively (i.e., they do not contribute to the final total surface area of the Metal/Pd5AC solid) (see Table 1). Then, the surface area of Al/Pd5AC (After Reaction) and Zn/Pd5AC (After Reaction) was reduced to 91 and 26 m^2/g, respectively, showing that there is a significant loss of catalyst's surface area, being of major magnitude for Zn than for Al. A pore collapse was noted as well, with a volume reduction from 0.7 cm^3/g of Pd5AC before reaction to 0.03-0.06 cm^3/g after reaction with Zn and Al, respectively. This indicates that Al/Pd5AC system has i) greater availability of catalytic active sites per surface area during the reaction, and ii) minor blockage of H_2

mobility/diffusion and adsorption on the metallic Pd active sites to form the Pd-hydride species (PdH_x) responsible of the reduction of HCO_3^- [17], thus reflecting a greater FA yield and selectivity.

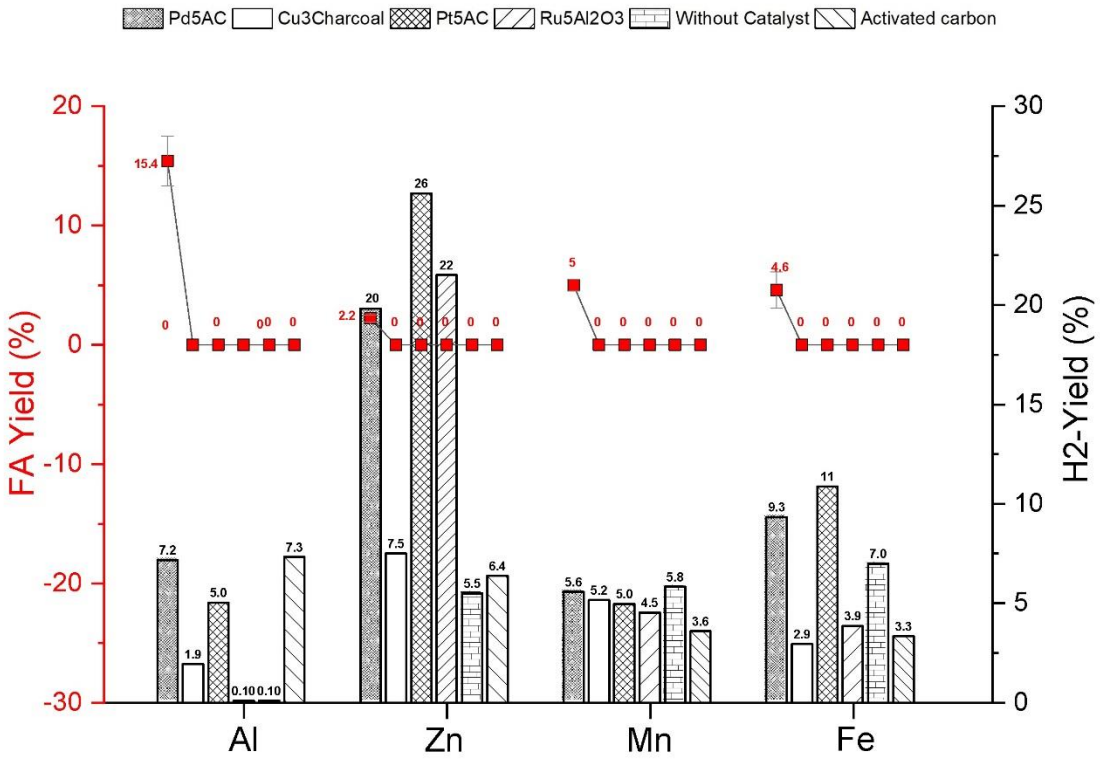

Fig. 2. FA and H_2 yields for the different metal-catalyst systems. Reaction conditions: 2 h, metal:carbamate molar ratio of 6, catalyst metal:carbamate molar ratio of 3.8 mmol, 70% of filling and 0.5 M of initial concentration.

Table 1. Textural properties of solids before and after reaction

Sample	**Surface area (m^2/g)**	**Pore volume (cm^3/g)**	**Pore size (Å)**
Before reaction	948.96	0.70	29.57
Pd5AC			
Cu3C	1234.71	0.99	32.05
Pt5AC	1490.63	1.22	32.74
Ru5Alu	168.58	0.15	36.11

Al powder	0.12	0.00	240.88
Zn powder	0.24	0.00	77.10
Mn powder	0.20	0.00	82.61
Fe powder	0.32	0.00	49.78
After reaction			
Residue of Al/Pd5AC	91.64	0.06	27.82
Residue Zn/Pd5AC	26.14	0.03	40.98

Effect of Al particle size and Al spall usage on the FA yield and selectivity

In Fig. 3, the effect of varying the particle size of reducing agent Al on FA yield and selectivity was investigated. 5 and 500 µm Al particles were employed, obtained by sieving granular aluminum (<1 mm), without further pretreatment. Additionally, an Al spall residue from BEFESA company, was also sieved with a final particle size in the range 500-800 µm, owing that the material presented a distribution of irregular geometries, mostly with a curly shape (see Fig. 4) that difficult the sieving, in contrast to the regular and round shape of Al 500 µm. The results for pure aluminum shows that FA yield decreased to 6% with larger particle size of 500 µm, while sustaining the selectivity toward FA formation (about 30%). Similarly, when testing the Al Spall 500 µm the FA yield decayed to 2.5%, attributed to stirring problems given the irregular geometry of the chips (see Fig. 4.). Nevertheless, this residue proved a potential to be used as cheap reducing agent in the conversion of capture CO_2, and hydrogen generation.

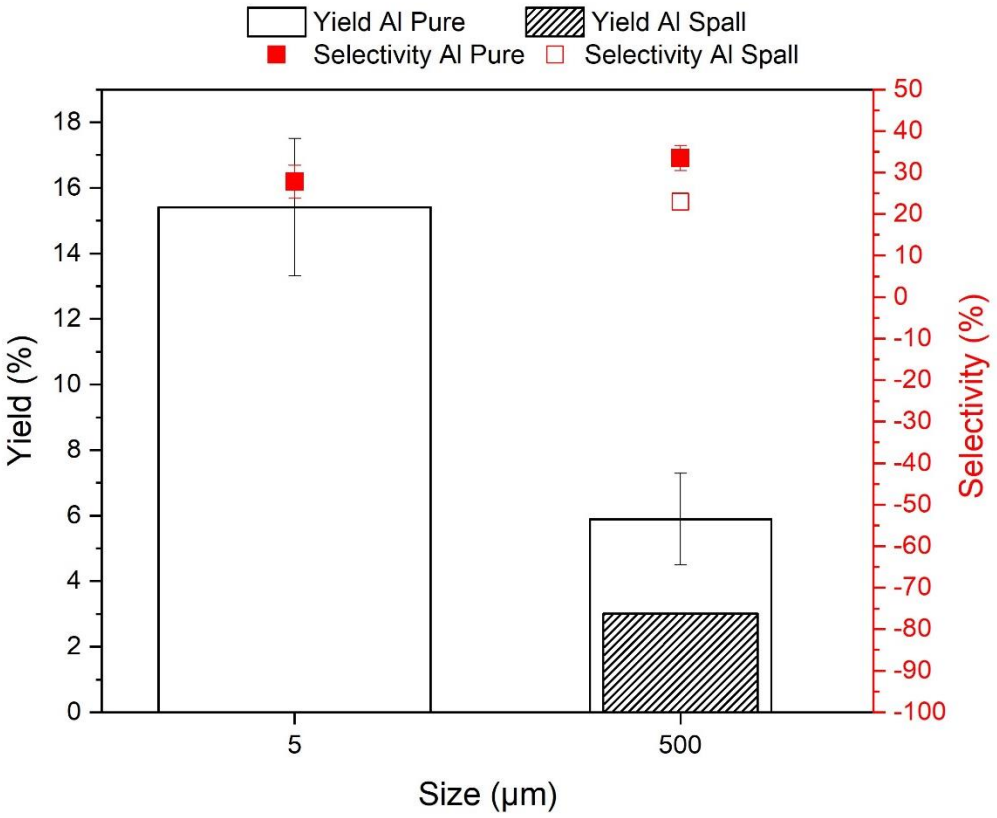

Fig. 3. FA yield as function of particle size of pure Al and Al spall residue. Reaction conditions: 2 h, metal:carbamate molar ratio of 6, catalyst metal:carbamate molar ratio of 3.8 mmol, 70% of filling and 0.5 M of initial concentration.

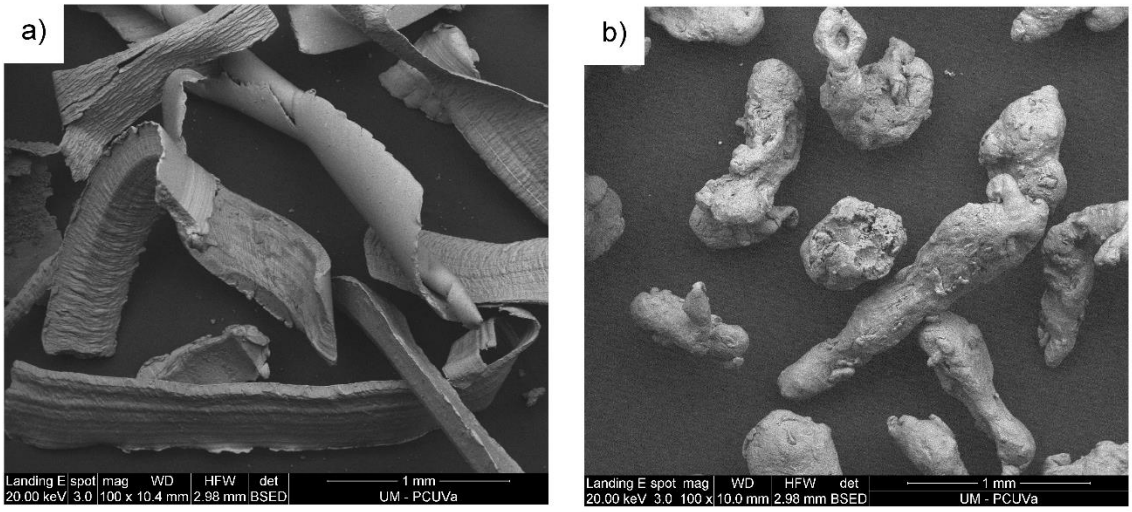

Fig. 4. Morphology of a) Al Spall chips 500 μm, and b) pure Al 500 μm

Hydrogen evolution analysis of Al and Zn under CO2RS and CO2LS

Given the remarkable performance Al showed for FA generation, and Zn in H_2 release, they were considered for further analysis of H_2 evolution during 10 h under CO_2-Rich stream (CO2RS) (aqueous AC and SB, 0.5 mol/L), and CO_2 Capture-Solvent Lean stream (CO2LS) (aqueous NH_3, 0.5 mol/L), in absence of catalyst. For these experiments, the Fig. 5 depicts the pressure evolution in the reactor, where the peaks observed correspond to the expected depressurization provoked by the gas samplings. In general, Zn presented faster H_2 generation rates under both solvent types at all times, and even after every sampling moment the pressure immediately started to recover, in contrast to Al that showed almost a flat behavior except for SB. For Al under aqueous SB (Fig. 5 (b)), the final pressure at 10 h (7.6 bar and H2 yield=25.1%) was higher than for Zn (6.4 bar and H2 yield=61.3%), because the gas sampling for at 8 h for Al was missed. In terms of H_2 yield of Zn for AC and SB (see Fig. 6 a)) there was not a significant difference because the yield at 10 h was 63.7 and 61.3%, respectively, while NH_3 had the lowest impact with 49.4% (Fig. 6 b)). The activation of Al in general was slower, at 2 h the yield was almost null for both AC and SB (0.1%) and started to be significant at hour 6 with SB (11%). When comparing at 10 h the system Al+SB (25.1 % H_2) and Al+AC (0.4 % H_2) is worth noting the significant promotion of SB. From the chapter 2 [17], it could also be observed a better result for SB compared to AC in the production of FA at increased temperature of 250 ºC, where it seems that Pd5AC and aluminum powder conformed a good catalytic system for the reduction of SB. From these observations, it can be concluded that i) SB responds better than AC to the increments of operation time and temperature toward FA and H_2 generation, ii) Al requires a stronger base (such as SB) for activating H2 generation, and iii) AC and NH_3, as a potential CO2RS for H_2 generation, can be accompanied by a more active metal, such as Zn.

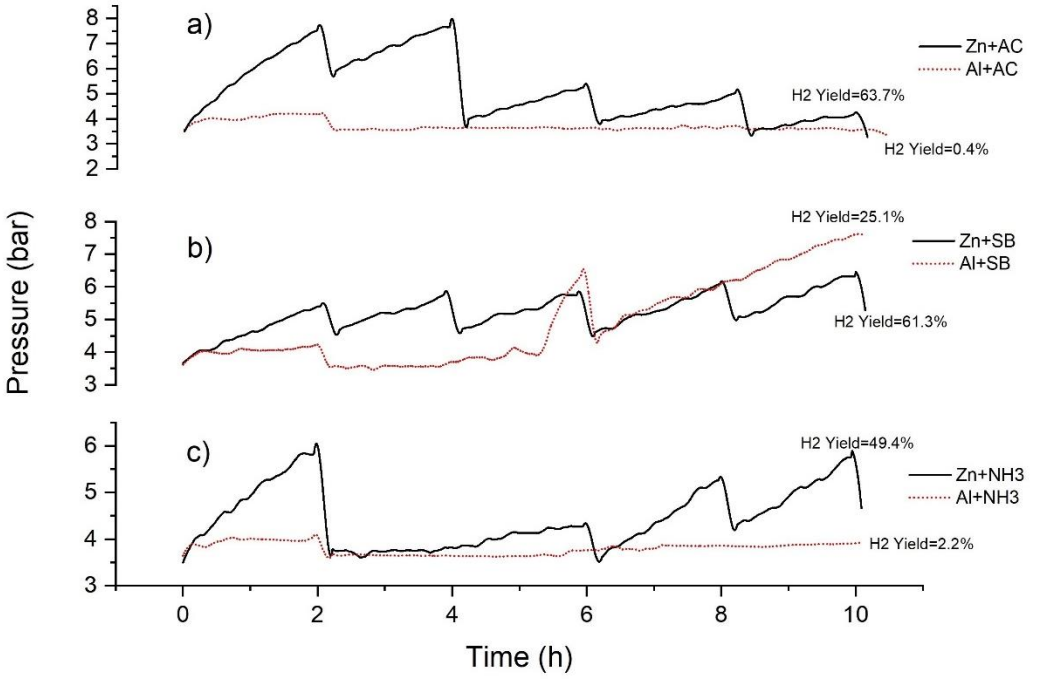

Fig. 5. Reactor's pressure evolution during 10 hours of hydrogen generation experiments at 120 ºC using Al & Zn under aqueous AC and SB as CO2RS (a and b respectively), and NH_3 as CO2LS (c).

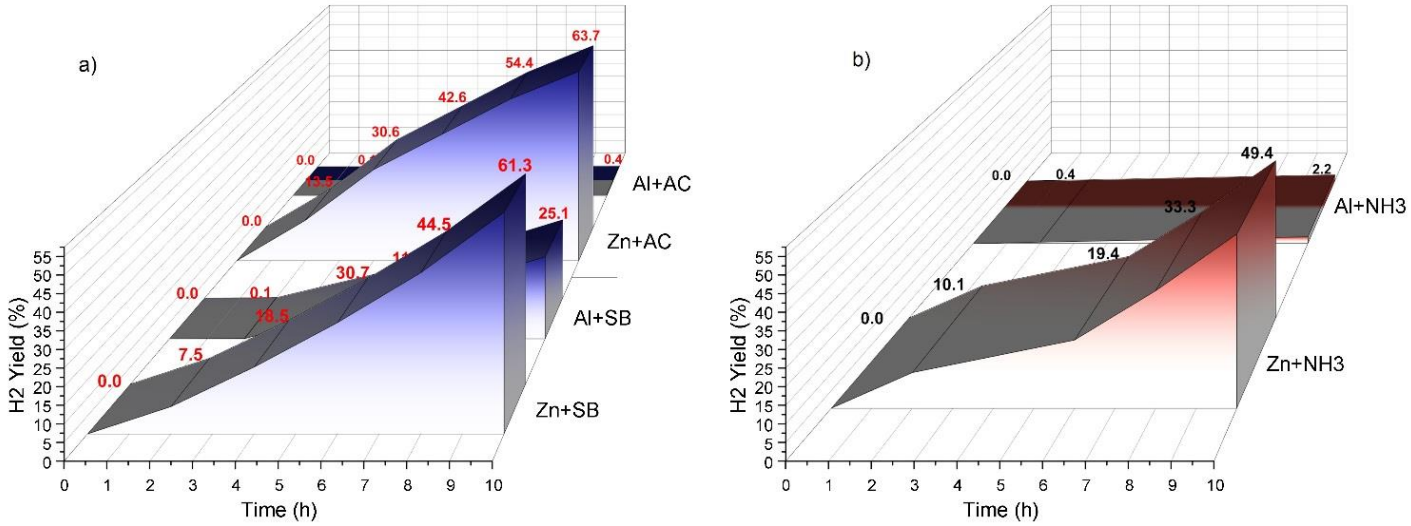

Fig. 6. H_2 evolution using Al and Zn during 10 hours experiments at 120 ºC under selected a) CO2RS (aqueous AC and SB respectively) and b) CO2LS (aqueous NH_3).

XRD results

The solid residue after reactions with the different metals, under catalyst Pd5AC, were characterized by XRD to determine oxidized by-products. Fig. 7 shows remaining unreacted elementary metals (Al, Zn, Mn and Fe) along with a mixture of oxides and hydroxides. Carbonates formation is detected for Al, Zn and Mn, suggesting that part of the conversion of the carbamate is due to this formation. From this, can be concluded that i) a complete conversion of the elementary metals is difficult to achieve it in 2 h, under the reaction conditions studied, and ii) reducing metals can react with the CO2RS, taking place an intake of CO_2 to form carbonates, while generating hydrogen that may falls into the definition of blue hydrogen since the carbon is not emitted but re-captured as carbonate.

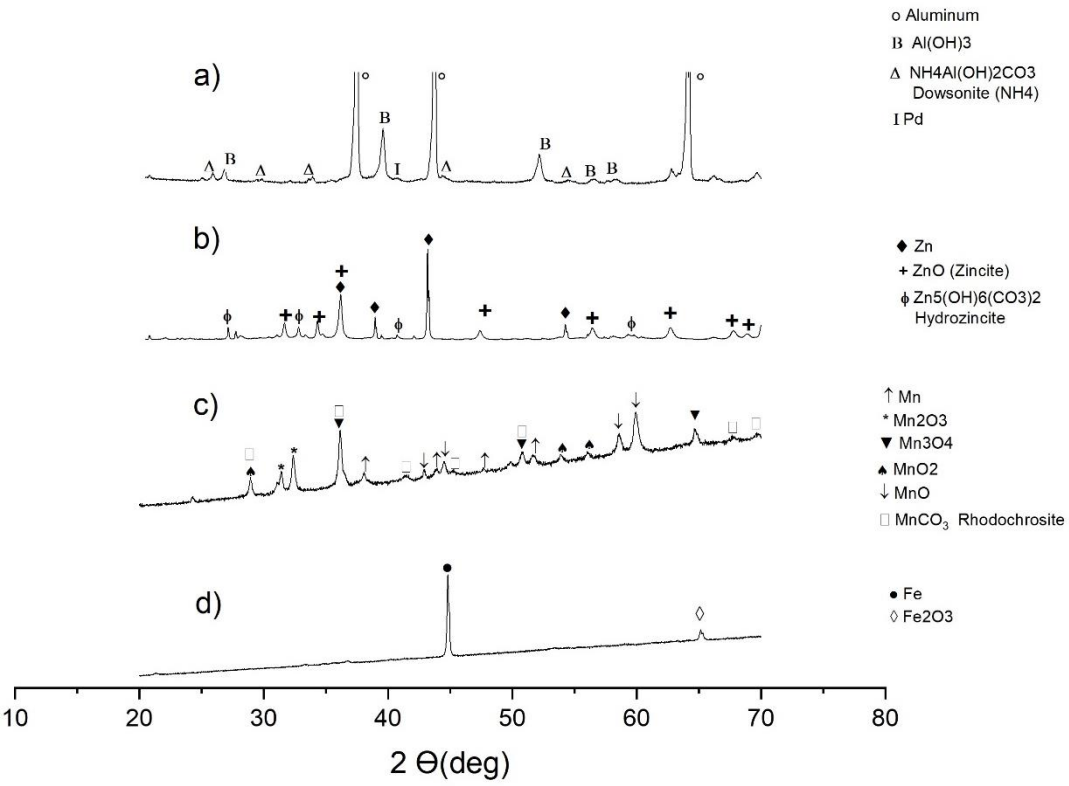

Fig. 7. XRD diffractograms of solid residue after reaction with catalyst Pd5AC and metals a) Al, b) Zn, c) Mn and d) Fe. Reaction conditions: 120 ºC, 2 h, metal:carbamate molar ratio of 6, catalyst metal:carbamate molar ratio of 3.8 mmol, 70% of filling and 0.5 M of initial concentration.

SEM Observations

The solid samples of reactions that presented FA formation were surface characterized by SEM-BSE. In this technique, the intensity of the backscattered-electrons (BSE) correlates with larger atoms (greater weight and atomic number Z), appearing as brighter areas, while dark areas are smaller atoms with lower number [40]. In Fig. 8 a), a smooth and bright layer appear covering the surface of unreacted elementary aluminum (round shape), ascribable to aluminum hydroxides and carbonates, detected by XRD. Fig. 8 b) reflects the high degree of oxidation of pure zinc to form ZnO (lighter areas), by the appearance of crystalline microestructures with needle like shapes. The globular darker shapes can be ascribed to carbon support, and unreacted metal. Fig. 8 c) also reflects the high degree of Mn exhausting/oxidation with different oxidative states, appearing as lighter areas in the form of flake-like shapes. Small crystalline filaments appear in the oxidation of Fe (Fig. 8 d)).

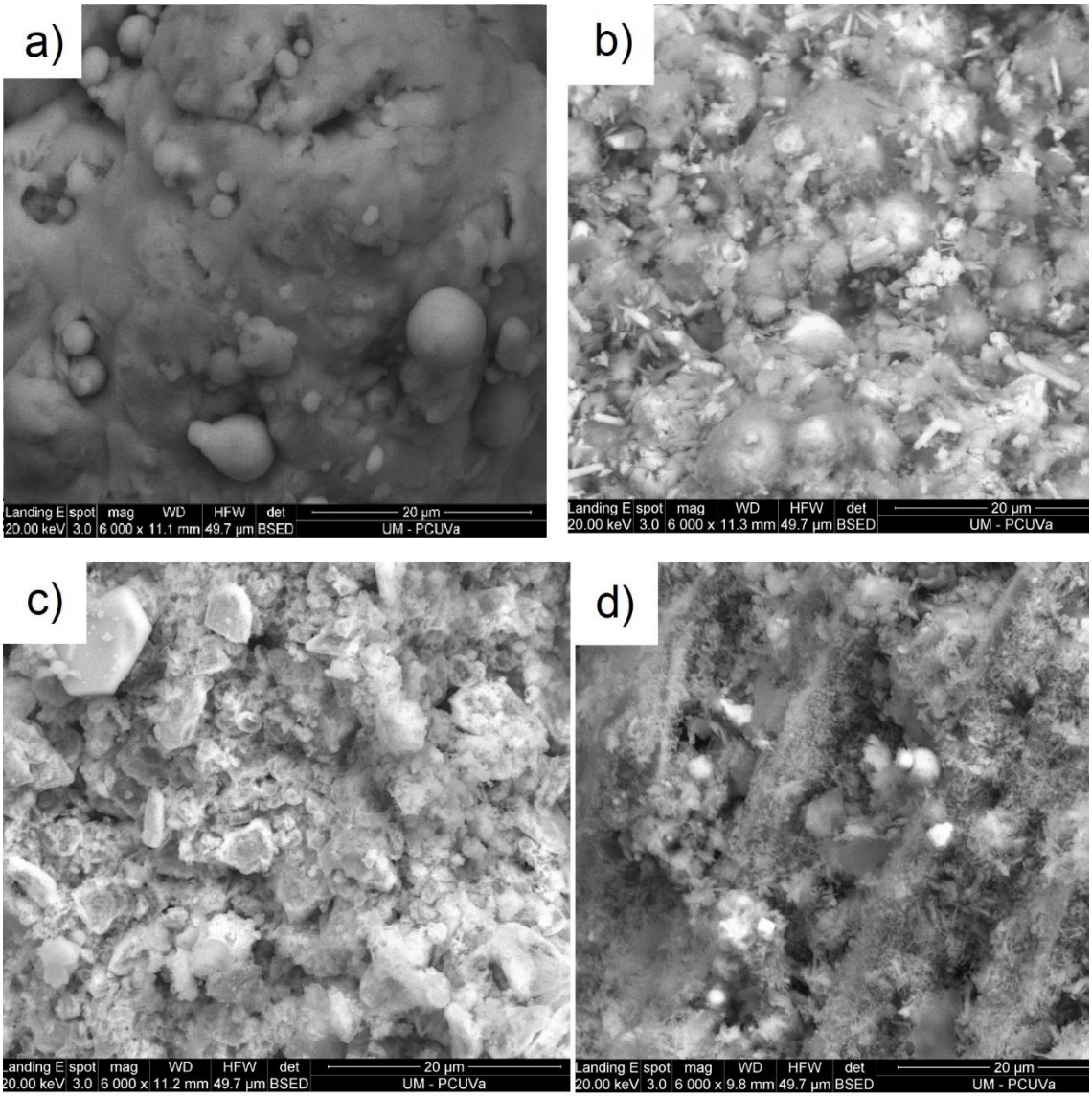

Fig. 8. Micrographs of solid residues after reduction with powder of a) Al, b) Zn, c) Mn and d) Fe

CHAPTER 3

Conclusions

Through the present chapter it was confirmed that, among selected catalyst, the Pd5AC displays the best performance toward FA production from captured CO_2 in aqueous ammonia. Among the metals. Aluminum was the most efficient for FA production given its lower affectation to the textural features of the catalyst in the solid mixing. However, in terms of hydrogen generation, zinc presents the best performance with H_2 yield up to 63.7% in 10 h under aqueous AC solution as CO2RS. Aluminum Spall, from BEFESA company, showed potential to be used as cheap reducing agent in the conversion of captured CO_2. The increase of size of the metal (Al) showed a detriment effect over FA yield. The present study suggests that both CO_2 Capture-Solvent Lean stream (CO2LS), and CO_2-Rich stream (CO2RS) are potential hydrothermal media for formic acid production and hydrogen generation, which are value-added chemicals with promising markets in the short term. This represents a potential integration of carbon capture utilization and storage (CCUS) with the hydrogen production in the frame CO_2 and hydrogen economies.

REFERENCES

[1] M. F. Bashir, “Oil price shocks, stock market returns, and volatility spillovers: a bibliometric analysis and its implications,” *Environ. Sci. Pollut. Res.*, pp. 1–20, 2022.

[2] H. Yu *et al.*, “Results from trialling aqueous ammonia-based post-combustion capture in a pilot plant at Munmorah Power Station: Gas purity and solid precipitation in the stripper,” *Int. J. Greenh. Gas Control*, vol. 10, pp. 15–25, 2012.

[3] F. Nocito and A. Dibenedetto, “Atmospheric CO2 mitigation technologies: carbon capture utilization and storage,” *Current Opinion in Green and Sustainable Chemistry*, vol. 21. Elsevier B.V., pp. 34–43, Feb. 2020, doi: 10.1016/j.cogsc.2019.10.002.

[4] H. A. Alalwan and A. H. Alminshid, “CO2 capturing methods: Chemical looping combustion (CLC) as a promising technique,” *Science of the Total Environment*, vol. 788. Elsevier B.V., Sep. 2021, doi: 10.1016/j.scitotenv.2021.147850.

[5] H. Wu *et al.*, “Membrane technology for CO2 capture: From pilot-scale investigation of two-stage plant to actual system design,” *Journal of Membrane Science*, vol. 624. Elsevier B.V., Apr. 2021, doi: 10.1016/j.memsci.2021.119137.

[6] H. Al Baroudi, A. Awoyomi, K. Patchigolla, K. Jonnalagadda, and E. J. Anthony, “A review of large-scale CO2 shipping and marine emissions management for carbon capture, utilisation and storage,” *Applied Energy*, vol. 287. Elsevier Ltd, Apr. 2021, doi: 10.1016/j.apenergy.2021.116510.

[7] S. Valluri, V. Claremboux, and S. Kawatra, “Opportunities and challenges in CO2 utilization,” *J. Environ. Sci.*, vol. 113, pp. 322–344, 2022.

[8] A. Gulzar, A. Gulzar, M. B. Ansari, F. He, S. Gai, and P. Yang, “Carbon dioxide utilization: A paradigm shift with CO2 economy,” *Chem. Eng. J. Adv.*, vol. 3, no. July, p. 100013, 2020, doi: 10.1016/j.ceja.2020.100013.

[9] E. I. Koytsoumpa, C. Bergins, and E. Kakaras, “The CO2 economy: Review of CO2 capture and reuse technologies,” *J. Supercrit. Fluids*, vol. 132, no. July 2017, pp. 3–16, 2018, doi:

10.1016/j.supflu.2017.07.029.

[10] C. Du, X. Wang, W. Chen, S. Feng, J. Wen, and Y. A. Wu, “CO2 transformation to multicarbon products by photocatalysis and electrocatalysis,” *Mater. Today Adv.*, vol. 6, 2020, doi: 10.1016/j.mtadv.2020.100071.

[11] S. M. Jarvis and S. Samsatli, “Technologies and infrastructures underpinning future CO2 value chains: A comprehensive review and comparative analysis,” *Renew. Sustain. Energy Rev.*, vol. 85, pp. 46–68, 2018.

[12] F. Jin *et al.*, “High-yield reduction of carbon dioxide into formic acid by zero-valent metal/metal oxide redox cycles,” *Energy Environ. Sci.*, vol. 4, no. 3, pp. 881–884, 2011, doi: 10.1039/C0EE00661K.

[13] A. Taheri Najafabadi, “CO2 chemical conversion to useful products: an engineering insight to the latest advances toward sustainability,” *Int. J. Energy Res.*, vol. 37, no. 6, pp. 485–499, 2013.

[14] C. He, G. Tian, Z. Liu, and S. Feng, “A Mild Hydrothermal Route to Fix Carbon Dioxide to Simple Carboxylic Acids,” *Org. Lett.*, vol. 12, no. 4, pp. 649–651, 2010, doi: 10.1021/ol9025414.

[15] X. Liu, H. Zhong, C. Wang, D. He, and F. Jin, “CO2 reduction into formic acid under hydrothermal conditions: A mini review,” *Energy Sci. Eng.*

[16] P. Verma *et al.*, “Recent strategies for enhancing the catalytic activity of CO2 hydrogenation to formate/formic acid over Pd-based catalyst,” *J. CO2 Util.*, vol. 54, no. August, p. 101765, 2021, doi: 10.1016/j.jcou.2021.101765.

[17] I. Juan, E. Pérez, D. León, Á. Martín, and M. D. Bermejo, “Catalytic hydrothermal conversion of CO2 captured by ammonia into formate using aluminum-sourced hydrogen at mild reaction conditions,” *J. Ind. Eng. Chem.*, vol. 97, pp. 539–548, 2021.

[18] C. Hao, S. Wang, M. Li, L. Kang, and X. Ma, “Hydrogenation of CO2 to formic acid on supported ruthenium catalysts,” *Catal. Today*, vol. 160, no. 1, pp. 184–190, 2011, doi:

10.1016/j.cattod.2010.05.034.

[19] Z. Huang *et al.*, “CO2 hydrogenation over mesoporous Ni-Pt/SiO2 nanorod catalysts: Determining CH4/CO selectivity by surface ratio of Ni/Pt,” *Chem. Eng. Sci.*, vol. 247, p. 117106, 2022.

[20] Z. Ma, P. Li, L. Ye, L. Wang, H. Xie, and Y. Zhou, “Selectivity reversal of photocatalytic CO 2 reduction by Pt loading,” *Catal. Sci. Technol.*, vol. 8, no. 20, pp. 5129–5132, 2018.

[21] Q.-H. Zhang, W.-D. Han, Y.-J. Hong, and J.-G. Yu, “Photocatalytic reduction of CO2 with H2O on Pt-loaded TiO2 catalyst,” *Catal. Today*, vol. 148, no. 3–4, pp. 335–340, 2009.

[22] M. Umeda, Y. Niitsuma, T. Horikawa, S. Matsuda, and M. Osawa, “Electrochemical reduction of CO2 to methane on platinum catalysts without overpotentials: strategies for improving conversion efficiency,” *ACS Appl. Energy Mater.*, vol. 3, no. 1, pp. 1119–1127, 2019.

[23] A. H. Valekar, K.-R. Oh, S.-K. Lee, and Y. K. Hwang, “Simultaneous production of lactate and formate from glycerol and carbonates over supported Pt catalysts,” *J. Ind. Eng. Chem.*, vol. 101, pp. 66–77, 2021.

[24] X. Wang, Y. Yang, H. Zhong, T. Wang, J. Cheng, and F. Jin, “Molecular H 2 O promoted catalytic bicarbonate reduction with methanol into formate over Pd 0.5 Cu 0.5/C under mild hydrothermal conditions,” *Green Chem.*, vol. 23, no. 1, pp. 430–439, 2021.

[25] Z. Huo, M. Hu, X. Zeng, J. Yun, and F. Jin, “Catalytic reduction of carbon dioxide into methanol over copper under hydrothermal conditions,” *Catal. today*, vol. 194, no. 1, pp. 25–29, 2012.

[26] N. Yan and K. Philippot, “Transformation of CO2 by using nanoscale metal catalysts: cases studies on the formation of formic acid and dimethylether,” *Curr. Opin. Chem. Eng.*, vol. 20, pp. 86–92, 2018, doi: 10.1016/j.coche.2018.03.006.

[27] A. K. Singh, S. Singh, and A. Kumar, “Hydrogen energy future with formic acid: A renewable chemical hydrogen storage system,” *Catal. Sci. Technol.*, vol. 6, no. 1, pp. 12–40, 2016, doi: 10.1039/c5cy01276g.

[28] I. V. Gürsel, T. Noël, Q. Wang, and V. Hessel, “Separation/recycling methods for

homogeneous transition metal catalysts in continuous flow," *Green Chem.*, vol. 17, no. 4, pp. 2012–2026, 2015.

[29] F. Jin *et al.*, "Highly efficient and autocatalytic H2O dissociation for CO2 reduction into formic acid with zinc," *Sci. Rep.*, vol. 4, p. 4503, 2014, doi: 10.1038/srep04503https://www.nature.com/articles/srep04503#supplementary-information.

[30] X. Krokidis, P. Raybaud, A.-E. Gobichon, B. Rebours, P. Euzen, and H. Toulhoat, "Theoretical study of the dehydration process of boehmite to γ-alumina," *J. Phys. Chem. B*, vol. 105, no. 22, pp. 5121–5130, 2001.

[31] O. F. Lopes *et al.*, "Zinc hydroxide/oxide and zinc hydroxy stannate photocatalysts as potential scaffolds for environmental remediation," *New J. Chem.*, vol. 39, no. 6, pp. 4624–4630, 2015, doi: 10.1039/c5nj00324e.

[32] A. Ali, M. Z. Hira Zafar, I. ul Haq, A. R. Phull, J. S. Ali, and A. Hussain, "Synthesis, characterization, applications, and challenges of iron oxide nanoparticles," *Nanotechnol. Sci. Appl.*, vol. 9, p. 49, 2016.

[33] H. Bacelo, A. M. A. Pintor, S. C. R. Santos, R. A. R. Boaventura, and C. M. S. Botelho, "Performance and prospects of different adsorbents for phosphorus uptake and recovery from water," *Chem. Eng. J.*, vol. 381, no. June 2019, p. 122566, 2020, doi: 10.1016/j.cej.2019.122566.

[34] P. Charvin, S. Abanades, F. Lemort, and G. Flamant, "Hydrogen production by three-step solar thermochemical cycles using hydroxides and metal oxide systems," *Energy & Fuels*, vol. 21, no. 5, pp. 2919–2928, 2007.

[35] H. Ishaq, I. Dincer, and C. Crawford, "A review on hydrogen production and utilization: Challenges and opportunities," *Int. J. Hydrogen Energy*, 2021.

[36] H. Zhong, L. Wang, Y. Yang, R. He, Z. Jing, and F. Jin, "Ni and Zn/ZnO Synergistically Catalyzed Reduction of Bicarbonate into Formate with Water Splitting," *ACS Appl. Mater. Interfaces*, vol. 11, no. 45, pp. 42149–42155, 2019.

[37] A. P. Umpierre, E. de Jesus, and J. Dupont, “Turnover numbers and soluble metal nanoparticles,” *ChemCatChem*, vol. 3, no. 9, pp. 1413–1418, 2011.

[38] J. Su, M. Lu, and H. Lin, “High yield production of formate by hydrogenating CO 2 derived ammonium carbamate/carbonate at room temperature,” *Green Chem.*, vol. 17, no. 5, pp. 2769–2773, 2015.

[39] H. Yao, Z. Xu, M. Cheng, J. Yun, Z. Jing, and F. Jin, “Catalytic conversion of formic acid to methanol with Cu and Al under hydrothermal conditions,” *BioResources*, vol. 7, no. 1, pp. 972–983, 2012.

[40] Z. L. Wang, Y. Liu, and Z. Zhang, *Handbook of Nanophase and Nanostructured Materials: Materials systems and applications I*, vol. 3. 清华大学出版社有限公司, 2003.

CHAPTER 4

Controlling the post-structure properties of metal-crosslinked carbon-aerogels from alginate for emerging technologies*

Abstract

In the present work, a series of metal nanoparticle decorated carbogels (MDCs) with prospective catalytic activity were synthesized via a facile and inexpensive strategy starting from metal ion (Ca^{+2}, Ni^{+2}, Cu^{+2}, Pd^{+2}, Pt^{+4}) crosslinked alginate aerogels (MCAs). The evolution of the aerogel (Agel) into carbogel (Cgel) was studied based on a thorough characterization, comprising techniques such as ICP-OES, CamSizer, TGA/DTG, UHV-XPS, H2-TPR, TPO, XRD, SEM-BSE, and N_2-adsorption (BET/BJH). The increase of metal ion concentration in the gelation bath (from 17 mmol/L to 380 mmol/L) did not result in the increase of the metal ion content in the hydrogel. Among the metal ions tested, Pd^{+2} showed the greatest incorporation in the aerogel, with a final metal content up to 13%, which is the greater than those found in the reviewed literature. From the TGA, the MCAs presented a DTG peak between 235-285 ºC, carrying the major mass loss (55-65%). Among the MDCs obtained by pyrolysis, Pd-Cgel remarkably lost the least mass, with only 58 %, up to 600 ºC. The textural features of the MCAs showed specific surface areas ranging from 480 to 687 m^2/g in dependence of crosslinking ion, and pore sizes in the mesoporous range (5< pore radius (Pr)<25 nm). Through different pyrolysis temperatures (150 - 600ºC) there was a decreasing trend of the textural features, with a huge change after approximately 285 °C, associated to an expected shrinkage, by the reduction of mesopore-radius between 66% and 90%. Interestingly, for Pd the thermal treatment between 130-265 ºC provoked the opposite effect, hence gaining pore size, but conserving the mesoporous range. Backscatter electron-based scanning electron microscopy imaging (SEM-BSE) of carbogels showed nanoparticles-clusters evolution through the different pyrolysis temperatures, developing well-defined shapes for Ni- and Cu-Cgel at 600 ºC, with average size of 14 nm +/- 7 nm and 85 nm +/- 29 nm, respectively. The combined analysis of XRD and TPR results of Ni-, Cu-, Pt- and Pd-Cgels indicated that the particles are composed of elementary metals and metal oxides in

varying ratios, while Pd-Agel was the sole aerogel to show the exclusive presence of zero-valent state by XPS and TPO analysis.

Keywords: *aerogels, Carbon aerogels, alginate crosslinking, catalyst synthesis, hydrogenation catalyst, pyrolysis treatment, metallic-clusters evolution, oxidative states*

** This chapter was done during the doctoral stay at the Institute of Thermal Separation Processes, from the Technische Universität. Hamburg (TUHH), under the supervision of professors Irina Smirnova, Pavel Gurikov and Baldur Schroeter*

CHAPTER 4

Introduction

Since the discovery of aerogels in 1930s [1-3], an important attention has been given to its development for a number of industrial applications. Given its nanoporous and thermal and electrical conductivity properties, breakthroughs in the past decades have been given in the sector of foods, biomedical, wastewater treatment, pollution, construction, electrode materials and catalysis [4][5]. For its part, carbon aerogels (carbogels) presented themselves, since late 1980s [6], as a promising alternative to natural carbonaceous materials, owing to the possibility of controlling its purity, mechanical strength and porosity from the synthesis steps. Other features like the large specific area, low density, low thermal and high electrical conductivity and hydrophobicity makes them ideal as supports for catalysts, chemical adsorbents and energy storage as capacitors [7].

The polycondensation of resorcinol with formaldehyde under alkaline conditions was the typical pathway for obtaining carbogels in the past decades. Other synthetic polymers have also been used as carbogels precursors, such as polybenzoxazines, polyureas, polyimides, polyamides, polyurethanes [8]. Nevertheless, the polysaccharides have gained much interest as an inexpensive and abundant carbon source, especially those derived from species with large capability of fixing carbon dioxide, such as the brown algae [9]. This represents an opportunity in the context of sustainable development, by encouraging the algae CO_2 capture with added value. On average, brown algae species has 40% alginate [10], an anionic biopolymer that can be easily crosslinked with cations for the preparation of hydrogels [11], and also for capturing pollutant cations as a bioremediation of environments contaminated with toxic heavy metals [12][13]. The tailorable textural and structural features of carbogels make possible the overcoming of some of the constraints encountered in heterogeneous catalysts, like the formation of metal aggregates, pore blocking and leaching of active sites. For instance, Raptopoulos *et al*. [14] produced MDCs from alginate crosslinked with polyurea, with an increased carbonization yield of up to 37%, which in turn improves the surface functionalities (e.g., electrical conductivity and catalytic activity) of the carbogel by contributing oxygen and nitrogen functional groups. In the work of Plaza *et al*. [15] a nitrogen enriched

carbon material exhibited CO_2 capture capacity by allocating basic sites in the microporous structure after a coating process with different alkylamines. Recently, Zhang *et al*. [16] developed a series of carbon aerogel electrocatalysts based on transition metal-nitrogen sites for the electroreduction of CO_2. The starting hydrogel was formed by the chemical crosslinking interaction between polypyrrole (PPY) and 2,2′-bipyridine-4,4′-dicarboxylic acid (BPDC) with the selected metal ions (Ni, Fe, Co, Mn and Cu). A freeze-drying method was chosen for obtaining the aerogel, which was afterwards carbonized at 1000 ºC during 4 h in Ar atmosphere. For the metals studied, the CO_2 electroreduction activity increased in the order Cu<Mn<Co<Fe<Ni. The Ni-Cgel was used as cathode for a Zn-CO_2 battery, delivering a maximum power density of 0.5 mW cm^{-2} and long-term stability.

Alginate aerogels can be used without further thermal treatment for catalytic applications [17][18], and they represent a promising alternative to the traditional materials used as catalysts support. The exploration of new and more efficient ways of supporting metals like Ni, Cu, Pd, Pt, Co is important because they are the most active transition metals for hydrogenation of carbon-carbon double bonds under moderate conditions [19]. In this matter, Primo *et al.* [17] synthetized native Pd aerogels with catalytic activity toward Suzuki carbon-carbon coupling reactions. During the solvent exchange step, the reduction of palladium occurred, but no further characterization of reduction/oxidative state of Pd species were provided in order to establish the reducibility degree of the catalyst. Likewise, Qiao *et al*. [20] fabricated a porous elementary Ni-containing alginate hybrid material with catalytic activity toward hydrogenation reactions. The catalyst consisted of a hydrogel obtained by coordinating Ni (II) ions with sodium alginate. The reduction of the metal was performed with $NaBH_4$, and the activity was maintained up to 20 cycles of the styrene hydrogenation reaction. Zhang *et al*. [21] crosslinked alginate by immobilizing nickel ions to form gel particles for the removal of the antibiotic ciprofloxacin from aqueous environments. The adsorbent beads were prepared by dripping sodium alginate to a 2% solution of Nickel (II) nitrate hexahydrate. The obtained gel was conventionally drained in a vacuum oven at 60 °C for 12 h, provoking a subsequent particle shrinkage due to water evaporation, yielding wrinkling and protrusions in the surface, observed by SEM. However, no surface area analysis was reported in order to determine the influence of the shrinkage over the final textural

properties. Wang *et al*. [22] produced Pd nanoparticles catalyst supported by natural polymer-based hydrogels of cationic (Ca^{+}) nanocellulose and alginate, through drop by drop addition of 10 mmol/L of $PdCl_2$, where the crosslinking takes places with the residual carbonyl groups in the cationic nanocellulose. The catalyst was suitable for the methylene blue removal batch and continuous systems, and a high yield of up to 99% for the Suzuki reaction, with up to 5 times recyclability. Bauman *et al*. [23] incorporated copper in a carbogel matrix from the polymerization of formaldehyde, achieving an uniform dispersion of spherical metal nanoparticles, ranging from 10-50 nm. This metal was selected based on its enhancing capacity of conductivity properties of the carbogel. In another work by Bauman *et al*. [24], carbogels of Ni, Co and Cu, with catalytic and transport prospective, were prepared from K^{+}-doped hydrogels of polystyrene spheres, pyrolyzed at 800 ºC. The materials obtained presented dense networks of interconnected carbon particles with hierarchical pore structure of micro and microporosity in the wall that facilitates the accessibility to the metal sites. They exhibited a nitrogen isotherm of type II, representative of microporous adsorbents, with an average BJH pore diameter of 6 nm, and average BET surface area of 530 m^2/g.

One of the problems in the synthesis of carbon 3-D-structures for catalysis is that metals have to be introduced as post-functionalization, with elaborated methods like supercritical deposition, chemical vapor deposition, traditional impregnation methods, among others [25]. This represents a not easy extra process step for as i) post-distributing metals clusters homogeneously through the adhesive-resistance feature of the carbon network, and ii) dispersed metal on carbon tends to aggregate, therefore the danger of too large metals cluster arises.

Based on the above information it is clear that the development of a carbon aerogel crosslinked with selected transition metals is strategic for covering up the catalytical needs of hydrogenation processes, like the reduction of CO_2 into green chemicals, and also could lead to an improved material with higher catalytical performance in terms of process yield, reusability, production cost, and carbon footprint, since the aerogels involve a facile and ecofriendly production process.

CHAPTER 4

In the present work, a series of aerogels (Agel) and carbogels (Cgel) with catalytic activity prospective were synthesized via a facile and inexpensive strategy from the crosslinking of anionic alginate with selected transition metals. The aim is to test metal-crosslinking and pyrolysis of alginate as alternative for the in-situ generation of monodispersed metal-nanoparticles with appropriate size for catalytic applications, without needing any additional post-modification step. The evolution of the Agel into Cgel was studied based on a thorough characterization, focusing on the textural features and metallic clusters development through different pyrolysis treatments, thus giving new information to the existing one in the literature.

Materials and methods

Chemicals

Fine powder of Alginate Hydagen 500, was used as received from BASF (Ludwigshafen, Germany). The metal precursors were: calcium chloride dihydrate ($CaCl_2.2H_2O$) (>99%, Carl Roth catalog number: T885.3), Nickel (II) nitrate hexahydrate (>99%, Bernd Kraft, catalog number: 15306), Copper (II) pentahydrate sulfate (>99%, Riedel-de Haën), Palladium (II) nitrate dihydrate (~40% Pd basis) (Sigma Aldrich, catalog number: 76070-1G) and Platinum (IV) chloride (assay 96%) (Sigma Aldrich, catalog number: 206113-1G). As a control/reference material, fine powder of commercial catalysts of 5 % Pd loading over activated carbon support (Pd5AC) was purchased from Sigma-Aldrich (catalog number: 205680-10G). Pd powder was used as control catalyst and was purchased from Sigma-Aldrich (catalog number: 326666-1G). All chemicals were used without further purification.

Metal-Crosslinked aerogels (MCAs) preparation

A 2 %wt solution of alginate was prepared by adding the powder to distillate water, stirred for 10 min at 500 RPM, and then stirred at 1000 RPM up to 2 h. Before using, it was left at room temperature overnight to allow the solution to settle. Nickel, copper, palladium, platinum and calcium aerogels were prepared by adding 35 g of the alginate solution into a separating funnel connected to compressed air supply and equipped with a nozzle made with a micropipette tip (10 mL) and a custom cut-syringe needle (0.6 mm ID and 3 mm length), as shown in Fig. 1. The droplets formation was controlled by manually graduating the pressure of the compressed air (below 0.5 bar), while allowing a gentle flow. The alginate droplets quickly form the hydrogels when contacting a stirred gelation bath of 17, 180 and 380 mmol/L concentration of the metal precursors. Afterwards, the gels were washed twice with distillate water and solvent exchanged with ethanol (99.8%) until its concentration was between 96-97%. This step produced an alcogel that conserved the initial bead shape, for a posterior drying in an autoclave at 70 ºC and 125 bar of supercritical CO_2 during 6 h.

Synthesis of Metal-Decorated Carbogels (MDCs)

The corresponding MDCs of Ni, Cu, Ca, Pd and Pt-crosslinked aerogels were obtained by pyrolysis under N2 atmosphere at 5 ºC/min, conditions at which the bond between metal ions with carboxylic groups is expected to cleave to mostly form metal oxides. Both TGA of aerogels and carbogel preparation took place at once in the same TGA equipment, as described in detail later. In the first place, the pyrolysis was taken up to 600 ºC, for determining the most important thermal changes, based on the behavior of the derivative curve (%/ºC). Then, five different pyrolysis temperatures were stablished, based on the different DTG curves that presented all MCAs, which will be analyzed in depth later as part of the thermal stability analysis. Given this, the temperatures were: 150 ºC, 285 ºC, 380 ºC, 450 ºC and 525 ºC. For Pd and Pt, 265 and 365 ºC were applied, instead of 285 ºC, 380 ºC,

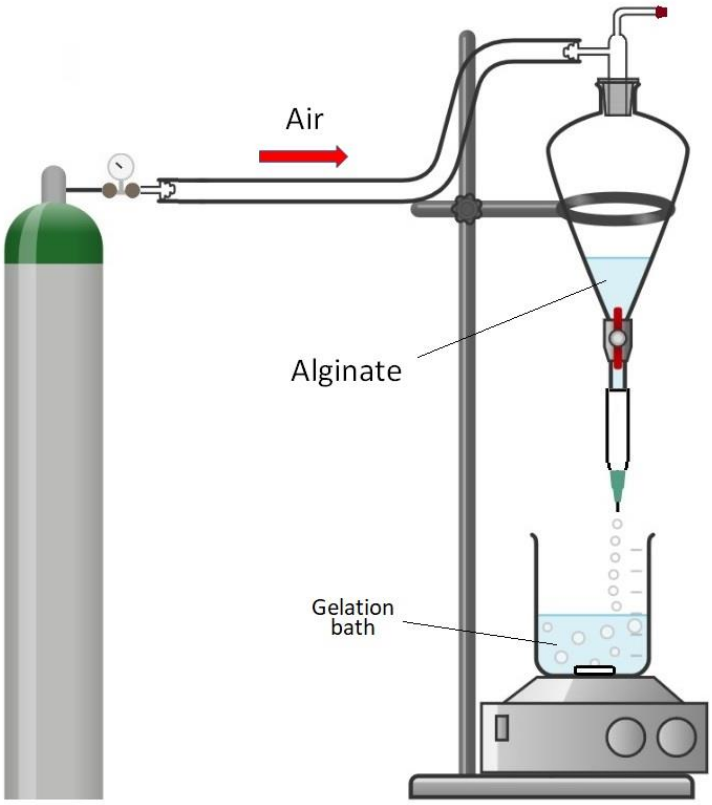

Fig. 1. Dripping device

Solid Characterization

Thermogravimetric analysis and derivative thermogravimetric analysis (TGA/DTG) were conducted in a Linseis STA-PT1600. The samples were heated up to 90 ºC at a 5ºC/min rate for 45 min, and raised to the desired temperature at 5ºC/min, with a dwelling time of 60 min. Textural properties analysis were conducted in a Nova 3000e Surface Area Analyzer (Quantachrome Instruments, Boynton Beach, FL, USA). An overall sample mass of 20–30 mg was used, and all samples were degassed under vacuum at 60 °C for at least 6 h prior to each analysis. The Brunauer-Emmett-Teller (BET) method was used to determine the specific surface area (SV). The pore volume of the mesopores and mean pore diameter of mesopores (dmeso) were determined by the Barrett-Joyner-Halendia (BJH). Metal content was measured by ICP-OES using a Perkin Elmer Optima 8300 DV, where the samples were previously digested in a combination of HNO_3, HCl and HF solution. The size and shape of the MCAs synthesized were determined by Camsizer XT system (Retsch

Technology) in free fall mode, its skeletal densities via Helium pycnometry, and bulk density calculated from the particles weight that occupied an untapped graduated cylinder.

Two Scanning electron microscopy (SEM) studies were conducted in the present work. The first one (from now on called as SEM1) was aimed at the outer-skin and inner pore structure morphology characterization of the MCAs, employing a Zeiss Supra VP55 equipment (Jena, Germany). In this case, samples were sputtered with a thin layer of gold (ca. 6 nm, Sputter Coater SCD 050, BAL-TEC) before analysis was started. The measurements were carried out under high vacuum at an accelerating voltage of 3–5 kV. The second one (from now on called as SEM2) is low voltage scanning electron microscopy (LVSEM) on the carbogels at different pyrolysis temperatures, in order to image the metallic nanoparticles (NPs). Backscattered electrons analysis (BSE) was applied. BSE electrons are from a deeper interaction volume of the incident beam. The interaction depth is dependent of the atomic number of the components of the sample which results in contrast between the elements in the resolution of the conventional SEM technique. The contrast correlates with atomic number: brighter regions correspond to higher atomic numbers. For this purpose, a ThermoFisher Scientific Scios 2 instrument was used. The electron beam resolution was 1.6 nm at the optimum working distance (<5 mm) at 2 kV accelerating voltage. The samples were fixed with a vacuum-resistant carbon tape on the sample holder. Sputter coating was not applied in this case because even a 5 nm thick sputtered gold layer can dramatically alter the morphology and the surface structure of the aerogel [26].

UHV-XPS analyses were carried out for the oxidative state and surface chemistry analysis of the pristine MCAs and the commercial catalyst Pd5AC, in a Specs brand X-ray photoelectronic spectrometer (NAPXPS) with a PHOIBOS 150 9MCD energy analyzer, using a non-monochromatic source of Al (1400 eV, 10 kV, 100W) with step energy of 50 eV for general spectra and 20 eV for high-resolution spectra. Previously, the MCAs beads were compressed using a press and die system, applying a force of 200 kN until obtaining a thin tablet.

A series of Temperature-programmed-technique experiments (TPX) where conducted in order to explore the catalytic features of MDCs and Pd-Agel. As a pretreatment before the experiments, the samples were heated at 10 ºC/min to 150 ºC and maintained for 0.5 h under a flow of 50 cm^3/min of pure Argon, in order to remove air and moisture, and finally returned to room temperature to start the data collecting. Temperature Programmed Reduction (H_2-TPR) experiments were conducted up to 1000 ºC under a flow of H_2/Ar (10% v/v; 50 cm^3/min) at a rate of 10 ºC/min, in a Autochem II 2920 Micromeritcs equipment, coupled to a quadrupole mass spectrometer (Pfeiffer-Vacuum Modelo Omnistar). Hydrogen consumption was monitored by the thermal conductivity detector. Before the detector, an ice trap was used to retain any water formed during the reduction. The TPO (temperature programmed oxidation) experiments consisted in heating the sample up to 1000 ºC at a rate of 10 ºC/min, under an O_2/Ar (5% O_2) flow of 50 mL/min, and CO and CO_2 formation is expected and followed up with the mass detector TPD (temperature programmed of desorption) was conducted under a flow of Ar, while following up the desorption of CO and CO_2 gases with the mass detector. Diffraction patterns of carbogels samples were collected under Cu-Kα1 radiation (Cu-Kα1 = 0.154059 nm) using a Rigaku SmartLab 9 kW X-ray diffractometer (XRD) with the following measurements conditions: Measurements were carried out in Bragg-Brentano (Θ/2Θ) mode, between 35°-80° using 5°/min scan rate.

Experiments of catalytical activity assessment of Pd-Agel

It was assayed in hydrothermal reaction for the reduction of the ammonia-based CO_2 captured species (1), mainly HCO_3^-, produced by the aqueous dissolution of ammonium carbamate in MiliQ water, in a concentration of 0.5 mol/L. The test consisted of filling a stainless-steel stirred reactor (Parr Instruments Series 4791 Micro Stirred Reactors of 25 mL, maximum pressure of 200 bar, and maximum temperature of 350 ºC), with the aqueous solution of carbamate up to 70% of the volume of the reactor, followed by the addition of 0.105 g of the catalyst Pd-Agel. Afterwards, the reactor was sealed and purged three times with 2.5 bar of nitrogen and hydrogen, subsequently, to remove the remaining air. Then, the reactor was pressurized, at room temperature, with Hydrogen (99.99%)

(provided by Linde) up to 26 bar. From this point, the system was heated at a ramp of 14 ºC/min using a band heater, up to 120 ºC and the stirring was kept at 500 RPM during the operation time of 5 h. The pressure meter device had an error of ±2 bar. After the reaction, the vessel was rapidly immersed in a cold-water bath. Then, the liquid sample was collected and filtered through a 0.22 mm filter before measurement of final concentration of formic acid (product of interest) and carbamate in the final liquid sample, through HPLC analysis (Waters, Alliance separation module e2695) using a RAZEX™ ROA-Organic Acid H+ column with RI detector (Waters, 2414 module). The mobile phase was 25 mM H_2SO_4 with a flow rate of 0.5 mL/min. The temperatures of the column and the detector were 40 °C and 30 °C, respectively. In order to stablish the effectiveness of the synthesized material two control reactions were conducted without Pd-AgeI catalyst, instead i) powder of metallic palladium was placed in the reactor, in a quantity equivalent to the metal content of Pd-Agel, and ii) no solid/catalyst in the reactor was placed (reaction blank). The conditions for both were the same as afore described (filling up to 70% of the volume of the reactor, 25 bar of H2, 120 ºC and 5 h). The yield of formic acid was calculated as shown in equation (2):

$HCO_3^- + H_2 \rightarrow HCOO^- + H_2O$ (1)

$$Y_{FA} = \frac{C_{FA,f}}{C_{cs,i}} x100 \quad (2)$$

Where $C_{FA,f}$ is the final molar concentration of formic acid, $C_{CS,i}$ is the initial molar concentration of ammonium carbamate

CHAPTER 4

RESULTS AND DISCUSSION

ICP-OES results

Fig. 2 depicts the relationship between the metal precursor bath concentration and the corresponding final metal content in the aerogel beads after the $scCO_2$ drying. A proportionality in the range 17-180 mmol/L is observed, but for higher bath concentration the metal content is not increasing in the aerogel, where Ni jumped from 9.54% to a maximum of 11%, and Ca to 9.36%. Comparatively, the nickel content reached seems to be efficient, in terms of metal precursor intake, since other approaches for vacuum dried gel films have used higher concentration of alginate (5 %) and nickel precursor (5 mol/L) for a final content of 12.95 wt% of Ni, and 15.32 wt% for Cu [27]. It is also worth noting that, among the metals, Pd gelation bath presented the highest metal content with 13%, while Cu the lowest with 1.11%. Platinum precursor also showed a marginal metal trapping of 3.4%. Metal content for all samples started to level off above 180 mmol/L, suggesting a saturation from the lowest concentration of 17 mmol/L. This shows that no greater amount of metal can be introduced in the hydrogel matrix, so it was decided to follow up the study with the lowest concentration samples. Interestingly, in the work by Primo *et al.* [17], Pd loading was lesser, of about 5%, when using 20 mmol/L of Na_2PdCl_4 as precursor with a 1 %wt solution of sodium alginate, previously crosslinked with 240 mmol/L of $CaCl_2$, where the cation exchange with Ca^{+} allowed controlling the Pd loading. More even, higher Pd^{+2} concentrations did not incorporate more Pd in the alginate beads.

In the case of Pt^{+4}, the gelation was very poor, and the alginate redissolved back to the aqueous gelation bath, so no beads were formed. Only after the solvent exchange step with ethanol the gelation occurred, in the shape of a sort of sponge that notably did not disperse well the metal precursor through the organic framework. After the drying, the Pt-Agel was in a sort of foam shape. This incapability of Pt^{+4} to crosslink well the alginate can be explained by the concept of the Lewis acid base theory and the hard-soft character of ions. Harder cations bond well to harder anions, and softer cations bond well to softer anions [28]. The crosslinking of alginate with metals strongly

depends on hard-soft character. [29]. Hard cations are preferably bound by oxygen atoms in negatively charged ligands such as carboxylate groups (hard anions) of β-D-mannurate (M) and of α-L-guluronate (G) of the alginate. The inclusion of Pt^{+2} as crosslinking agent could be considered, but given its complex coordination chemistry, which shares with Pt^{+4}, it must be taken into account the original ligands in the precursor to be used, besides pH and other factors. However, this Pt^{+2} specie has proven activity in heterogeneous catalysis [30].

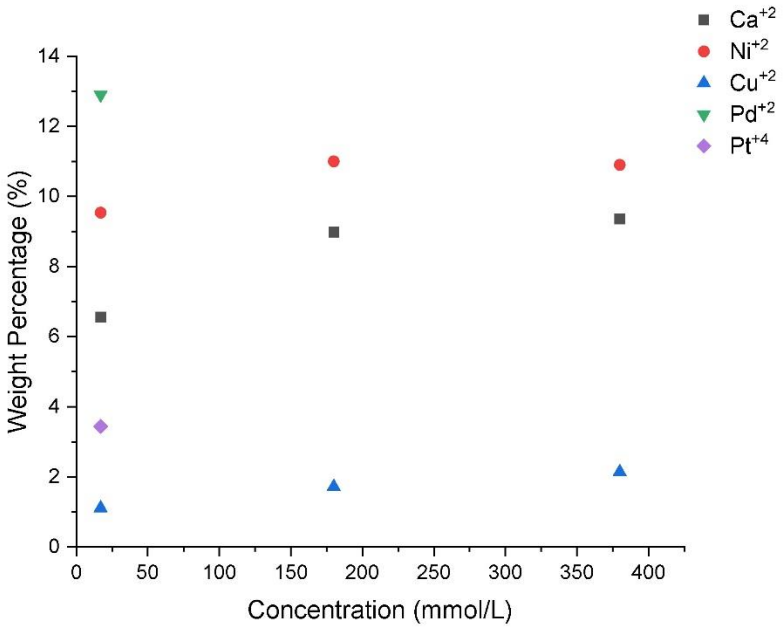

Fig. 2. Metal content in Agel beads at different metal precursor batch concentrations

CamSizer results

Table 1 summarizes the granulometric characteristics of the MCAs beads at the lowest concentration of gelation bath (17 mmol/L). In general, the particle size remained almost equal for all samples, with an average of 1.37 mm and a low deviation of 0.0363 mm. The smallest spherical particle frequency (SPHT3) was 0.82 for Ni-Agel, and the greatest for Pd-Agel with 0.91, showing acceptable sphericity and marginal symmetricity (average of 0.75) for all samples, which is consistent with the images of Fig. 3. All materials are highly porous, above 99% in average.

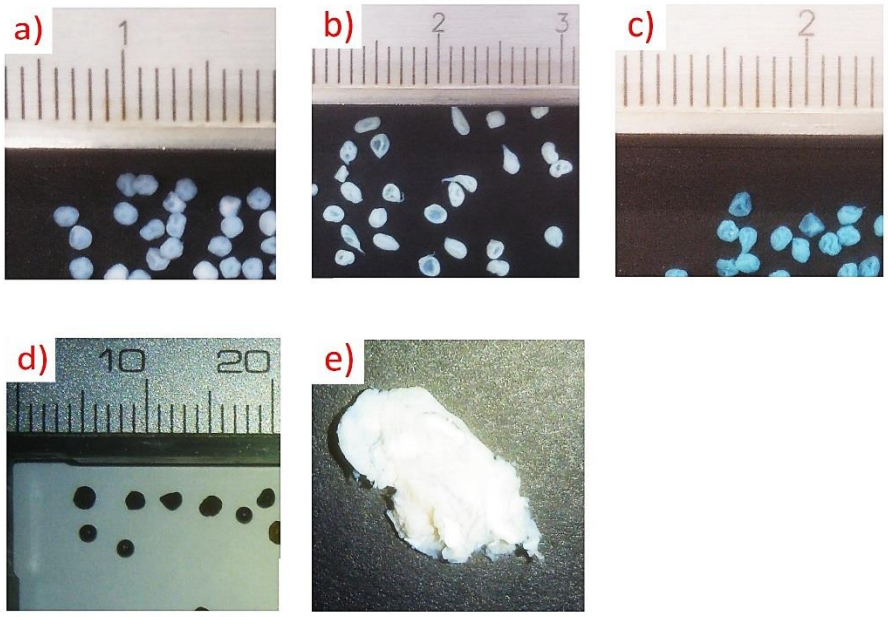

Fig. 3. MCAs beads of a) Ca^{+2}, b) Ni^{+2}, c) Cu^{+2}, d) Pd^{+2} and e) Pt^{4+} foam.

Table 1. Granulometric analysis of MCAs

Aerogel sample	Mean particle diameter Mv3(x)(mm)*	Mean value SPHT3*	Mean value b/l3*	Bulk density (g/cm^3)	Skeletal density (g/cm^3)	Total porosity (%)
Ca-Agel	1.41	0.90	0.74	5.5E-03 ± 1.6E-9	1.72 ± 0.12	99.68
Ni-Agel	1.30	0.82	0.68	5.3E-03 ± 4.1E-10	1.87 ± 0.28	99.72
Cu-Agel	1.40	0.86	0.70	5.5E-03 ± 3.7E-9	2.25 ± 0.14	99.76
Pd-Agel	1.38	0.91	0.87	7.8E-03 ± 0.0	4.61 ± 0.87	99.83
Pt-Agel	-	-	-	-	1.69 ± 0.14	-
Average	1.37	0.87	0.75	6.03E-03	2.43	99.75
Deviation	0.0363	0.0343	0.0618	8.88E-04	0.87	4.74E-02

* Values taken from Camsizer file X_{Femin} (width of particle projection)

Thermogravimetric analysis (TGA) and derivative thermogravimetry (DTG) of MCAs

The thermograms for pristine MCAs are presented in Fig. 4, showing more than 2 different pyrolysis steps. In general, for all samples a moisture loss (10-20%) occurred between 70-85 ºC (70ºC for Pt-Agel). All samples presented a second peak between 235-285 ºC. This thermal event carried the major mass loss (55-65%), and can be associated with the biopolymer decomposition through the thermal scission of the carboxylate/carboxylic acid groups of the alginate into metal-carbonate [31]. During pyrolysis process, metal ions can catalyze the thermal decomposition at a lower temperature, through reactions of decarboxylation/decarbonylation, dehydration and biopolymer chain break [27]. Above 285 ºC, a minor third peak appeared for Ni (318 ºC) and Pd (285 ºC) samples, ascribable to different decomposition steps of the remaining metal-precursor, most probably into metal oxides [32][33]. For copper sample, a DTG duplet peak is warned at 165 and 203 ºC, which may correspond to the formation of trihydrate and monohydrate species of the pentahydrate sulfate, that use to be at lower temperature (45-58 ºC) [34][35]. However, this phenomenon took place at higher temperature, indicating a strong interaction of the remaining precursor with the MDC in formation. This duplet was observed similarly in the work of Raptopoulos *et al*. [14], but its characterization was not discussed. The great mass loss for most of the materials synthesized suggests that even after introduction of metals the alginate is not too thermally stable. Nevertheless, among the metals tested, Pd remarkably lost the least, with only 58 %, up to 600 ºC, followed by Cu with 66 %, Ca with 74 %, Ni with 89 %, and 95.3 % for Pt. The oxidative state of the materials, whether metal-oxide or elementary metal, will be discussed further based on XRD, XPS and TPR/TPO analyses.

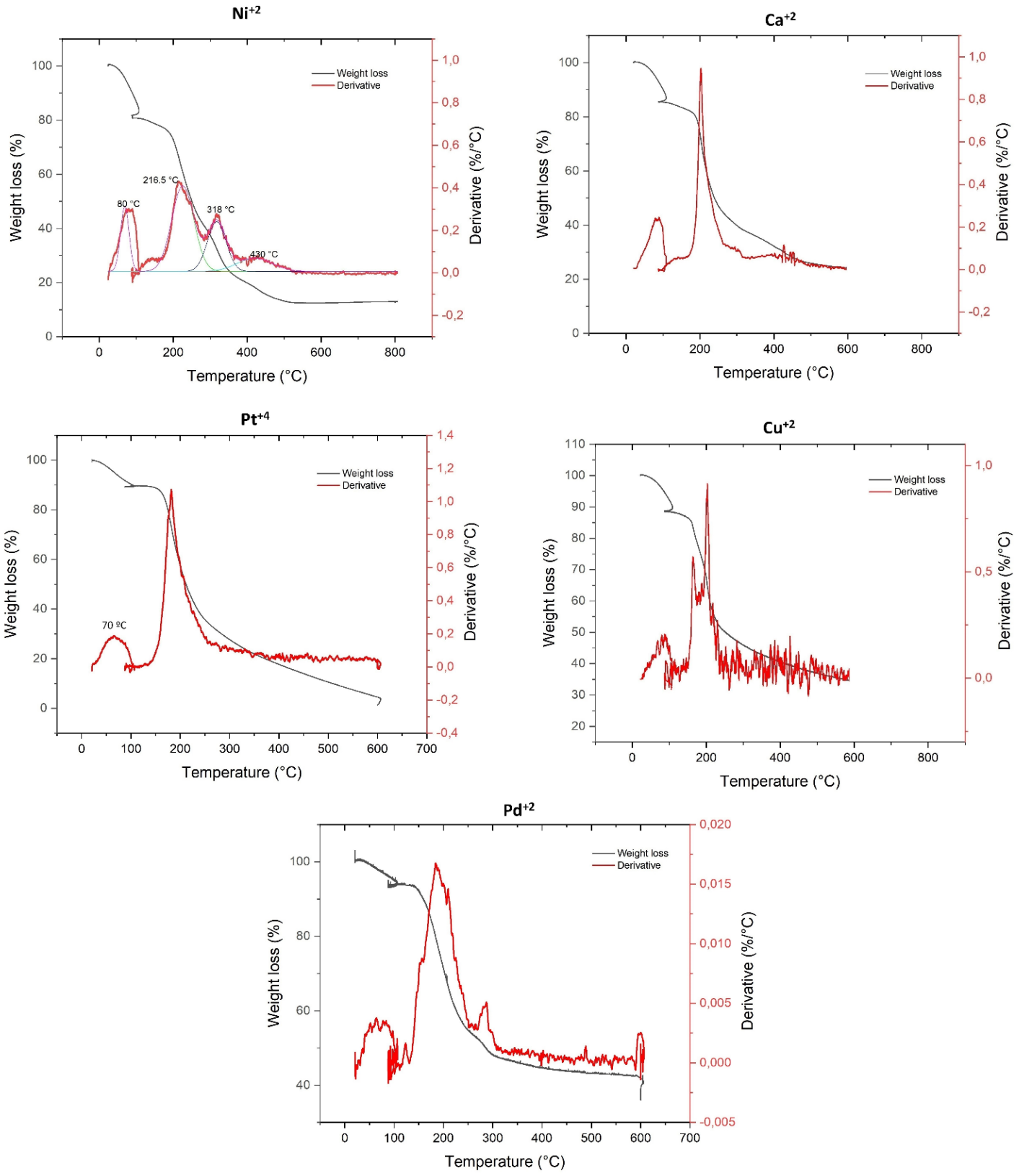

Fig. 4. Thermogravimetric analysis (TGA) and derivative thermogravimetry (DTG) of MCAs

Textural properties analysis

Textural properties of specific surface area (Sv), Pore volume (Pv) and pore radius (Pr) were measured for both MCAs and MDCs synthesized, illustrated in the Fig. 5, where “0” correspond to the pristine MCA at the lowest gelation bath concentration of 17 mmol/L. The values of Sv obtained, ranging from 480 to 687 m^2/g, were even higher of those of native alginates elsewhere (up to 541 m^2/g) [14]. Remarkably, Sv of Pd-Agel (242 m^2/g) was considerably higher than reported elsewhere for Pd alginate aerogel (52 m^2/g) [17]. The data of Sv, Pv and Pr showed decreasing pattern at higher temperatures, repeated for ions Ca, Cu and Ni, with a huge change after approximately 285 °C, while for Pd at 265 ºC, which is consistent with the major thermal biopolymer’s decomposition suggested by the second DTG peak (Fig. 4). The shrinkage of the aerogels during the pyrolysis process is a very well-known issue [36], and in the present work it was observed between 285-380 ºC by the reduction of pore radius between % 66 and 90%. Even though, the spherical shape was retained, in concordance with Bauman *et al*. [24], who found that the sizes of the macropores are 40-50 % smaller than the voids in the uncarbonized material, and the addition of metals allows a volumetric shrinkage in a uniform fashion.

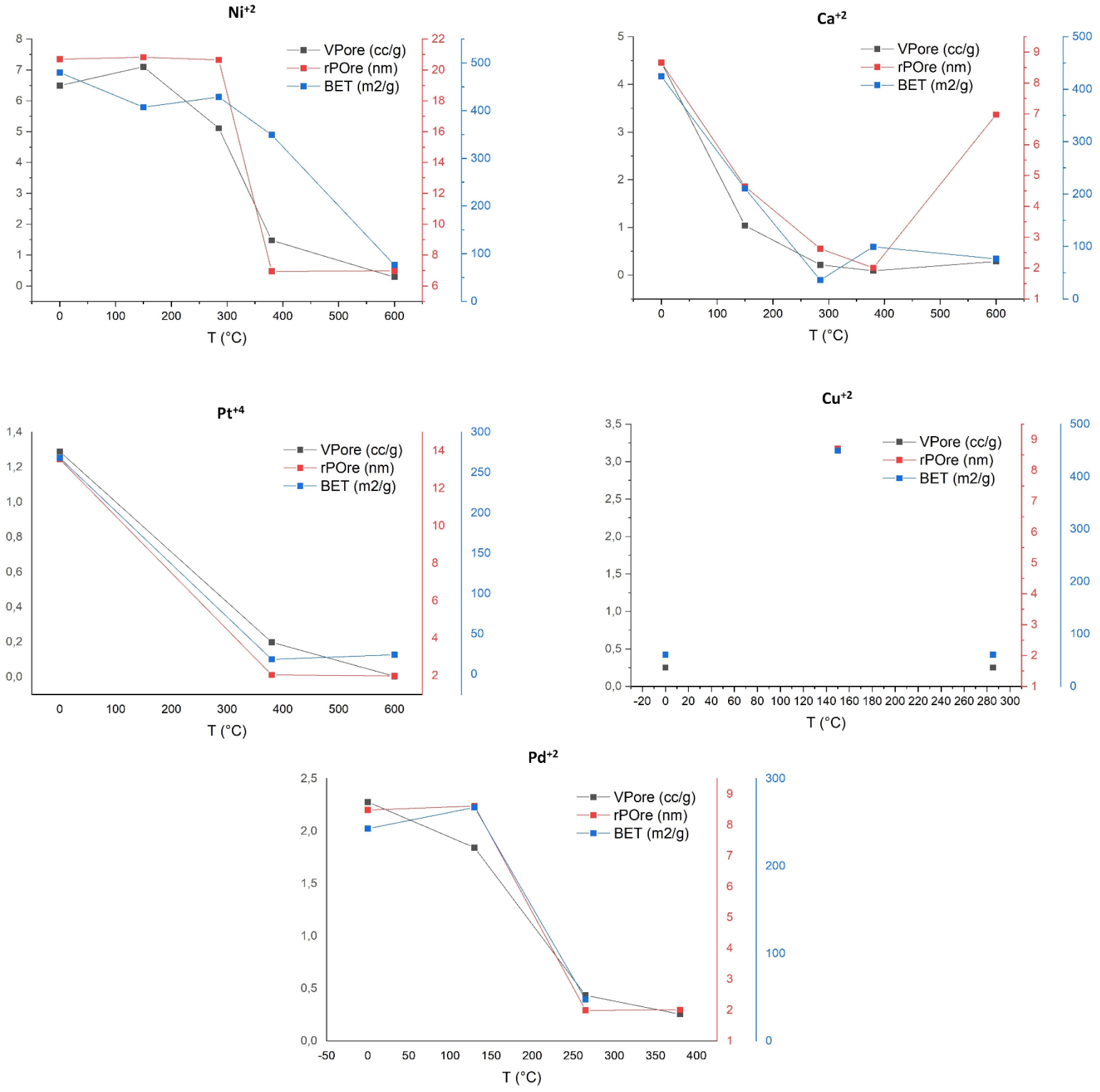

Fig. 5. Textural properties of MCAs (denoted as “0”) and MDCs at different pyrolysis temperatures

Based on Fig. 2, the metal content starts to level off above 180 mmol/L, leaving a considerable amount of unreacted metal salt in the gelation bath. During the dropping process, once gelation took place the excess of free metal salt can accumulate over the bead surface, thus hindering the surface area, reflected in the decrease of the parameter above 180 mmol/L, as seen in Fig. 6. This fact is supported by the findings of Miller *et al*. [37], who obtained a decreased Sv with the increment of metal loading in Ru/carbogel nanocomposite, given the large difference in atomic mass of the transition metals compared to carbon. The pore sizes of all selected MCAs were mesoporous range (5<Pr<25 nm) (see Fig. 5). N_2-adsorption-desorption experiments were not possible for the Cu and Pd carbogel at 600 ºC, most probably because at this temperature they lost all the mesopores.

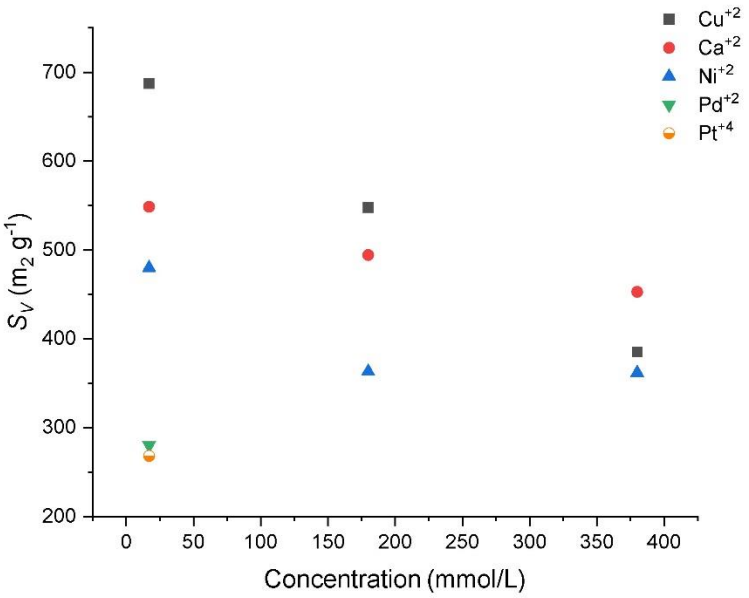

Fig. 6. Specific surface area of metal aerogels at different concentrations of precursor bath.

The $dV/DlogR_{normalized}$ *Vs* r_{pore} is a type of curve that allows presenting the pore size distribution and the importance of the larger pore ranges in a sample [38]. It was evaluated for the MCAs and MDCs. The data of this curve was normalized in order to better point out the changes between the different pyrolysis temperatures. As observed in Fig. 7, a significant change of mesopore-radius occurred for

the Ni-, Cu- and Ca-Cgel between 285-380 °C, where only small mesopores were left afterwards, while big pores were destroyed. Interestingly, for Pd the thermal treatment between 130-265 ºC provoke the opposite effect than the other metals, thus gaining pore size, but conserving the mesoporosity. In the case of Pt-Agel (not shown), the available data was insufficient and inconclusive, because it was not possible to get the minimum mass quantity out of the pyrolysis to perform pore size distribution analysis for the different pyrolysis temperatures, as the weight loss (95.3 % up to 600 ºC) was the greatest among the metals tested.

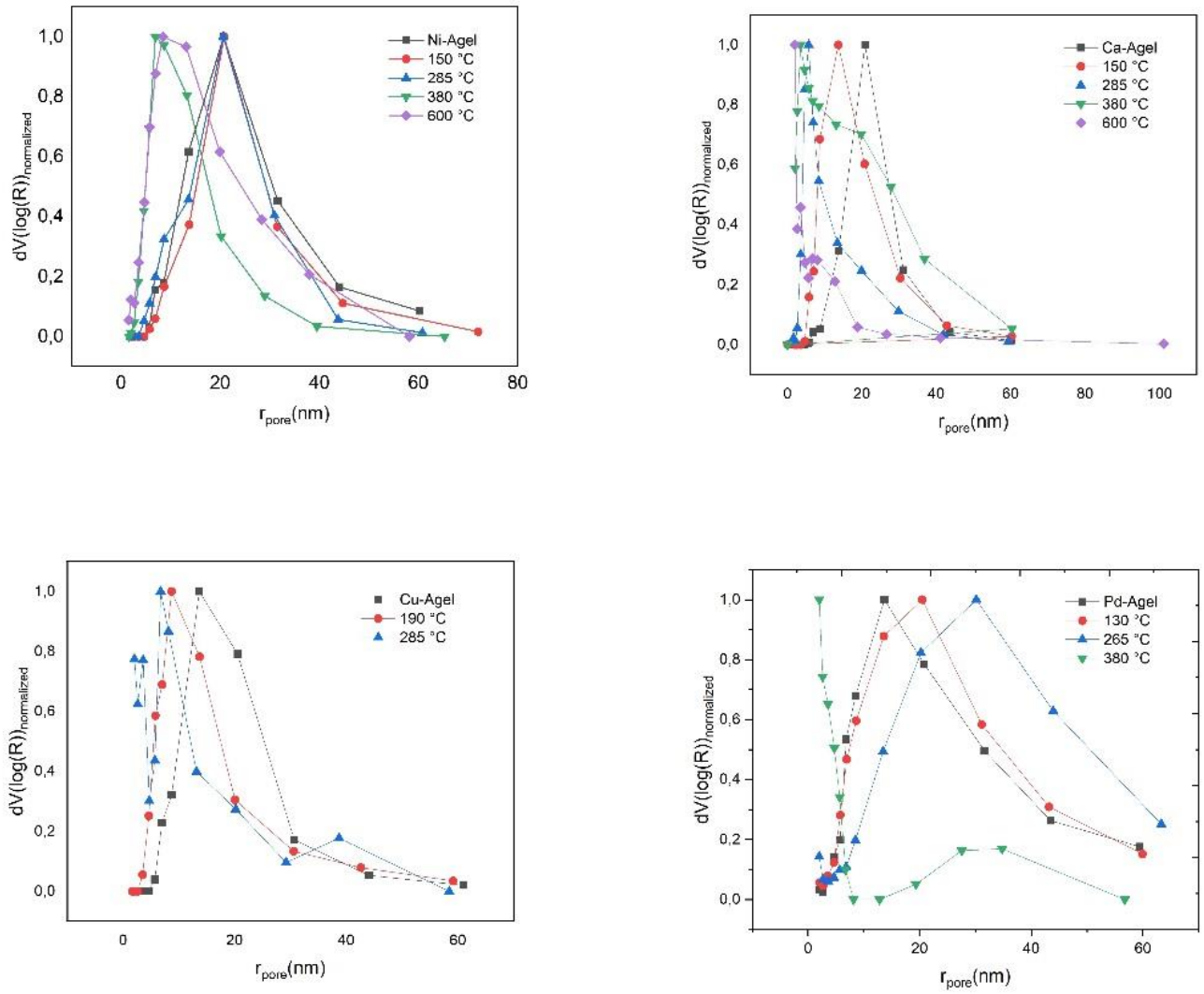

Fig. 7. Effect of pyrolysis temperature over the pore size distribution of MCAs and MDCs

Scanning Electron microscopy (SEM) and Backscattered electrons analysis (BSE)

SEM images (Fig. 8) (SEM1) reflected that both outer skin and inner structure of all MCAs are mostly homogeneous and highly porous in nature. Only in the case of Pd-Agel, its outer skin is covered up with Pd particles well distributed. Its pores are formed by well-defined thin strings and channels that may be good for diffusion of reactants in catalytic applications.

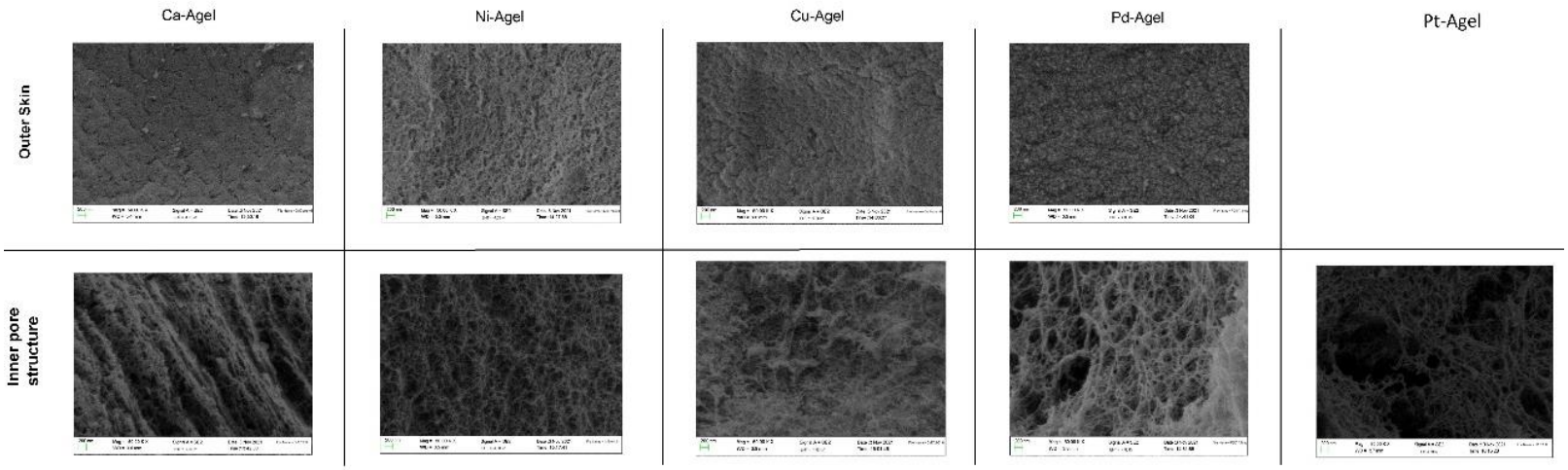

Fig. 8. Outer-skin and inner pore structure morphology characterization of MCAs by SEM1

BSE examination (see Fig. 9) (SEM2) permitted locating smooth bright areas in the porous structure of Ni-Cgel obtained below 380 ºC, but no NPs were observed. These areas were acquiring round-nanoparticle shape as the pyrolysis temperature increased, showing a metallic-clusters evolution, developing its best round shape at 600 ºC, compared to the lower temperatures. Pyrolysis at 600°C resulted in the formation of NPs, highly dispersed across the inner pore structure of the carbogel, and image analysis of the BSE images showed average size of NP to be 14 nm +/- 7 nm, while for Cu-Cgel was significantly larger, of 40 nm +/- 20 nm and 85 nm +/- 29 nm at 285 ºC and 600 ºC, respectively.

In the case of Pd-Agel, Pd formed an atomic layer on the nanostructured carbon framework, making impossible to define a size by SEM images, most probably due to the high final metal content (c.a. 13%), that can be adjusted by the gelation bath concentration. For control sample Pd5AC, average particle size of NP was estimated in 21 nm+/- 13 nm, using BSE image (see Fig. 10).

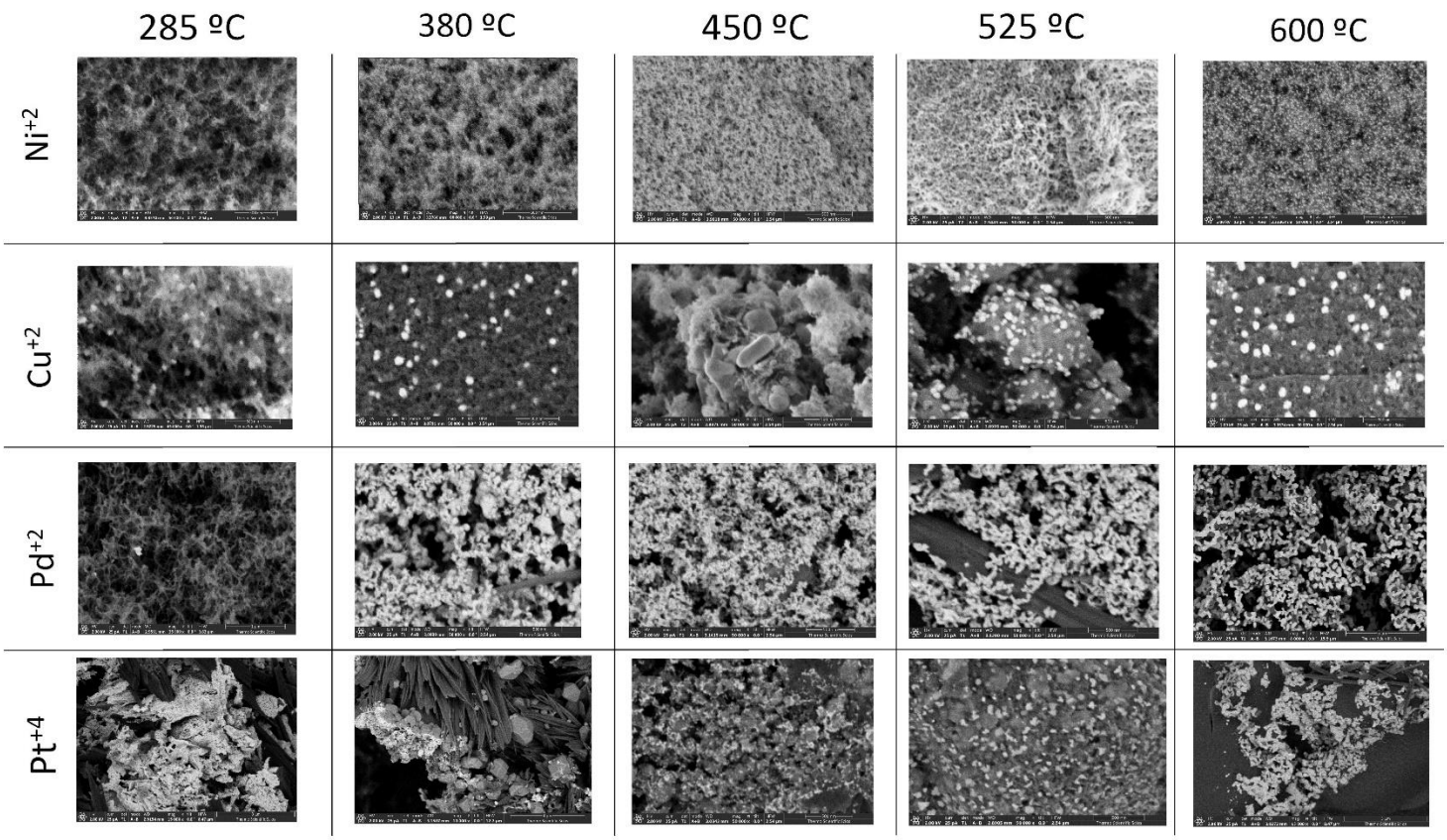

Fig. 9. SEM-BSE (SEM2) images of MDCs at different pyrolysis temperatures

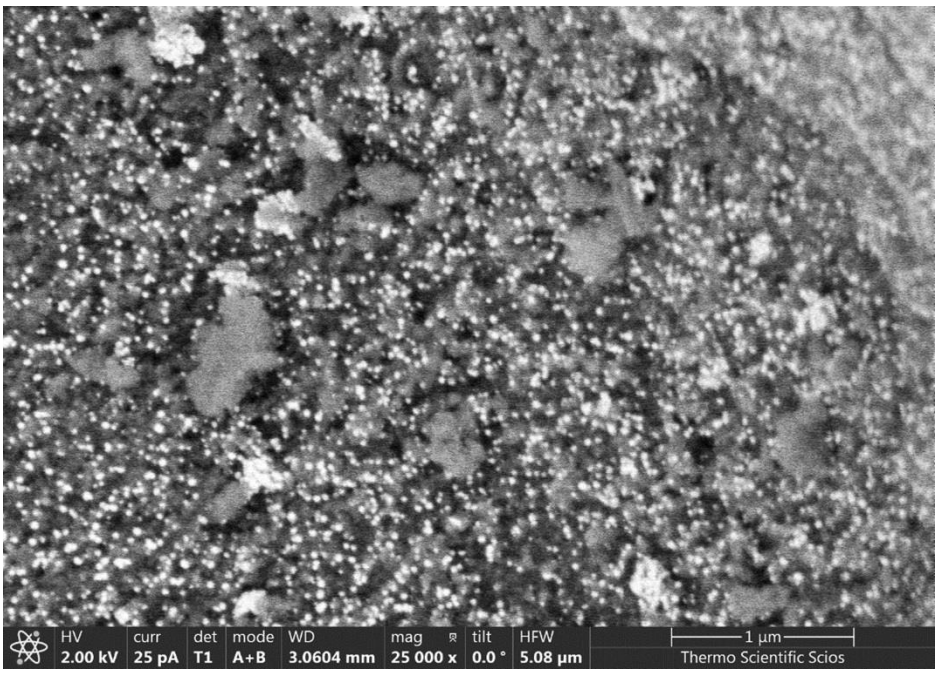

Fig. 10. SEM-BSE (SEM2) image of commercial control catalyst Pd5AC

Table 2 shows the average particle size and crystallite size for the different MDCs, where the effect of the increased pyrolyzing temperature is clearly seen in the case of Ni and Cu contained samples i.e., the higher the pyrolyzing temperature the larger NPs appear on the carbogel. Under the temperature increment, pyrolysis process also provoked the loss of macropores into denser micro and meso porous and crystalline metallic structures. This finding suggests that the size of both metal nanoparticles and pores can be tailored by the control of gelation bath concentration and pyrolysis temperature, in agreement with [24], which can in turn prevent the metal agglomeration related to deactivation of catalysts [17].

Table 2. Average particle size and average crystallite size of metal NPs in different MDCs.

Specie	Pyrolysis Temperature (ºC)	NP size using image analysis (nm)	Crystallite size estimated from XRD data (nm)
NiO	800	-	8+/- 1
NiO	600	14 +/- 7	23 +/- 2
Pt	525	33 +/- 23	25 +/- 5
PtO_2	525		35 +/- 7
Cu	285	40 +/- 19	15 +/- 5
Cu_2O	285		23 +/- 15
Cu	600	85 +/- 29	21 +/- -
CuO	600		25 +/- 6

In the case of Pt^{+4}, NPs could be detected in the carbogel only after pyrolyzing at 525°C. However, the shape of the NPs is not well-defined compared to the Ni-, Cu-, Pd- carbogels. BSE image of Pt-Cgel sample clearly shows (Fig. 9) the appearance of large, irregular shaped NPs. The size of NPs is 33 nm +/- 23 nm according to the image analysis of BSE images.

CHAPTER 4

X-ray Photoemission spectrometry (XPS) of MCAs and commercial Pd5AC catalyst.

Survey XPS spectra for Pd, Pt-Agel and Pd5AC catalyst are depicted in Fig. 11, while results for Ca, Ni and Cu-Agel are presented in Fig. 12. The elements in common for all samples were carbon (C1s) and oxygen (O1s). Sodium (Na) was present in all samples except for catalyst Pd5AC, most probably coming from the type of alginate used to prepare de MCAs. Other elements like S and Cl were detected, originated from the metal precursors: calcium chloride dihydrate, copper (II) pentahydrate sulfate and Platinum (IV) chloride. Given the non-conducting nature of the samples the accumulation of positive charges during the measurements caused a chemical shift of all core-level peaks toward higher binding energy values [39]. Also, all samples' surfaces were exposed to ambient air for several weeks before the analysis. Therefore, it was necessary, as a reference, to calibrate the main C1s peak to *adventitious carbon* (AdC) at 284.5 eV, and applying a corresponding shift to all other spectra, based on ASTM standard and literature for in-nature-polysaccharides samples [40-42].

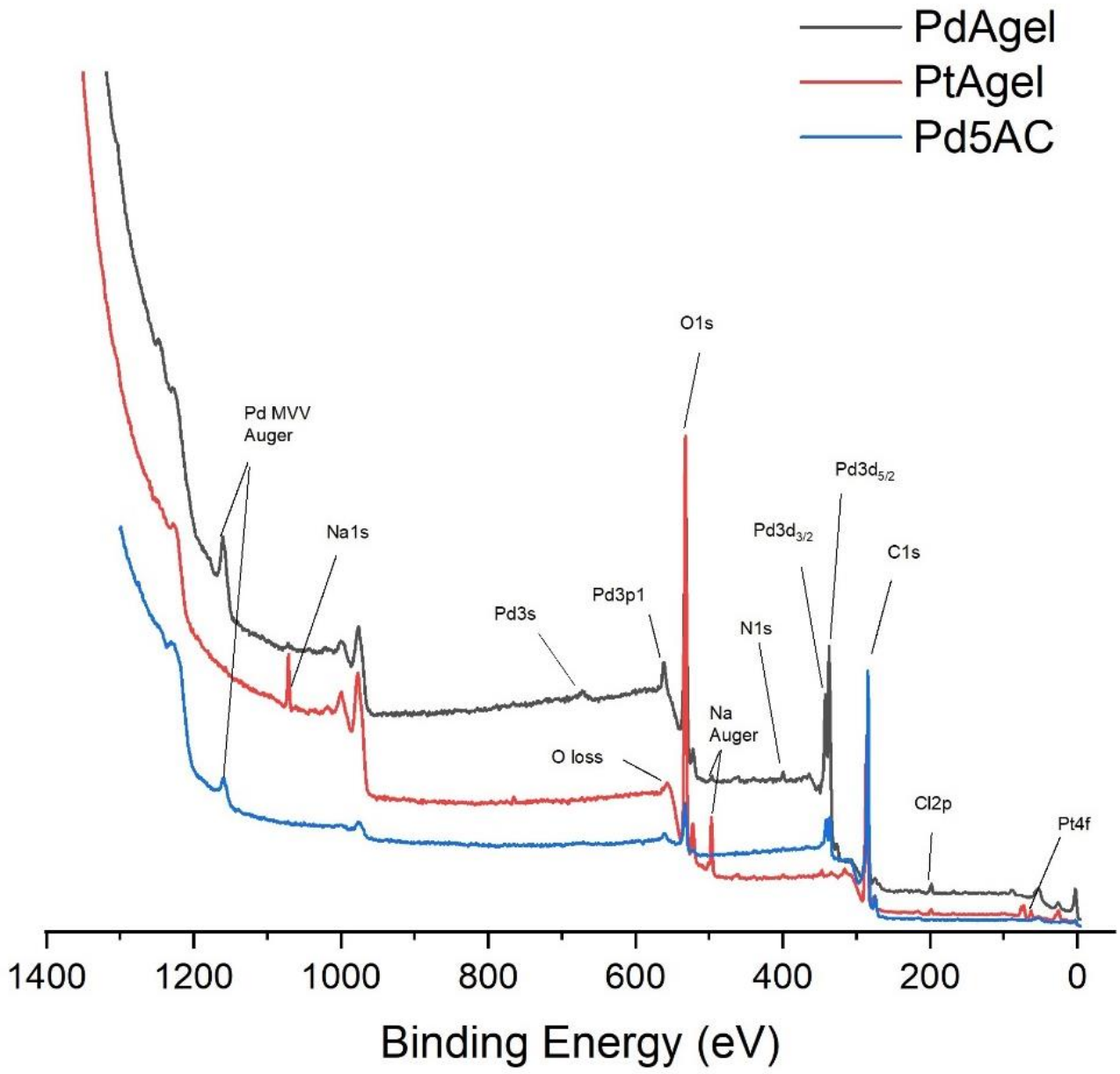

Fig. 11. Overall XPS survey spectra for Pd, Pt-Agel and Pd5AC catalyst

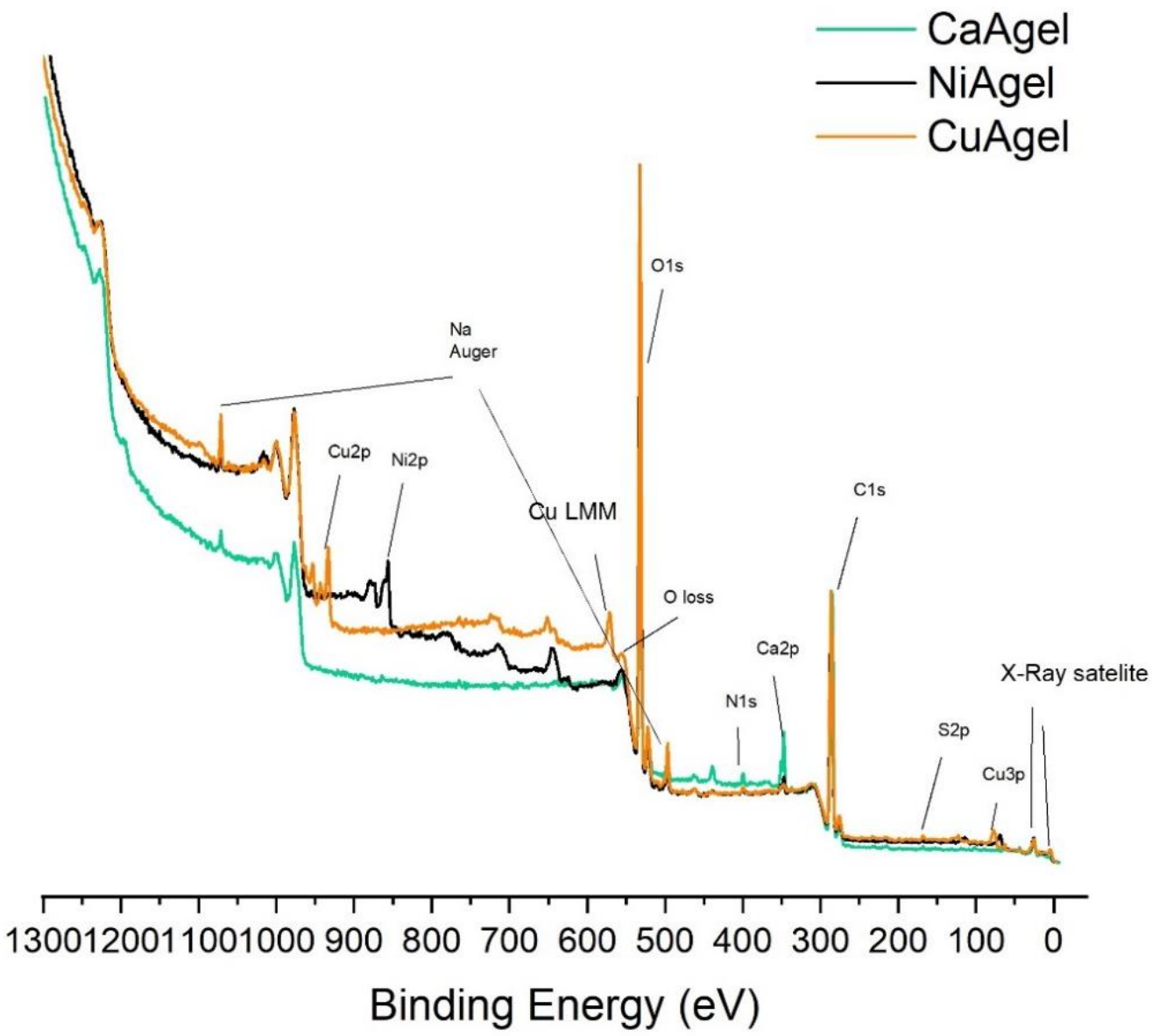

Fig. 12. Overall XPS survey spectra for Ca, Ni and Cu-Agel

C1s photoemission lines of Fig. 13 were successfully deconvoluted into 3 curves for all samples. The C1s in the commercial catalyst Pd5AC appeared at 284.4 eV (C-C bond), indicating it is graphite [43], and component at 285.6 eV matches the C-OH, C-O-C bond [44]. Intensities at average 287.7 eV (third peak from right to left) for all samples expect Pd5AC confirmed the formation of carbonates (CO_3^{2-}) [44][45], firstly suspected by the TGA/DTG analysis. The two components from the deconvolution of *O1s photoemission lines* of Ca-Agel sample (Fig. 14) suggest that the metal ion

formed different compounds, as oxide (CaO at 530.8 eV) and hydroxide ($Ca(OH)_2$ at 532.4 eV) [46]. These two deconvolution components were repeated for Ni, Cu, Pd and Pt, allowing inferring that these metal ions also formed oxides and hydroxides after the aerogel preparation procedure. All samples except Pd5AC showed symmetrical *N1s photoemission line* at average 399.8 eV (Fig. 15), in the form of nitrogen of organic matrix [43] as C-N bond (carbon nitride) [47]. Therefore, nitrate-based precursors of the gelation bath contributed to nitrogen-doping the MCAs, ergo to its surface basicity, which is an important feature linked to electrical conductivity improvement in electrochemistry applications [48], to the development of improved electro-catalysts for oxygen reduction [49], and useful in catalytic applications enhanced by a basic environment, such as the hydrothermal reduction of captured CO_2 [50].

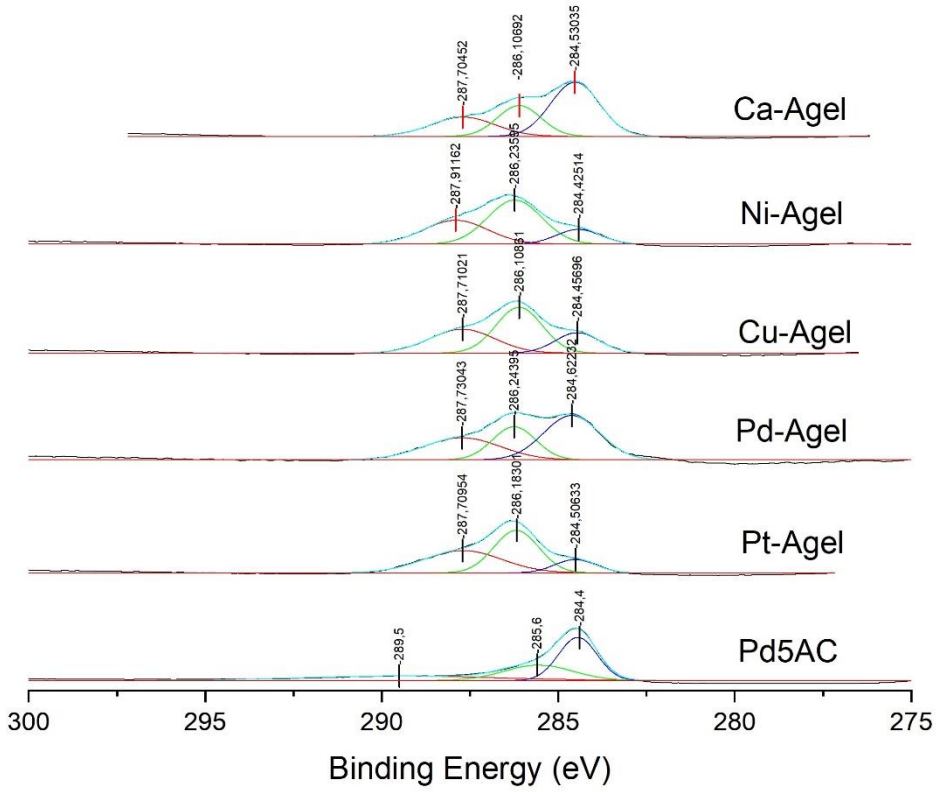

Fig. 13. C1s photoemission lines of MCAs and catalyst Pd5AC

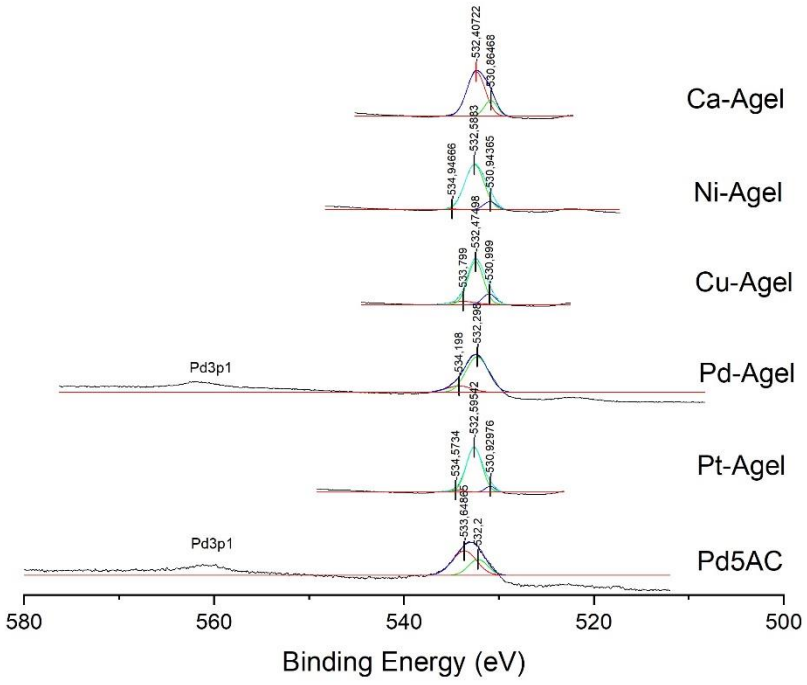

Fig. 14. O1s photoemission lines of MCAs and catalyst Pd5AC

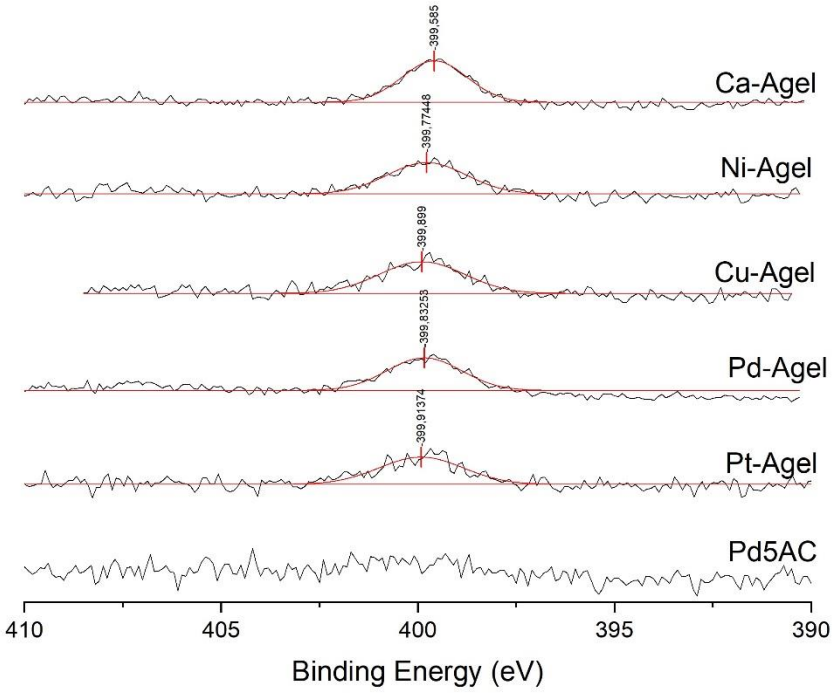

Fig. 15. N1s photoemission lines of MCAs and catalyst Pd5AC

For samples Pd-Agel and Pd5AC the corresponding peaks for $Pd3d_{5/2}$ and $P3d_{3/2}$ [51] appeared as doublet at 335 and 340 eV, respectively, with the respective ΔBE=5.3 eV (Fig. 15). The deconvolution of high-resolution spectra of $Pd3d_{5/2}$ for Pd-Agel showed two peaks at 337.1 and 335.1 eV, with a ΔBE=2.0 eV, which corresponds to Pd^0 and PdO, respectively [52], being the latter of relative greater magnitude, meaning that the Pd-Agel was only partially reduced through the solvent exchange with ethanol. Oppositely, Pd5AC catalyst had relative greater peak of Pd^0 than Pd^{+2}, similarly to Palladium nano-catalyst of Wang *et al*. [22], explaining its effective activity for hydrogenation processes like the conversion of captured CO_2 into green chemicals [50]. Pd MVV Auger lines at 1160.1 and 1159.5 eV confirmed the reduced state of palladium in both Pd-Agel and Pd5AC catalyst.

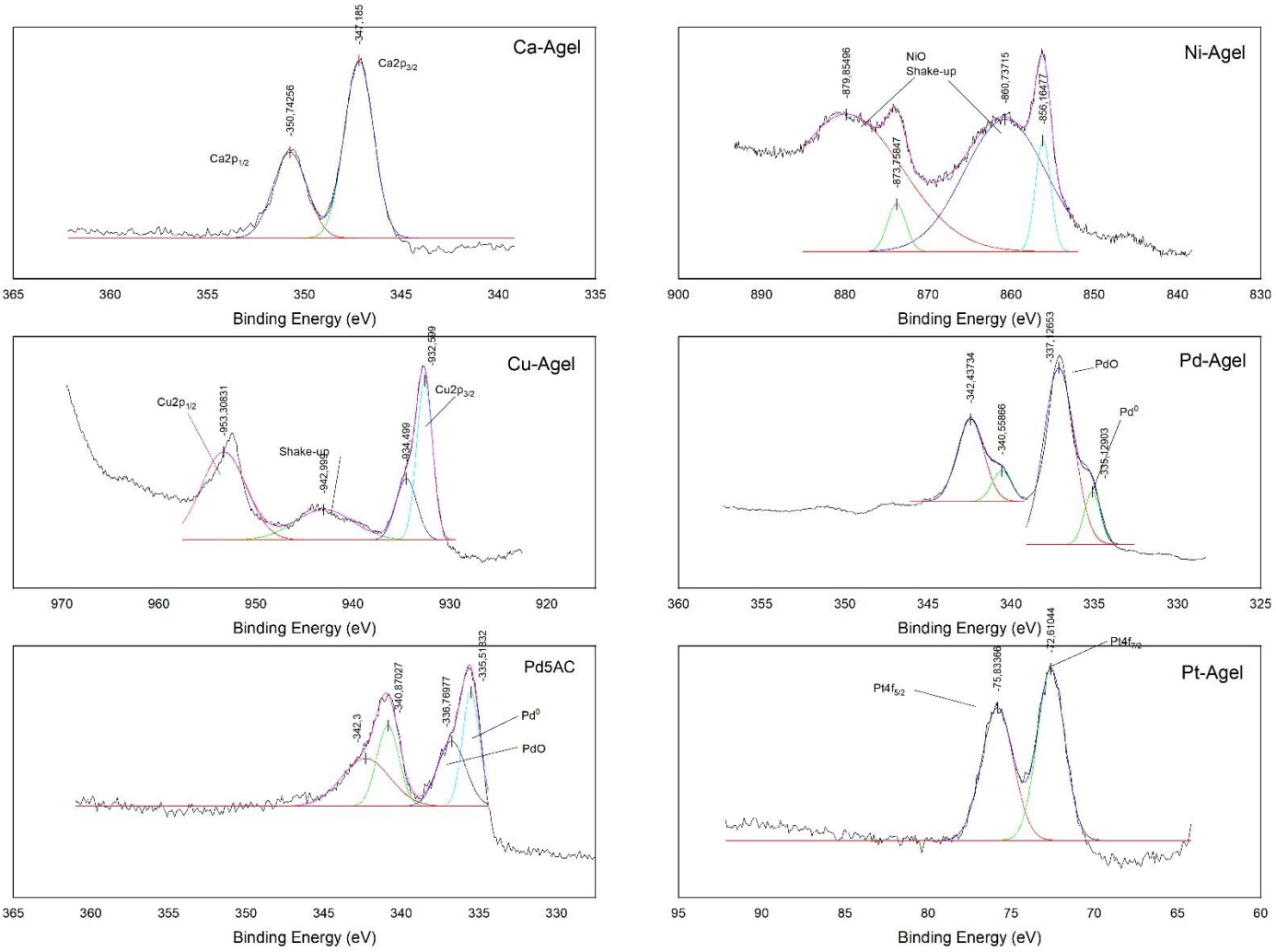

Fig. 16. High resolution spectra of MCAs and control catalyst Pd5AC

The doublet structure of $Pt4f_{7/2}$ and $Pt4f_{5/2}$ had lines at 72.6 (possibly to PtO line based on [53]) and 75.8 eV with a ΔBE=3.2 eV, respectively. However, $Pt4f_{7/2}$ and $Pt4f_{5/2}$ lines of the present work match better with $Pt(OH)_2$ and $PtCl_4$ [43]. Among the aerogels, only Pt-Agel sample presented a clear Na1s line at 1071.3 eV [54], and considering that the Pt precursor used was the worst crosslinking the alginate, it suggests that in fact the Na^+ present in the alginate plays an important role by allowing an ion exchange with the metallic cations, in a similar way found by Primo *et al.* [17], where the cation exchange with Ca^+ allowed controlling the Pd loading. Pt-Agel sample contained Cl2p, coming from the metal precursor that could not be washed out. No Cl2p line (usually between 190-220 eV) for Ca-Agel, and only a weak S2p line for Cu-Agel (168.2 eV), indicating its successful removing during the washing step.

A multiplate structure can be observed for Ni2p, fitting curves by deconvolution with binding energies at 856.1 ($2p_{3/2}$) and 873.7 eV ($2p_{1/2}$). Nearby, the satellite “shake-up” peak at 860.7 and 879.8 eV are indicative of oxidative state of Ni^{+2} specie [21]. In an analogous way, Cu-Agel sample had a multiplate structure of Cu2p, with main emission lines at 932.5 ($2p_{3/2}$) and 953.3 ($2p_{1/2}$). The fitting curves by deconvolution are contributions of Cu^{+1} and Cu^{+2}, at 932.5 and 934.4 eV, respectively, indicating the presence of a mixture of Cu-oxides and hydroxides [55]. The satellite line intensity at 942.9 eV is entirely ascribable to Cu^{+2} [56][57]. Concerning calcium, the doublet of Ca2p appearing at 347.1 ($2p_{3/2}$) and 350.7 eV ($2p_{1/2}$) are representative of $Ca(OH)_2$ [58].

XRD of MDCs

Bragg peaks of nickel (II)-oxide (NiO) were detected (see Fig. 17), and the average crystallite size at 380 ºC is approximately 8 nm +/-1 nm. However, the widths of the peaks became much narrower at 600 ºC, which means a significantly larger crystallite size than at 380 ºC, so the average crystallite size of NiO NPs is 23 nm +/- 2 nm. The diffraction peaks at 44, 52 and 76º are indicative of face-centered cubic (fcc) phase of crystalline Ni (JCPDS no. 04–0850) corresponding to (111), (200), and (220) planes of crystalline Ni [59]. At pyrolysis temperature of 600 ºC, these peaks become more

intense, with NiO peaks still present but weaker than at 380 ºC. The different crystal forms of metallic Nickel (111, 200, 220), with the temperature increase can cause the sintering of nickel into larger particles of metal [60]. In the work of Raptopoulos [14] after pyrolysis under argon atmosphere of the X-Cu-alginate, metallic Cu and Cu_2O were detected in XRD patterns, as a result of the redox reaction between Cu^{+2} and sugars, suggesting that during pyrolysis occurred a carbothermal reduction of the metal ion. It is also worth noting that before pyrolysis the metal ions are molecularly dispersed in the aerogel, and pyrolysis results in metallic-clusters conformation, leading in turn to partial reduction of Ni^{+2} species to form elementary metal nanoparticles. In a similar way, this was evidenced by Bauman *et al*. [24] in the preparation of Ni, Co and Cu carbogels, where the M^{+2} ions formed metal particles (but with no sign of metal-oxides in the XRD patterns) during pyrolysis of the organic aerogel for as no visible metal particles or precipitated metal salts appeared in the micrographs of the pre-carbonized metal-doped materials. The reason for the complete reduction in this case, compared to the partial reduction of the present work, can be that the resorcinol-formaldehyde resin is a reductive matrix, while the alginate is not necessarily. Cu containing gels pyrolyzed at different temperatures resulted in different chemical composition NPs. Bragg's peak of elementary copper and copper (I) oxide was observed in samples pyrolyzed at 285°C, however, copper (II) oxide dominates next to traces of elementary copper in the NPs after pyrolysis at 600°C. The general trend that crystallite size increases with increasing pyrolyzing temperature is true for all components.

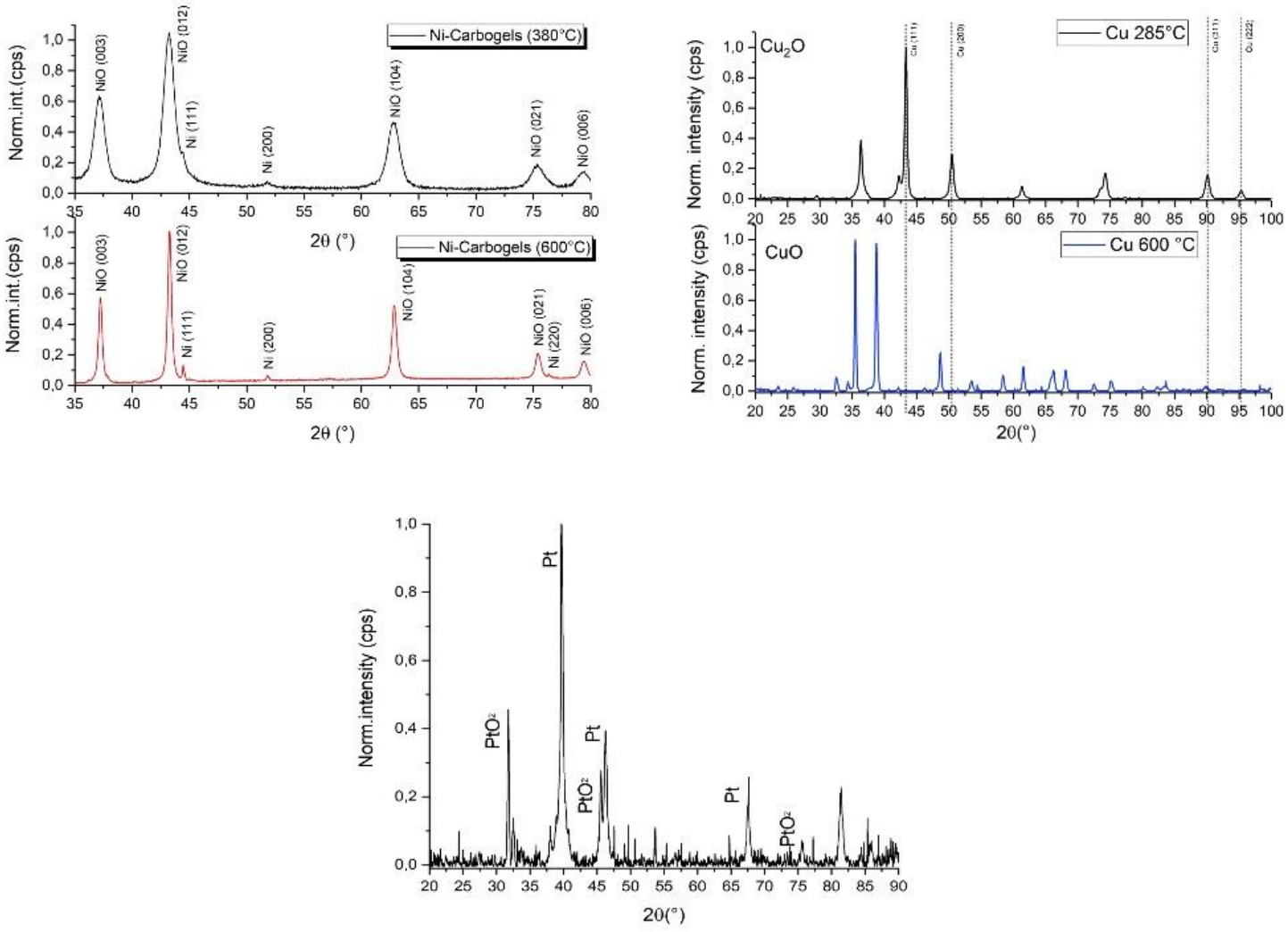

Fig. 17. XRD Diffractograms of MDCs at different temperatures of pyrolysis

XRD measurements also confirmed that elementary Pt is the dominant component of the NPs for Pt-Cgel sample at 525 ºC. However, Bragg peaks of PtO_2 were also detected. The crystallite size is 25 nm+/- 5 nm for Pt and 35 nm +/- 7 nm for PtO_2. Bragg's peak of Pd in Pd5AC sample were not detected, i.e., the Pd do not have a crystalline structure, and it seems to be amorphous.

Temperature programmed reduction (TPR) of MDCs

H_2-TPR of Ni-Cgel (Fig. 18 (a)) showed a main broad peak at 334.3 ºC, characteristic of the reduction region of Ni^{+2} to Ni^0 (378 ºC for bulk NiO [61], and 382 ºC for a Ni4.3%/AC catalyst [62]), confirming that there is only one oxidative state in Ni-Cgel, as observed in XPS. This also matches with the DTG peak at 318 ºC (Fig. 4) that suggested the formation of the metal oxide at this temperature. The slightly lower reduction temperature (334.3 ºC) may be related to the higher content of metal in the Ni-Cgel (9.5%), also reflected by the broad shape of the reduction peak, thus providing a surface level weak interaction between Ni and hydrogen. This higher reducibility is comparatively competitive to other Ni based catalysts with similar metal content and lower reducibility, such as Ni10%/AC (main peak at 430 ºC [63]). This imply it would be required an easier activation pretreatment of Ni-Cgel before a catalytical application. Moreover, the Ni-Cgel presented no significant gasification of the carbon lattice, that usually onsets from 600 ºC for carbon supports [64][65], hence supporting evidence of its thermal stability.

Fig. 18 (b) illustrates the reduction of copper at different oxidative states, observing two major steps. First one start developing from 60 ºC and completely achieved at 420 ºC, corresponding to the reduction CuO specie (Cu^{+2}) to Cu_2O (Cu^{+1}) and Cu^0 [63]. Second one onset at 520 ºC, with a maximum at 673 ºC. Since copper oxides species completely reduce to metallic Cu^0 at temperatures no further than 420 ºC [66][67], this second step should be explained by the gasification of the carbon lattice in the Cu-Cgel sample.

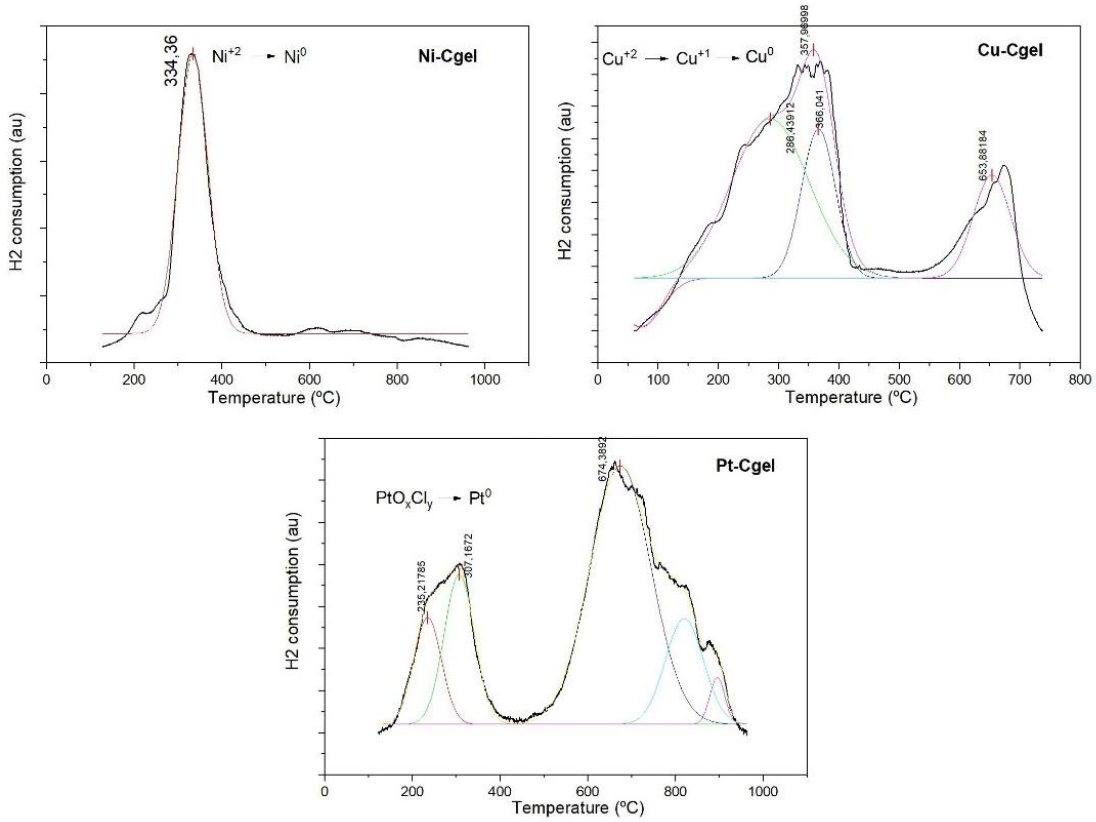

Fig. 18. H_2-TPR curves of a) Ni-Cgel, b) Cu-Cgel and c) Pt-Cgel, produced at 600 ºC

The deconvoluted reduction peaks of Pt-Cgel at 235.2 and 307.2 ºC (Fig. 18. (c)) can be ascribable to reduction of bulk and inter surficial PtO_xCl_y, as suggested by [68], coming from traces of $PtCl_4$ precursor. Additionally, at this temperature range the desorption of HCl have been also identified [69]. It appears that there is an absence of typical PtO_x reduction peaks that use to appear below 200 ºC [70], probably associated to the poor crosslinking that displayed the Pt-Agel. This means that unlike Ni, Cu and Pd, Pt does not catalyze the oxides formation during carbonization. Finally, the gasification of the Pt-Agel sample is observed from 450 up to 950 ºC.

TPR curves of Pd-Cgel where not possible to obtain with the method used, in order to avoid serious damage on the chemisorption equipment, due to the detection of condensable substances. In compensation, TPR curves of Pd-Agel are provided in the next section.

Study of Pd^0 presence in Pd-Agel by TPR/TPO analysis

The former Pd^{+2}-hydrogel beads were of dark-brown color alike the metal precursor bath. Within minutes after the solvent exchange step started, it was observed that the forming Pd-Agel was turning partially black-colored, which is indicative of Pd^{+2} reduction to Pd^{+0}. To confirm this, separate TPR and TPO analyses were conducted over Pd-Agel with the purpose to verify its reduced state after the solvent exchange. In Fig. 19 (a) the TPO curves depicts the O_2 consumption as well as the evolution of CO (mass 28 amu) and CO_2 (mass 44 amu), clearly showing two burn-off steps at 252 and 308 ºC. A weak O_2 consumption peak is warned at 355.5 ºC, but is not accompanied with appreciable acceleration of CO/CO_2 formation, so it could be associated to a contribution of PdO formation by Pd^0 oxidation, which has been reported with maximum rates at 327 ºC [71] and 380 ºC [72]. In Fig. 19 (b) the TPR of Pd-Agel showed a main broad peak of asymmetrical hydrogen consumption, probably due to the high metal loading (~13%), with three deconvolution peaks, suggesting that Pd^{+2} does not undergo a single step reduction. Instead, while the main peak at 197.8 ºC matches with the reduction of Pd^{+2} strongly interacting with the support [73], the peaks at 255.9 and 295.9 ºC may indicate reduction of i) other Pd^{+2} species with even stronger interactions with the support, and/or ii) a two-step reduction ($Pd^{+2} \rightarrow Pd^{+1} \rightarrow Pd^0$) [74]. This results, combined to the deconvolution of XPS high-resolution spectra of $Pd3d_{5/2}$, confirm that the Pd atomic layer observed by SEM contains elementary metal (Pd^0) in mixture with metal oxides. This finding is in concordance with the results of Primo *et al.* [17], who also observed this proceeding during solvent exchange with ethanol of Pd-hydrogel. In this sense, an induction of the Pd reduction, at 80 ºC and 2h, may lead to a higher degree conversion, based on *Wang et al*. [22].

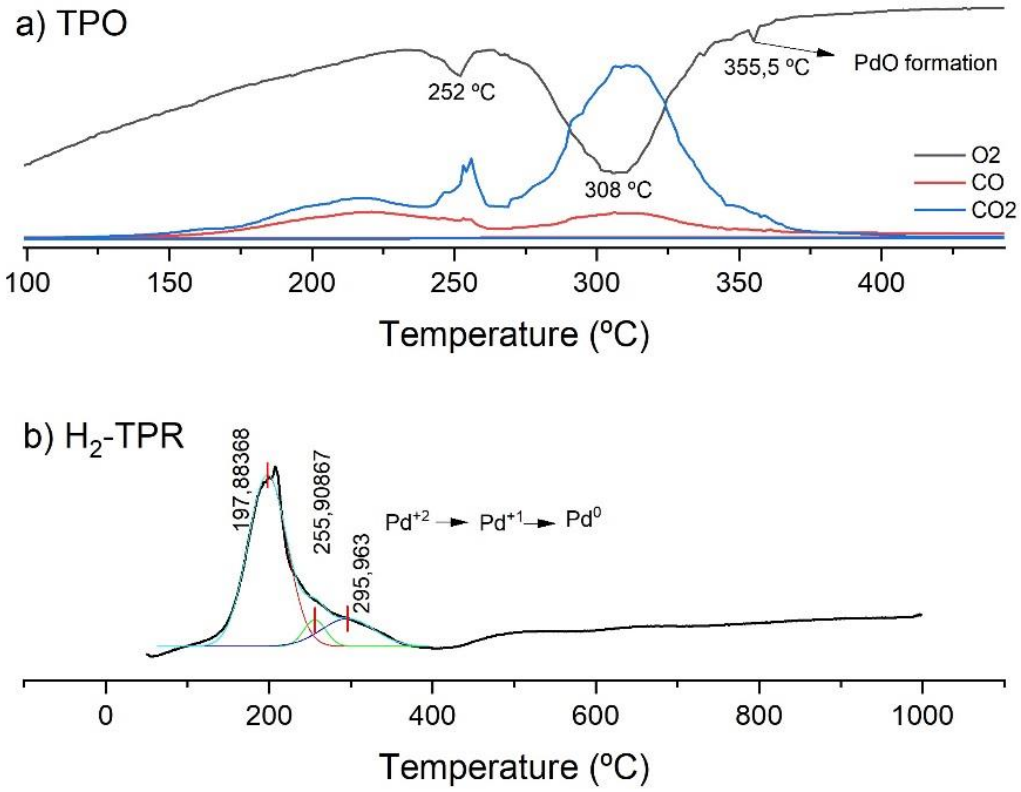

Fig. 19 a) TPO and b) H_2-TPR curves for Pd-Agel

Catalytical activity assessment of Pd-Agel

Among the materials synthetized, Pd-Agel was selected for catalytical test, based on its mass quantity availability, and the presence of reduced (metallic) sites detected by XPS. As it can be observed in Fig. 20, the reaction with catalyst Pd-Agel presented a clear consumption of hydrogen reflected by the decrease in the pressure over the time, while the formic acid yield was 34.3%. In contrast, the blank reaction showed no H_2 consumption, as the pressure remained flat over the time, and the final liquid characterization (HPLC chromatograph in Fig. 20) showed no formic acid signal. On the other hand, reaction with Pd powder as catalyst showed a negligible yield of 2.97%, while commercial catalyst Pd5AC showed, in chapter 2, a yield of 56% at the same conditions of pressure of hydrogen,

temperature and reactor's filling, but in less time of 2 h. These results show that the Pd-Agel is active toward the hydrogenation of captured CO_2 in water into formic acid. The disadvantage encountered for this catalyst is the poor physical stability under the alkaline conditions of the reaction solution (pH=9.2), because after the hydrothermal reduction process the beads collapsed and teared apart, although the residue could be separated and recovered. Future work concerning optimizing the production scale of the Pd-Agel into Pd-Cgel will allow studying its performance as more chemically and thermally stable carbonous material, while stablishing the improvements needed for its competitiveness against commercial catalysts.

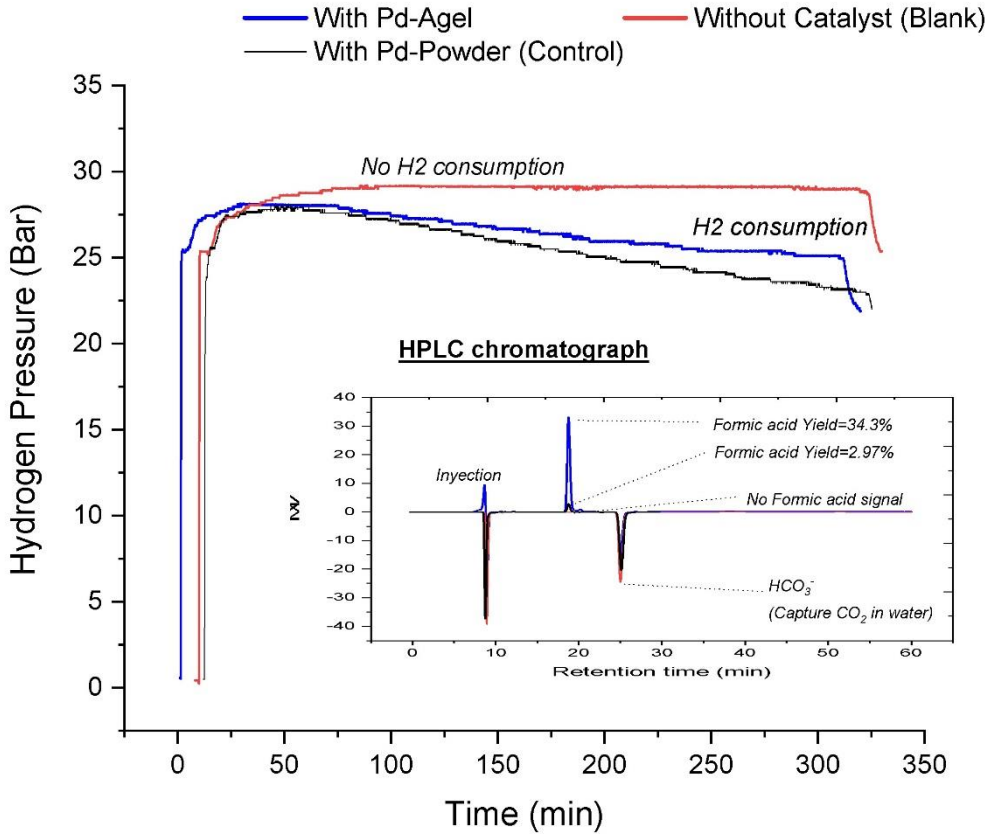

Fig. 20. Hydrogen pressure evolution during the reduction of captured CO2 into formic acid using no catalyst, catalyst Pd-Agel and Pd Powder.

CHAPTER 4

Conclusions

In the present work, different properties of the post-structure of metal-crosslinked carbogels from alginate were obtained by varying the synthesis conditions, such as the type of metal ion, the concentration of the metal precursor in the gelation bath and the pyrolysis temperature. The metal content in the aerogel can be tuned by adjusting the concentration of the gelation bath up to 180 mmol/L, where above this value no greater amount of metal can be introduced in the hydrogel matrix. Likewise, the surface area of MCAs was dependent of the concentration of gelation bath, showing an indirect proportionality. Expect for Pt^{+4}, all MCAs beads presented a good sphericity, and high porosity (99% in average) in the mesoporous range. In the pyrolysis step, up to 600 ºC, all MCAs presented significant mass loss, suggesting a marginal thermal stability of the material. Nevertheless, among the MDCs, Pd-Cgel remarkably lost the least mass, with only 58 %. Through the pyrolysis, the spherical shape of MCAs was kept, but reduction of pore radius between 66% and 90% evidenced a shrinkage, expect for Pd-Agel which on the contrary gained pore size. For all Cgels, nanoparticles-clusters evolution, through the different temperatures, was detected by SEM-BSE, where Ni- and Cu-Cgel at 600 ºC, with average size of 14 nm +/- 7 nm and 85 nm +/- 29 nm, respectively. The combined analysis of XRD and TPR results of Ni-, Cu-, Pt- and Pd-Cgels indicated that the particles are composed of elementary metals and metal oxides in varying ratios, while Pd-Agel was the sole aerogel to present a reduction to elementary Pd during solvent exchange. The assessment experiments of Pd-Agel showed that the material, without any thermal treatment, is catalytically activity toward reduction of captured CO_2 in water into formic acid. However, it is necessary to optimize the production scale of the carbogel stage for trying to find a more chemically and thermally stable catalyst, with competitiveness against commercial catalysts.

CHAPTER 4

REFERENCES

[1] S. S. Kistler, “Coherent expanded aerogels and jellies,” *Nature*, vol. 127, no. 3211, p. 741, 1931.

[2] S. S. Kistler, “Coherent expanded aerogels,” *Rubber Chem. Technol.*, vol. 5, no. 4, pp. 600–603, 1932.

[3] S. S. Kistler, “Coherent expanded-aerogels,” *J. Phys. Chem.*, vol. 36, no. 1, pp. 52–64, 2002.

[4] A. C. Pierre and G. M. Pajonk, “Chemistry of aerogels and their applications,” *Chem. Rev.*, vol. 102, no. 11, pp. 4243–4266, 2002.

[5] C. Moreno-Castilla and F. J. Maldonado-Hódar, “Carbon aerogels for catalysis applications: An overview,” *Carbon N. Y.*, vol. 43, no. 3, pp. 455–465, 2005.

[6] R. W. Pekala, “Organic aerogels from the polycondensation of resorcinol with formaldehyde,” *J. Mater. Sci.*, vol. 24, no. 9, pp. 3221–3227, 1989.

[7] J.-H. Lee and S.-J. Park, “Recent advances in preparations and applications of carbon aerogels: A review,” *Carbon N. Y.*, vol. 163, pp. 1–18, 2020.

[8] P. Paraskevopoulou, D. Chriti, G. Raptopoulos, and G. C. Anyfantis, “Synthetic polymer aerogels in particulate form,” *Materials (Basel).*, vol. 12, no. 9, p. 1543, 2019.

[9] O. K. Lee and E. Y. Lee, “Sustainable production of bioethanol from renewable brown algae biomass,” *Biomass and Bioenergy*, vol. 92, pp. 70–75, 2016.

[10] L. Pereira and J. Cotas, “Introductory chapter: Alginates-A general overview,” *Alginates-Recent Uses This Nat. Polym.*, 2020.

[11] E. M. Ahmed, “Hydrogel: Preparation, characterization, and applications: A review,” *J. Adv. Res.*, vol. 6, no. 2, pp. 105–121, 2015.

[12] S. A. Qamar, M. Qamar, A. Basharat, M. Bilal, H. Cheng, and H. M. N. Iqbal, “Alginate-based nano-adsorbent materials–Bioinspired solution to mitigate hazardous environmental pollutants,” *Chemosphere*, p. 132618, 2021.

[13] H. Maleki, “Recent advances in aerogels for environmental remediation applications: A review,” *Chem. Eng. J.*, vol. 300, pp. 98–118, 2016.

[14] G. Raptopoulos *et al.*, “Metal-doped carbons from polyurea-crosslinked alginate aerogel beads,” *Mater. Adv.*, vol. 2, no. 8, pp. 2684–2699, 2021.

[15] M. G. Plaza, C. Pevida, A. Arenillas, F. Rubiera, and J. J. Pis, “CO2 capture by adsorption with nitrogen enriched carbons,” *Fuel*, vol. 86, no. 14, pp. 2204–2212, 2007.

[16] Y. Zhang *et al.*, “Hierarchical Cross-Linked Carbon Aerogels with Transition Metal-Nitrogen Sites for Highly Efficient Industrial-Level CO2 Electroreduction,” *Adv. Funct. Mater.*, vol. 31, no. 45, p. 2104377, 2021.

[17] A. Primo, M. Liebel, and F. Quignard, “Palladium coordination biopolymer: A versatile access to highly porous dispersed catalyst for suzuki reaction,” *Chem. Mater.*, vol. 21, no. 4, pp. 621–627, 2009.

[18] S. Frindy, A. el Kadib, M. Lahcini, A. Primo, and H. García, “Copper nanoparticles stabilized in a porous chitosan aerogel as a heterogeneous catalyst for C− S cross-coupling,” *ChemCatChem*, vol. 7, no. 20, pp. 3307–3315, 2015.

[19] G. Agrimi *et al.*, *Biorefineries: an introduction*. Walter de Gruyter GmbH & Co KG, 2015.

[20] X. Qiao, L. Niu, H. Zhang, X. Wen, Y. Cao, and G. Bai, “Controllable fabrication of a novel porous Ni-alginate hybrid material for hydrogenation,” *Appl. Catal. B Environ.*, vol. 218, pp. 721–730, 2017.

[21] X. Zhang *et al.*, “Novel alginate particles decorated with nickel for enhancing ciprofloxacin removal: characterization and mechanism analysis,” *Ecotoxicol. Environ. Saf.*, vol. 169, pp. 392–401, 2019.

[22] B. Wang *et al.*, “Palladium nano-catalyst supported on cationic nanocellulose–alginate hydrogel for effective catalytic reactions,” *Cellulose*, vol. 27, pp. 6995–7008, 2020.

[23] T. F. Baumann, G. A. Fox, J. H. Satcher, N. Yoshizawa, R. Fu, and M. S. Dresselhaus, “Synthesis and characterization of copper-doped carbon aerogels,” *Langmuir*, vol. 18, no. 18, pp. 7073–7076, 2002.

[24] T. F. Baumann and J. H. Satcher, “Homogeneous incorporation of metal nanoparticles into ordered macroporous carbons,” *Chem. Mater.*, vol. 15, no. 20, pp. 3745–3747, 2003.

[25] B. A. T. Mehrabadi, S. Eskandari, U. Khan, R. D. White, and J. R. Regalbuto, “A review of

preparation methods for supported metal catalysts," *Adv. Catal.*, vol. 61, pp. 1–35, 2017.

[26] L. Juhász *et al.*, "False Morphology of Aerogels Caused by Gold Coating for SEM Imaging," *Polymers (Basel).*, vol. 13, no. 4, p. 588, 2021.

[27] Y. Liu *et al.*, "Bio-based nickel alginate and copper alginate films with excellent flame retardancy: preparation, flammability and thermal degradation behavior," *RSC Adv.*, vol. 5, no. 79, pp. 64125–64137, 2015.

[28] L. B. Railsback, "Some fundamentals of mineralogy and geochemistry," *On-line book, quoted from www. gly. uga. edu/railsback*, 2006.

[29] R. P. Narayanan, G. Melman, N. J. Letourneau, N. L. Mendelson, and A. Melman, "Photodegradable iron (III) cross-linked alginate gels," *Biomacromolecules*, vol. 13, no. 8, pp. 2465–2471, 2012.

[30] T. Baran, N. Y. Baran, and A. Menteş, "Preparation, structural characterization, and catalytic performance of Pd (II) and Pt (II) complexes derived from cellulose Schiff base," *J. Mol. Struct.*, vol. 1160, pp. 154–160, 2018.

[31] M. J. Zohuriaan and F. Shokrolahi, "Thermal studies on natural and modified gums," *Polym. Test.*, vol. 23, no. 5, pp. 575–579, 2004.

[32] W. Brockner, C. Ehrhardt, and M. Gjikaj, "Thermal decomposition of nickel nitrate hexahydrate, Ni (NO3) 2· 6H2O, in comparison to Co (NO3) 2· 6H2O and Ca (NO3) 2· 4H2O," *Thermochim. Acta*, vol. 456, no. 1, pp. 64–68, 2007.

[33] A. Alba, M. A. Aramendia, V. Borau, C. Jimenez, and J. M. Marinas, "Influence of preparation variables on the activity and selectivity of PdAlPO4 catalysts," *J. Catal.*, vol. 98, no. 2, pp. 288–295, 1986.

[34] E. Widjaja, H. H. Chong, and M. Tjahjono, "Use of thermo-Raman spectroscopy and chemometric analysis to identify dehydration steps of hydrated inorganic samples—application to copper sulfate pentahydrate," *J. Raman Spectrosc. An Int. J. Orig. Work all Asp. Raman Spectrosc. Incl. High. Order Process. also Brillouin Rayleigh Scatt.*, vol. 41, no. 2, pp. 181–186, 2010.

[35] R. L. White, "Variable temperature infrared study of copper sulfate pentahydrate dehydration,"

Thermochim. Acta, vol. 528, pp. 58–62, 2012.

[36] J. Gross, C. T. Alviso, and R. W. Pekala, “Structural evolution in carbon aerogels as a function of precursor material and pyrolysis temperature,” *MRS Online Proc. Libr.*, vol. 431, 1996.

[37] J. M. Miller and B. Dunn, “Morphology and electrochemistry of ruthenium/carbon aerogel nanostructures,” *Langmuir*, vol. 15, no. 3, pp. 799–806, 1999.

[38] K. Liu and M. Ostadhassan, “The impact of pore size distribution data presentation format on pore structure interpretation of shales,” *Adv. Geo-Energy Res.*, vol. 3, no. 2, pp. 187–197, 2019.

[39] G. Greczynski and L. Hultman, “X-ray photoelectron spectroscopy: towards reliable binding energy referencing,” *Prog. Mater. Sci.*, vol. 107, p. 100591, 2020.

[40] R. Zhang *et al.*, “Preparation of hierarchical porous carbons from sodium carboxymethyl cellulose via halloysite template strategy coupled with KOH-activation for efficient removal of chloramphenicol,” *J. Taiwan Inst. Chem. Eng.*, vol. 80, pp. 424–433, 2017.

[41] G.-J. Kwon *et al.*, “Adsorption characteristics of Ag nanoparticles on cellulose nanofibrils with different chemical compositions,” *Polymers (Basel).*, vol. 12, no. 1, p. 164, 2020.

[42] A. E1523-15, “Standard guide to charge control and charge referencing techniques in X-ray photoelectron spectroscopy.” ASTM International West Conshohocken, 2015.

[43] J. F. Moulder, “Handbook of X-ray photoelectron spectroscopy,” *Phys. Electron.*, pp. 230–232, 1995.

[44] M. Peuckert, “XPS investigation of surface oxidation layers on a platinum electrode in alkaline solution,” *Electrochim. Acta*, vol. 29, no. 10, pp. 1315–1320, 1984.

[45] Y. Yu *et al.*, “CO 2 activation and carbonate intermediates: an operando AP-XPS study of CO 2 electrolysis reactions on solid oxide electrochemical cells,” *Phys. Chem. Chem. Phys.*, vol. 16, no. 23, pp. 11633–11639, 2014.

[46] J.-C. Dupin, D. Gonbeau, P. Vinatier, and A. Levasseur, “Systematic XPS studies of metal oxides, hydroxides and peroxides,” *Phys. Chem. Chem. Phys.*, vol. 2, no. 6, pp. 1319–1324, 2000.

[47] X. Yan, T. Xu, G. Chen, S. Yang, H. Liu, and Q. Xue, “Preparation and characterization of

electrochemically deposited carbon nitride films on silicon substrate," *J. Phys. D. Appl. Phys.*, vol. 37, no. 6, p. 907, 2004.

[48] H. Chen *et al.*, "Nitrogen doping effects on the physical and chemical properties of mesoporous carbons," *J. Phys. Chem. C*, vol. 117, no. 16, pp. 8318–8328, 2013.

[49] K. Elumeeva, J. Ren, M. Antonietti, and T. Fellinger, "High Surface Iron/Cobalt-Containing Nitrogen-Doped Carbon Aerogels as Non-Precious Advanced Electrocatalysts for Oxygen Reduction," *ChemElectroChem*, vol. 2, no. 4, pp. 584–591, 2015.

[50] I. Juan, E. Pérez, D. León, Á. Martín, and M. D. Bermejo, "Catalytic hydrothermal conversion of CO2 captured by ammonia into formate using aluminum-sourced hydrogen at mild reaction conditions," *J. Ind. Eng. Chem.*, vol. 97, pp. 539–548, 2021.

[51] B. V. Crist and D. B. V Crisst, *Handbook of monochromatic XPS spectra*, vol. 1. Wiley New York, 2000.

[52] M. Brun, A. Berthet, and J. C. Bertolini, "XPS, AES and Auger parameter of Pd and PdO," *J. Electron Spectros. Relat. Phenomena*, vol. 104, no. 1–3, pp. 55–60, 1999.

[53] J. Z. Shyu and K. Otto, "Identification of platinum phases on γ-alumina by XPS," *Appl. Surf. Sci.*, vol. 32, no. 1–2, pp. 246–252, 1988.

[54] B. C. Beard, "Sodium salts of chlorine oxyacid anions, Cl (+ 7), perchlorate, xps comparison spectra," *Surf. Sci. Spectra*, vol. 2, no. 2, pp. 97–103, 1993.

[55] M. C. Biesinger *et al.*, "Quantitative chemical state XPS analysis of first row transition metals, oxides and hydroxides," in *Journal of Physics: Conference Series*, 2008, vol. 100, no. 1, p. 12025.

[56] R. P. Vasquez, "CuO by XPS," *Surf. Sci. Spectra*, vol. 5, no. 4, pp. 262–266, 1998.

[57] D. P. Drolet, D. M. Manuta, A. J. Lees, A. D. Katnani, and G. J. Coyle, "FT-IR and XPS study of copper (II) complexes of imidazole and benzimidazole," *Inorganica Chim. Acta*, vol. 146, no. 2, pp. 173–180, 1988.

[58] T. Sugama, L. E. Kukacka, N. Carciello, and N. J. Hocker, "Study of interactions at water-soluble polymer/Ca (OH) 2 or gibbsite interfaces by XPS," *Cem. Concr. Res.*, vol. 19, no. 6, pp. 857–867, 1989.

[59] C. Teng *et al.*, “Fabrication and characterization of monodisperse magnetic porous nickel microspheres as novel catalysts,” *Nanoscale Res. Lett.*, vol. 10, no. 1, pp. 1–8, 2015.

[60] E. D. Garbowski, C. Mirodatos, and M. Primet, “Nickel in Mordenites–Formation and Activity of Metallic complexes, Clusters and Particles,” in *Studies in Surface Science and Catalysis*, vol. 12, Elsevier, 1982, pp. 235–243.

[61] A. Alihosseinzadeh, B. Nematollahi, M. Rezaei, and E. N. Lay, “CO methanation over Ni catalysts supported on high surface area mesoporous nanocrystalline γ-Al2O3 for CO removal in H2-rich stream,” *Int. J. Hydrogen Energy*, vol. 40, no. 4, pp. 1809–1819, 2015.

[62] Q. Zeng *et al.*, “Adsorption and oxidation of elemental mercury from coal-fired flue gas over activated coke loaded with Mn–Ni oxides,” *Environ. Sci. Pollut. Res.*, vol. 26, no. 15, pp. 15420–15435, 2019.

[63] R. Merabti, K. Bachari, D. Halliche, Z. Rassoul, and A. Saadi, “Synthesis and characterization of activated carbon-supported copper or nickel and their catalytic behavior towards benzaldehyde hydrogenation,” *React. Kinet. Mech. Catal.*, vol. 101, no. 1, pp. 195–208, 2010.

[64] M. Trépanier, A. Tavasoli, A. K. Dalai, and N. Abatzoglou, “Co, Ru and K loadings effects on the activity and selectivity of carbon nanotubes supported cobalt catalyst in Fischer–Tropsch synthesis,” *Appl. Catal. A Gen.*, vol. 353, no. 2, pp. 193–202, 2009.

[65] G. Zhang, Z. Li, H. Zheng, T. Fu, Y. Ju, and Y. Wang, “Influence of the surface oxygenated groups of activated carbon on preparation of a nano Cu/AC catalyst and heterogeneous catalysis in the oxidative carbonylation of methanol,” *Appl. Catal. B Environ.*, vol. 179, pp. 95–105, 2015.

[66] G. Fierro, M. Lojacono, M. Inversi, P. Porta, R. Lavecchia, and F. Cioci, “A study of anomalous temperature-programmed reduction profiles of Cu2O, CuO, and CuO-ZnO catalysts,” *J. Catal.*, vol. 148, no. 2, pp. 709–721, 1994.

[67] K. Sonobe, M. Tanabe, T. Imaoka, W. Chun, and K. Yamamoto, “Low-Temperature H2 Reduction of Copper Oxide Subnanoparticles,” *Chem. Eur. J.*, vol. 27, no. 33, pp. 8452–8456, 2021.

[68] C.-P. Hwang and C.-T. Yeh, “Platinum-oxide species formed by oxidation of platinum

crystallites supported on alumina," *J. Mol. Catal. A Chem.*, vol. 112, no. 2, pp. 295–302, 1996.

[69] M. A. Fraga, E. Jordao, M. J. Mendes, M. M. A. Freitas, J. L. Faria, and J. L. Figueiredo, "Properties of carbon-supported platinum catalysts: role of carbon surface sites," *J. Catal.*, vol. 209, no. 2, pp. 355–364, 2002.

[70] T. Huizinga, J. Van Grondelle, and R. Prins, "A temperature programmed reduction study of Pt on Al2O3 and TiO2," *Appl. Catal.*, vol. 10, no. 2, pp. 199–213, 1984.

[71] S. C. Su, J. N. Carstens, and A. T. Bell, "A Study of the Dynamics of Pd Oxidation and PdO Reduction by H2and CH4," *J. Catal.*, vol. 176, no. 1, pp. 125–135, 1998.

[72] G. Farkas, A. Beck, A. Tungler, and A. Sárkány, "Characterization of Pd blacks by temperature programmed oxidation," *React. Kinet. Catal. Lett.*, vol. 70, no. 2, pp. 331–339, 2000.

[73] A. Aznarez, A. Gil, and S. A. Korili, "Performance of palladium and platinum supported on alumina pillared clays in the catalytic combustion of propene," *RSC Adv.*, vol. 5, no. 100, pp. 82296–82309, 2015.

[74] B. Ngamsom, N. Bogdanchikova, M. A. Borja, and P. Praserthdam, "Characterisations of Pd–Ag/Al2O3 catalysts for selective acetylene hydrogenation: effect of pretreatment with NO and N2O," *Catal. Commun.*, vol. 5, no. 5, pp. 243–248, 2004.

Part 3. On the design and construction of a semicontinuous facility for integrating CO_2 and hydrogen economies and its concept proof by experimental study

CHAPTER 5

Coupling the solvent-based co_2 capture processes to the metal-water-splitting for hydrogen generation in a semi-continuous fashion

Abstract

Increasingly, green hydrogen is occupying a protagonist place in the energy and manufacturing markets as one of the most promising sustainable sources, under the lens of the so-called hydrogen economy. For its part, CO_2-economy is experiencing this increasing trend as well, suggesting that the conjugation of both will represent a powerful strategy for the achievement of the sustainable-development goals in the future. The present work aims at coupling for the first time, in a novel semicontinuous facility, the CO_2-Rich stream (CO2RS) and CO_2 Capture-Solvent Lean stream (CO2LS), from traditional solvent-based CO_2 capture processes (NH_3, NaOH and MEA), with the hydrogen generation from the metal-water splitting reaction, using common elements such as Al, Zn, Mn and Fe. The purpose of doing this is to give an added value to those alkaline streams with the capability of activating/promoting the hydrogen generation from metals, thus offering important scale-up information. The hydrogen produced was collected and quantified to stablish the yields of hydrogen for comparison of the different metal/stream type. The liquid (HPLC) and solid characterization (XRD and FTIR analyses) allowed determining the changes of CO2R concentration, and the oxidative state of the exhausted metals, respectively. The experimental study showed that H_2 yield increased in the order Mn<Al<Fe<Zn, using aqueous AC as CO2RS. The yield was proportional to temperature and concentration, and indirectly to particle size. For Al, among the streams used, aqueous NaOH (CO2LS) showed the showed the highest H_2 relative yield, up to 85.5%, within only 50 min and 200 ºC. Based on the results, the most basic CO2RSs and CO2LSs like aqueous SB and NaOH, respectively, would do a better match with less active metals like Al and Mn, while highly active metals like Zn and Fe would do a better match with less basic CO2RS like AC, or a CO2LS like aqueous ammonia or MEA.

Keywords: *CO_2-economy, H_2-economy, green hydrogen, carbon capture, CO_2-Rich stream, CO_2-Lean stream, metal-water splitting, superheated water, semicontinuous facility, concept proof*

CHAPTER 5

Introduction

In recent times the increasing demand of electricity, along with its associated energy and fuel security, is leading to a diversification of the energy basket in many countries [1]. As a response to the global environmental problems, demographic growth and carbon emissions from fossil fuels, the hydrogen economy driven by renewable sources supposes a breakthrough in future's sustainability [2], and a priority for the EU's post-COVID-19 economic recovery package [3][4]. Hydrogen is largely used as a reactant in the chemical and petroleum industries for ammonia production (around 50%), followed by crude oil processing (slightly less than 40%) [5]. Pure hydrogen is a promising fuel because of its high calorific value (120-143 MJ/kg) compared to coal (14-29.6 MJ/kg) [6-8], currently almost entirely supplied from natural gas (steam methane reforming), but can be obtained by a number of processes such as water electrolysis, natural gas reforming, gasification of coal and biomass, water splitting by high temperature heat, photo-electrolysis and biological processes [9]. However, its production from fossil sources has a significant carbon emission (around 830 million tons of carbon dioxide per year) [10] making necessary to change to low- or zero-carbon hydrogen production [11]. In this context, three main types of hydrogen are recognized (grey, blue and green), depending on the source and emissions during the production [12]. Grey-hydrogen comes from the traditional steam reforming of natural gas, and the waste carbon dioxide is released to the atmosphere. Blue-hydrogen is cleaner version of grey where the carbon emissions are captured and geologically stored or reused. Green hydrogen is the cleanest version, is generated by renewable energy sources (i.e., water electrolysis) without producing carbon emissions, using low or zero-carbon electricity [13][14]. Although only green hydrogen is considered by EU as the future, and blue hydrogen does not comply the IPCEI rules (important projects of common European interests) [15], it may have an important place as an intermediate solution in the coming decades, especially if the CO_2 capture rate can be kept to 99% [16]. The main problem with blue hydrogen is that its reduction impact on the greenhouse effect has not been fully proven, since the effective reduction of CO_2 emissions is only 9-12% less than gray, and the footprint of greenhouse gases can be more than 20% higher than burning natural gas or coal, and 60% higher than burning diesel, according to recent life cycle analysis proposed by Howarth *et*

al. [17]. Even so, blue hydrogen has competitive advantages, and its achievement cannot be ruled out in the medium term, since it will be cheaper than green hydrogen, especially by 2030 [18], and with greater potential for industrial scaling [19][20].

In consequence, the efforts are addressed toward a cleaner and environmentally sustainable way of production of green or renewable hydrogen from the electrolysis of water powered by solar and/or wind energy [21]. The electrolysis of water as hydrogen production system is a proven technology in small and large scale [21]. The most widespread electrolysis system is based on alkaline and PEM (proton exchange membrane) electrolyzer, but its disadvantages are the high cost of components, use of noble catalysts, low durability, corrosion, among others [22][23]. In general, electrolysis is still a more expensive method (10.3 $/kg and efficiency of 60-80%)) compared to traditional steam reforming (2.27$/kg and 85% efficiency) and only applied if high-purity hydrogen is required [10][24]. Other possible method for producing hydrogen is based on the release from ammonia, but is not a well-established technology, as it does not form a significant part of the existing markets for ammonia [25]. Recently, hydrogen generated from the reaction or corrosion of aluminum/aluminum alloys with water becomes interesting because of its low cost, relatively high hydrogen storage capacity and simplicity of the hydrogen generation system [26]. In spite of the need of further economic assessments to ensure feasibility of aluminum as feedstock, the process is promising in terms of sustainability, owing to the recyclability of aluminum from scrap, using renewable energy [27], as aluminum can be regenerated through a solar thermochemical cycle [28-30]. Recycled scrap aluminum not suitable for secondary aluminum production can be consumed for hydrogen generation, making the cost of aluminum-based hydrogen production potentially low [31]. Other aluminum containing waste materials like capacitors, aluminum cans and packaging, supposes an important feedstock for H_2 generation, because they would not require complicated separation processes, as the non-aluminum parts (plastic, paper, etc) did not have substantial influence on the mechanism of hydrogen production [32]. Besides, the hydrogen mass yield of the Aluminum-water splitting of 11.1% is competitive with other renewable sources of hydrogen like steam gasification of biomass (hydrogen

yield potential of 7.6-12.6%), and can be obtained under milder reaction temperature, where gasification requires above 700 ºC [33].

The possible mechanisms of the water–aluminum reaction to produce hydrogen are [32]:

$$2Al+6H_2O \rightarrow 2Al(OH)_3+3H_2 \quad (1)$$

$$2Al + 4H_2O \leftrightarrow 2AlO(OH) + 3H_2 \quad (2)$$

$$2Al + 3H_2O \leftrightarrow Al_2O_3 + 3H_2 \quad (3)$$

The reaction (1) forms the polymorphs of aluminum hydroxide (gibbsite/bayerite) and hydrogen, reaction (2) forms the aluminum hydroxide boehmite (AlO(OH)) and hydrogen, and (3) forms aluminum oxide and hydrogen. It should be noted that both gibbsite and bayerite are different polymorphic forms of the aluminum hydroxide $Al(OH)_3$ (gibbsite is slightly more thermodynamically stable than bayerite). From room temperature to 280 ºC, $Al(OH)_3$ is the most stable product, while from 280-480 ºC, AlO(OH) is the most stable. Above 480 ºC, Al_2O_3 is the most stable product [34]. These byproducts form a dense layer that cut off the contact between water and aluminum surface, so the reactions do not take place at mild conditions [35], requiring a reaction-induction step of 12 h, followed by two hydrogen generation steps, up to 40 h, at 30 ºC, based on calorimetric measurements of the reaction by Nie *et al* [36].

The hydrogen release rate from the activated aluminum powder is low, only of the order of 8×10^{-7} g H_2/sec/g of Al [34]. This is why aluminum has to be surface-activated, and many approaches have been studied, like milling and ultrasonic treatment, higher reaction temperatures, preparation of alloys of aluminum by adding other metals, like Gallium [37], reducing the size of aluminum particles, use of acids or bases, and inorganic water-soluble salts like KCl and NaCl [38-42]. Aluminum powders can be activated by ball-milling them in water, followed by a rapid heating and cooling thermal shock treatment [43]. Alumina can also promote the hydrogen release when using metal powders like iron oxide, in the steam iron process at high temperature (645°C) [44]. Alumina modified with Ni and Co, in the aluminum water splitting, can catalyze and significantly decrease the reaction induction time

and promote the hydration of passive oxide film on Al surface [45]. Also, Deng, et. al. [46] showed that Al_2O_3-modified Al powder could continuously react with water and generate hydrogen at room temperature under atmospheric pressure.

The activation of aluminum by alkaline solutions, mainly NaOH, has been widely reported [26][47-51], which can be expressed as follows (reaction 4) [52]:

$$2Al + 2NaOH + 6H_2O \rightarrow 2NaAl(OH)_4 + 3H_2 \quad (4)$$

This technology has proven to be efficient, where the hydrogen generation is proportional to the concentration of the base. Its disadvantages are the extreme corrosion nature of NaOH and its additional cost as raw material. Another alkaline solution like KOH was tasted under flow conditions in an annular reactor, syringe pumped through an annular reactor where it contacts the Al foil wrapped on the surface of the inner rod [53]. A similar efficiency to NaOH was obtained, given its strong base nature, but disadvantageous dense layer formation of Al_xOH_y is also present, being fluffy and sticky, covering the Al surface, thus preventing the hydrogen generation to proceed continuously, so an instant removal is a challenge to be solved [26]. For instance, for Manganese (Mn) corrosion (reaction 5) the addition of ammonium salts, like CH_3COONH_4, has been studied to coagulate the $Mn(OH)_2$ passive layer that prohibits the H_2 generation reaction to proceed [54]. Michiels *et al.* [55] also demonstrated the benefits of using carbon dioxide in the hydrogen generation from Fe powder (reaction 6), because a carbonate intermediate is formed in mild hydrothermal reaction, where the oxidation of zerovalent iron to magnetite takes place via iron(II) carbonate $FeCO_3$, a unstable intermediate that hydrates to Fe_3O_4, H_2 and CO_2 ($3FeCO_3+H_2O \rightarrow Fe_3O_4+H_2+3CO_2$).

$$Mn+H_2O \rightarrow MnO+H_2 \quad (5)$$

$$2Fe+3H_2O \rightarrow Fe_2O_3+3H_2 \quad (6)$$

$$Zn+H_2O \rightarrow ZnO+H_2 \quad (7)$$

CHAPTER 5

There is a vast number of studies in batch mode, but it is evident from the literature [56] that *"It is necessary to consider reactor operation in different regimes such as pulse, quasicontinuous, and flowing"*, which only counted works have attempted. Among them, it can be mentioned the work of Hikari *et al*. [57], who also implemented a semi-continuous system for the generation of high-pressure hydrogen (30 MPa), using waste aluminum with 15% content of metallic Al, under subcritical water, yielding 16.7g H_2/kg Al. In the work of Takahashi *et al*. [58], a flow-type equipment was implemented for the continuous reduction of CO_2 dissolved in 0.01 mol/L HCl aqueous solution, at 20 bar through a Fe powder bed, mainly yielding methane, ethylene, ethane and propylene. The use of carbon steel (S-45C) cutting chaffs as the reductant, with Ni powder as hydrogenation catalyst, made possible to generate hydrogen, CO and formic acid.

Despite these reports, the CO_2 Capture-Solvent Lean stream (CO2LS) and CO_2-Rich stream (CO2RS) coming from the solvents-based CO_2 capture processes (mainly aqueous NH_3, NaOH and MEA), have not been proposed nor studied as activators/catalyzers of the metal water-splitting reaction for hydrogen production in a semicontinuous fashion. As a precedent, from the previous chapter 3, both CO2LS and CO2RS showed effectiveness as hydrothermal media in batch mode for the hydrogen generation, using different metals (Al, Zn, Mn and Fe). Therefore, the present study is important because for the first time represents a potential integration of two of the most strategic goals for the sustainable development nowadays, that is the carbon capture and the green hydrogen production. For that, a novel semicontinuous facility was designed and constructed, giving important information for a future scale-up process. This approach allowed determining the most active metals, the catalyzing effect of using a CO_2-Rich stream (CO2RS) and a CO_2 Capture-Solvent Lean stream (CO2LS) in the green hydrogen generation. Solids by-products were analyzed by XRD, SEM-EDS, ATR-FTIR and N_2-Absorption analysis.

Materials and methods

Chemicals

Ammonium carbamate (AC) (99%), sodium bicarbonate (SB) (100%), as the CO_2-Rich stream (CO2RS), and aqueous solutions of ammonia (0.35 to 5 mol/L), ethanolamine (MEA) (5 mol/L) or sodium hydroxide (NaOH) (0.5 M), as the CO_2 Capture-Solvent Lean stream (CO2LS), were used as activators of the hydrogen generation reaction from metals and water. Fine powder of Zn (pure), Mn (≥99% trace metals basis), and Fe (≥99%), were purchased from Sigma-Aldrich. Fine powder of Al (<5 mm, 99.5%) was purchased from Panreac. Granular aluminum (<1 mm, 99.7% trace metals basis, Sigma-Aldrich) and aluminum spall (provided by BEFESA company) were sieved into 250 and 500 μm sizes, and further employed as reactants without any other treatment.

Liquid and Gas characterization

The carbamate and sodium bicarbonate liquid samples were analyzed by HPLC (Waters, Alliance separation module e2695) using an RAZEX™ ROA-Organic Acid H+ column with RI detector (Waters, 2414 module). The mobile phase was 25 mM H_2SO_4 with a flow rate of 0.5 mL/min. The temperatures of the column and the detector were 40 °C and 30 °C, respectively.

The gas phase composition of the hydrogen generation experiments was online-quantified using a GC-TCD Varian 4900, equipped with Molsieve 5A-10m and Poraplot Q -10m columns. Two reference gas standard mixtures of H_2 at two different concentrations (5.0086 mol% H_2 and 94.9914 mol% CH_4; 50.0322 mol% H_2 49.9678 mol% CH_4), provided by BAM institute from Germany were employed

CHAPTER 5

Design and operation of the semi-continuous H_2-generation facility

In a simplified way, Fig. 1 shows the block-flow diagram (BFD) of the semi-continuous setup constructed for hydrogen production and measurement. In more detail, Fig. 2 shows the piping and instrumentation diagram (P&ID) of the system, where the main operation circuit is defined by the flow path of either CO2RS or CO2LS, starting in tank T-101, then the pump P-101 (HPLC pump Jasco), heater H-101, Fixed bed reactor R-101, cooler C-101 (using ethylenglicol as refrigerant) and finally the flash drum S-101 (316L Stainless Steel Double Ended DOT-Compliant Sample Cylinder-Swagelok). Before each experiment, the circuit is dried out of any reminding water/moisture from a previous run, by flowing compressed air (opening V-01 and V-02), followed by leaks testing with nitrogen (valve V-02) at 10 bar above the vapor pressure of water at the corresponding experiment operation temperature (e.g., for 250 ºC the leak testing pressure is 50 bar (40 bar [vapor pressure] + 10 bar). To reach and control the desired pressure, a back-pressure regulator (BPR) was installed before the three-way valve V-04. In a regular experience, the CO2RS or CO2LS are pumped through the circuit afore described, and the three-phase fixed bed reactor (ID 0.9525 cm, Length 10 cm and 2 g of the metal bed) is operated in co-current upflow mode, so the generated hydrogen follows the liquid motion, in likeness to the packed-bed bubble flow described by Dudukovic [59], while the reaction between water and the metals proceed in a semi-continuous fashion. Upstream the reactor, the two-phases fluid (liquid and gas) is collected in liquid-gas separator S-101. The operational temperature of the facility ranges from room temperature up to conditions of superheated water (250 °C and 50 bar), reaction time from 0.5 to 2 h of steady-state operation time (SSOT), where time zero starts when reaching the working temperature, after a heating ramp of 30 ºC/min. During the SSOT, valves V-05 and V-06 remain closed, so S-101 is gradually filled with liquid and gas, making the internal pressure to increase proportionally to the volumetric flow of liquid and gas collected. Temperatures T1 and T2, and pressure P3 are measured and recorded by means of a Temperature Picotech instrument USB TC-08, and a digital manometer Druck DPI-104-IS, respectively. The majority of the experiments were duplicated in order to stablish the experimental error.

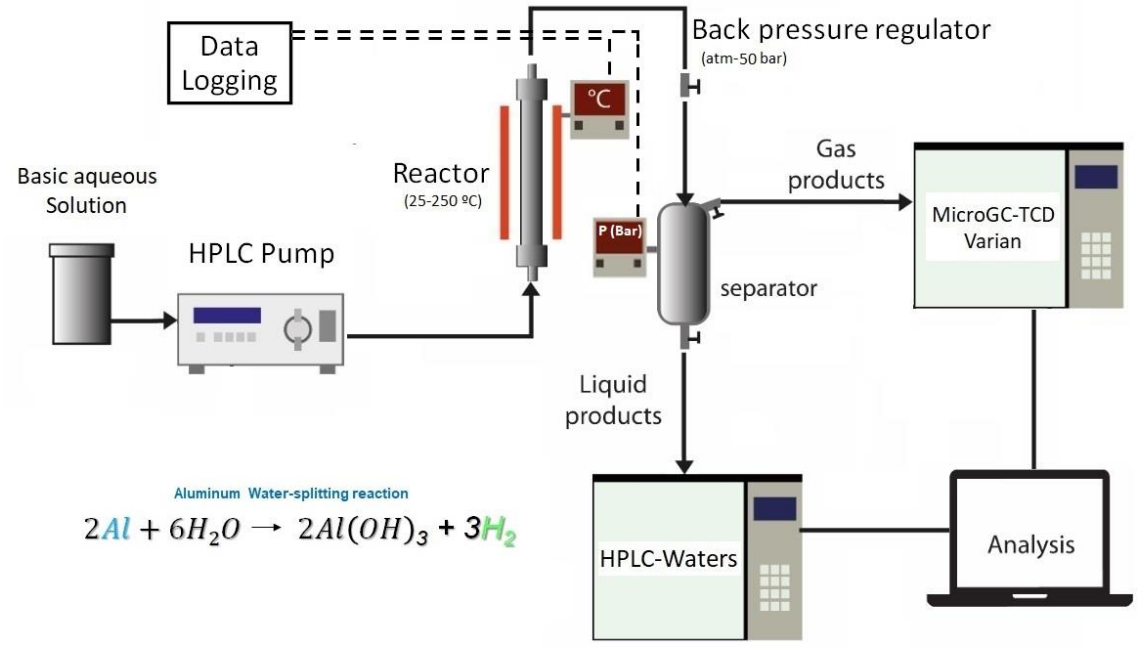

Fig. 1. BFD of the semicontinuous hydrogen generation facility

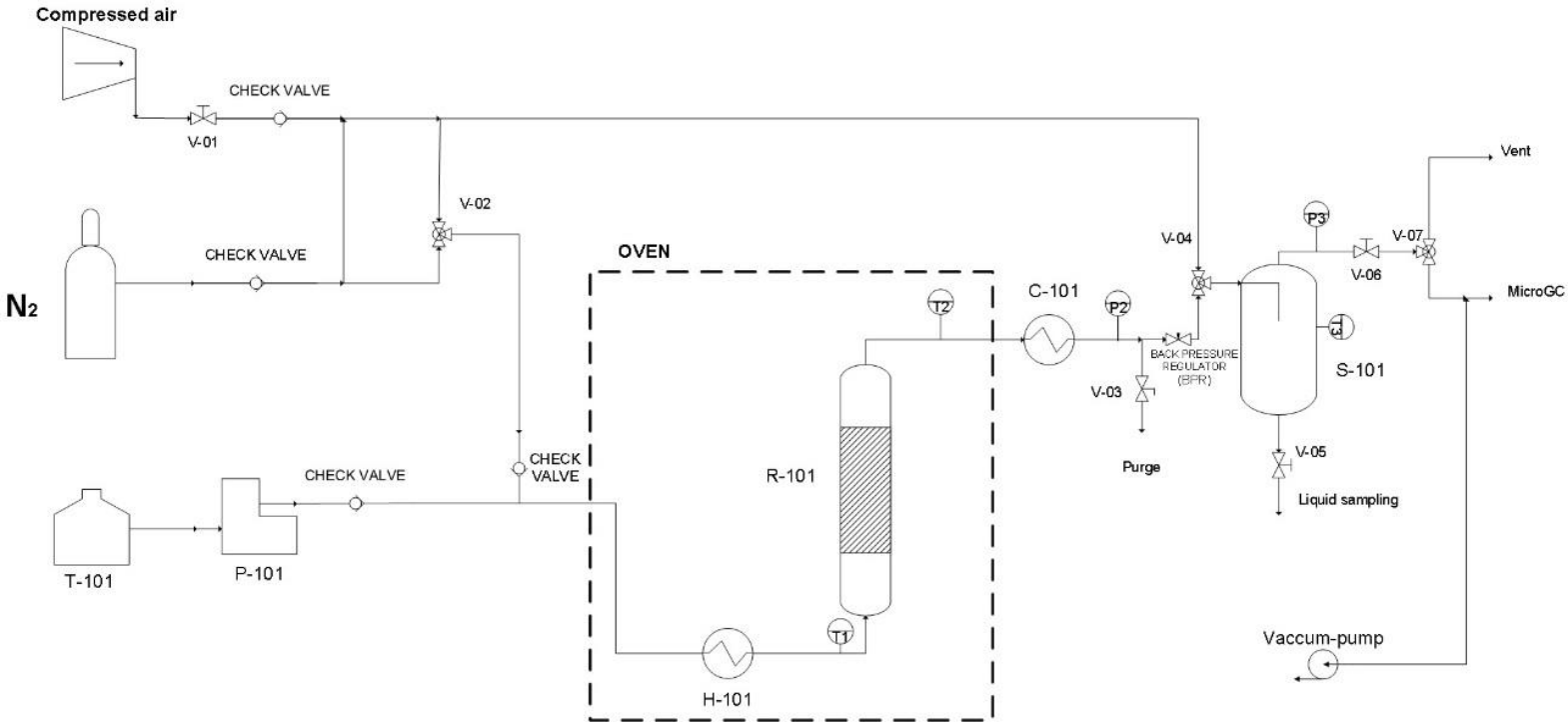

Fig. 2. P&ID of the semicontinuous hydrogen generation facility

The moles of hydrogen produced ($n\mathrm{H2}$) are calculated by equations 8 and 9:

$$n\mathrm{H2} = \frac{P_{s,f} * V_{s,f}}{R * T_{s,f}} * xH2 \quad (8)$$

$$V_{s,f} = V_{s,t} - V_{s,l} \quad (9)$$

Where, once completed the SSOT, $P_{s,f}$ is the final absolute pressure (P3) inside the unit S-101; $T_{s,f}$ is the final temperature (T3) measured with a PT-100 sensor; $V_{s,f}$ is the final overhead (gas) volume inside unit S-101; $V_{s,t}$ is the total volume of S-101; $V_{s,l}$ is the final volume of liquid collected in S-101; R is the ideal gas constant (83.14472 L*mbar*K^{-1}*mol^{-1}); *xH2* is the fractional molar composition of hydrogen, measured by gas chromatography. Given the low pressure (<3.75 bar) and temperature (room) of the hydrogen-containing gas inside the unit S-101, its behavior can be considered as ideal gas [60], and the application of the equation of ideal gases is adequate, so it is not necessary invoke a more complex equation.

The dependent variables: molar yield of hydrogen ($y\mathrm{H2}$), relative hydrogen yield ($\Upsilon\mathrm{H2}$) and hydrogen generation rate (φH2) (mL/min) were calculated by equations 10-12:

$$y\mathrm{H2} = \frac{n\mathrm{H2}}{n\mathrm{M}} * 100 \quad (10)$$

$$\Upsilon\mathrm{H2} = \frac{n\mathrm{H2}}{n_{t,M}} * 100 \quad (11)$$

$$\varphi\mathrm{H2} = \frac{(n\mathrm{H2} * \mathrm{PMH2})/\rho\mathrm{H2}}{SSOT} * 100 \quad (12)$$

Where, $n\mathrm{H2}$ is the moles of hydrogen produced; $n\mathrm{M}$ is the moles of metal M used; $n_{t,M}$ are the stoichiometry moles of hydrogen produced by mol of metal M (Al, Zn, Mn or Fe), according to theoretical reactions 5-7, $\rho\mathrm{H2}$ is the density of hydrogen (consulted in the NIST [61]) at T3 and P3 (see Fig. 2) and SSOT is the steady-state operation time.

The loss of carbamate and bicarbonate ions ($lCO2$) after H_2 generation was calculated by equation 13:

$$lCO2 = \mathrm{abs}(\frac{C_{cs,f} - C_{cs,i}}{Ccs,i}) * 100 \quad (13)$$

Where $C_{cs,i}$ is the initial molar concentration of carbon source and $C_{cs,f}$ is the final molar concentration of carbon source.

Solid Characterization

The solid samples were dried overnight in a vacuum-oven at 45 °C, to remove the remaining moisture. They were analyzed by X-ray diffraction (XRD), using a BRUKER D8 DISCOVER A25 equipment, with 3 kW Generator, 2.2 kW type FFF Cu-ceramic tube, LynxEye Detector, operating at 40 kV and 30 mA. The database used for identifying the phases was the PDF-2 Released 2013 (ICDD). SEM micrographs observations were conducted over the exhausted metals after the H_2 release experiments, to determine the morphology, surface particle changes and chemical composition. For this, a Quanta 200FEG ESEM (Environmental Scanning Electron Microscope) equipment was used, operating at 20kV. Firstly, EDS (Energy Dispersive Spectroscopy) microanalysis was performed, targeted over 2-3 spots in the sample for the elementary analysis; afterwards, the samples were coated with gold in a K575 sputter coater, and the images generated with a BSED detector. Textural properties analysis of the solids after reaction were conducted in an ASAP 2420 equipment with nitrogen adsorption at 77 K, all samples were degassed prior to each analysis. The surface area was determined by the BET method, whereas pore size and volume were calculated by the BJH method. The solid residue after activation with aqueous NaOH was analyzed by ATR-FTIR, using an ALPHA-Bruker equipment.

Results and discussion

Performance of different metals on the hydrogen yield under aqueous AC stream

Fig. 3 presents the hydrogen yield with respect to the metals tested at the condition of superheated water (200 ºC, 25 bar), 2 h of SSOT and 0.5 mL/min of 1.5 mol/L of AC as CO2RS. The hydrogen produced is considered blue because a reduction of carbamate concentration (Carbamate loss-lCO2) in the final liquid sample was detected by HLPC, for all metals, so the lCO2 had a maximum of 7.7%, when using Mn, indicating that the CO_3^- anion has been either chemisorbed into the metal bed (recaptured) or decomposed to the gas phase, as will be discussed later in more detail with the solid characterization. It is also observed that the H_2 yield increased in the order Mn<Al<Fe<Zn, with a maximum of 75.3% for Zn, only followed by Fe with 34%. Al and Mn showed marginal yields of about 9%, indicating that, among the metals, zinc is the most active toward hydrogen release in a weak basic aqueous stream like AC. This result is in concordance with the batch experiments of hydrogen generation in chapter 3, where zinc showed better performance than Al, with H_2 yield up to 63.7% in 10 h under aqueous AC solution as CO2RS. The results for Zn and Fe powder are outstanding because it means they responded well to the proposed activation method without further modification or pretreatment (e.g., costly alloy preparation or doping process). The differences of metals reactivity with water can be explained by the concept of metallicity, which is, on the contrary to electronegativity, the ability of metal atoms to lose electrons. The stronger the metallicity of a metal the more reactive with water. Metals with low electronegativity like lithium, sodium, potassium (among others) are active enough at ambient temperature to react with cold water, producing relative metal hydroxide and hydrogen [62], while metals like Al, Zn, Mn and Fe require activation. Aluminum powder performance could be enhanced toward hydrogen generation, even at ambient conditions, by a modification with fine ɣ-Al_2O_3 through a ceramic processing procedure [46], but this may add more costs and processes steps, and a limited concentration 4.8 wt% of hydrogen. Similarly to the aim of the present work of utilizing CO_2 as activator of hydrogen generation, Xi *et al* [54] studied the promoting effect that has the addition of ammonium salts like CH_3COONH_4 (among others) to Mn, owing to its anions'

(CH_3COO-) capacity to coagulate of $Mn(OH)_2$ passive layer (that prohibits the reaction to proceed). Likewise, Michiels *et al.* [55] also demonstrated the benefit of CO_2 in the oxidation of Iron to generate hydrogen and magnetite, by the formation of unstable intermediate iron (II) carbonate $FeCO_3$ that promotes the overall reaction.

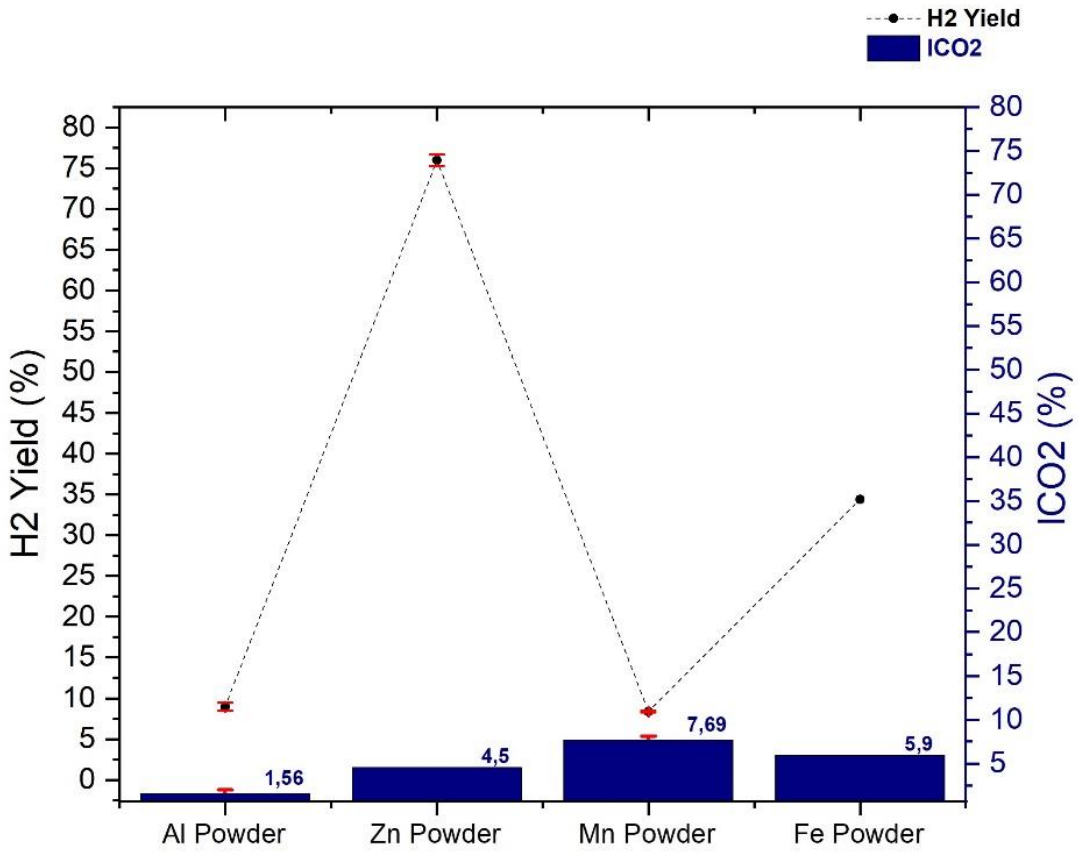

Fig. 3. H_2 yield and carbamate loss as function of metal powder type. Reaction conditions: 200 ºC, 25 bar, 2 h of SSOT and 0.5 mL/min of 1.5 mol/L of AC as CO2RS.

Effect of aluminum type and textural parameters on hydrogen yield

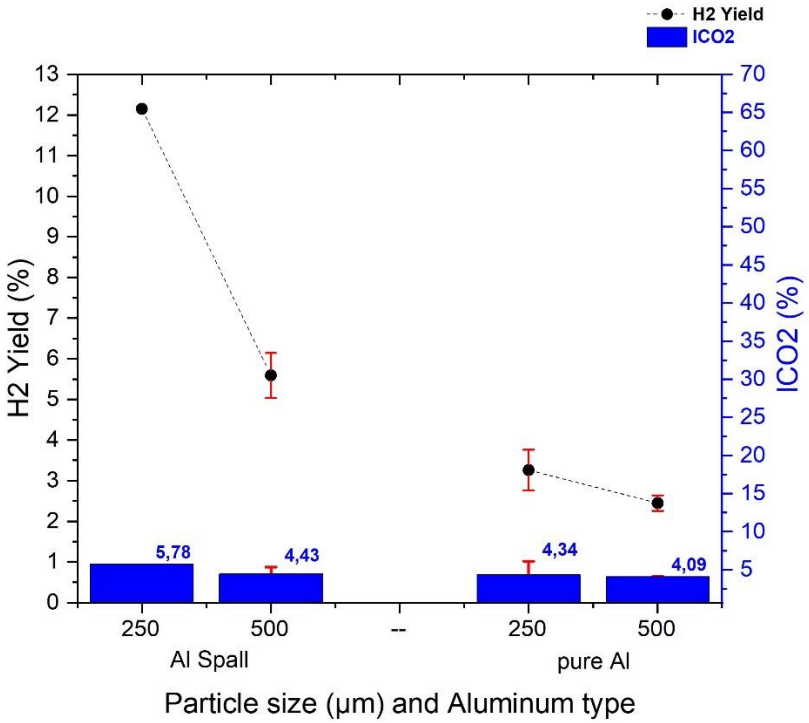

Fig. 4. H_2 yield as function of particle size and type of Al. Reaction conditions: 200 ºC, 25 bar, 2 h of SSOT and 0.5 mL/min of 1.5 mol/L of AC as CO2RS

In order to stablish the effect of particle size, hydrogen generation experiments were conducted with pure aluminum at 250 and 500 µm, at conditions: 200 ºC, 25 bar, 2 h of SSOT and 0.5 mL/min of 1.5 mol/L of AC as CO2RS (see Fig. 4). As expected, a proportionality between the H_2-yield and the particle size for both aluminum types were found, where yield increased up to 12% for Al spall at 250 µm. This type of Al-waste showed better performance, in comparison to the pure aluminum, probably because of its higher surface area (4.68 m^2/g against 0.17 m^2/g for Al 250µm), pore volume (6.05E-03 cm^3/g) (see Table 1) and its chemical composition is not limited only to elemental Al (34.16%), but also includes Fe (32.98%), which has higher metallicity. Other elements like Si (1.43%), Cl (0.72%), C (6.64%) and O (24.07%) are also present (determined by SEM-EDS) (see Fig. 5). This result makes the Al spall a very promising residue for hydrogen generation, which can be reutilized without further pretreatments than a size classification.

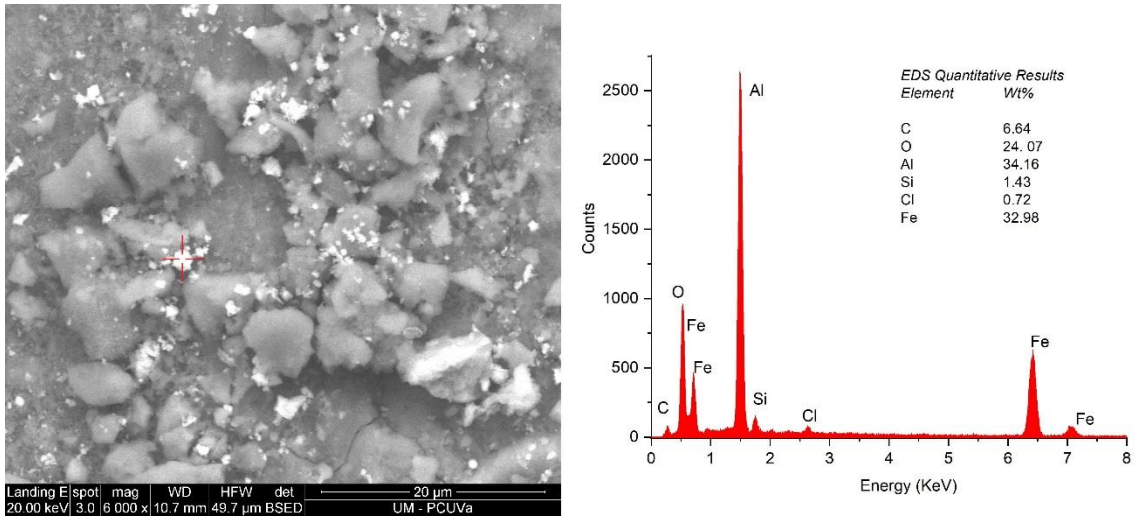

Fig. 5. Elementary composition analysis of Al Spall 250 µm by SEM-EDS

Table 1. Textural characterization of the metals used

Metal	Surface area (m^2/g)	Pore volume (cm^3/g)*	Pore diameter (nm)*
Al powder	0.12	7.12E-04	24.09
Zn powder	0.24	4.54E-04	7.71
Mn powder	0.21	4.22E-04	8.26
Fe powder	0.32	3.98E-04	4.98
Al 250 µm	0.17	2.54E-04	6.07
Al 500 µm	0.10	1.14E-04	4.71
Al Spall 250 µm	4.68	6.05E-03	5.18
Al Spall 500 µm	1.17	2.17E-03	7.46

Effect of temperature and concentration of CO2RS on hydrogen yield

The influence of temperature and concentration over the H_2 generation was studied from 25 to 250 ºC (25-50 bar) using Al 500 µm, a flow of 0.5 mL/min of the CO2RS (AC and SB) in the concentration range of 0-3.0 mol/L, and 2 of SSOT (Fig. 6). It is known that the increase of temperature results in a faster Al-water reaction and a higher flow rate of produced hydrogen [63]. Accordingly, the dependence and proportionality of H_2 yield to temperature variable was found with AC as activator,

reaching its highest at 250 ºC. Yield is also proportional to concentration of AC and starts to level off above 1.5 mol/L, a trend that can be better observed at temperatures from 130 to 250 ºC. For its part, SB as activator contrast radically with AC, as its performance is higher by far, measured as relative yield (relative to the stoichiometry H_2), reaching 71%, and hydrogen generation rate of 19 mL/min (with hydrogen density 2.77E-04 g/mL, taken at T3=21.8 ºC and P3=3.3 bar), in only 0.5 h of SSOT at 200 ºC and 1.0 mol/L concentration. Hydrogen generation is known to be faster at increased pH [64], so at concentration of 1.0 mol/L the SB solution has a pH of 10.2, while for AC at the same concentration is 9.38, evidencing the difference in the results.

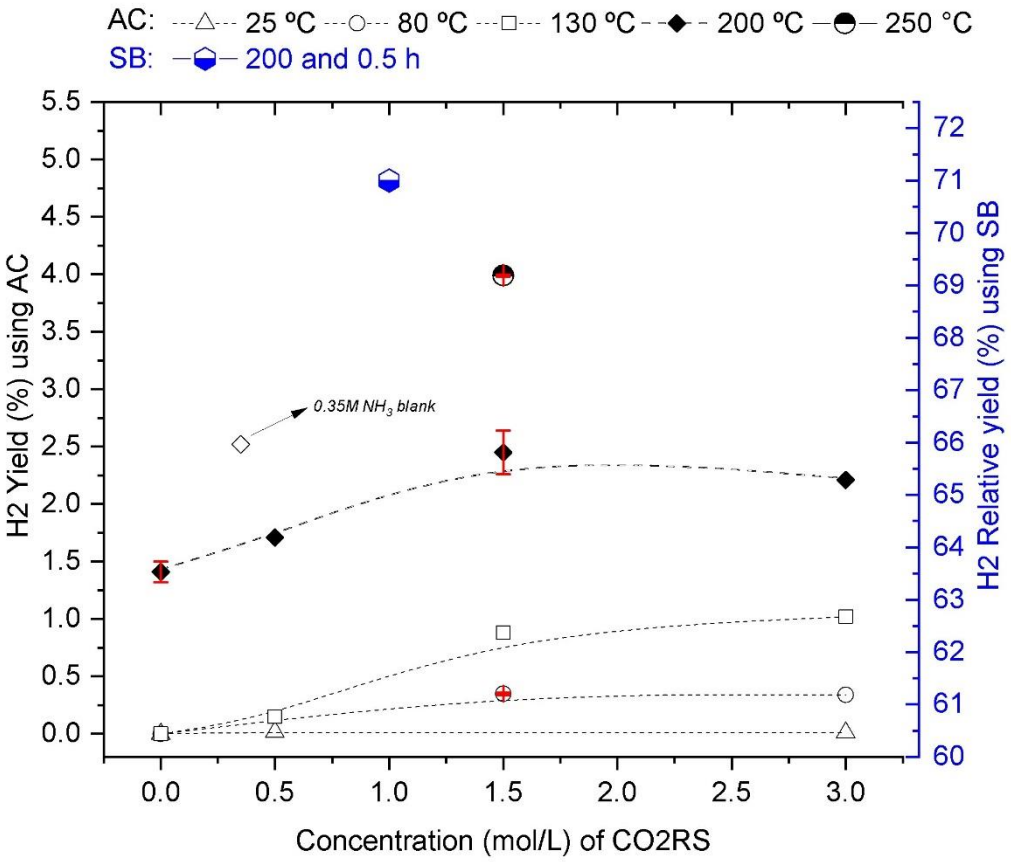

Fig. 6. H_2 yield as function of temperature and concentration of AC. Reaction conditions: Al 500 µm, 25-250 ºC (25-50 bar), Al 500 µm, 0.5 mL/min of the CO2RS (AC and SB), 0-3.0 mol/L, 2 h of SSOT.

In order to stablish whether captured CO_2 from ammonia-based CO_2 absorption has a catalyzing role in the hydrogen generation, a reaction blank was performed with 0.35 mol/L of NH_3 at 200 ºC, keeping the rest of reaction conditions unvaried. The H_2 yield was nearly the same as 1.5 mol/L of AC and 200 ºC, indicating that captured CO_2 in ammonia (mainly in the form of an equilibria of NH_2COO^-, CO_3^- and HCO_3^- anions in aqueous solution [65]) does not has appreciable catalyzing role in the aluminum water-splitting, considering two main reasons: i) carbamate is an amino-acid anion with a neutral character, ii) no carbonate intermediate is formed in the aluminum water-splitting, unlike carbonate-assisted hydrogen generation from iron, where CO_2 has a catalyzing role by the formation of the intermediate $FeCO_3$ compound that undergoes decomposition to Fe_3O_4 and CO_2 [55][66].

Effect aqueous AC flow rate on hydrogen yield

Fig. 7 presents the H_2 yield as function of volumetric flow of AC aqueous solution using Al 500 µm at conditions of 1.5 mol/L, 130-200 ºC and 2 h. Apparently, the SSOT of 2 h was long enough to allow both activation and deactivation of aluminum, so no significant differences were observed by changing the flow rate of AC in this case, given that the maximum hydrogen production rates can occur at the very beginning of the aluminum corrosion, before surface deactivation. Nevertheless, it is to worth mention that for a stronger base (NaOH 1N) and shorter times (below 23 min), Tekade *et al.* [67] observed that the rate of hydrogen generation increases with increase in flow rate of aqueous NaOH from 0.2 ml/min to 10 ml/min.

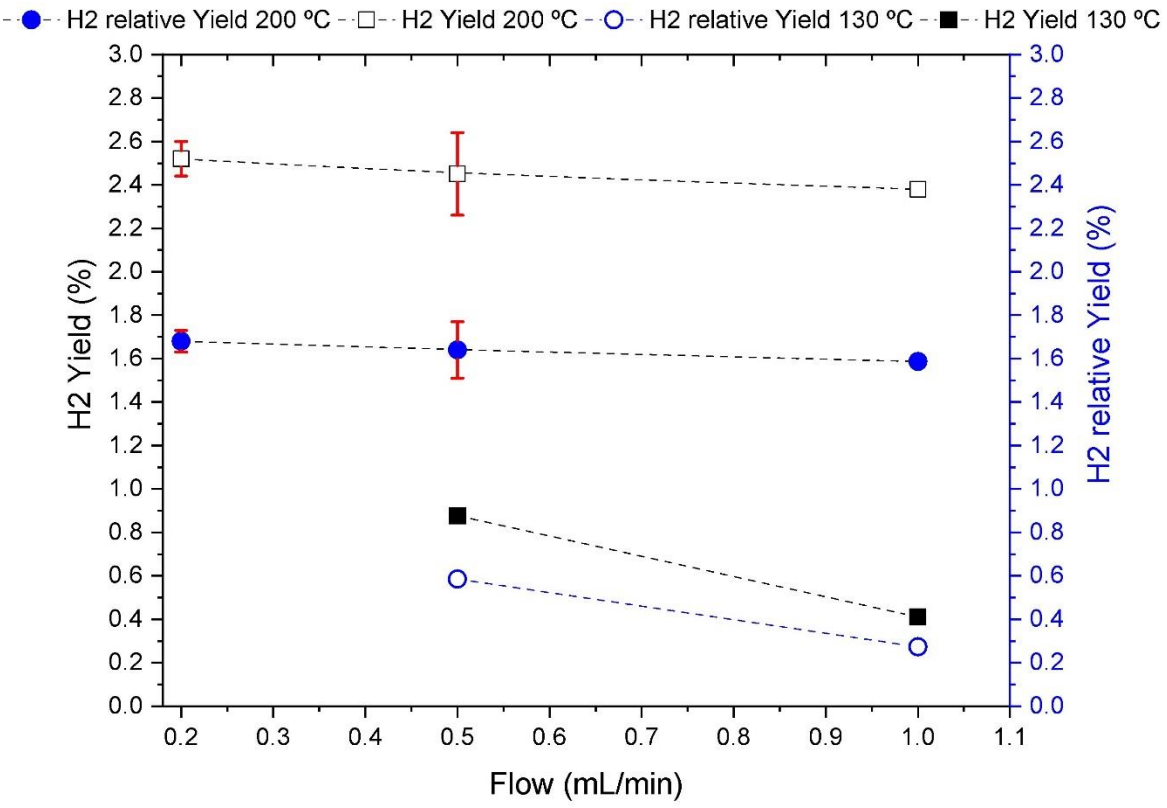

Fig. 7. H_2 yield as function of flow of AC. Reaction conditions: Al 500 µm, 130-200 ºC, 1.5 mol/L, and 2 h of SSOT.

Green-hydrogen generation from aluminum using CO2LSs

Fig. 8 depicts the hydrogen yield with respect to type and concentration of CO2LS (aqueous solutions of NH_3, NaOH and MEA) using pure aluminum 500 µm, at the conditions of superheated water (200 ºC and 25 bar), during 2 h of SSOT and 0.5 mL/min. The hydrogen produced is considered green because no CO_2 emission is involved. It is remarkable that among the solvents used, NaOH showed the highest Green-H_2 relative yield (up to 85.5%), within only 50 min, at a low concentration of 0.5 mol/L. This experiment accounts for a hydrogen rate of 1.9±0.02 mmol/min or 12.8±0.1 mL/min (with hydrogen density 2.97E-04 g/mL, taken at T3=25 ºC and P3=3.7 bar), while 10.7 mL/min was obtained at 25 ºC, atmospheric pressure but under much higher flow of 10 mL/min of KOH 0,5 M [53], and 8 mL/min also at higher flow rate (10 mL/min) of 0.5 M NaOH [67]. These results fit well with what

is stated in the field of sodium hydroxide for clean hydrogen production, because as compared to other activation methods, NaOH provides the higher rate of hydrogen generation [68]. In the case of NH_3, the H_2 yield reached a maximum of 3.1% at concentration of 1.5 mol/L, and leveled off up to 5.0 mol/L, and for MEA the yield was marginal of 2.4% also at 5.0 mol/L. The disadvantage of using NaOH as an activator is its corrosive nature and its prohibitive cost. However, through the present work, it is proposed to potential stakeholders (thermal power stations, ironmaking factories, concrete and cement factories, among others) to overcome this cost disadvantage by utilizing the lean stream from the NaOH CO_2 capturing process before the capture, thus adding value to the CO_2 capture by generating green hydrogen, while minimizing the loss of the CO2LSs by the high-pressure of the superheated-water condition. The increase of pressure not only can minimize the CO2LS loss, but also improve the removal of CO_2 in the subsequent absorption column [69].

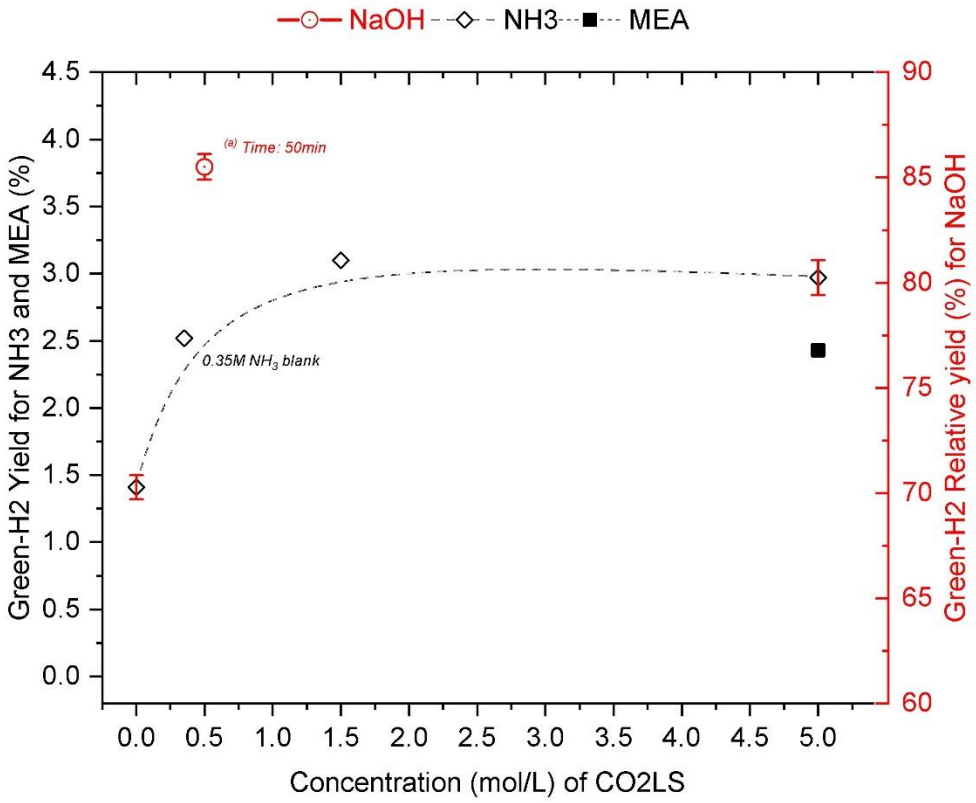

Fig. 8. H_2 yield as function of concentration of different CO2LS. Reaction conditions: Al 500 μm, 200 ºC (25 bar), 0.5 mL/min and 2 h of SSOT.

Given the outstanding performance of 0.5 mol/L NaOH, it was desired to conduct its evaluation at a much lower temperature of 25 ºC, because is the lowest temperature for capturing CO_2 in NaOH, while comparing it with AC under the same conditions. In Fig. 9, the H_2 yield for NaOH in 3 h was computed in 68 %, while for AC less than 0.1%, and it was stopped at 2 h due to the evidence of no hydrogen generation. Interestingly, when registering the temperature in the outlet of the tubular reactor (T2 in Fig. 2), which corresponds to a point quite near of the aluminum bed, the behavior for NaOH showed temperature peaks pattern throughout the reaction time, observing three main peaks of 28, 28.2, and 28.3 ºC at 88.7, 136 and 183.5 min, respectively, while for AC the T2 behavior was flat, it did not change. Likewise, when data-logging the pressure in the flash (P3 in Fig. 2), for NaOH it could also be observed peaks that matches well with the temperature peaks, indicating that the hydrogen generation reaction is exothermic, exhibiting a pulses pattern, and demonstrating that, under the studied conditions, it can proceed in a self-sustaining way without external energy at ambient temperature. For AC the increase of pressure is due to the continuous pumping of liquid and the subsequent filling of the flash that compresses the gas headspace.

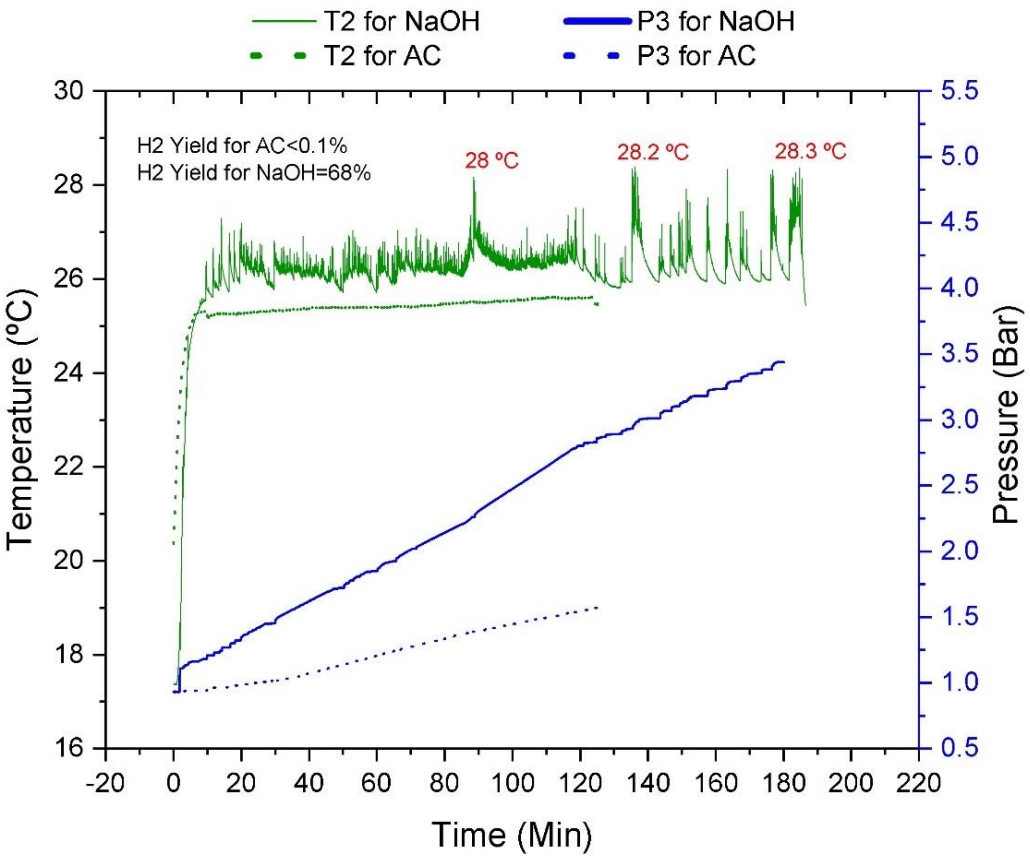

Fig. 9. Temperature T2 and pressure P3 behavior during the activation of Al with aqueous AC and NaOH streams. Reaction conditions: Al 500 μm, 25 ºC, atmospheric pressure, 0.5 mol/L, and 2-3 h of SSOT

Solid byproducts characterization

After activation of selected metals with aqueous AC stream (CO2RS)

Fig. 10 depicts the XRD diffractograms of the solid byproduct from the experiments with selected metals that were analyzed in Fig. 3. For the case of Al, Fig. 10 a) shows the typical signals of the cubic structure of elemental aluminum, with diffraction peaks at 2ɵ= 38, 45 and 65º [70][71] (PDF 00-004-0787) confirming that is only partially exhausted into boehmite (2ɵ = 28, 49 and 55º) (PDF 00-021-1307) [72] to generate hydrogen. Diffractogram of Fig. 10 b) confirms the almost complete

exhausting of Zn (weak peaks at 39, 43,3 and 54,3º) (PDF 00-004-0831) into ZnO (31.8, 34.2, 36.2, 47.5, 56.6, 62.9, 66.2, 68 and 69º) [73] (PDF 00-036-1451) for the highest Blue-H_2 yield of 75% (Fig. 3). Diffractogram of Fig. 10 c) suggest that the capture CO_2 of the CO2RS was chemisorbed by Mn bed (40.5, 42.9, 47.7 and 52.3) to form $MnCO_3$ Rhodochrosite (24.1, 31.2, 37.6, 41.3, 45.1, 51.5, 60, 63.9, 67.8º) [74] (PDF 00-044-1472). Diffractogram of Fig. 10 d) also suggests that the capture CO_2 of the CO2RS was chemisorbed by Fe-bed (30, 35.5, 43, 44.7, 53.5, 57, 62.6 and 65º) (PDF 00-006-0696) to form the hydrogen-promoting intermediate $FeCO_3$ Siderite [55] (PDF 00-029-0696) [75], and the oxidation product $Fe^{2+}Fe^{3+}{}_2O_4$ Magnetite (PDF 00-019-0629) was also detected.

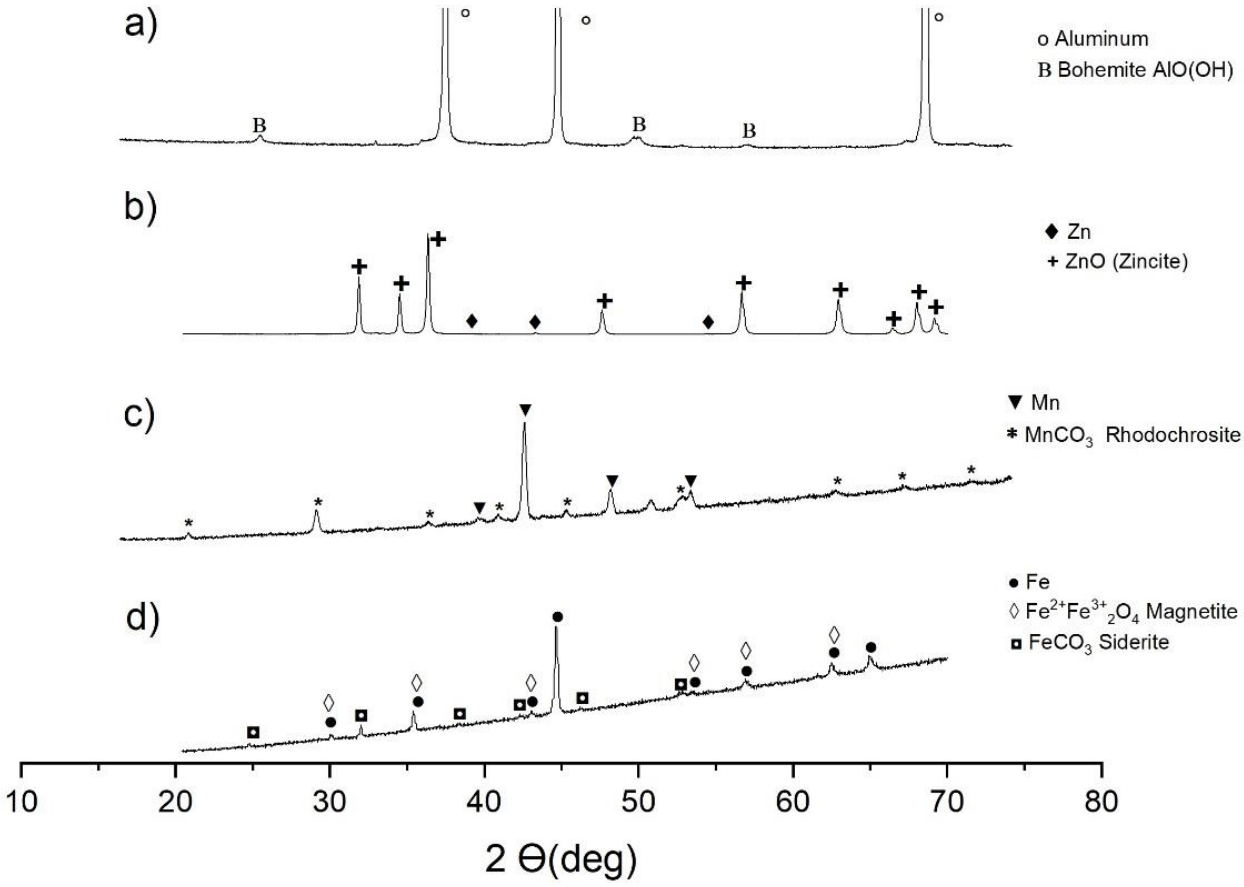

Fig. 10. XRD diffractograms of solid byproducts after hydrogen generation with a) Al, b) Zn, c) Mn and d) Fe, using aqueous AC as CO2RS

After activation of aluminum with NaOH and $NaHCO_3$ (SB) solutions as CO2LS

Based on diffractogram of Fig. 11 (a) the full conversion of aluminum by NaOH 0.5 M at 200 ºC and 0.8 h for a Green-H_2 yield of 85.5% (Fig. 8) is confirmed as the three possible oxidation products appeared, namely Bohemite AlO(OH)(PDF 01-083-2384), Bayerite $Al(OH)_3$ (PDF 00-020-0011) and Gibbsite $Al(OH)_3$ (PDF 00-007-0324). The water splitting reaction of aluminum with the aid of sodium hydroxide is written as in reaction (4), where two moles of sodium aluminate $NaAl(OH)_4$ are formed. However, this compound was not detected by the XRD, therefore it could have been completely transformed to NaOH and $Al(OH)_3$, according to reaction (14), thanks to the high conversion degree of the overall process:

$NaAl(OH)_4 \rightarrow NaOH + Al(OH)_3$ (14) [76].

The diffractogram of byproduct after activation with NaOH 0.5 M at 25 ºC and 3 h (Fig. 11. (b)) confirms its efficacy even at low temperature (Green-H_2 yield of 68%), while the proportion of bayerite peaks are lower to the elemental aluminum. The diffractogram of SB byproduct at 200 º and 0.5 h (Fig. 11. (c)) is consistent with the high oxidation degree of aluminum (H_2 relative yield of 71%), in which elemental aluminum signals are faded by boehmite and $NaAlCO_3(OH)_2$ Dawsonite signals (PDF 00-045-1359). In the same way, the diffractogram of AC byproduct at 200 º and 2 h (Fig. 11. (d)) is consistent with the low oxidation degree of aluminum (Blue-H_2 yield of 2.5%), in which elemental aluminum signal is the predominant, only accompanied by weak peaks of Bohemite.

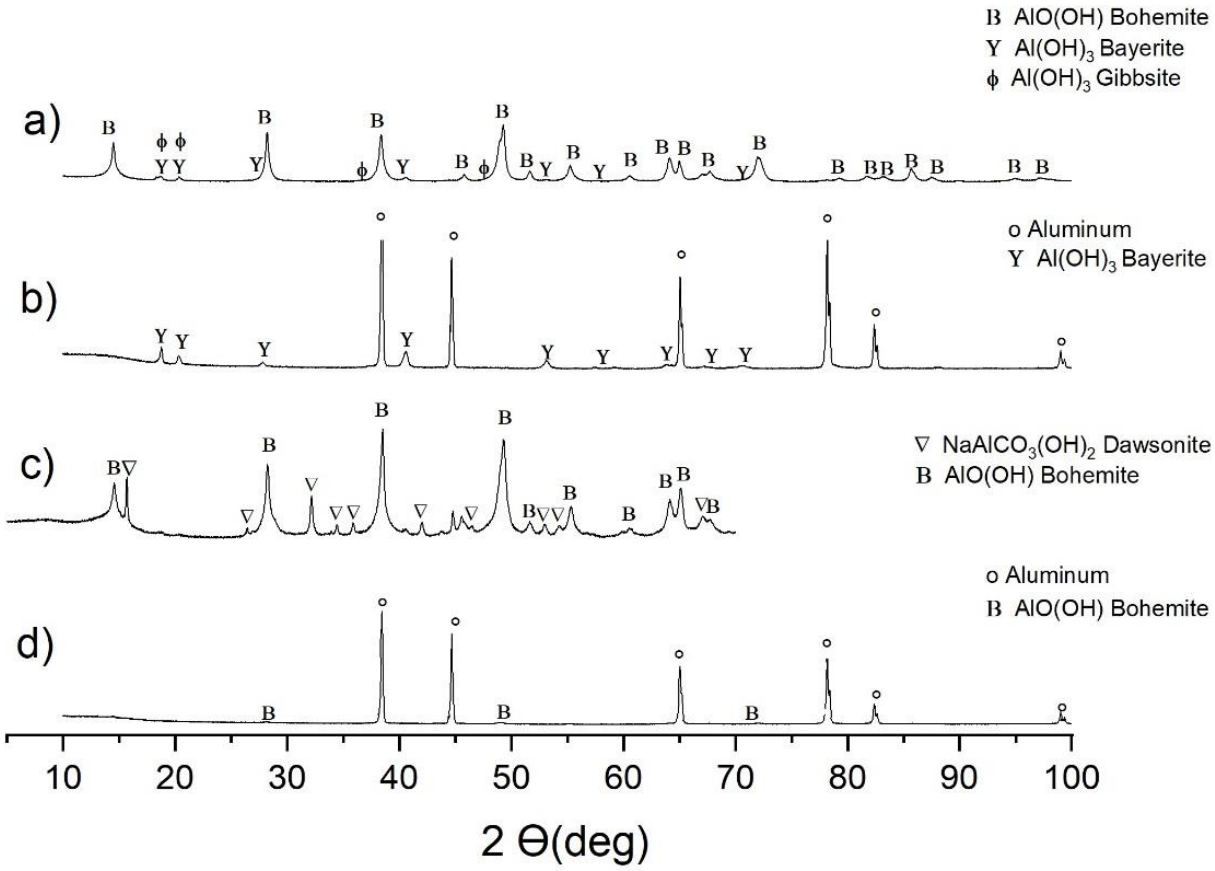

Fig. 11. XRD diffractograms of solid byproduct after activation of Al with a) NaOH at 200 ºC and 0.8 h, b) NaOH at 25 ºC and 3 h, c) SB at 200 ºC and 0.5 h, and d) AC at 200 ºC and 2 h.

Before starting the XRD analysis of the solid byproduct from Al activation with NaOH at 200 ºC and 0.8 h, it was observed an unusual depressurization of the plastic bottle containing the solid sample, suggesting that it may had absorbed gas, probably by the formation of a metal hydride comprising Al and H (AlH_4-), considering that the absorption of hydrogen to form this complex compound happens under high pressures processes [77]. To try to confirm this, ATR-FTIR analysis was performed, where the ATR spectrum of Fig. 12 presents what appears to be Al-H bond characteristic bands at the neighborhood of 1640-1660 cm−1 and 710-760 cm−1 [78][79]. The possible mechanism is as described by Wang *et al*. [78], where activated aluminum can directly react with hydrogen to form aluminum hydride (AlH_3), further reacting with NaH and hydrogen to form $NaAlH_4$. The high gravimetric hydrogen capacity of $NaAlH_4$ (5.6%wt_H_2), makes it a good candidate for solid-state

hydrogen storage systems, sharing an important place with other metal hydrides like $NaBH_4$ (10.8 %wt_H_2), $LiBH_4$ (18.4 %wt_H_2) and Mg_2FeH6 (5.2%wt_H_2) [25] [77][80].

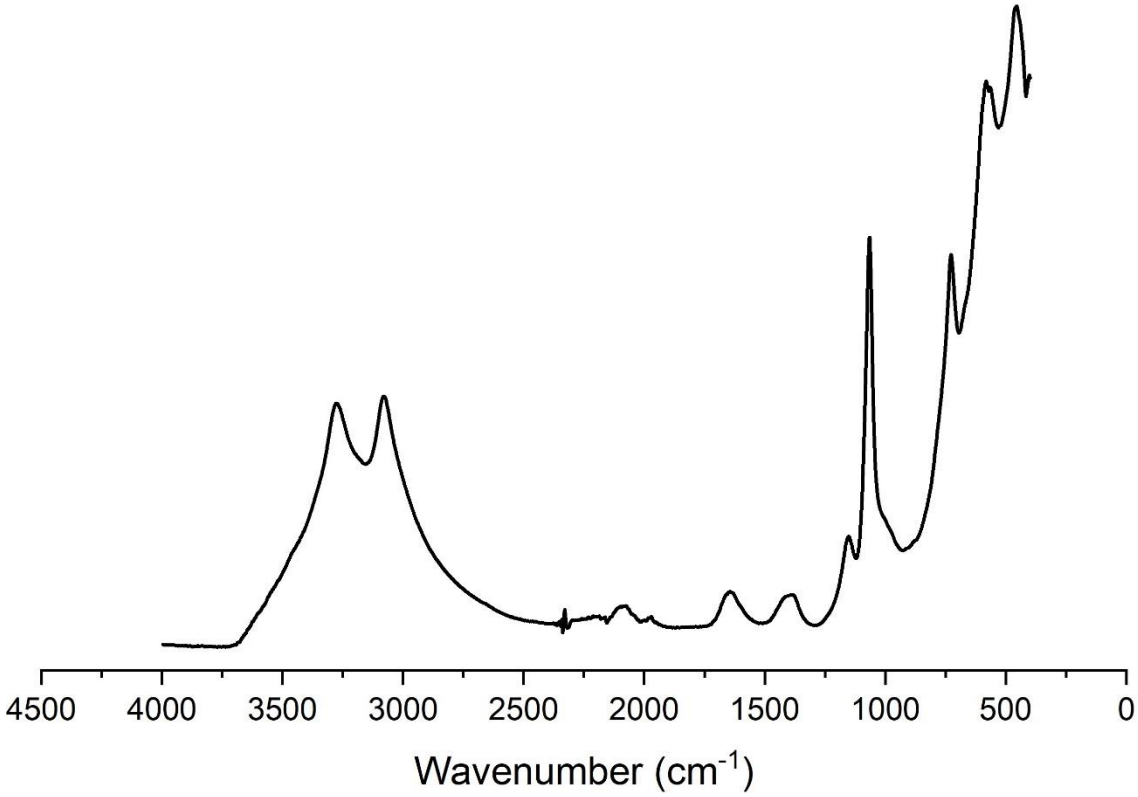

Fig. 12. ATR-FTIR spectra of solid byproduct after activating Al with NaOH solution

CHAPTER 5

Conclusions

For the first time, the coupling of CO2-Rich stream (CO2RS) and CO2 Capture-Solvent Lean stream (CO2LS) with the metals-based hydrothermal generation of hydrogen was successfully accomplished via the construction of a semi-continuous facility. The experimental study showed that, similarly to chapter 3, Zn powder had the highest H_2 yield (75.3%) and increased in the order Mn<Al<Fe<Zn. The liquid and solid characterization allowed concluding that the hydrogen generated, when using a CO2RS, led to carbamate/bicarbonate loss, which is recaptured in the solid in the form of metal carbonates. As expected, and in accordance to chapter 3, the particle size of the metal used affected the H_2 yield, where the smaller the size the higher the yield. Once again, as in chapter 3, the aluminum spall tested from BEFESA company showed outstanding results in terms of hydrogen yield, up to 12% for Al spall at 250 μm, compared to pure Al 250 μm (c.a. 3%). H_2 yield was proportional to the variables temperature and concentration of AC, while the variable flow of aqueous stream showed no significant effect. Remarkably, aqueous sodium bicarbonate (SB) (CO2RS) showed a greater performance in comparison to AC, by reaching 71% of H_2 relative yield, using Al, in only 0.5h of SSOT at 200 ºC and 1.0 mol/L concentration. Likewise, aqueous NaOH 0.5 mol/L (CO2LS) showed the highest H_2 relative yield (up to 85.5%), using Al, within only 50 min. This suggests that the most basic CO2RSs and CO2LSs like aqueous SB and NaOH, respectively, would do a better match with less active metals like Al and Mn. Following this logic, highly active metals like Zn and Fe would do a better match with less basic CO2RS like AC, or a CO2LS like aqueous ammonia or MEA.

Potential stakeholders for the present proposed technology are those implementing solvents-based CO_2 capture plants in its facilities: thermal power stations, ironmaking factories, concrete and cement factories, among others. This offers the opportunity for giving value-added to the process streams in a renewed and demanding market for hydrogen. These results will also allow optimizing the continuous hydrogen production from the metal-water-splitting reaction for reducing CO_2 into green chemicals, like formic acid, and for further applications in the framework of hydrogen economy.

CHAPTER 5

REFERENCES

[1] M. Rubio-Varas and B. Muñoz-Delgado, “200 years diversifying the energy mix? Diversification paths of the energy baskets of European early comers vs. latecomers,” 2017.

[2] J. O. Abe, A. P. I. Popoola, E. Ajenifuja, and O. M. Popoola, “Hydrogen energy, economy and storage: review and recommendation,” *Int. J. Hydrogen Energy*, vol. 44, no. 29, pp. 15072–15086, 2019.

[3] S. van Renssen, “The hydrogen solution?,” *Nat. Clim. Chang.*, vol. 10, no. 9, pp. 799–801, 2020.

[4] E. C. E. Commission, “Europe’s moment: repair and prepare for the next generation.” 2020.

[5] H. Dagdougui, R. Sacile, C. Bersani, and A. Ouammi, *Hydrogen infrastructure for energy applications: production, storage, distribution and safety*. Academic Press, 2018.

[6] I. Dincer, M. A. Rosen, and F. Khalid, “3.16 Thermal Energy Production,” I. B. T.-C. E. S. Dincer, Ed. Oxford: Elsevier, 2018, pp. 673–706.

[7] T. Mirowski and P. Janusz, “Hydrogen in energy balance–selected issues,” *Zesz. Nauk. Inst. Gospod. Surowcami Miner. Pol. Akad. Nauk*, 2018.

[8] M. F. Hordeski, *Alternative fuels: the future of hydrogen*. CRC Press, 2020.

[9] P. Nikolaidis and A. Poullikkas, “A comparative overview of hydrogen production processes,” *Renew. Sustain. energy Rev.*, vol. 67, pp. 597–611, 2017.

[10] M. Ball and M. Wietschel, “The future of hydrogen – opportunities and challenges,” *Int. J. Hydrogen Energy*, vol. 34, no. 2, pp. 615–627, 2009, doi: https://doi.org/10.1016/j.ijhydene.2008.11.014.

[11] J. Bartlett and A. Krupnick, “Decarbonized Hydrogen in the US Power and Industrial Sectors: Identifying and Incentivizing Opportunities to Lower Emissions,” 2020.

[12] H. Ishaq, I. Dincer, and C. Crawford, “A review on hydrogen production and utilization: Challenges and opportunities,” *Int. J. Hydrogen Energy*, 2021.

[13] N. Van Hulst, “The clean hydrogen future has already begun,” *IEA Comment. Int. Energy Agency. https//www. iea. org/comme ntari es/the-clean-hydro gen-futur e-has-alrea dy-begun.*

Accessed April, vol. 1, p. 2021, 2019.

[14] M. Yu, K. Wang, and H. Vredenburg, “Insights into low-carbon hydrogen production methods: Green, blue and aqua hydrogen,” *Int. J. Hydrogen Energy*, vol. 46, no. 41, pp. 21261–21273, 2021.

[15] L. L. Meldahl, “A clean hydrogen market in the making. Comparing Norway’s and the Netherland’s roles in the European hydrogen transition.” NTNU, 2021.

[16] C. Philibert, “Perspectives on a Hydrogen Strategy for the European Union,” *Etudes l’Ifri, Ifri*, 2020.

[17] R. W. Howarth and M. Z. Jacobson, “How green is blue hydrogen?,” *Energy Sci. Eng.*, vol. 9, no. 10, pp. 1676–1687, 2021.

[18] J. Neff, C. Bataille, and B. Shaffer, “The role of hydrogen in decarbonizing Alberta’s electricity system,” *Sch. Public Policy Publ.*, 2021.

[19] D. Hjeij, Y. Biçer, and M. Koç, “Hydrogen strategy as an energy transition and economic transformation avenue for natural gas exporting countries: Qatar as a case study,” *Int. J. Hydrogen Energy*, 2021.

[20] J. Lof, “SURVEY OF HEAVY-DUTY HYDROGEN FUEL CELL ELECTRIC VEHICLES.”

[21] C. Acar and I. Dincer, “Review and evaluation of hydrogen production options for better environment,” *J. Clean. Prod.*, vol. 218, pp. 835–849, 2019.

[22] M. M. Rashid, M. K. Al Mesfer, H. Naseem, and M. Danish, “Hydrogen production by water electrolysis: a review of alkaline water electrolysis, PEM water electrolysis and high temperature water electrolysis,” *Int. J. Eng. Adv. Technol*, vol. 4, no. 3, pp. 2249–8958, 2015.

[23] K. E. Ayers *et al.*, “Research advances towards low cost, high efficiency PEM electrolysis,” *ECS Trans.*, vol. 33, no. 1, p. 3, 2010.

[24] S. S. Kumar and V. Himabindu, “Hydrogen production by PEM water electrolysis–A review,” *Mater. Sci. Energy Technol.*, vol. 2, no. 3, pp. 442–454, 2019.

[25] M. Hirscher *et al.*, “Materials for hydrogen-based energy storage–past, recent progress and future outlook,” *J. Alloys Compd.*, vol. 827, p. 153548, 2020.

[26] X. Huang *et al.*, “A review: Feasibility of hydrogen generation from the reaction between

aluminum and water for fuel cell applications," *J. Power Sources*, vol. 229, pp. 133–140, 2013.

[27] M. Kutz, *Environmentally conscious materials and chemicals processing*, vol. 3. Wiley Online Library, 2007.

[28] A. Steinfeld, P. Kuhn, A. Reller, R. Palumbo, J. Murray, and Y. Tamaura, "Solar-processed metals as clean energy carriers and water-splitters," *Int. J. Hydrogen Energy*, vol. 23, no. 9, pp. 767–774, 1998.

[29] L. D'Souza, "Thermochemical hydrogen production from water using reducible oxide materials: a critical review," *Mater. Renew. Sustain. Energy*, vol. 2, no. 1, p. 7, 2013.

[30] Y. S. Cho and J. H. Kim, "Hydrogen production by splitting water on solid acid materials by thermal dissociation," *Int. J. Hydrogen Energy*, vol. 36, no. 14, pp. 8192–8202, 2011.

[31] H. Z. Wang, D. Y. C. Leung, M. K. H. Leung, and M. Ni, "A review on hydrogen production using aluminum and aluminum alloys," *Renew. Sustain. Energy Rev.*, vol. 13, no. 4, pp. 845–853, 2009, doi: https://doi.org/10.1016/j.rser.2008.02.009.

[32] P. Setiani, N. Watanabe, R. R. Sondari, and N. Tsuchiya, "Mechanisms and kinetic model of hydrogen production in the hydrothermal treatment of waste aluminum," *Mater. Renew. Sustain. Energy*, vol. 7, no. 2, p. 10, 2018.

[33] S. Turn, C. Kinoshita, Z. Zhang, D. Ishimura, and J. Zhou, "An experimental investigation of hydrogen production from biomass gasification," *Int. J. Hydrogen Energy*, vol. 23, no. 8, pp. 641–648, 1998.

[34] J. Petrovic and G. Thomas, "A study of issues related to the use of aluminum for-On-board vehicular hydrogen storage," *US Dep. Energy version*, vol. 1, no. 0, pp. 1–26, 2008.

[35] K. Mahmoodi and B. Alinejad, "Enhancement of hydrogen generation rate in reaction of aluminum with water," *Int. J. Hydrogen Energy*, vol. 35, no. 11, pp. 5227–5232, 2010.

[36] H. Nie, M. Schoenitz, and E. L. Dreizin, "Calorimetric investigation of the aluminum–water reaction," *Int. J. Hydrogen Energy*, vol. 37, no. 15, pp. 11035–11045, 2012.

[37] S. P. Tekade, A. S. Pednekar, G. R. Jadhav, S. E. Kalekar, D. Z. Shende, and K. L. Wasewar, "Hydrogen generation through water splitting reaction using waste aluminum in presence of gallium," *Int. J. Hydrogen Energy*, vol. 45, no. 44, pp. 23954–23965, 2020.

[38] S. S. Razavi-Tousi and J. A. Szpunar, “Effect of structural evolution of aluminum powder during ball milling on hydrogen generation in aluminum–water reaction,” *Int. J. Hydrogen Energy*, vol. 38, no. 2, pp. 795–806, 2013.

[39] Y. Yang, W.-Z. Gai, Z.-Y. Deng, and J.-G. Zhou, “Hydrogen generation by the reaction of Al with water promoted by an ultrasonically prepared Al (OH) 3 suspension,” *Int. J. Hydrogen Energy*, vol. 39, no. 33, pp. 18734–18742, 2014.

[40] J. Macanás, L. Soler, A. M. Candela, M. Muñoz, and J. Casado, “Hydrogen generation by aluminum corrosion in aqueous alkaline solutions of inorganic promoters: The AlHidrox process,” *Energy*, vol. 36, no. 5, pp. 2493–2501, 2011.

[41] S. P. Tekade, D. Z. Shende, and K. L. Wasewar, “Hydrogen generation in water splitting reaction using aluminum: effect of NaOH concentration and reaction modelling using SCM,” *Int. J. Chem. React. Eng.*, vol. 16, no. 7, 2018.

[42] T. Troczynski and E. Czech, “Compositions and methods for generating hydrogen from water.” Google Patents, Oct. 20, 2005.

[43] M. Watanabe, X. Jiang, and R. Saito, “Method for generating hydrogen gas utilizing activated aluminum fine particles.” Google Patents, Jun. 26, 2007.

[44] M. Damizia, M. P. Bracciale, B. De Caprariis, V. Genova, and P. De Filippis, “High Thermal Stability Fe2O3-Al2O3 System to Produce Renewable Pure Hydrogen in Steam Iron Process,” *Chem. Eng. Trans.*, vol. 86, pp. 547–552, 2021.

[45] W.-Z. Gai, X. Zhang, K. Sun, and Z.-Y. Deng, “Hydrogen generation from Al-Water reaction promoted by MB/γ-Al2O3 (M= Co, Ni) catalyst,” *Int. J. Hydrogen Energy*, vol. 44, no. 45, pp. 24377–24386, 2019.

[46] Z. Deng, J. M. F. Ferreira, Y. Tanaka, and J. Ye, “Physicochemical mechanism for the continuous reaction of γ-Al2O3-modified aluminum powder with water,” *J. Am. Ceram. Soc.*, vol. 90, no. 5, pp. 1521–1526, 2007.

[47] Y. A. Aleksandrov, E. I. Tsyganova, and A. L. Pisarev, “Reaction of Aluminum with Dilute Aqueous NaOH Solutions,” *Russ. J. Gen. Chem.*, vol. 73, no. 5, 2003.

[48] A. Irankhah, S. M. S. Fattahi, and M. Salem, “Hydrogen generation using activated

aluminum/water reaction," *Int. J. Hydrogen Energy*, vol. 43, no. 33, pp. 15739–15748, 2018.

[49] L. Soler, J. Macanás, M. Munoz, and J. Casado, "Aluminum and aluminum alloys as sources of hydrogen for fuel cell applications," *J. Power Sources*, vol. 169, no. 1, pp. 144–149, 2007.

[50] S. S. Martínez, W. L. Benítes, A. A. Á. Gallegos, and P. J. Sebastián, "Recycling of aluminum to produce green energy," *Sol. energy Mater. Sol. cells*, vol. 88, no. 2, pp. 237–243, 2005.

[51] G.-L. Ma, H.-B. Dai, D.-W. Zhuang, H.-J. Xia, and P. Wang, "Controlled hydrogen generation by reaction of aluminum/sodium hydroxide/sodium stannate solid mixture with water," *Int. J. Hydrogen Energy*, vol. 37, no. 7, pp. 5811–5816, 2012.

[52] D. Belitskus, "Reaction of aluminum with sodium hydroxide solution as a source of hydrogen," *J. Electrochem. Soc.*, vol. 117, no. 8, p. 1097, 1970.

[53] S. P. Tekade, D. Z. Shende, and K. L. Wasewar, "Hydrogen Generation in an Annular Micro-Reactor: an Experimental Investigation of Water Splitting Reaction Using Aluminum in Presence of Potassium Hydroxide," *Int. J. Chem. React. Eng.*, vol. 17, no. 2, 2018.

[54] X. Xi, J. Chang, and Z. Huang, "The study of kinetics and reaction between metallic manganese and water in (NH~ 4)~ 2SO~ 4 solution," *J. Funct. Mater.*, vol. 34, no. 3, pp. 320–322, 2003.

[55] K. Michiels, J. Spooren, and V. Meynen, "Production of hydrogen gas from water by the oxidation of metallic iron under mild hydrothermal conditions, assisted by in situ formed carbonate ions," *Fuel*, vol. 160, pp. 205–216, 2015.

[56] V. Shmelev, V. Nikolaev, J. H. Lee, and C. Yim, "Hydrogen production by reaction of aluminum with water," *Int. J. Hydrogen Energy*, vol. 41, no. 38, pp. 16664–16673, 2016.

[57] T. Hiraki, S. Yamauchi, M. Iida, H. Uesugi, and T. Akiyama, "Process for recycling waste aluminum with generation of high-pressure hydrogen," *Environ. Sci. Technol.*, vol. 41, no. 12, pp. 4454–4457, 2007.

[58] H. Takahashi, T. Kori, T. Onoki, K. Tohji, and N. Yamasaki, "Hydrothermal processing of metal based compounds and carbon dioxide for the synthesis of organic compounds," *J. Mater. Sci.*, vol. 43, no. 7, pp. 2487–2491, 2008.

[59] M. P. Dudukovic, F. Larachi, and P. L. Mills, "Multiphase reactors–revisited," *Chem. Eng. Sci.*,

vol. 54, no. 13–14, pp. 1975–1995, 1999.

[60] Y. A. Cengel, M. A. Boles, and M. Kanoğlu, *Thermodynamics: an engineering approach*, vol. 5. McGraw-hill New York, 2011.

[61] E. W. Lemmon, “Thermophysical properties of fluid systems,” *NIST Chem. Webb.*, 1998.

[62] S. Xu and J. Liu, “Metal-based direct hydrogen generation as unconventional high density energy,” *Front. Energy*, vol. 13, no. 1, pp. 27–53, 2019.

[63] Y. Yavor, S. Goroshin, J. M. Bergthorson, D. L. Frost, R. Stowe, and S. Ringuette, “Enhanced hydrogen generation from aluminum–water reactions,” *Int. J. Hydrogen Energy*, vol. 38, no. 35, pp. 14992–15002, 2013.

[64] L. Soler, J. Macanas, M. Muñoz, and J. Casado, “Synergistic hydrogen generation from aluminum, aluminum alloys and sodium borohydride in aqueous solutions,” *Int. J. Hydrogen Energy*, vol. 32, no. 18, pp. 4702–4710, 2007.

[65] C. K. Ahn *et al.*, “Determination of ammonium salt/ion speciation in the CO2 absorption process using ammonia solution: Modeling and experimental approaches,” *Energy Procedia*, vol. 4, pp. 541–547, 2011, doi: https://doi.org/10.1016/j.egypro.2011.01.086.

[66] F. Jin *et al.*, “High-yield reduction of carbon dioxide into formic acid by zero-valent metal/metal oxide redox cycles,” *Energy Environ. Sci.*, vol. 4, no. 3, pp. 881–884, 2011, doi: 10.1039/C0EE00661K.

[67] S. P. Tekade, D. Z. Shende, and K. L. Wasewar, “Hydrogen Generation in an Annular Micro-Reactor: An Experimental Investigation and Reaction Modelling by Shrinking Core Model (SCM),” *Int. J. Chem. React. Eng.*, vol. 16, no. 7, 2018.

[68] S. Kumar, *Clean hydrogen production methods*. Springer, 2015.

[69] G. Qi, S. Wang, H. Yu, P. Feron, and C. Chen, “Rate-based modeling of CO2 absorption in aqueous NH3 in a packed column,” *Energy Procedia*, vol. 37, pp. 1968–1976, 2013.

[70] M. Ravichandran, A. Naveen Sait, and V. Anandakrishnan, “Densification and deformation studies on powder metallurgy Al–TiO2–Gr composite during cold upsetting,” *J. Mater. Res.*, vol. 29, no. 13, pp. 1480–1487, 2014, doi: 10.1557/jmr.2014.143.

[71] H. Kwon and M. Leparoux, “Hot extruded carbon nanotube reinforced aluminum matrix

composite materials," *Nanotechnology*, vol. 23, no. 41, p. 415701, 2012.

[72] Y. Liu *et al.*, "Hydrothermal synthesis of microscale boehmite and gamma nanoleaves alumina," *Mater. Lett.*, vol. 62, no. 8–9, pp. 1297–1301, 2008.

[73] L.-L. Xing, C.-H. Ma, Z.-H. Chen, Y.-J. Chen, and X.-Y. Xue, "High gas sensing performance of one-step-synthesized Pd–ZnO nanoflowers due to surface reactions and modifications," *Nanotechnology*, vol. 22, no. 21, p. 215501, 2011.

[74] W. Liang *et al.*, "Crystal structure of impurity-free rhodochrosite (MnCO3) and thermal expansion properties," *Phys. Chem. Miner.*, vol. 47, no. 2, pp. 1–11, 2020.

[75] Y. Roh, C.-L. Zhang, H. Vali, R. J. Lauf, J. Zhou, and T. J. Phelps, "Biogeochemical and environmental factors in Fe biomineralization: magnetite and siderite formation," *Clays Clay Miner.*, vol. 51, no. 1, pp. 83–95, 2003.

[76] L. Soler, J. Macanás, M. Munoz, and J. Casado, "Hydrogen generation from aluminum in a non-consumable potassium hydroxide solution," in *Proceedings International Hydrogen Energy Congress and Exhibition IHEC*, 2005, pp. 13–15.

[77] A. Züttel, "Hydrogen storage methods," *Naturwissenschaften*, vol. 91, no. 4, pp. 157–172, 2004.

[78] J. Wang, J. Gao, Z. Wu, G. Ou, and Y. Wang, "Synthesis of renewable energy materials, sodium aluminum hydride by grignard reagent of Al," *J. Nanomater.*, vol. 2015, 2015.

[79] I. Franke, O. Hentschel, D. Nitsche, M. Stops, H.-D. Bauer, and B. Scheppat, "Parallel FTIR-ATR and gravimetrical in-situ measurements on sodium alanate powder samples during hydrogen desorption," *Int. J. Hydrogen Energy*, vol. 38, no. 36, pp. 16161–16167, 2013.

[80] U. B. Demirci and P. Miele, "Chemical hydrogen storage:'material'gravimetric capacity versus 'system'gravimetric capacity," *Energy Environ. Sci.*, vol. 4, no. 9, pp. 3334–3341, 2011.

CONCLUSIONS AND FUTURE WORK

In the present study of converting captured CO_2 into value added chemicals, several conclusions have been addressed in supporting the convenience of considering CO_2 as a renewable resource. The analysis of relevance for CO_2 utilization technologies showed that the sector of production of Fuels and chemicals (formic acid and green Hydrogen) occupy a high rank within the emerging technologies. In this matter, the selection of proper solvent-based capture technology is a key in utilizing CO_2 as feedstock, and will affect the performance of the simultaneous processes of CO_2 thermochemical reduction, and the *in situ* generation of hydrogen aided by metals. It was observed that, in the catalytic process to obtain formic acid, the ammonium carbamate (ammonia-based CO_2 capture derivative) showed the best performance under mild reaction temperature (120 ºC), while sodium bicarbonate (NaOH-based CO_2 capture derivative) showed outstanding performance but needed higher temperature (250 ºC) for an increased yield. The bicarbonate (HCO_3^-) anion was identified as the reducible specie, and its conversion toward formic acid was proportional to the hydrogen pressure. The process is also greatly improved by the increase of catalyst content, where Palladium 5 wt% over activated carbon showed the highest activity, by the formation of palladium hydride species that can play a reducing role, while the carbonaceous type supports were identified as the most adequate for reducing captured CO_2 and generating hydrogen. Among the metals tested, aluminum was the most efficient for FA production given its lower affectation to the textural features of the catalyst in the solid mixing. Importantly, by the present thesis it was identified for the first time the potential of giving value-added to the streams of basic solvent-based capture technologies, by activating the hydrogen generation from metals, for the purpose of leading to the integration of CO_2 and hydrogen economies. In this matter, zinc presented the best performance with H_2 yield up to 63.7% in 10 h under aqueous AC solution as CO_2-Rich stream. Besides, it was demonstrated that the inclusion of residues from metal-processing factories (aluminum spall) can increase the hydrogen yield, representing a strategy in the search for an economic and environmental feasibility of the proposed technology.

The high dependency of the CO_2 thermochemical reduction process to the type and content of catalyst suggested the need of developing, in collaboration with researchers from TUHH, new catalytic materials, but in a more facile and ecofriendly manner. In this sense, two types of potential materials with catalytic activity were synthesized using alginate and transition metals, namely metal-crosslinked aerogels (MCAs) and metal-decorated carbogels (MDCs) from the pyrolysis of the former. By controlling the pyrolysis temperature, metal ion type and concentration of gelation bath, the post-structure properties of MDCs different post-structure properties were obtained. A nanoparticles-cluster evolution was observed for all carbogels, through the pyrolysis process, in which the increase in crystallite size with increasing pyrolysis temperature was true for all metal ions. Remarkably, among the MDCs, Pd-Agel showed the best features in terms of thermal stability and reducibility, being the only to exhibit zero-valent state conformation during the solvent exchange step in the synthesis process. This conferred catalytic features to the aerogel that were proven in the CO_2 thermochemical reduction process, showing a yield of formic acid of 34.3%, at 120 ºC and 5 h.

The construction and start-up of a semicontinuous facility allowed for the first time coupling the CO_2-Rich stream (CO2RS) and CO_2 Capture-Solvent Lean stream (CO2LS) with the metals-based hydrothermal generation of hydrogen, under the lens an integration of CO_2 economy and Hydrogen economy. Several metals were tasted, where Zn powder had the highest H_2 yield (75.3%) and increased in the order Mn<Al<Fe<Zn. A carbamate/bicarbonate migration from the liquid (CO2RS) to the metallic residue, by the formation of a metallic carbonate, was detected. The process was positively affected by the condition of super-heated water that made possible to rise the temperature and pressure while conserving the liquid state of water. Aqueous sodium bicarbonate and sodium are strong bases that should be better used in activating less active metals like Al and Mn. For its part, highly active metals like Zn and Fe should be better used with less basic aqueous streams like ammonium carbamate, ammonia and MEA.

Future work

The main recommended aspects for a future work are as follows:

Evaluating various sources of industrial metallic wastes as reducing agents for the conversion of captured CO_2. Simultaneously, these wastes should be evaluated for the green hydrogen generation, accompanied by the study of its pretreatments, size reduction and/or sieving.

Scaling up the production of aerogels and carbogels for trying to find a more chemically and thermally stable catalyst, which will permit to conduct a wider study of its catalytical performance under different reaction conditions, to improve its competitiveness against commercial catalysts.

Optimizing the continuous hydrogen production from the metal-water-splitting reaction to feed the design parameters of a future continuous process of reducing captured CO_2 into green chemicals.

Stablishing a techno-economical assessment of the processes of producing formic acid and green hydrogen, to determine the potential profit and revenues.

RESUMEN

Introducción.

Para el 2050 alrededor del 50 % de la producción de energía mundial provendrá de combustibles fósiles, lo cual exige desde ahora el avance en el desarrollo de nuevas y mejores tecnologías de aprovechamiento del CO_2. Por su parte, la investigación en nuevos métodos de obtención de hidrógeno verde está creciendo rápidamente como una forma de descarbonizar la energía utilizada en todo el mundo. En el **Capítulo 1** de la presente tesis se realizó un análisis de Indicadores de estado de avance y relevancia de las tecnologías de aprovechamiento de CO_2, con base en la literatura, y reveló que el sector de Combustibles y productos químicos, en donde se puede ubicar la producción de ácido fórmico, tiene la mayor relevancia dentro de las tecnologías emergentes no tradicionales. A su vez, el ácido fórmico muestra un gran potencial de producción en medio catalítico hidrotermal con condiciones moderadas de reacción, en donde el tipo de soporte del catalizador juega un papel crucial. Dadas sus propiedades texturales y superficiales y estabilidad en el medio hidrotermal, los soportes carbonosos se han constituido como el mejor aliado para este tipo de proceso, representando una oportunidad de investigación el desarrollo de catalizadores nuevos y alternativos a los disponibles en el comercio. El medio hidrotermal es estratégico a su vez porque éste se aprovecha para generar *in situ* el hidrógeno necesario para la reducción de CO_2 capturado en fórmico, mediante la adición de metales reductores, y, dentro del contexto de cero emisiones y desarrollo sostenible, esta generación va más allá y se convierte en una oportunidad integradora de las dos potentes economías de CO_2 e hidrógeno. Por ello, tanto la reducción hidrotermal de CO_2, como la generación térmica de hidrógeno con metales reductores hacen parte del foco de la presente tesis, la cual propone por primera vez el uso novedoso de las corrientes CO2RS y CO2LS, del proceso de captura de CO_2 con solventes básicos, como activadores de la generación de hidrógeno verde en un sistema semicontínuo de diseño y fabricación propia.

Objetivos

Como objetivo principal de la tesis, se desea integrar la captura de CO_2 con la generación de hidrógeno para la producción de **ácido fórmico** e **hidrógeno verde**, a la luz de las economías tanto de CO_2 como de hidrógeno. Para ello, se establecieron los siguientes objetivos de investigación, divididos en la **Parte 2** y la **Parte 3** de la tesis.

Parte 2: Sobre el estudio catalítico de la reducción de derivados de la absorción de CO_2 en amoníaco como materiales de partida para la producción de productos químicos de valor agregado

• Evaluación de materiales de partida para la producción hidrotermal de ácido fórmico en condiciones leves de reacción (Capítulo 2).

• Estudio paramétrico de los efectos de las principales variables de proceso en la producción de ácido fórmico (Capitulo 2).

• Cribado y comparación de diferentes catalizadores metálicos soportados y metales reductores en busca del sistema metal/catalizador más activo para la reducción de CO_2 y la generación de H_2 (Capítulo 3).

• Uso de las corrientes CO2RS/CO2LS como medio de reacción en la generación de hidrógeno en un proceso simultáneo con reducción de CO_2 capturado (Capítulo 3).

• Desarrollo de soportes carbonosos alternativos a partir de fuentes renovables con mejores costos de producción y huella de carbono a través de procesos de producción sencillos y amigables con el ambiente (Capítulo 4). (Colaboración internacional con la Universidad Técnica de Hamburgo TUHH).

• Caracterización exhaustiva de catalizadores comerciales y sintetizados y metales gastados, usando técnicas instrumentales con tecnologías de punta (Capítulos 2, 3 y 4)

Parte 3: Sobre el diseño y construcción de una instalación semicontinua para la integración de las economías de CO2 e hidrógeno y su prueba de concepto mediante un estudio experimental

• Diseño y construcción de una novedosa instalación semicontinua para la generación de hidrógeno verde y azul a partir de metales y residuos industriales en condiciones de agua sobrecalentada (Capítulo 5).

• Evaluación de prueba de concepto del uso de una corriente rica en CO_2 (CO2RS) y una corriente de solvente de captura pobre en CO_2 (CO2LS) como activadores de la generación de hidrógeno a partir de la reacción de división del agua con metales en modo semicontinuo (Capítulo 5).

Resultados y discusión

En el **Capítulo 2** el estudio en batch del proceso de reducción catalítica de CO_2 en medio hidrotermal mostró que, como material de partida, el carbamato de amonio fue el de mejor rendimiento hacia fórmico a una temperatura de reacción moderada de 120 ºC, mientras que el bicarbonato de sodio presentó el mayor rendimiento, pero a una temperatura más elevada de 250 ºC (Fig. 1).

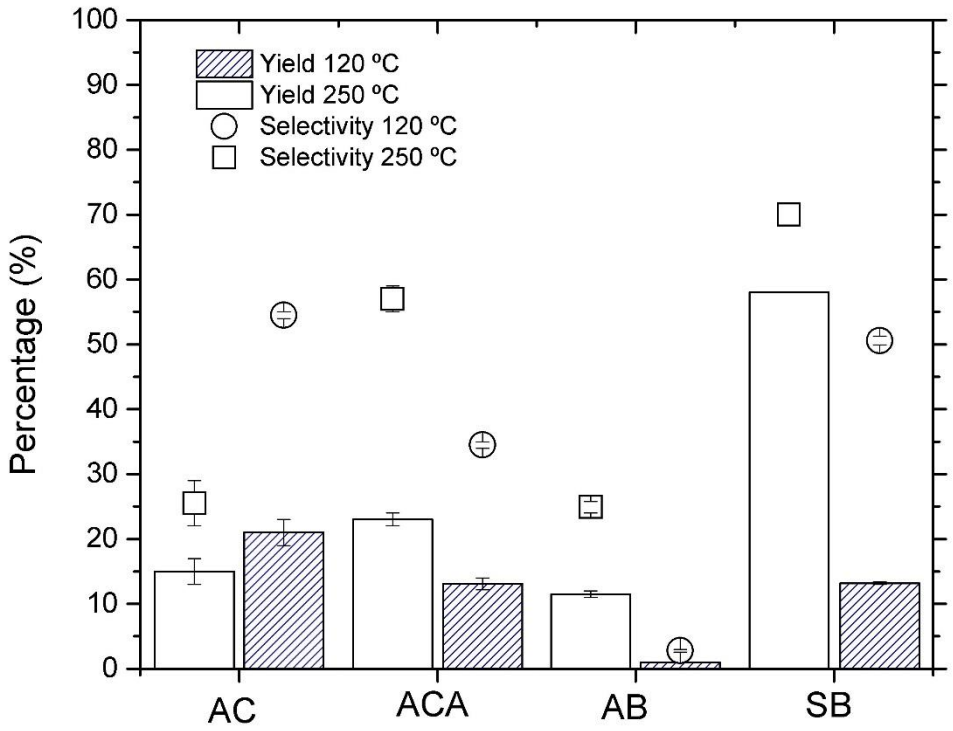

Fig. 1. Comparación de rendimiento de diferentes fuentes de carbono a 120 y 250 ºC. Condiciones de reacción: 2 h, relación molar Al:fuente de carbono de 6, 15% de catalizador, 70% de relleno y 0,5 M de concentración inicial. (AC: carbamato de amonio, ACA: carbonato de amonio, AB: bicarbonato de amonio y SB: bicarbonato de sodio).

El rendimiento de fórmico, a partir de AC, está limitado por la descomposición térmica de la especie reducible HCO_3^-, y del ion formato, por lo que la temperatura mostró un máximo de rendimiento en 120 ºC (Fig. 2).

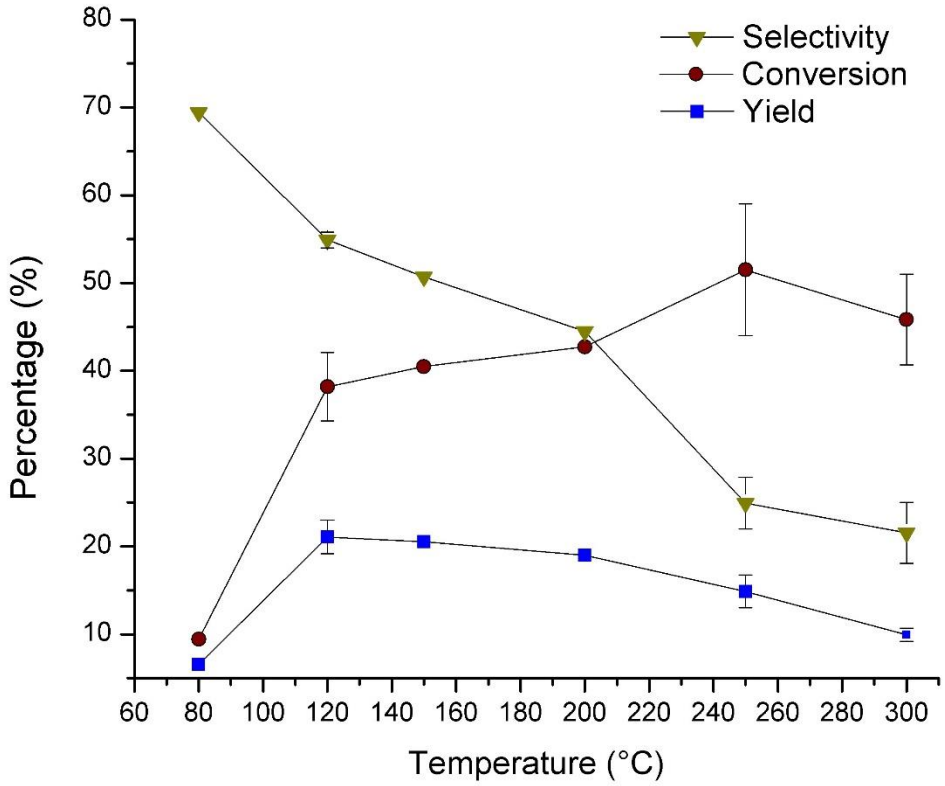

Fig. 2. Efecto de la temperatura sobre el rendimiento, conversión y selectividad. Las condiciones de reacción son: 2 h, relación molar Al:AC de 6, 15 % de catalizador, 70 % de relleno y 0,5 M de concentración inicial de AC.

El rendimiento de fórmico fue directamente proporcional con el contenido de catalizador de paladio 5%wt en carbón activo, obteniéndose un rendimiento de casi el 40%, para la concentración más alta, sugiriendo que el proceso es altamente sensible a la naturaleza y cantidad del catalizador (Fig. 3).

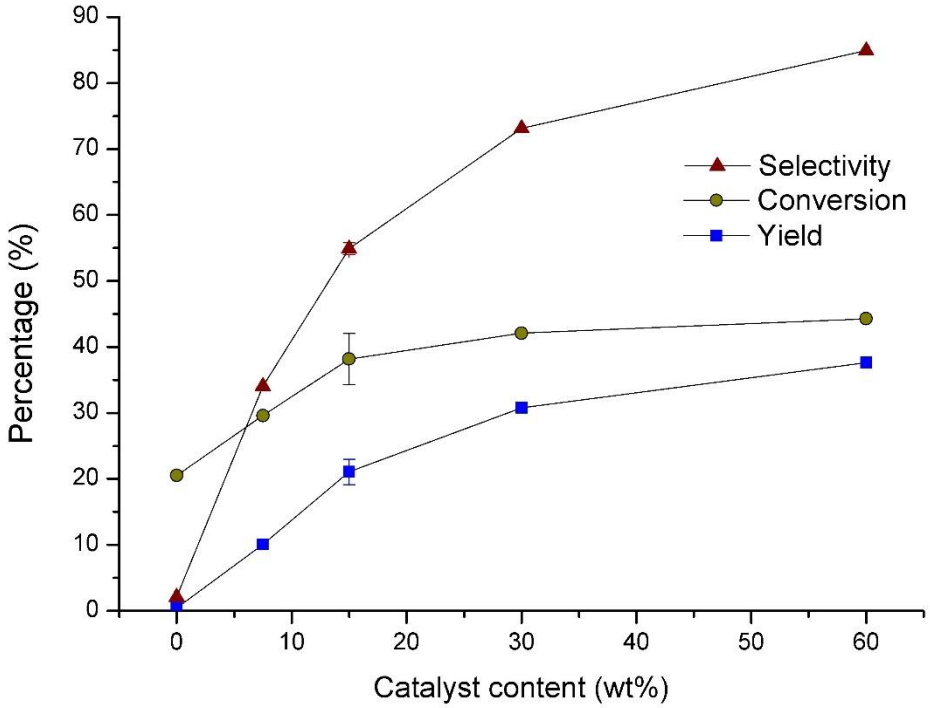

Fig. 3. Efecto del contenido de catalizador Pd/C 5% en peso con respecto al carbamato de amonio. Las condiciones de reacción son: 120 ºC, 2 h, relación Al:AC de 6, 70% de llenado y 0,5 M de concentración inicial de AC.

A través de la caracterización del sólido gastado después de reacciones sucesivas de reutilización, se identificó que el aluminio no se consume totalmente, inclusive hasta el quinto re-uso. Además, se logró elucidar la evolución del catalizador en los diferentes ciclos de reutilización, con el análisis H_2-TPR. Este permitió identificar la formación de especies de hidruro de paladio, las cuales pueden jugar un rol reductivo del CO_2 capturado en fórmico (Fig. 4).

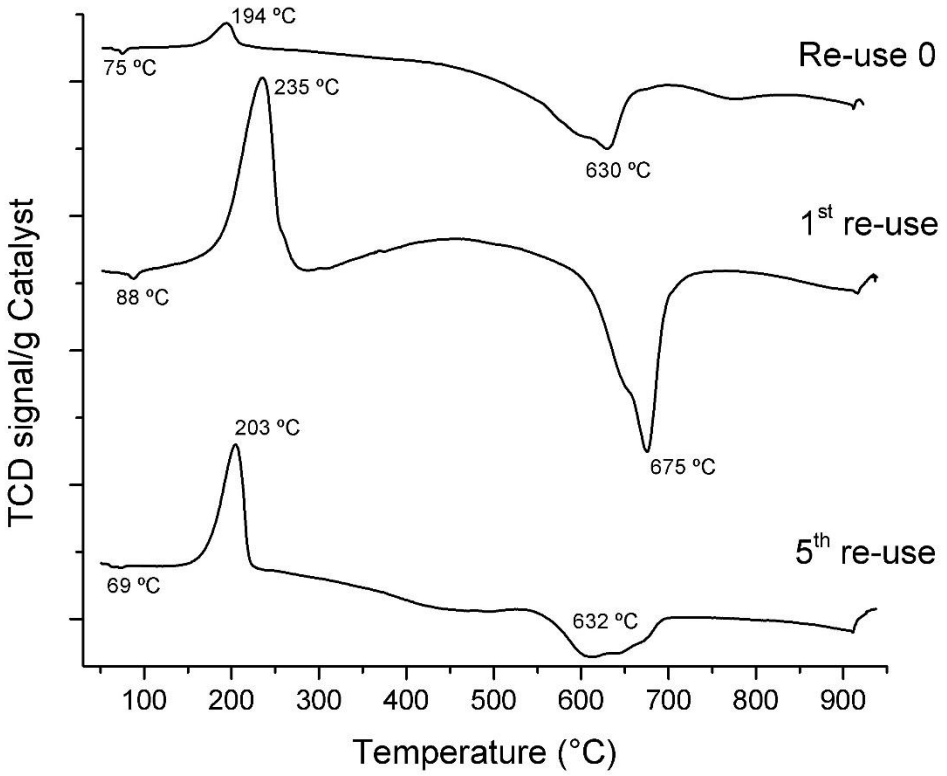

Fig. 4. Perfil TPR del sólido resultante (Al+Pd/C 5% en peso) después de reacción en el punto central (Reutilización 0), 1ª y 5ª reutilización.

En el **Capítulo 3** el estudio en batch de la reducción hidrotermal de CO_2 capturado en amoniaco se amplió a la evaluación de diferentes metales reductores y catalizadores, así como su incidencia en la producción simultánea de hidrógeno verde. Dentro de un cribado de catalizadores, diferenciados entre ellos por el tipo de soporte y metal activo, el Paladio 5% wt en carbón activo fue el único que mostró actividad hacia la producción de ácido fórmico, para todos los metales reductores usados (Fig. 5). Entre estos metales, el Zinc mostró la mayor presión autógena, correspondiente con un mayor rendimiento de hidrógeno verde, de hasta 26% (Fig. 6).

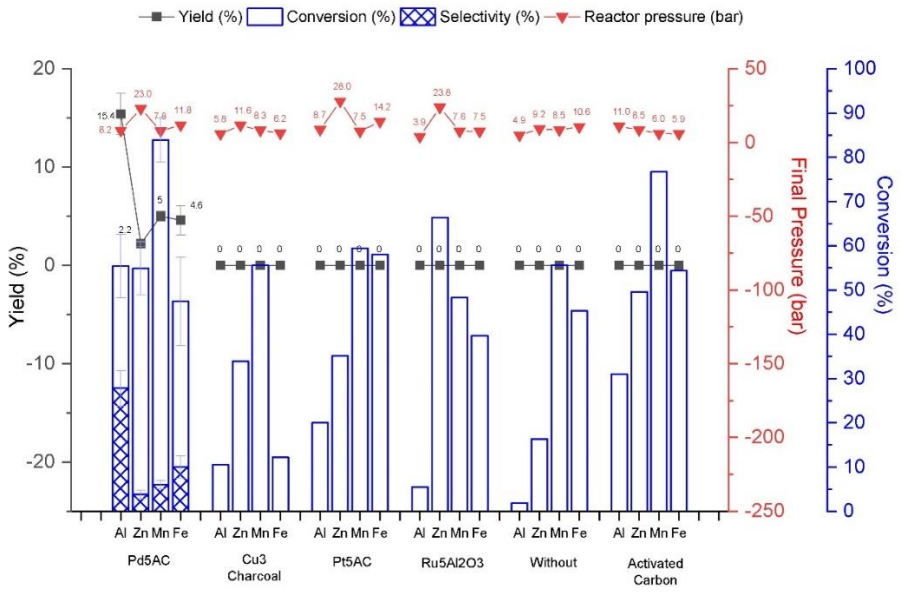

Fig. 5. Rendimiento catalítico de diferentes sistemas metal/catalizador. Condiciones de reacción: 2 h, relación molar metal:carbamato de 6, relación molar catalizador metal:carbamato de 3,8 mmol, 70% de relleno y 0,5 M de concentración inicial.

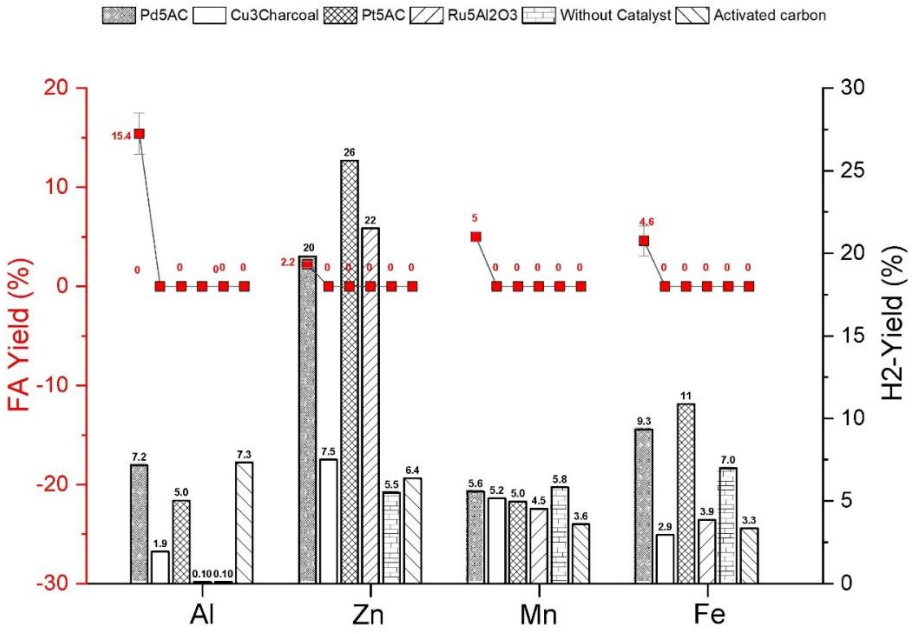

Fig. 6. Rendimientos de FA y H2 para los diferentes sistemas metal-catalizador. Condiciones de reacción: 2 h, relación molar metal:carbamato de 6, relación molar catalizador metal:carbamato de 3,8 mmol, 70% de relleno y 0,5 M de concentración inicial.

En esta oportunidad se pudo analizar el efecto que tiene el tamaño de partícula del metal reductor y su pureza, usando para ello aluminio 500 µm y un residuo de aluminio de la compañía BEFESA, en forma de virutas. En comparación con el polvo (<5 µm), dicho tamaño, tanto para el aluminio puro como para el residuo, hizo decaer el rendimiento a fórmico, pero esto permitió demostrar que el residuo presenta actividad hacia la generación *in situ* de hidrógeno verde.

Para el estudio de la generación de hidrógeno verde se consideraron dos medios/corrientes, uno rico en CO_2 capturado (CO2RS), y otro libre de CO_2 o solvente fresco (CO2LS), en experimentos con ausencia de catalizador y por 10 horas. En general, zinc presentó ratas de generación de H_2 más rápidas bajo ambos tipos de corrientes en todo momento, con un rendimiento de hasta 63.7% con AC acuoso. La activación de Al en general fue más lenta, sólo empezó a ser significativo a las 6 h con SB, para un rendimiento de H_2 del 11 %.

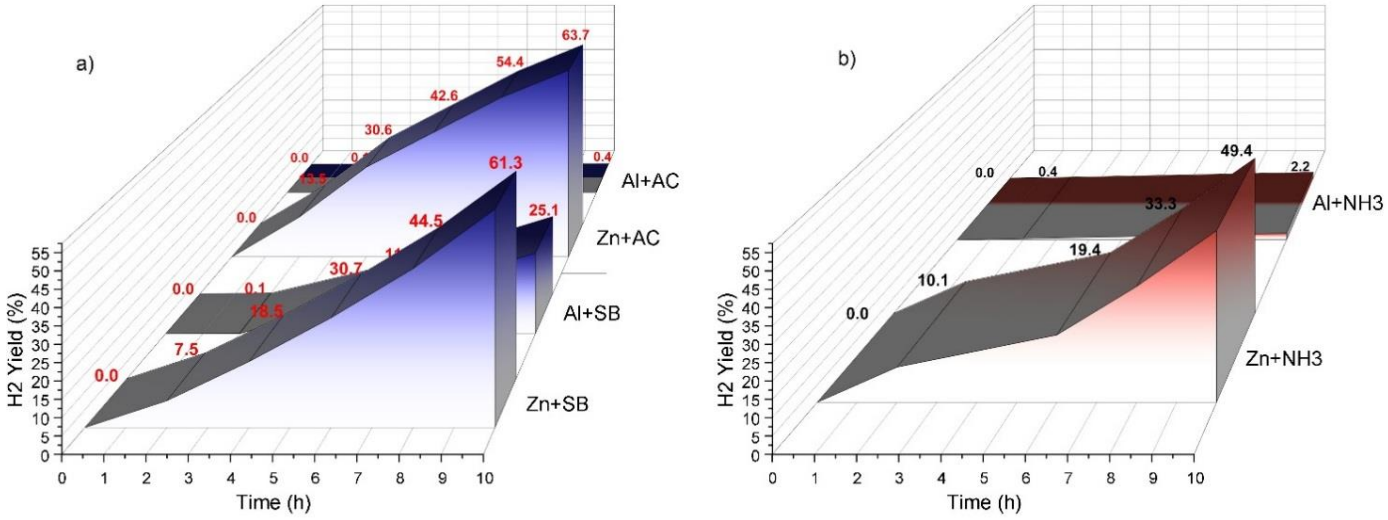

Fig. 7. Evolución de H2 usando Al y Zn durante experimentos de 10 horas a 120 ºC bajo los medios a) CO2RS (AC y SB acuoso), y b) CO2LS (NH_3 acuoso).

El análisis XRD de los sólidos mostró, además de la esperada formación de oxidación de los metales usados, la aparición de carbonatos metálicos, sugiriendo que parte de la conversión del carbamato se debe a este producto.

La síntesis de aerogeles entrecruzados con metales (MCAs) y carbogeles decorados con metales (MDCs) del **Capítulo 4** se realizó en el marco de la estancia doctoral. En el primer paso de síntesis, preparación de hidrogel, se varió la concentración de la solución de precursor de metal en el baño de gelificación, pero el contenido final de metal se estabilizó a partir de una concentración de 170 mmol/L. Pd^{+2} mostró la mayor incorporación en aerogel, con un contenido final de metal de hasta 13% (Fig. 8), que es mayor a los encontrados en la literatura revisada, y después de la pirólisis el Pd-Cgel fue notablemente el que perdió menos masa, con sólo el 58 %, hasta 600 ºC (Fig. 9).

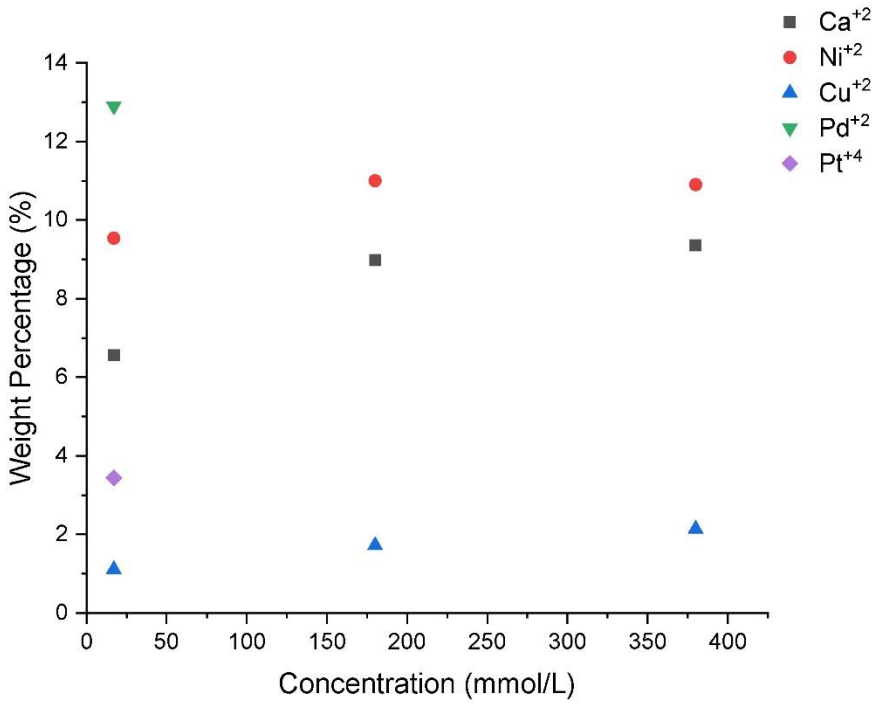

Fig. 8. Contenido de metal en esferas de aerogel a diferentes concentraciones de precursor metálico

A diferentes temperaturas de pirólisis (150 - 600ºC) hubo una tendencia decreciente en las características texturales, con un gran cambio después de aproximadamente 285 °C, asociado a un encogimiento esperado (Fig. 10). SEM-BSE de carbogeles mostró una evolución de closters de nanopartículas a través de las diferentes temperaturas de pirólisis, desarrollando formas bien

definidas para Ni- y Cu-Cgel a 600 ºC, con tamaño promedio de 14 nm +/- 7 nm y 85 nm +/- 29 nm, respectivamente (Fig. 11).

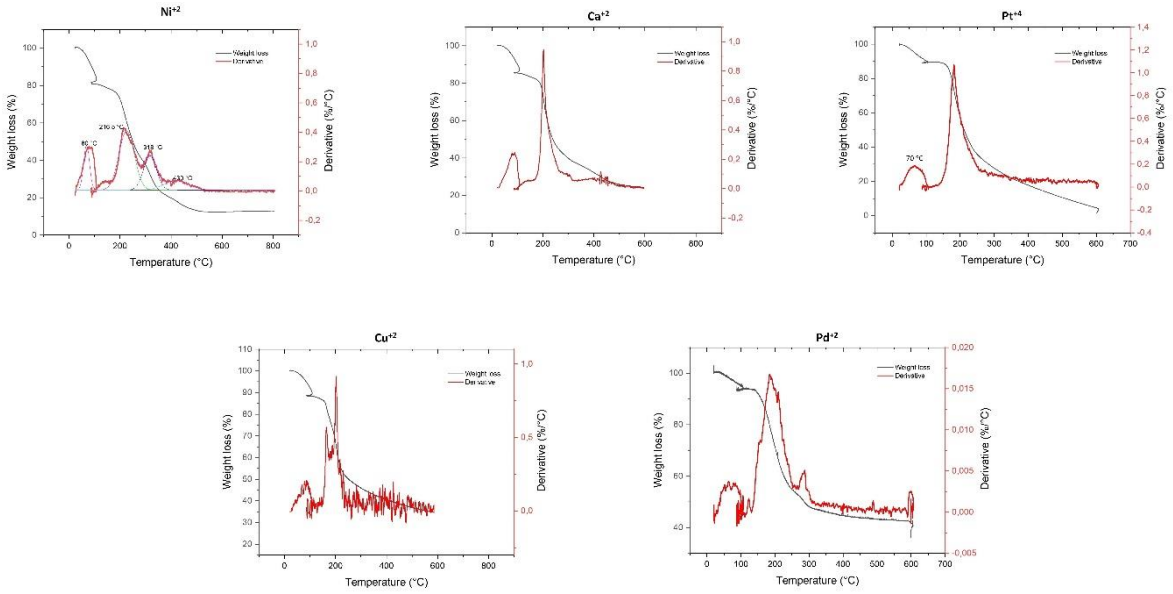

Fig. 9. Análisis termogravimétrico (TGA) y termogravimetría derivada (DTG) de MCA

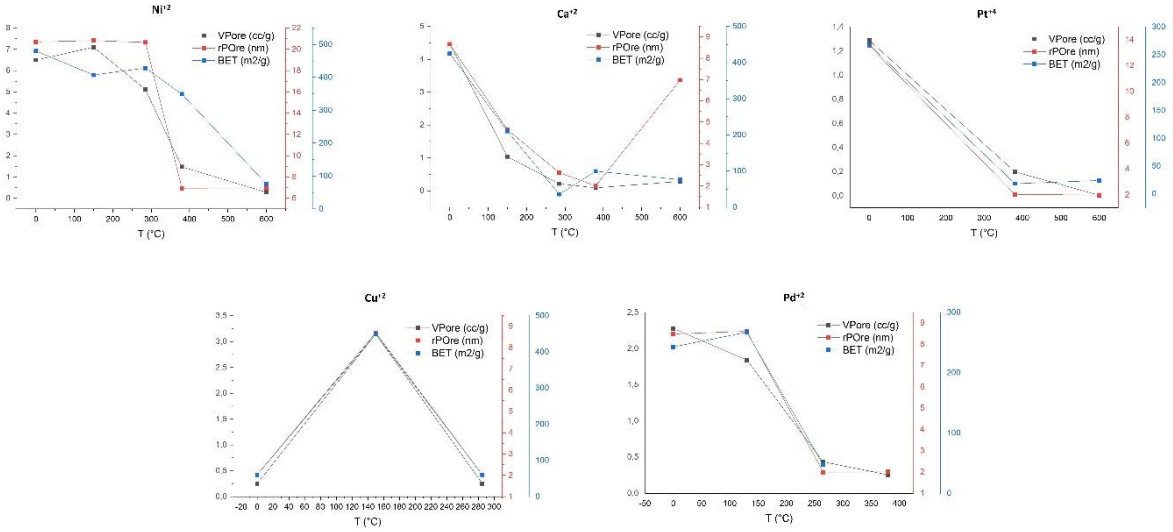

Fig. 10. Propiedades texturales de los MCAs (indicados como "0") y MDCs a diferentes temperaturas de pirólisis

Los resultados XRD (Fig. 12) y TPR (Fig. 13) de Ni-, Cu-, Pt- y Pd-Cgels indicaron que las partículas están compuestas de metales elementales y óxidos metálicos en proporciones variables, mientras que Pd-Agel fue el único aerogel en mostrar la presencia exclusiva del estado de valencia cero por análisis XPS (Fig. 14) y TPO (Fig. 15).

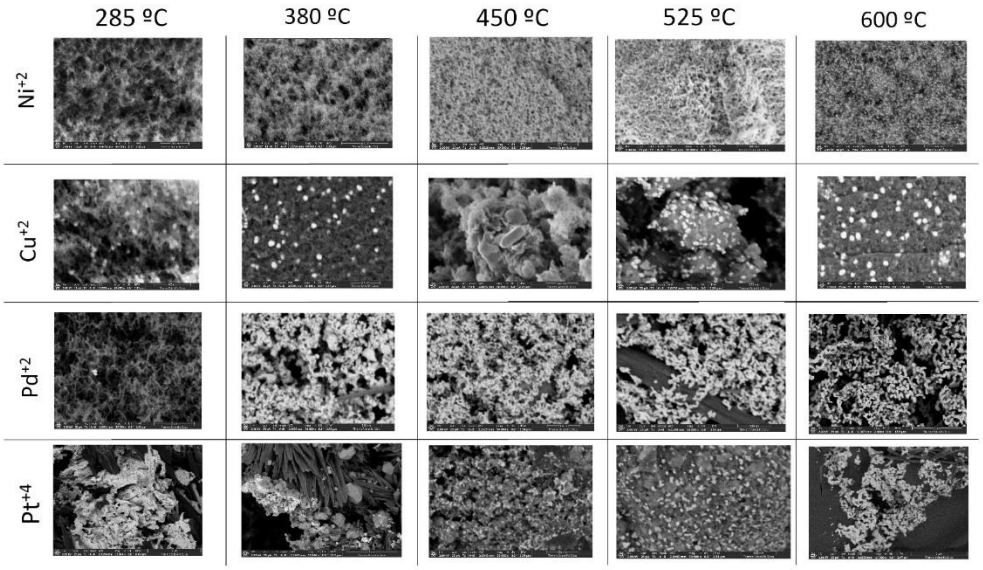

Fig. 11. Imágenes SEM-BSE (SEM2) de MDCs a diferentes temperaturas de pirólisis

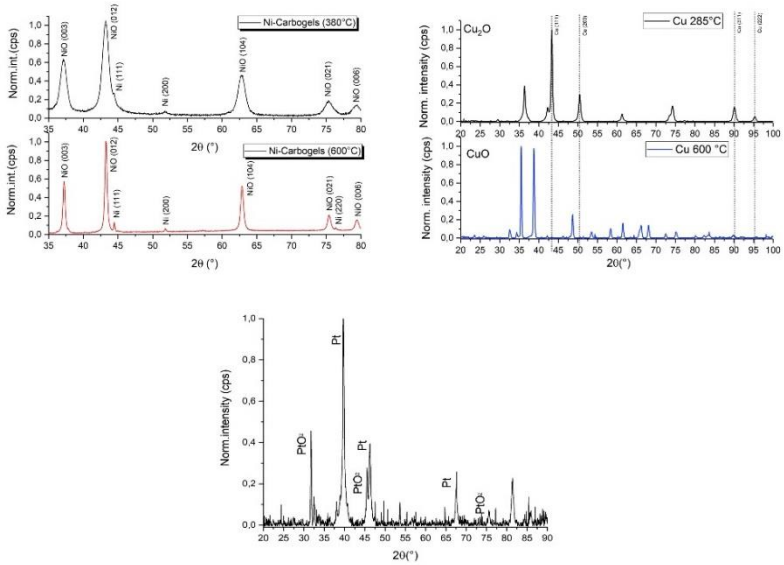

Fig. 12. Difractogramas XRD de MDCs a diferentes temperaturas de pirólisis

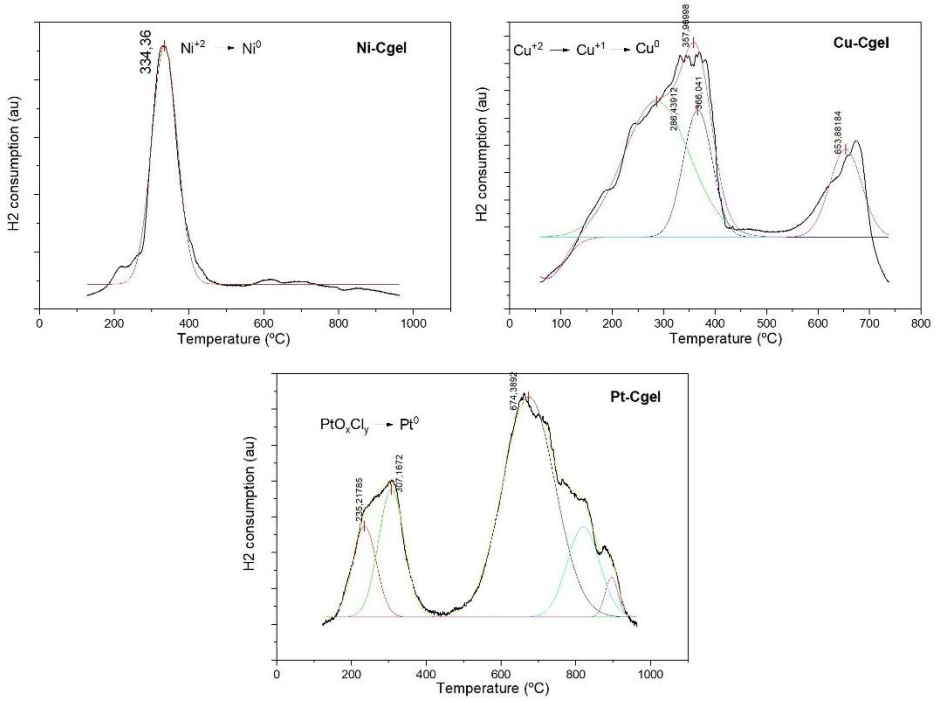

Fig. 13. Curvas H2-TPR de a) Ni-Cgel, b) Cu-Cgel yc) Pt-Cgel, producidos a 600 ºC

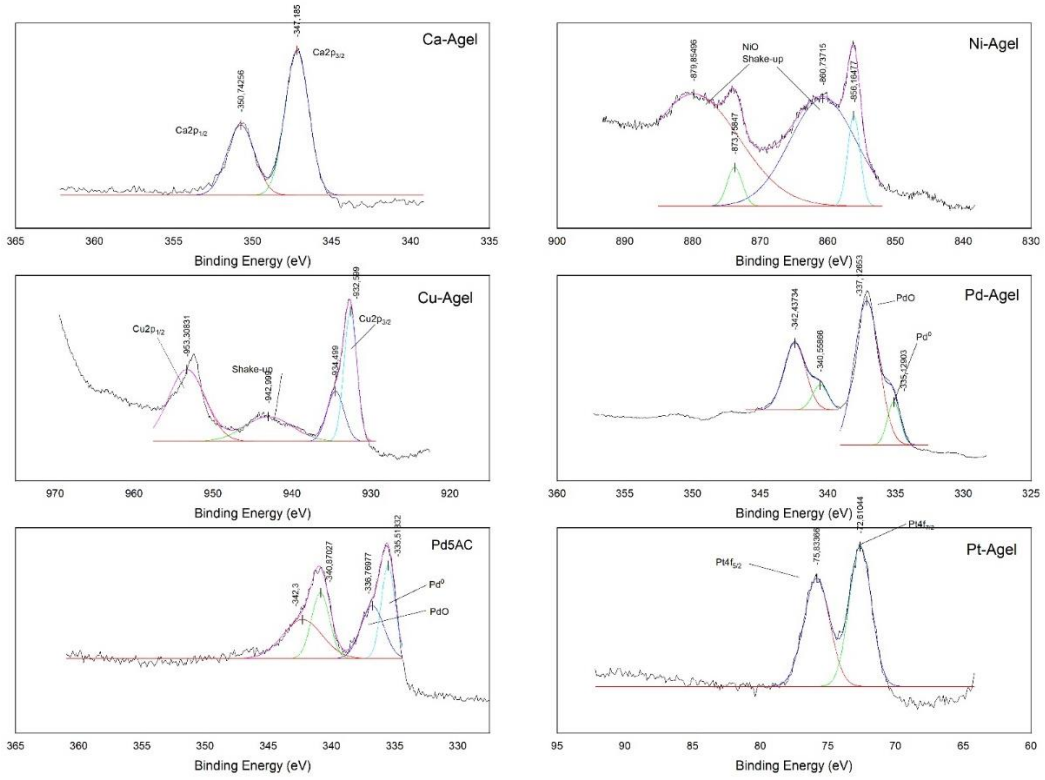

Fig. 14. Espectros de alta resolución de MCA y catalizador de control Pd5AC

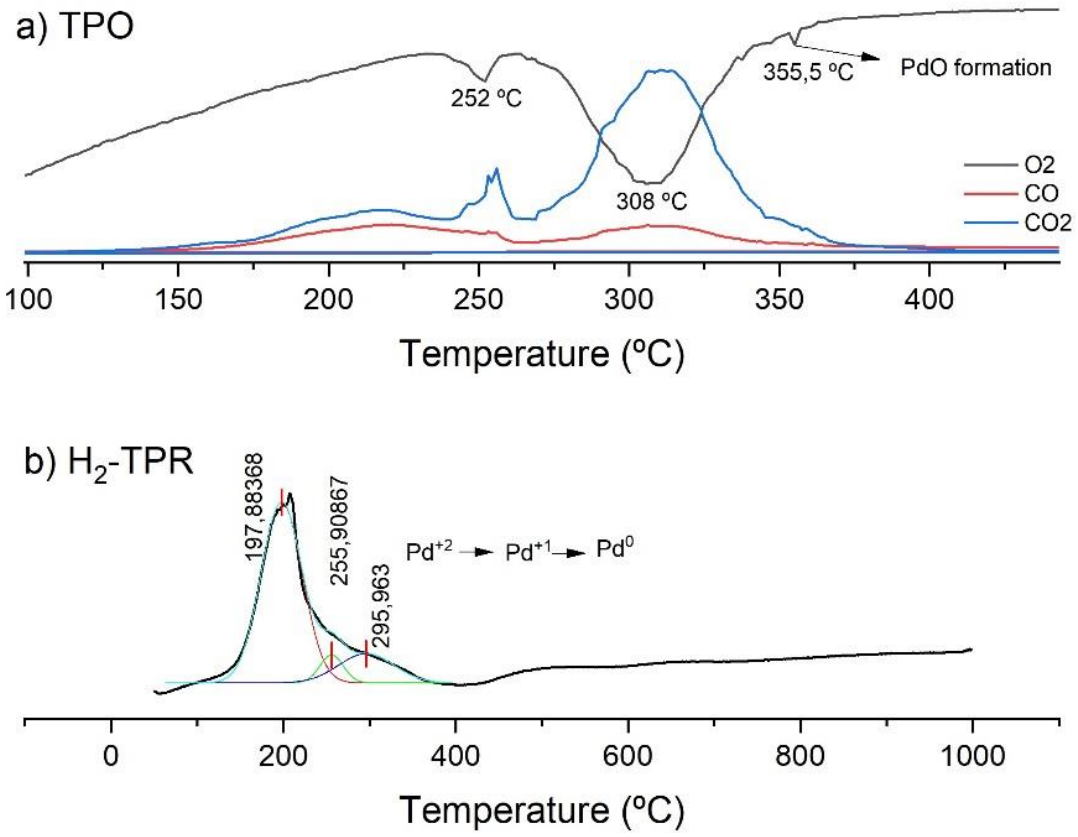

Fig. 15 a) Curvas TPO y b) H_2-TPR para Pd-Agel

Al ensayar el Pd-Agel como catalizador en la reacción de reducción de CO2 capturado el rendimiento de ácido fórmico fue de 34.3%, en contraste con la reacción blanco (sin catalizador) que no mostró consumo de H_2 y/o señal de ácido fórmico. Por otro lado, la reacción con polvo de Pd como catalizador (reacción control) mostró un rendimiento insignificante de 2,97% (Fig. 16).

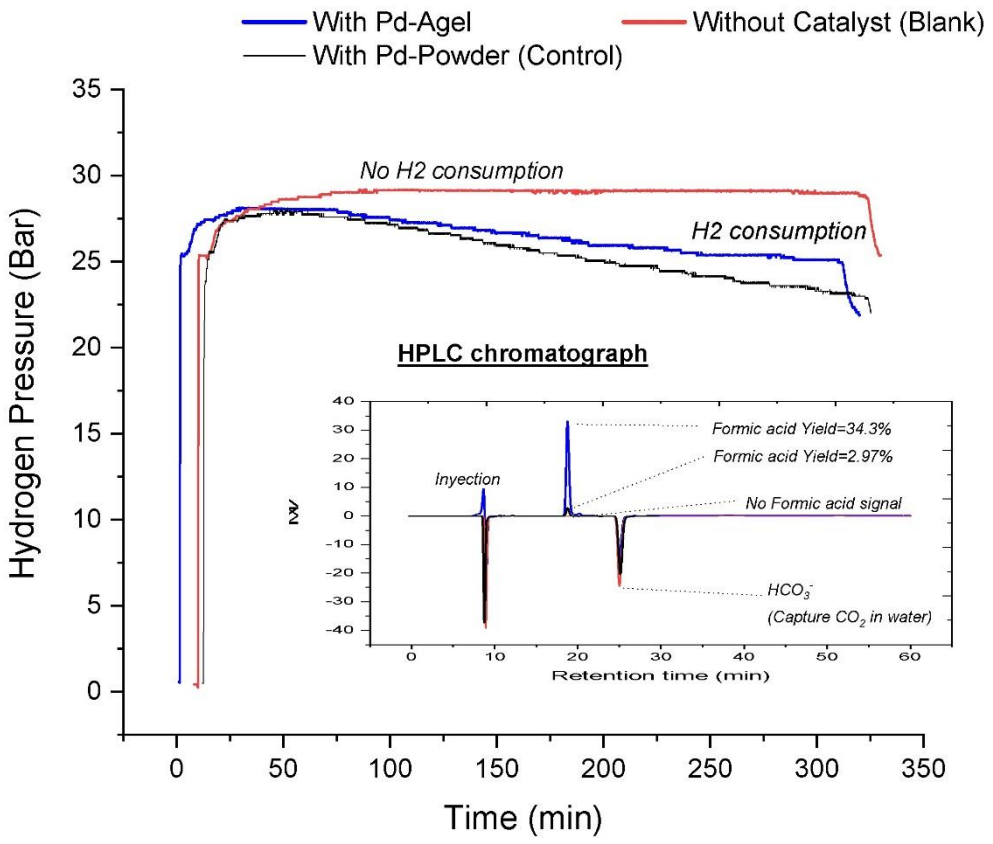

Fig. 16. Evolución de la presión de hidrógeno durante la reducción del CO_2 capturado hacia ácido fórmico sin catalizador (blanco), con catalizador Pd-Agel y Pd en polvo (control).

Por primera vez, el **Capítulo 5** propone una instalación novedosa operada en semicontínuo, de construcción propia, para el aprovechamiento de las corrientes de solventes básicos que median en las plantas típicas de captura de CO_2 (CO2RS y CO2LS) para la generación de hidrógeno verde a partir de metales (Fig. 17). El estudio experimental mostró que la producción de H_2 aumentó en el orden Mn<Al<Fe<Zn, usando AC acuoso como corriente CO2RS (Fig. 18). El rendimiento fue proporcional a la temperatura y la concentración, e indirectamente al tamaño de partícula. Una vez más, el residuo de aluminio en forma de viruta de la compañía BEFESA mostró un alto desempeño, alcanzando un rendimiento del 12 % para el tamaño de 250 µm, usando AC acuoso como CO2RS. El rendimiento de H_2 fue proporcional a las variables temperatura y concentración de AC, mientras que la variable flujo de corriente acuosa no mostró efecto significativo. Es de remarcar que el

bicarbonato de sodio acuoso (SB) (CO2RS) mostró un mayor rendimiento en comparación con AC, al alcanzar un rendimiento relativo del 71 % de H_2, utilizando Al, en solo 0,5 h de SSOT a 200 ºC y una concentración de 1,0 mol/L (Fig. 19). Asimismo, el NaOH acuoso 0,5 mol/L (CO2LS) mostró el mayor rendimiento relativo de H_2 (hasta 85,5 %), utilizando Al, en solo 50 min (Fig. 20). Así mismo, al igual que en el capítulo 3 se detectó la interacción de los CO2RS con los metales por formación de carbonatos metálicos, y por ATR-FTIR se detectó la formación de hidruros de aluminio.

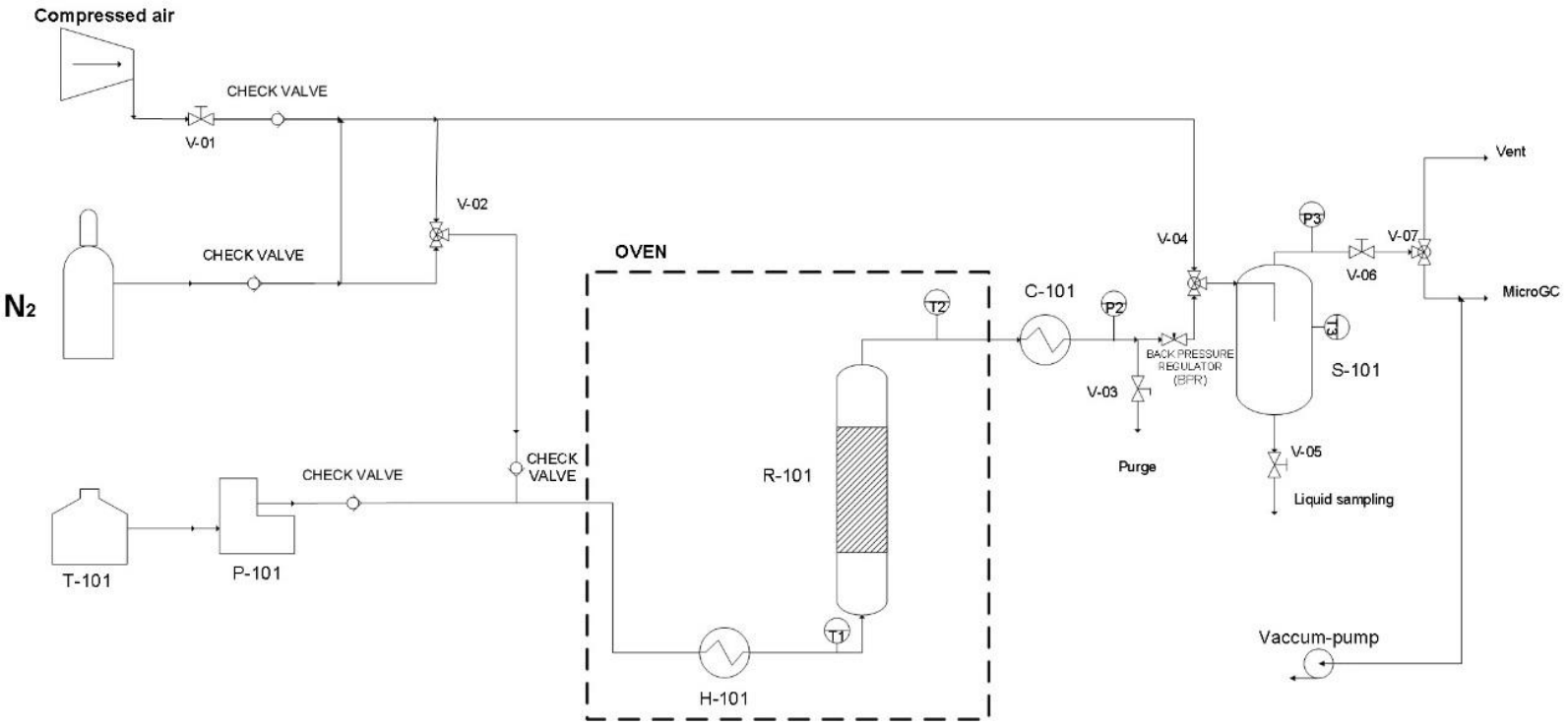

Fig. 17. P&ID de la instalación de generación de hidrógeno en semicontinuo

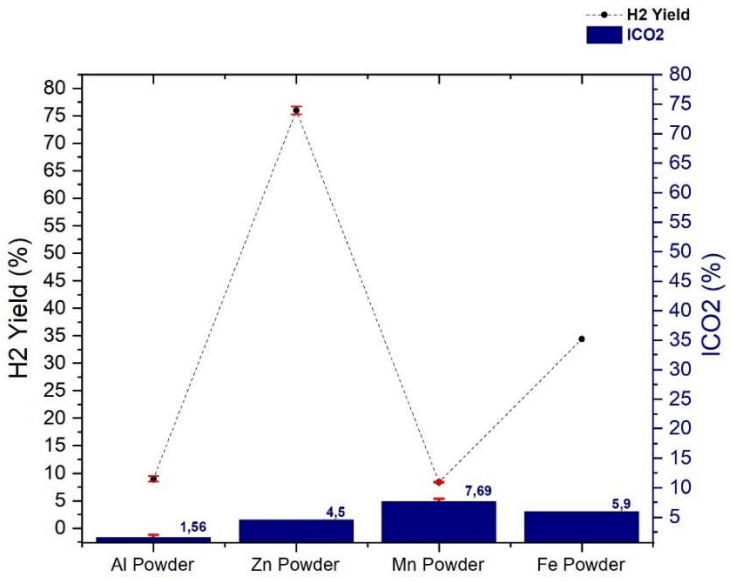

Fig. 18. Rendimiento de H_2 y pérdida de carbamato en función del tipo de polvo metálico. Condiciones de reacción: 200 ºC, 25 bar, 2 h de SSOT y 0,5 mL/min de 1,5 mol/L de AC como CO2RS.

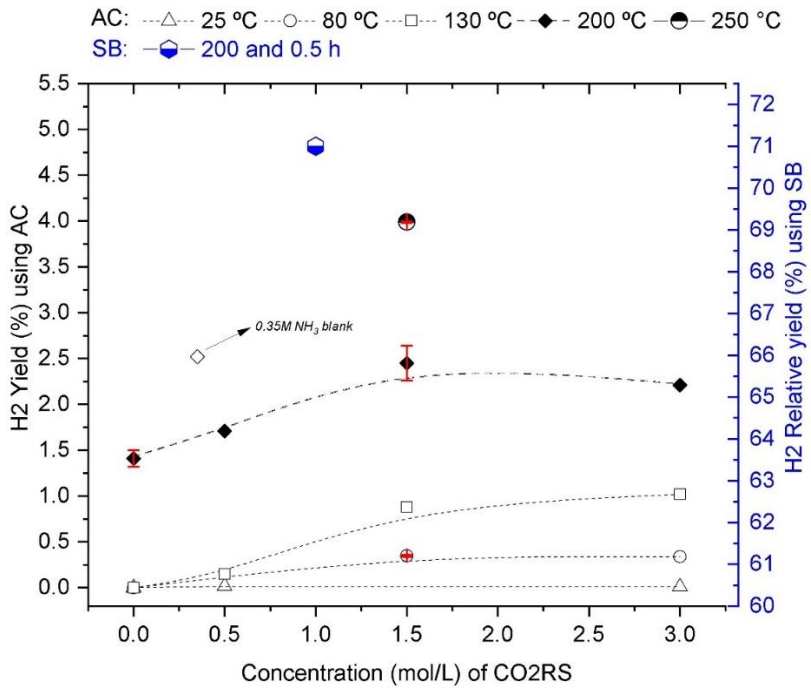

Fig. 19. Rendimiento de H_2 en función de la temperatura y la concentración de AC. Condiciones de reacción: Al 500 µm, 25-250 ºC (25-50 bar), Al 500 µm, 0,5 mL/min de CO2RS (AC y SB), 0-3,0 mol/L, 2 h de SSOT.

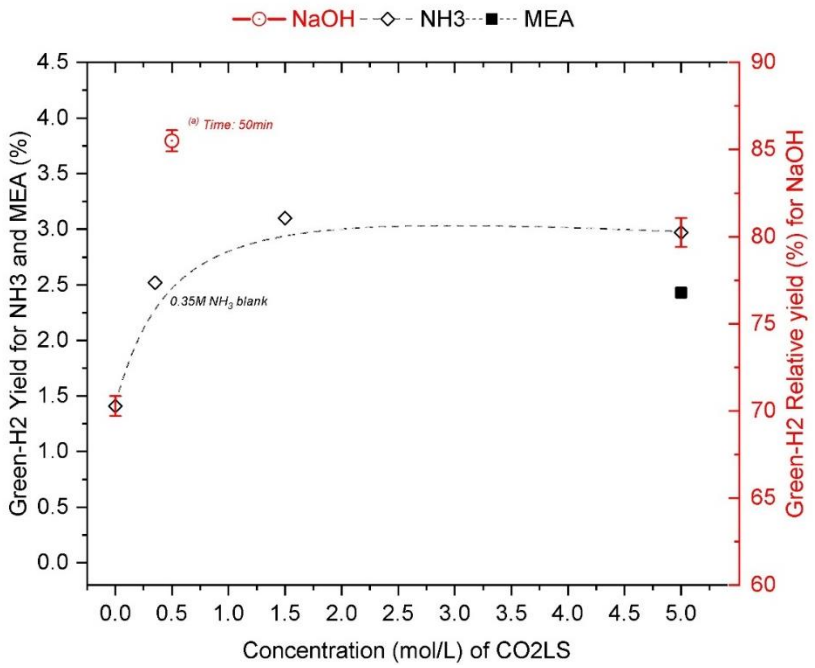

Fig. 20. Rendimiento de H_2 en función de la concentración de diferentes CO2LS. Condiciones de reacción: Al 500 µm, 200 ºC (25 bar), 0,5 mL/min y 2 h de SSOT.

ABOUT THE AUTHOR

Juan Ignacio del Río Blandón was born in Medellín-Colombia in 1986. He obtained a Swiss scholarship to course Process Engineering degree at the Universidad Eafit (2004-2010), in Medellín. In 2008 was granted an undergraduate internship scholarship at the University of Oklahoma, to work in the Biofuels research group of Professor Daniel Resasco in the deoxygenation reactions of vegetable oils into olefins. In 2009-2011 he worked in operations management with Lean Six Sigma in the coal company Cerrejón, and in Maillard reactions research at the company Tecnas S.A., for developing reaction flavors. In 2012 he joined the Industrial Chemical Processes (PQI) research group from Universidad de Antioquia (UdeA), to work in the field of applied catalysis for production of bio-hydrocarbons from vegetable oils. He was granted the tuitions fees waver for coursing the master degree of engineering with chemistry emphasis at UdeA (2013-2016) and was awarded with the meritorious distinction. During this period, he also taught the laboratories of Heat transfer, Mass transfer, and chemical reactions and reactors, at the Department of Chemical Engineering (UdeA). From 2012 to 2014 he was an English copy editor of the Journal Vitae, from UdeA. In 2017 he enrolled to the doctoral program of thermodynamic engineering of fluids, at Universidad de Valladolid, obtaining a predoctoral fellowship to study the conversion of captured CO_2 into value-added chemicals. In 2021, with the aid of an Erasmus scholarship, he was a guest scientist in the Institute of Thermal Separation Processes of Professor Irina Smirnova, at the Technische Universität. Hamburg (TUHH), to conduct studies in the synthesis of alginate derived aerogels and carbogels with catalytic properties.

ORCID number: 0000-0002-5045-4567
Scopus Author ID: 7201580631

LIST OF PUBLICATIONS:

del Río, J. I., Pérez, E., León Mediavilla, D., Martín Martínez, Á., & Bermejo Roda, M. D. (2021). Catalytic hydrothermal conversion of CO2 captured by ammonia into formate using aluminum-sourced hydrogen at mild reaction conditions, Journal of Industrial and Engineering Chemistry, 97, 539-548.

del Río, J. I., Pérez, W., Cardeño, F., Marín, J., & Rios, L. A. (2021). Pre-hydrogenation stage as a strategy to improve the continuous production of a diesel-like biofuel from palm oil. Renewable Energy, 168, 505-515.

del Río, J. I., Cardeño, F., Pérez, W., Peña, J. D., & Rios, L. A. (2018). Catalytic hydrotreating of jatropha oil into non-isomerized renewable diesel: Effect of catalyst type and process conditions. Chemical Engineering Journal, 352, 232-240.

Pérez, W., Marín, J., del Río, J., Peña, J., & Rios, L. (2017). Upgrading of palm oil renewable diesel through hydroisomerization and formulation of an optimal blend. Fuel, 209, 442-448.

del Río, J. I., Cardeño, F., Ríos, L. A., & Peña, J. D. (2015). Hidrogenación de aceite crudo de Jatropha para aplicaciones industriales. Información tecnológica, 26(6), 03-12.

In preparation: Juan I. del Río, Laura Juhász, József Kalmár, Zoltán Erdélyi, María D. Bermejo, Ángel Martín, Irina Smirnova, Pavel Gurikov, Baldur Schroeter, Controlling the post-structure properties of metal-crosslinked carbon-aerogels from alginate for emerging technologies.

In preparation: Juan I. del Río, María D. Bermejo, Ángel Martín, Coupling the solvent-based CO2 capture processes to the metal-water-splitting for hydrogen generation in a semi-continuous fashion

LIST OF ORAL PRESENTATION:

Accepted: Juan I. del Río, Angel Martín, María D. Bermejo, Green and blue hydrogen generation in a semi-continuous fashion by activating the metal-water-splitting with CO_2 capture derivatives and solvents, in CHISA - 26th International Congress of Chemical and Process Engineering, Prague (Czech Republic), 21-25 August 2022.

Juan I. del Río, Baldur Schroeter, María D. Bermejo, Ángel Martín, Irina Smirnova, Pavel Gurikov, Controlling the post-structure properties of metal-crosslinked carbon-aerogels from alginate for emerging technologies, in the Spanish-portuguese industry-academia aerogel meeting, held in Coimbra, Portugal, March 1-2, 2022. Awarded Second best Oral presentation.

Juan I. del Río, Angel Martín, María D. Bermejo, Activating the metal-water-splitting for hydrogen generation in a semi-continuous fashion, in 10th International seminar on thermodynamic engineering of fluids, held online in Tarragona (Spain), July 22nd-23rd, 2021.

Angel Martín, Juan I. del Río, Eduardo Perez, María D. Bermejo, Using aluminum as reducing agent for the catalytic conversion of ammonia-based CO_2 absorption derivatives, in 1er Encuentro ibérico de fluidos supercríticos- EIFS2020, held on 18-20 February 2020 in Santiago de Compostela (Spain).

Juan I. del Río, Angel Martín, María D. Bermejo, A comparison of ammonia-co2absorption derivatives as starting materials for the catalytic production of formic acid in hydrothermal media, in CIBIQ iberoamericano de ingeniería química, held in Santander (Spain) from 19th to 21st June, 2019.

Juan I. del Río, María D. Bermejo, Angel Martín, Conversion of CO_2 capture by amines into value-added chemicals, in ESS-HPT Summer School, held in Maribor – Graz, 8.7. – 22.7.2018.

del Río, J. I., Cardeño, F., Rios, L. A, Hydrogenation of crude jatropha oil for industrial applications, in XXIV Congreso iberoamericano de catálisis CICAT Medellín, Colombia, 2014

LIST OF POSTERS:

Juan I. del Río, Angel Martín, María D. Bermejo, Effect of process conditions in the reduction of CO_2 captured by ammonia, in The 12th European congress of chemical engineering ECCE12, Florence, Italy, 15-19 September 2019.

Juan I. del Río, Eduardo Perez, Angel Martín, María D. Bermejo, Formic acid production from the Catalytic transfer-hydrogenation of ammonium carbamate, in 17th reunión europea en fluidos supercriticos, Ciudad real (Spain), 8-11 April 2019

Juan I. del Río, Eduardo Perez, Angel Martín, María D. Bermejo, Catalytic recycling of CO_2 captured by amines for obtaining formic acid, in IX reuniòn de expertos en tecnologías de fluidos comprimidos FLUCOMP, Madrid (Spain), 14-15 June 2018.

Juan I. del Río, William Perez, Luis A. Ríos, Juan D. Peña, Diesel renovable de aceite de palma: el biocombustible líquido avanzado de Colombia, in Primer congreso nacional de bioenergía - BION, Cali (Colombia), 27-28 April 2017. Awarded best poster.

Juan I. del Río, William Perez, Luis A. Ríos, Juan D. Peña, A performance comparison of NiMoS and CoMoS catalysts on the hydrotreating of Jatropha oil for the production of green diesel, in V jornada técnica de Ingeniería Química e Ingeniería Biológica, Universidad Nacional de Colombia, Medellin (Colombia), 13-17 March, 2017.